

# **Design of Polymeric Sensing Materials for Volatile Organic Compounds: Optimized Material Selection for Ethanol with Mechanistic Explanations**

by

Katherine Mariann Elizabeth Stewart

A thesis  
presented to the University Of Waterloo  
in fulfilment of the  
thesis requirement for the degree of  
Doctor of Philosophy  
in  
Chemical Engineering

Waterloo, Ontario, Canada, 2016

© Katherine Mariann Elizabeth Stewart 2016

## **Author's Declaration**

I hereby declare that I am the sole author of this thesis. This is a true copy of the thesis, including any required final revisions, as accepted by my examiners.

I understand that my thesis may be made electronically available to the public.

## Abstract

There are many applications in which sensing and monitoring volatile organic compounds (VOCs) and other gas analytes are important. This thesis focusses on finding suitable sensing materials for ethanol to reduce the instances of people driving while intoxicated. To find suitable sensing materials, many constraints must be taken into consideration. For example, a sensing material and sensor must have the appropriate sensitivity and selectivity required.

The goal is to create a sensing material or multiple materials capable of detecting ethanol that is emitted from the skin (transdermally). This requires highly sensitive sensing materials and sensors capable of detecting ethanol close to 5 ppm. This limit of 5 ppm was confirmed by measuring transdermal ethanol. In addition, to avoid false positives, the sensor must be able to selectively identify ethanol (i.e. respond preferentially to ethanol).

To achieve this goal, polymeric sensing materials were used because of their ability to be tailored towards a target analyte. Multiple polymeric sensing materials were designed, synthesized, and evaluated as a sensing material for ethanol. Both the sensitivity and selectivity of the sensing materials were evaluated using a specially designed experimental test set-up that included a highly sensitive gas chromatograph (GC) capable of detecting down to the ppb range.

In total, over thirty potential sensing materials were evaluated for ethanol. These sensing materials, which include polyaniline (PANI) and two of its derivatives, poly (*o*-anisidine) (PoANI) and poly (2,5-dimethyl aniline) (P25DMA), doped with various concentrations of five different metal oxide nanoparticles ( $\text{Al}_2\text{O}_3$ , CuO, NiO,  $\text{TiO}_2$ , and ZnO), were synthesized and evaluated for sensitivity and selectivity to ethanol. In addition, specialized siloxane-based polymers and other polymers such as poly (methyl methacrylate) (PMMA) and polypyrrole (PPy) were evaluated.

From these thirty plus sensing materials, P25DMA doped with  $\text{TiO}_2$ , NiO, and  $\text{Al}_2\text{O}_3$ , along with PPy, had the best sensitivity towards ethanol. Most of the materials tested, with the exception of the CuO doped P25DMA, P25DMA doped with 20% ZnO, poly (ethylene imine) (PEI), and the siloxane-based sensing materials, were able to sorb, and therefore detect, 5 ppm of ethanol. Therefore, the sensitivity requirement of 5 ppm was satisfied. In terms of selectivity, P25DMA doped with 5%  $\text{Al}_2\text{O}_3$  and P25DMA doped with 10%  $\text{TiO}_2$  had the best selectivity towards ethanol with respect to five typical interferent gases (acetaldehyde, acetone, benzene, formaldehyde, and methanol).

Some of the most promising polymeric sensing materials were then deposited onto two different kinds of sensors: a capacitive radio frequency identification (RFID) sensor and a mass-based microcantilever microelectromechanical systems (MEMS) sensor. These sensors were evaluated for sensitivity, selectivity, and response and recovery times. It was found that P25DMA doped

with 20% NiO had a detection limit of 3 ppm on the RFID sensor, whereas P25DMA had a detection limit of 5 ppm on the MEMS sensor. It should be noted that not all sensing materials work well on all sensors.

To improve the selectivity of a sensor, a sensor array or electronic nose can be used. These use a pattern-recognition algorithm to separate the responses for different gas analytes. A proof-of-principle study was done using principal component analysis that was capable of distinguishing between six different VOCs using five different polymeric sensing materials. In addition, a three sensor array was evaluated on the RFID platform. Using PCA as the filtering algorithm, four gas analytes (ethanol, methanol, acetone, and benzene) were able to be identified. These four analytes could also be identified even when in gas mixtures of twos and threes and when all four gas analytes were present.

After this wide experimentation, and based on the knowledge gained from the sorption responses between various VOCs and polymers, along with what has been reported in the literature, various sensing mechanisms were proposed. These sensing mechanisms explain why certain VOCs sorb more preferentially onto certain polymers. Therefore, identifying the dominant sensing mechanisms for a target analyte can improve sensing material selection.

Based on these sensing mechanisms, potential sensing materials can be chosen for a target analyte. By including other constraints from the specific application target and sensor, this list of potential sensing materials can be further narrowed. From here, these sensing materials can be evaluated for sensitivity and selectivity, before the most promising ones are deposited onto sensors for further testing.

This has led to prescriptions that can be followed when designing a new sensing material for a target application. These prescriptions take into consideration the chemical nature of the target analyte (and thus, the dominant mechanisms by which it is likely to interact), any constraints of the target application (including operational temperature and type of sensor), and the chemical nature of the common interferences present with the target analyte. These prescriptions allow one to narrow down a list of hundreds or thousands of potential sensing materials to a manageable few, which can then be evaluated.



## **Acknowledgements**

I would like to thank my supervisor, Prof. Alexander Penlidis, for his guidance and support throughout my PhD. I looked forward to our biweekly meetings for his advice, humour, and focus. Special thanks to Prof. Neil McManus, Prof. Eihab Abdel-Rahman, Mahmoud Khater, and Scott Chen.

Many thanks to my colleagues and friends Yasaman Amintowlieh, Nicole Cathcart, Holly Gray, Mark Hazlett, Hadi Izadi, Niousha Kazemi, Marzieh Riahinezhad, Pouyan Sardashti, and Alison Scott who all lent an ear from time to time and kept me going and sane.

My parents have always been my staunchest supporters. I would like to thank my dad, Ken Stewart and my mom, Marilyn Stone, for taking the time to proofread my thesis and papers. Finally, I would like to thank my husband, Brian Abernethy, for his unrelenting support.

# Table of Contents

Author’s Declaration.....	ii
Abstract.....	iii
Acknowledgements.....	v
Table of Contents.....	ix
List of Figures.....	xvii
List of Tables.....	xxiv
1. Outline and Objectives.....	1
1.1 Introduction and Motivation.....	1
1.2 Objectives.....	1
1.3 Outline.....	2
2. Literature Background.....	5
2.1 Volatile Organic Compound (VOC) Detection.....	5
2.1.1 Gas Sensors.....	5
2.2.2 Ethanol Sensors.....	5
2.2 Sensing Characteristics.....	5
2.2.1 Sensitivity.....	6
2.2.2 Selectivity.....	7
2.2.3 Response and Recovery Times.....	8
2.2.4 Operational Temperature.....	9
2.3 Transdermal Ethanol.....	10
2.4 Sensing Materials.....	11
2.4.1 Polymeric Materials.....	12
2.4.2 Metals and Metal Oxides.....	12
2.4.3 Dopants.....	13
2.4.4 Polymeric Nanocomposites.....	14
2.4.5 Sensing Materials for Volatile Organic Compounds (VOCs).....	14
2.5 Types of Sensors.....	14

2.5.1 Resistive Sensors .....	15
2.5.2 Capacitive Sensors .....	16
2.5.3 Mass-based Sensors .....	17
2.5.4 Optical and Spectroscopic Sensors .....	17
2.5.5 Sensor Arrays and Electronic Noses .....	18
2.5.6 Other Sensors .....	18
2.6 Sensing Materials and Sensors for Ethanol .....	19
2.6.1 Polymeric Sensing Materials .....	19
2.6.1.1 Polyaniline (PANI) .....	19
2.6.1.2 Poly (o-anisidine) (PoANI).....	20
2.6.1.3 Poly (2,5-dimethyl aniline) (P25DMA).....	21
2.6.2 Metal Oxide Sensing Materials and Dopants.....	23
2.6.2.1 Aluminum Oxide (Al <sub>2</sub> O <sub>3</sub> ) .....	23
2.6.2.2 Copper Oxide (CuO).....	24
2.6.2.3 Nickel Oxide (NiO).....	25
2.6.2.4 Titanium Dioxide (TiO <sub>2</sub> ).....	27
2.6.2.5 Zinc Oxide (ZnO) .....	28
3. Experimental .....	31
3.1 Gas Test System.....	31
3.1.1 Experimental Set-up.....	31
3.1.2 Specialized Gas Chromatograph.....	32
3.1.3 Gas Analytes Tested .....	33
3.2 Transdermal Gas Determination .....	34
3.2.1 Transdermal Volatile Organic Compounds (VOCs).....	34
3.2.2 Transdermal Ethanol Concentration .....	35
3.3 Sensing Material Preparation .....	36
3.4 Deposition onto Sensors .....	38
3.4.1 Radio Frequency Identification (RFID) Sensor .....	38
3.4.2 Microelectromechanical Systems (MEMS) Microcantilever Sensor .....	38
3.5 Evaluation of Sensing Materials and Sensors .....	38

3.5.1 Evaluation of Sensing Materials .....	38
3.5.2 Evaluation of Sensors .....	39
3.5.2.1 RFID Sensors .....	39
3.5.2.2 MEMS-based Sensors .....	39
3.6 Statistical Analysis .....	40
3.7 Polymerization Kinetics of Aniline .....	42
4. Results and Discussion: Sensing Material Analysis .....	47
4.1 Transdermal Gas Studies .....	47
4.1.1 Transdermal Volatile Organic Compounds (VOCs).....	47
4.1.2 Transdermal Ethanol Concentration .....	49
4.2 Characterization of Polymer Nanocomposites.....	54
4.2.1 Dopant Concentration (EDX) and Morphology (SEM).....	54
4.2.1.1 P25DMA doped with CuO.....	55
4.2.1.2 P25DMA doped with Al <sub>2</sub> O <sub>3</sub> .....	56
4.2.1.3 P25DMA Doped with ZnO .....	57
4.2.1.4 P25DMA doped with NiO .....	59
4.2.1.5 P25DMA doped with TiO <sub>2</sub> .....	59
4.2.2 Crystallinity (XRD) .....	60
4.3 Ethanol Sorption Studies.....	62
4.3.1 Polyaniline (PANI) and its Derivatives .....	62
4.3.2 Doped Polyaniline (PANI) and Poly (o-anisidine) (PoANI) .....	63
4.3.3 Doped Poly (2,5-dimethyl aniline) (P25DMA) .....	64
4.3.3.1 P25DMA Doped with Al <sub>2</sub> O <sub>3</sub> .....	65
4.3.3.2 P25DMA Doped with CuO.....	66
4.3.3.3 P25DMA Doped with NiO .....	67
4.3.3.4 P25DMA Doped with TiO <sub>2</sub> .....	68
4.3.3.5 P25DMA Doped with ZnO.....	69
4.4 Selectivity Studies.....	69
4.4.1 P25DMA Doped with Al <sub>2</sub> O <sub>3</sub> .....	70
4.4.2 P25DMA Doped with ZnO .....	71

4.4.3 P25DMA Doped with NiO .....	71
4.4.4 P25DMA Doped with TiO <sub>2</sub> .....	72
4.5 Optimal Sensing Materials for Ethanol.....	73
4.6 Sensor Array .....	74
5. Results and Discussion: Sensors and Further Analysis .....	79
5.1 Sensor Evaluation .....	79
5.1.1 Radio Frequency Identification (RFID).....	79
5.1.1.1 Rigid versus Flexible RFID Sensor .....	79
5.1.1.2 RFID Rigid Sensor.....	96
5.1.1.3 RFID Sensor Array .....	99
5.1.2 Microelectromechanical Systems (MEMS) Microcantilever .....	108
5.2 Polymer Backbone Studies .....	110
5.2.1 No Side Chains or Groups .....	110
5.2.2 Dimethyl Side Groups.....	111
5.2.3 Effect of Polymeric Backbones .....	113
5.3 Polymer Functional Groups and Side Chain Studies.....	113
5.3.1 Linear Polyethylene Backbone .....	113
5.3.2 Polyaniline Backbone .....	114
5.3.3 Siloxane Backbone.....	115
5.3.4 Effect of Functional Groups and Side Chains.....	117
5.4 Sample Stability .....	117
5.5 Further Comparisons.....	118
5.5.1 Batch to Batch Comparison .....	118
5.5.2 Operator Comparison.....	119
5.5.3 Day to Day Comparison.....	119
5.5.4 Powder vs. Film .....	120
6. Results and Discussion: Mechanistic Explanations.....	123
6.1 Primary Sensing Mechanisms.....	123
6.1.1 Polarity and Hydrogen Bonding .....	123

6.1.2 Lewis Acid-Base Interactions .....	125
6.1.3 p-orbitals and $\pi$ -bonds .....	125
6.1.4 Metal Coordination .....	127
6.1.5 Steric Hindrance.....	129
6.1.6 Dispersion and van der Waals Forces .....	129
6.2 Secondary Sensing Mechanisms .....	130
6.2.1 Swelling .....	130
6.2.2 Solvent Effects .....	131
6.3 Multiple Mechanisms.....	131
6.4 Solubility and Solubility Parameters .....	131
6.5 Dominant Mechanisms for Different Volatile Organic Compounds (VOCs) .....	135
6.5.1 Alcohols .....	135
6.5.2 Aldehydes and Ketones.....	139
6.5.3 Amines .....	146
6.5.4 Aromatics .....	148
6.5.5 Alkanes .....	151
6.6 Final Remarks about Sensing Mechanisms .....	153
7. Results and Discussion: Selecting a Sensing Material .....	155
7.1 Sensor Application Requirements.....	155
7.1.1 Sensitivity .....	155
7.1.2 Selectivity .....	156
7.1.3 Operational Temperature .....	156
7.1.4 Response and Recovery Times .....	157
7.2 Target Analyte's Chemistry (Mechanisms) .....	157
7.3 Case Studies .....	158
7.3.1 Examples.....	158
7.3.1.1 Effect of Hydrogen Bonding.....	158
7.3.1.2 Incorporation of Metal Oxide Dopants into a Polymeric Sensing Material .....	160
7.3.1.3 Competing Mechanisms.....	161
7.3.2 Counter Examples .....	162

7.3.2.1 Competing Analytes (Poor Selectivity) .....	163
7.3.2.2 Incompatible Metal Oxides and Polymers .....	163
7.4 Practical Prescriptions.....	166
7.4.1 Practical Prescriptions.....	166
7.4.2 Polymeric Sensing Material Selection Example.....	169
8. Concluding Remarks and Recommendations .....	173
8.1 Concluding Remarks.....	173
8.3 Future Work .....	175
8.3.1 Short Term Goals.....	175
8.3.1.1 Improve the Sensor Array for Six VOCs.....	175
8.3.1.2 Improve Understanding of Sensing Mechanisms and Dopant Incorporation .....	175
8.3.1.3 Improve Understanding of Sensing Mechanisms for Inorganic Analytes .....	175
8.3.2 Long Term Goals .....	176
8.3.2.1 Build and Evaluate a Prototype of the Ethanol Sensing Device for a Vehicle ...	176
8.3.2.2 Design, Synthesize, and Evaluate Sensing Materials for Acetone .....	176
8.3.2.3 Design, Synthesize, and Evaluate Sensing Materials for Benzene .....	176
8.3.2.4 Sensing Materials for Inorganic Pollutants.....	177
8.3.2.5 Sensing Materials for Toxic Aqueous Analytes .....	177
8.3.2.6 Modelling of the Interactions between Sensing Materials and Analytes.....	177
References.....	179
Appendix A: Volatile Organic Compounds (VOCs) Emitted from the Human Body .....	207
Appendix B: Sensing Materials for Volatile Organic Compounds .....	211
Appendix C: Selectivity towards Ethanol.....	227
Appendix D: Miscellaneous Chromatograms.....	231
D.1: Gas Chromatograms.....	231

D.2 Gel Permeation Chromatography (GPC) Responses .....	236
Appendix E: Data.....	239
E.1 Chapter 4 Data.....	239
E.1.1 Polyaniline (PANI) Nanocomposites (Section 4.3.2).....	239
E.1.2 Poly (o-anisidine) (PoANI) Nanocomposites (Section 4.3.2) .....	239
E.1.3 Poly (2,5-dimethyl aniline) (P25DMA) Nanocomposites (Section 4.3.3) .....	240
E.2 Chapter 5 Data.....	242
E.2.1 RFID Sensor (Section 5.1.1) .....	242
E.2.2 MEMS Sensor (Section 5.1.2).....	244
E.2.3 Backbone Studies (Section 5.2).....	244
E.2.4 Functional Group Studies (Section 5.3) .....	244
E.2.5 Batch to Batch Comparison (Section 5.5.1) .....	245
E.2.6 Operator Comparison (Section 5.5.2).....	245
E.2.7 Day to Day Comparison (Section 5.5.3) .....	245
E.2.8 Powder vs. Film (Section 5.5.4) .....	246
E.3 Chapter 7 Data.....	246
E.3.1 PANI vs. PNMA (Section 7.3.1.1).....	246
E.3.2 Commercial Polymers (Section 7.4.2).....	246
Appendix F: Statistical Analysis Tables .....	249
F.1 Analysis from Chapter 4.....	251
F.1.1 Analysis for PANI and Its Derivatives (Section 4.3.1) .....	251
F.1.2 Analysis for Doped PANI and PoANI (Section 4.3.2).....	252
F.1.3 Analysis for Doped P25DMA (Section 4.3.3).....	253
F.1.4 Analysis for Other Polymers (Section 4.3.4).....	257
F.1.5 Analysis for Selectivity Studies (Section 4.4) .....	258
F.2 Analysis for Chapter 5 .....	259
F.2.1 Analysis for RFID Ethanol Sensitivity (Section 5.1.1) .....	259
F.2.2 Analysis for Backbone Studies (Section 5.2) .....	260
F.2.3 Analysis for Functional Group Studies (Section 5.3).....	261



F.2.4 Analysis for Sample Stability (Section 5.4) .....	263
F.2.5 Analysis for Batch to Batch Comparison (Section 5.5.1).....	263
F.2.6 Analysis for Operator Comparison (Section 5.5.2) .....	264
F.2.7 Analysis for Day to Day Comparison (Section 5.5.3).....	264
F.2.8 Analysis for Powder versus Film (Section 5.5.4).....	265
F.3 Analysis for Chapter 7 .....	266
F.3.1 Effect of Hydrogen Bonding (Section 7.3.1.1).....	266
F.3.2 Polymeric Sensing Material Selection Example (Section 7.4.2).....	267
Appendix G: Characterization Details .....	269
G.1 Additional Energy Dispersive X-ray (EDX) Data .....	269
G.2 Additional X-ray Diffraction (XRD) Data.....	270
Appendix H: Sensor Array Analysis.....	271
H.1 P25DMA Five Sensor Array (Section 4.6) .....	271
H.2 RFID Three Sensor Arrays (Section 5.1.1.3).....	274
H.2.1 RFID Siloxane-based Three Sensor Array.....	274
H.2.2 RFID P25DMA-based Three Sensor Array .....	276
Appendix I: Potential Polymeric Sensing Materials for Ethanol.....	279
Appendix J: Safety Considerations .....	289

## List of Figures

Figure 2.1: Comparison of ethanol sensitivity ( $R-R_0/R_0$ , where R is the response to ethanol and $R_0$ is the response to air) of ZnO nanoparticles and nanorods (Singh et al., 2008).....	6
Figure 2.2: Chromatogram of 0.05 ppm formaldehyde. ....	7
Figure 2.3: Selectivity of Ag doped $\text{In}_2\text{O}_3$ gas sensor (Wang et al., 2009a).....	8
Figure 2.4: Response and recovery times of ZnO gas sensor for acetone at (a) multiple concentrations and (b) 100 ppm (Jia et al., 2014). ....	9
Figure 2.5: Sensitivity versus operational temperature for various doped ZnO sensing materials for (a) benzene and (b) toluene (Zhu et al., 2004).....	9
Figure 2.6: Emission rate of gas analytes emitted from the skin. Note the compounds (analytes) are colour coded by compound class (Mochalski et al., 2014). ....	11
Figure 2.7: Adsorption and absorption of ethanol. ....	12
Figure 2.8: Schematic of PANI-acid doping mechanism (Virji et al., 2004). Note that this figure shows HCl as the acid, but the mechanism can be extended to all other acids. ....	14
Figure 2.9: (a) Sensor A, (b) Sensor B, (c) Sensor C, and (d) response of all three sensors to 100 ppm of ethanol at different temperatures (Shen et al., 2012). ....	15
Figure 2.10: E-field distribution across a capacitor using low frequencies (left) and RF frequencies (right) (Chen et al., 2015b). ....	16
Figure 2.11: Schematic of microcantilever sensor (Khater et al., 2009). ....	17
Figure 2.12: Three dimensional PCA plot for six different VOCs (Li et al., 2013a). ....	18
Figure 2.13: Chemical structure of polyaniline (PANI). ....	19
Figure 2.14: Chemical Structure of PoANI. ....	21
Figure 2.15: Chemical Structure of P25DMA .....	22
Figure 2.16: Sensitivity to ethanol versus temperature for ZnO doped with 0 atomic (at.) % (C05), 1 at. % (C15), 2 at. % (C25), 3 at. % (C35), and 4 at. % (C45) (Yang et al., 2009b)....	24
Figure 2.17: Effect of NiO dopant concentrations on the sensitivity of $\text{SnO}_2$ to ethanol (Liu et al., 2011a). ....	27
Figure 2.18: Effects of NiO addition on sensitivity and selectivity (Zheng et al., 2012). ....	27
Figure 3.1. Schematic of the test system, where MFC, PC, and FM are mass flow controller, pressure controller, and flow meter, respectively. Note that the analytes shown are ethanol, methanol, and benzene, but represent the individual tanks of all the different analytes used. .	31

Figure 3.2: Chromatogram of four different gas analytes (formaldehyde, acetaldehyde, ethanol, and benzene), eluting out at different times. ....	32
Figure 3.3: Chromatogram of formaldehyde at 0.09 ppm. ....	33
Figure 3.4: Chromatogram of lab air (reference point for further determinations). ....	35
Figure 3.5: Chromatogram from the palm of a hand. Note formaldehyde and acetic acid labels are overlapping. ....	35
Figure 3.6: Schematic of the test chamber used for evaluation of the MEMS-based sensor. ....	40
Figure 3.7: Proposed oxidation mechanism for the polymerization of aniline (Bocchini et al., 2013). ....	44
Figure 3.8: Typical conversion versus time graph for the polymerization of polyaniline. ....	45
Figure 4.1: Gases emitted from one individual’s hand over time. ....	48
Figure 4.2: Gas chromatogram of unidentified (unknown) compounds emitted from the person’s hand. ....	49
Figure 4.3: Comparison of the transdermal ethanol concentration and BAC measured from the mouth, March 25, 2015. ....	50
Figure 4.4: Comparison of the transdermal ethanol concentration and BAC measured from the mouth, April 1, 2015. ....	50
Figure 4.5: Comparison of the transdermal ethanol concentration and BAC measured from the mouth, April 14, 2015. ....	51
Figure 4.6: Transdermal ethanol concentration shown for different days over three months in 2015. ....	51
Figure 4.7: BAC from the breathalyzer shown for different days over three months in 2015. ....	52
Figure 4.8: Transdermal ethanol concentration and BAC from the breathalyzer for the double shot (3 oz.), February 19, 2015. ....	53
Figure 4.9: Transdermal ethanol concentration measurements for six days plus the double shot (shown as the first bar, February 19) for comparison. ....	53
Figure 4.10: SEM of (a) P25DMA, (b) P25DMA 5% CuO, (c) P25DMA 10% CuO, and (d) P25DMA 20% CuO. ....	56
Figure 4.11: SEM images of (a) P25DMA, (b) P25DMA 5% Al <sub>2</sub> O <sub>3</sub> , (c) P25DMA 10% Al <sub>2</sub> O <sub>3</sub> , and (d) P25DMA 20% Al <sub>2</sub> O <sub>3</sub> . ....	57
Figure 4.12: SEM images of (a) P25DMA, (b) P25DMA 5% ZnO, (c) P25DMA 10% ZnO, and (d) P25DMA 20% ZnO. ....	58

Figure 4.13: SEM images of (a) P25DMA, (b) P25DMA 5% NiO, (c) P25DMA 10% NiO, and (d) P25DMA 20% NiO.....	59
Figure 4.14: SEM images of (a) P25DMA, (b) P25DMA 5% TiO <sub>2</sub> , (c) P25DMA 10% TiO <sub>2</sub> , and (d) P25DMA 20% TiO <sub>2</sub> .....	60
Figure 4.15: XRD of (a) P25DMA, (b) P25DMA 5% CuO, (c) P25DMA 5% Al <sub>2</sub> O <sub>3</sub> , (d) P25DMA 5% NiO, (e) P25DMA 5% TiO <sub>2</sub> , and (f) P25DMA 5% ZnO .....	61
Figure 4.16: XRD of P25DMA, NiO nanoparticles, P25DMA, and P25DMA 10% NiO. ....	62
Figure 4.17: Amount of ethanol sorbed onto PANI, PoANI, and P25DMA. ....	62
Figure 4.18: Ethanol sorption onto undoped and doped PANI and PoANI.....	63
Figure 4.19: Ethanol sorption onto undoped and doped P25DMA. ....	65
Figure 4.20: Ethanol sorption of P25DMA and P25DMA doped with 5%, 10%, and 20% Al <sub>2</sub> O <sub>3</sub> . ....	66
Figure 4.21: Ethanol sorption of P25DMA doped with CuO. ....	67
Figure 4.22: Amount of sorbed analyte for P25DMA, P25DMA 5% NiO, P25DMA 10% NiO, and P25DMA 20% NiO. ....	67
Figure 4.23: Amount of sorbed analyte for P25DMA, P25DMA 5% TiO <sub>2</sub> , P25DMA 10% TiO <sub>2</sub> , and P25DMA 20% TiO <sub>2</sub> .....	68
Figure 4.24: Amount of sorbed analyte for P25DMA, P25DMA 5% ZnO, P25DMA 10% ZnO, and P25DMA 20% ZnO. ....	69
Figure 4.25: (a) Ethanol sorption of P25DMA and P25DMA doped with 5%, 10%, and 20% Al <sub>2</sub> O <sub>3</sub> and (b) Amount of sorbed analyte for P25DMA and P25DMA 5% Al <sub>2</sub> O <sub>3</sub> . Note that for (b), the gases, from left to right (black to white), are ethanol, formaldehyde, methanol, acetaldehyde, acetone, and benzene. ....	70
Figure 4.26: Amount of sorbed analyte for P25DMA and P25DMA 5% ZnO. Note that from left to right (black to white), the gases are ethanol, formaldehyde, methanol, acetaldehyde, acetone, and benzene. ....	71
Figure 4.27: Amount of sorbed analyte for P25DMA, P25DMA 5% NiO, P25DMA 10% NiO, and P25DMA 20% NiO. ....	72
Figure 4.28: Amount of sorbed analyte for P25DMA, P25DMA 5% TiO <sub>2</sub> , P25DMA 10% TiO <sub>2</sub> , and P25DMA 20% TiO <sub>2</sub> .....	73
Figure 4.29: Amount of gas analyte sorbed onto each sensing material. Note that from left to right, the bars represent acetaldehyde, acetone, benzene, ethanol, formaldehyde, and methanol, respectively.....	75
Figure 4.30: PCA reference plot. ....	76
Figure 4.31: Scree plot showing the percent of variability for each Factor.....	77

Figure 4.32: PCA plot with unknowns (single gases).....	77
Figure 4.33: Unknown gas mixture. ....	78
Figure 5.1: Response schematic of RFID sensor. A change in capacitance ( $\Delta C$ ) results in a change in response amplitude as the resonant frequency shifts (Stewart et al., 2015). ....	80
Figure 5.2: Rigid RFID sensor (left) and flexible RFID (right) sensors, with a Canadian quarter for scale. The flexible RFID sensor is bent at 90° in an acrylic form. ....	80
Figure 5.3: The response amplitude (unitless) for all six sensing materials for both the rigid and flexible sensor. Each analyte (ethanol, blue; methanol, green; acetone, orange; benzene, yellow) was individually exposed to the sensing materials at 1250 ppm. ....	82
Figure 5.4: Response Amplitude (unitless) of all six sensing materials when exposed to ethanol and one other interferent simultaneously at 1250 ppm for both the rigid (grey) and flexible (orange) sensors. The second and fourth column for each sensing material show the response amplitude when the concentration of ethanol was halved to 625 ppm (lighter columns).....	84
Figure 5.5: Response Amplitude (unitless) of all six sensing materials when exposed to ethanol and two interferents simultaneously at 1250 ppm for both the rigid (grey) and flexible (orange) sensors. The second and fourth column for each sensing material show the response amplitude when the concentration of ethanol was halved to 625 ppm (lighter columns).....	88
Figure 5.6: Response Amplitude (unitless) of all six sensing materials when exposed to all four gases simultaneously at 1250 ppm for both the rigid (grey) and flexible (orange) sensors. The second and fourth column for each sensing material show the response amplitude when the concentration of ethanol was halved to 625 ppm (lighter columns). ....	91
Figure 5.7: The amplitude and delay response and recovery curves for P25DMA for each analyte individually tested at 5000 ppm. ....	93
Figure 5.8: The amplitude and delay response and recovery curves for P25DMA 20% NiO for each analyte individually tested at 5000 ppm. ....	93
Figure 5.9: The amplitude and delay response and recovery curves for P25DMA 20% ZnO for each analyte individually tested at 5000 ppm. ....	94
Figure 5.10: The amplitude and delay response and recovery curves for OV 275 for each analyte individually tested at 5000 ppm. ....	94
Figure 5.11: The amplitude and delay response and recovery curves for OV 225 for each analyte individually tested at 5000 ppm. ....	95
Figure 5.12: The amplitude and delay response and recovery curves for SXFA for each analyte individually tested at 5000 ppm. ....	95

Figure 5.13: Change in sensor response amplitude for each sensing material at different concentrations of ethanol. Note that for clarity, the concentration has been placed on a log scale with a concentration of 0 ppm of ethanol equal to 1 on the scale. ....	96
Figure 5.14: The change in resonant frequency measured at equilibrium for different analytes at (a) 5000 ppm and (b) 625 ppm for each sensing material. ....	98
Figure 5.15: Response and recovery times for each sensing material measured for ethanol at 5000 ppm. Relative response amplitude is the percent change in the amplitude of the response from the baseline, when the sensing material is exposed to an analyte. ....	99
Figure 5.16: The three sensor array on the rigid RFID platform. These RFID arrays are the same size as those shown in Figure 5.2. ....	100
Figure 5.17: Sample readout of the RFID three sensor array for the P25DMA-based sensing materials. Note that the peaks for each sensing material are separate and distinct (Chen, 2015). ....	100
Figure 5.18: Single gas analytes for (a) the siloxane-based and (b) the P25DMA-based sensor arrays. ....	101
Figure 5.19: Two gas mixtures for (a) the siloxane-based and (b) the P25DMA-based sensor arrays. Note that E, M, A, and B denote ethanol, methanol, acetone, and benzene, respectively. ....	102
Figure 5.20: Three gas mixtures for (a) the siloxane-based and (b) the P25DMA-based sensor arrays. Note that E, M, A, and B denote ethanol, methanol, acetone, and benzene, respectively. ....	103
Figure 5.21: All four gases for (a) the siloxane-based and (b) the P25DMA-based sensor arrays. ....	104
Figure 5.22: PCA plot for the siloxane-based RFID sensor array. Note that E is ethanol, M is methanol, A is acetone, and B is benzene in the gas mixtures. ....	105
Figure 5.23: PCA plot for the P25DMA-based RFID sensor array. Note that E is ethanol, M is methanol, A is acetone, and B is benzene in the gas mixtures. ....	106
Figure 5.24: Factor 2 vs. Factor 3 projection of variables onto the 2 x 3 plane for the siloxane-based RFID sensor array. ....	107
Figure 5.25: Factor 1 vs Factor 4 PCA plot for the siloxane-based RFID sensor array. The two squares emphasize ethanol and benzene. Note that E is ethanol, M is methanol, A is acetone, and B is benzene in the gas mixtures. ....	108
Figure 5.26: (a) before and (b) after ethanol sorption onto the MEMS microcantilever (Khater et al., 2014). ....	109
Figure 5.27: Chemical structure of (a) PANI and (b) PPy. ....	110
Figure 5.28: Amount of ethanol sorbed onto PANI and PPy. ....	110

Figure 5.29: Chemical structure of (a) P25DMA and (b) PPO.....	111
Figure 5.30: Amount of ethanol sorbed onto P25DMA and PPO. ....	111
Figure 5.31: Amount of methanol sorbed onto P25DMA and PPO. ....	112
Figure 5.32: Chemical structure of (a) PMMA and (b) PVP.....	113
Figure 5.33: Amount of ethanol sorbed onto PMMA and PVP.....	114
Figure 5.34: Chemical structure of (a) PANI, (b) PoANI, and (c) P25DMA.....	114
Figure 5.35: Amount of ethanol sorbed onto PANI, PoANI, and P25DMA.....	115
Figure 5.36: Chemical structure of (a) OV 225, (b) OV 275, and (c) SXFA. ....	116
Figure 5.37: Response to ethanol for OV 225, OV 275, and SXFA.....	116
Figure 5.38: Amount of ethanol sorbed onto varying ages of PANI (five, two, and zero years old).....	117
Figure 5.39: Amount of ethanol sorbed onto two different batches of P25DMA 5% NiO. ....	118
Figure 5.40: Amount of ethanol sorbed onto two different batches of P25DMA 5% NiO made by two different operators. ....	119
Figure 5.41: Amount of ethanol sorbed onto P25DMA 5% NiO on multiple days.....	120
Figure 5.42: Ethanol sorption onto film and powder forms of PVP and PMMA. ....	121
Figure 6.1: Overlap of p-orbitals and $\pi$ -bonds.....	126
Figure 6.2: Ni coordination to the nitrogens in the quinoid ring (Han et al., 2006). ....	128
Figure 6.3: a) Polyaniline (PANI) and b) Polypyrrole (PPy).....	136
Figure 6.4: a) Poly (diallyldimethyl ammonium chloride) (PDDAC), b) Poly(3,4-ethylenedioxy thiophene): poly(styrene sulfonate) (PEDOT: PSS), c) OV 275.....	137
Figure 6.5: Schematic of an (a) aldehyde and a (b) ketone. ....	139
Figure 6.6: (a) Poly (ethylene imine) (PEI), (b) poly (methyl methacrylate) (PMMA), (c) poly (vinyl alcohol) (PVA), and (d) poly (2,5-dimethyl aniline) (P25DMA).....	141
Figure 6.7: Substitution of $\alpha$ -naphthalene sulfonate ( $\alpha$ -NS <sup>-</sup> ) with acetic acid in polypyrrole (PPy). ....	144
Figure 6.8: Benzene $\pi$ -stacking onto SXFA. ....	149
Figure 6.9: (a) MCD and (b) single wall carbon nanotubes doped with iron-tetraphenylporphyrin (SWCNT-Fe-TPP).....	150
Figure 6.10: Cryptophane-A .....	152

Figure 7.1: Schematic of (a) polyaniline (PANI) and (b) poly (N-methyl aniline) (PNMA).....	158
Figure 7.2: Amount of ethanol (circles) and acetone (squares) sorbed onto both PANI and PNMA. ....	159
Figure 7.3: Sorption of different gases (left to right, ethanol, formaldehyde, methanol, acetaldehyde, acetone, and benzene) to P25DMA and P25DMA 5% Al <sub>2</sub> O <sub>3</sub> .....	160
Figure 7.4: SEM images of (a) P25DMA and (b) P25DMA doped with Al <sub>2</sub> O <sub>3</sub> .....	161
Figure 7.5: Ethanol sorption on P25DMA and P25DMA doped with different concentrations of NiO. ....	161
Figure 7.6: Schematic of polyethyleneimine (PEI).....	163
Figure 7.7: Amount of ethanol sorbed onto P25DMA doped with CuO. ....	164
Figure 7.8: SEM images of (a) P25DMA, (b) P25DMA doped with 5% CuO, (c) P25DMA doped with 10% CuO, and (d) P25DMA doped with 20% CuO. ....	165
Figure 7.9: Prescription Flow Chart for Sensing Material Selection.....	168
Figure 7.10: Sorption of the four polymers to ethanol, methanol, and acetone.....	171
Figure D.1: Gas chromatogram of all six gas analytes evaluated. Note the separation between all the gases, except methanol and acetaldehyde. Benzene eluted after 17 minutes (lone peak on the right). There was also a water peak to the right of formaldehyde around 5.5 minutes. ...	231
Figure D.2: Two ethanol chromatograms measured at 48 minutes (red) and 60 minutes (black). Note that the two chromatograms are on top of one another. This shows that equilibrium has been reached. ....	232
Figure D.3: Gas chromatogram of acetaldehyde. ....	233
Figure D.4: Gas chromatogram of acetone. ....	233
Figure D.5: Gas chromatogram of benzene. ....	234
Figure D.6: Gas chromatogram of ethanol. ....	234
Figure D.7: Gas chromatogram of formaldehyde. ....	235
Figure D.8: Gas chromatogram of methanol. ....	235
Figure D.9: Gel permeation chromatogram of polyaniline (PANI), where the RI is red, the RALS is green, and the LALS is black. ....	236
Figure G.1: XRD for P25DMA 5% NiO and a P25DMA 5% NiO Replicate.....	270



## List of Tables

Table 2.1: Mean Concentration of Compounds from Three Different Volunteers.....	10
Table 2.2: Summary of Sensing Characteristics for Various PANI Sensors for Ethanol.....	20
Table 2.3: Summary of Sensing Characteristics for Various PoANI Sensors for Ethanol.....	21
Table 2.4: Summary of Sensing Characteristics for Various P25DMA Sensors for Ethanol.....	22
Table 2.5: Summary of Sensing Characteristics for Various Al <sub>2</sub> O <sub>3</sub> Sensors.....	23
Table 2.6: Summary of Sensing Characteristics for Various CuO Sensors.....	25
Table 2.7: Summary of Sensing Characteristics for Various NiO Sensors .....	26
Table 2.8: Summary of Sensing Characteristics for Various TiO <sub>2</sub> Sensors .....	28
Table 2.9: Summary of Sensing Characteristics for Various ZnO Sensors .....	29
Table 3.1: Gas Analytes and Concentrations Used.....	34
Table 3.2: Polymerization Kinetic Aspects of Aniline from the Literature.....	43
Table 3.3: Recipe used to Synthesize Polyaniline .....	44
Table 3.4: Rates Constant Values for Ammonium Persulfate (APS) .....	44
Table 3.5: Molecular Weight of PANI .....	45
Table 4.1: Ethanol Concentration for both Hand and Mouth at 20 and 30 Minutes.....	52
Table 4.2: Weight Percent of Metal in Each Polymer Nanocomposite at Different Concentrations.....	55
Table 4.3: Selectivity of Doped and Undoped P25DMA towards Ethanol .....	74
Table 5.1: Percentage by which the Response Dropped when Ethanol Concentration was Halved for Both Sensors .....	83
Table 5.2: Percentage by which the Response Dropped when Ethanol Concentration was Halved for the Rigid Sensor.....	85
Table 5.3: Percentage by which the Response Dropped when Ethanol Concentration was Halved for the Flexible Sensor .....	85
Table 5.4: Percentage by which the Response Dropped when Ethanol Concentration was Halved for the Rigid Sensor.....	89
Table 5.5: Percentage by which the Response Dropped when Ethanol Concentration was Halved for the Flexible Sensor .....	89

Table 5.6: Percentage by which the Response Dropped when Ethanol Concentration was Halved for Both Sensors .....	91
Table 5.7: Noise and Limit of Detection for Ethanol for each Sensing Material on the RFID Sensor .....	97
Table 5.8: Percent Drop of Response when the Ethanol Concentration was Halved .....	102
Table 5.9: Percent Drop of Response when the Ethanol Concentration was Halved .....	103
Table 5.10: Percent Drop of Response when the Ethanol Concentration was Halved .....	104
Table 5.11: Ethanol Response.....	109
Table 5.12: Selectivity towards Ethanol with respect to methanol for P25DMA and PPO .....	112
Table 6.1: Dipole Moment of Common Volatile Organic Compounds (VOCs).....	124
Table 6.2: Hansen and Hildebrand Solubility Parameters for Various VOCs.....	133
Table 6.3: Hansen and Hildebrand Solubility Parameters for Various Polymers.....	134
Table 6.4: Hildebrand Solubility Parameters for Polystyrene .....	135
Table 6.5: Polymeric Sensing Materials for Alcohols .....	138
Table 6.6: Hansen and Hildebrand Solubility Parameters for P25DMA, PANI, and Gas Analytes.....	143
Table 6.7: Polymeric Sensing Materials for Aldehydes and Ketones .....	145
Table 6.8: Polymeric Sensing Materials for Amines .....	148
Table 6.9: Polymeric Sensing Materials for Aromatics.....	151
Table 6.10: Polymeric Sensing Materials for Alkanes .....	153
Table 7.1: EDAX Measurements for P25DMA Doped with CuO .....	164
Table 7.2: Potential Polymeric Sensing Materials for Ethanol.....	170
Table A.1: Selected VOCs Emitted from the Human Body .....	207
Table B.1: Sensing Materials for Acetone .....	211
Table B.2: Sensing Materials for Acetaldehyde .....	214
Table B.3: Sensing Materials for Benzene .....	216
Table B.4: Sensing Materials for Ethanol.....	217
Table B.5: Sensing Materials for Formaldehyde .....	221

Table B.6: Sensing Materials for Methanol .....	224
Table B.7: Sensing Materials for Toluene .....	225
Table C.1: Selectivity of Sensors towards Ethanol with Respect to Other VOCs.....	227
Table D.1: dn/dc Values .....	237
Table D.2: Molecular Weight Averages of PANI .....	237
Table D.3: Pullulan Standard ( $M_w = 108,000$ Da).....	238
Table E.1 Amount of Ethanol Sorbed onto Each PANI Nanocomposite .....	239
Table E.2 Amount of Ethanol Sorbed onto Each PoANI Nanocomposite .....	239
Table E.3: Amount of Ethanol Sorbed onto the P25DMA Nanocomposites .....	240
Table E.4: Amount of Acetaldehyde Sorbed onto the P25DMA Nanocomposites .....	240
Table E.5: Amount of Acetone Sorbed onto the P25DMA Nanocomposites.....	241
Table E.6: Benzene onto the P25DMA Nanocomposites.....	241
Table E.7: Formaldehyde onto the P25DMA Nanocomposites.....	241
Table E.8: Methanol onto the P25DMA Nanocomposites .....	242
Table E.9: Flexible vs. Rigid RFID Sensor .....	242
Table E.10: Rigid vs Flexible Sensor .....	243
Table E.11. RFID Sensor Array Data .....	243
Table E.12: MEMS Sensor .....	244
Table E.13: PANI vs PPy to Ethanol .....	244
Table E.14: P25DMA vs PDPMO to Ethanol .....	244
Table E.15: PMMA vs PVP to Ethanol .....	244
Table E.16: PANI and Derivatives to Ethanol.....	244
Table E.17: Percent Response to Ethanol, Methanol, and Acetone.....	245
Table E.18: Amount of Ethanol Sorbed onto Two Batches of PANI 5% NiO.....	245
Table E.19: Amount of Ethanol Sorbed onto PANI 5% NiO Prepared by Two Operators.....	245
Table E.20: Amount of Ethanol Sorbed onto PANI 5% NiO Measured on Different Days .....	245
Table E.21: Amount of Ethanol Sorbed onto PVP and PMMA Powders and Films .....	246
Table E.22: Amount of Analyte Sorbed onto PANI and PNMA.....	246

Table E.23: Amount of Ethanol Sorbed.....	246
Table E.24: Amount of Acetone Sorbed.....	246
Table E.25: Amount of Methanol Sorbed.....	247
Table F.1: ANOVA Comparing Ethanol Sorption on PANI, PoANI, and P25DMA .....	251
Table F.2: Bonferroni t-test and Fisher’s LSD Comparing Ethanol Sorption PANI and Its Derivatives.....	251
Table F.3 Percent Error for Ethanol Sorption onto PANI, PoANI, and P25DMA.....	252
Table F.4: ANOVA Comparing Ethanol Sorption on Doped and Undoped PANI and PoANI..	252
Table F.5: Bonferroni t-test and Fisher’s LSD Comparing Ethanol Sorption on Doped and Undoped PANI and PoANI.....	252
Table F.6: Percent Error Comparing Ethanol Sorption on Doped and Undoped PANI and PoANI.....	253
Table F.7: ANOVA Comparing Ethanol Sorption on P25DMA and P25DMA Doped with Al <sub>2</sub> O <sub>3</sub> .....	253
Table F.8: Bonferroni t-test and Fisher’s LSD Comparing Ethanol Sorption on P25DMA and P25DMA Doped with Al <sub>2</sub> O <sub>3</sub> .....	253
Table F.9: Percent Error Comparing Ethanol Sorption on P25DMA and P25DMA Doped with CuO .....	254
Table F.10: ANOVA Comparing Ethanol Sorption on P25DMA and P25DMA Doped with CuO .....	254
Table F.11: Bonferroni t-test and Fisher’s LSD Comparing Ethanol Sorption on P25DMA and P25DMA Doped with CuO .....	254
Table F.12: Percent Error Comparing Ethanol Sorption on P25DMA and P25DMA Doped with CuO .....	255
Table F.13: ANOVA Comparing Ethanol Sorption on P25DMA and P25DMA Doped with NiO .....	255
Table F.14: Bonferroni t-test and Fisher’s LSD Comparing Ethanol Sorption on P25DMA and P25DMA Doped with NiO.....	255
Table F.15: Percent Error Comparing Ethanol Sorption on P25DMA and P25DMA Doped with NiO .....	255
Table F.16: ANOVA Comparing Ethanol Sorption on P25DMA and P25DMA Doped with TiO <sub>2</sub> .....	256

Table F.17: Bonferroni t-test and Fisher’s LSD Comparing Ethanol Sorption on P25DMA and P25DMA Doped with TiO <sub>2</sub> .....	256
Table F.18: Percent Error Comparing Ethanol Sorption on P25DMA and P25DMA Doped with TiO <sub>2</sub> .....	256
Table F.19: ANOVA Comparing Ethanol Sorption on P25DMA and P25DMA Doped with ZnO.....	256
Table F.20: Bonferroni t-test and Fisher’s LSD Comparing Ethanol Sorption on P25DMA and P25DMA Doped with ZnO .....	257
Table F.21: Percent Error Comparing Ethanol Sorption on P25DMA and P25DMA Doped with ZnO.....	257
Table F.22: ANOVA Comparing Ethanol Sorption on the Other Polymers .....	257
Table F.23: Bonferroni t-test and Fisher’s LSD Comparing Ethanol Sorption on the Other Polymers.....	258
Table F.24: Percent Error Comparing Ethanol Sorption on the Other Polymers .....	258
Table F.25: ANOVA Comparing Different Analyte Sorption on P25DMA .....	258
Table F.26: Bonferroni t-test and Fisher’s LSD Comparing Different Analyte Sorption on P25DMA .....	259
Table F.27: Percent Error Comparing Different Analyte Sorption on P25DMA.....	259
Table F.28: ANOVA Comparing Rigid vs Flexible Sensors.....	259
Table F.29: Bonferroni t-test and Fisher’s LSD Comparing the Rigid and Flexible Sensors .....	260
Table F.30: Percent Error Comparing the Siloxane-based and P25DMA-based Sensing Materials.....	260
Table F.31: PANI vs PPy.....	260
Table F.32: Percent Error Comparing PANI and PPy .....	260
Table F.33: P25DMA vs PPO for Ethanol.....	261
Table F.34: Percent Error Comparing P25DMA and PPO for Ethanol.....	261
Table F.35: P25DMA vs PPO for Methanol.....	261
Table F.36: Percent Error Comparing P25DMA and PPO for Methanol.....	261
Table F.37: PMMA vs PVP .....	261
Table F.38: Percent Error Comparing PMMA vs PVP.....	262
Table F.39: PANI, PoANI, P25DMA.....	262
Table F.40: Bonferroni t-test and Fisher’s LSD Comparing .....	262
Table F.41: Percent Error Comparing PANI, PoANI, P25DMA .....	262

Table F.42: OV 275, OV 225, SXFA .....	262
Table F.43: Bonferroni t-test and Fisher’s LSD Comparing OV 275, OV 225, SXFA.....	263
Table F.44: Percent Error Comparing OV 275, OV 225, SXFA .....	263
Table F.45: ANOVA Table Comparing Sample Stability of PANI .....	263
Table F.46: Percent Error Comparing Sample Stability of PANI .....	263
Table F.47: ANOVA Table Comparing Batches .....	264
Table F.48: Percent Error Comparing Batches .....	264
Table F.49: ANOVA Table Comparing Operators.....	264
Table F.50: Percent Error Comparing Operators .....	264
Table F.51: ANOVA Table Comparing Days .....	265
Table F.52: Percent Error Comparing Days .....	265
Table F.53: ANOVA Table Comparing Powder vs Film Deposition.....	265
Table F.54: Percent Error Comparing Powder vs Film Deposition.....	265
Table F.55: ANOVA Comparing PANI vs PNMA .....	266
Table F.56: Bonferroni t-test and Fisher’s LSD Comparing PANI and PNMA.....	266
Table F.57: Percent Error Comparing PANI to PNMA.....	266
Table F.58: ANOVA Comparing Potential Sensing Materials for Ethanol.....	267
Table F.59: Percent Error Comparing Potential Sensing Materials for Ethanol.....	267
Table F.60: ANOVA Comparing Potential Sensing Materials for Methanol.....	267
Table F.61: Bonferroni t-test and Fisher’s LSD Comparing Potential Sensing Materials for Methanol.....	267
Table F.62: Percent Error Comparing Potential Sensing Materials for Methanol.....	268
Table F.63: ANOVA Comparing Potential Sensing Materials for Acetone.....	268
Table F.64: Bonferroni t-test and Fisher’s LSD Comparing Potential Sensing Materials for Acetone.....	268
Table F.65: Percent Error Comparing Potential Sensing Materials for Ethanol.....	268
Table G.1: EDX Data.....	269
Table G.2: Representative Percent Error for Three EDX Samples .....	269
Table H.1: Data Used for the P25DMA Five Sensor Array .....	271

Table H.2: Factor Coordinates of Cases for the P25DMA Five Sensor Array .....	272
Table H.3: Factor Coordinates of Variables for the P25DMA Five Sensor Array .....	273
Table H.4: Eigenvalues for the P25DMA Five Sensor Array .....	273
Table H.5: Data Used for the Siloxane-based RFID Three Sensor Array .....	274
Table H.6: Factor Coordinates of Cases for the Siloxane-based RFID Three Sensor Array.....	275
Table H.7: Factor Coordinates of Variables for the Siloxane-based RFID Three Sensor Array.....	275
Table H.8: Eigenvalues for the Siloxane-based RFID Three Sensor Array .....	276
Table H.9: Data Used for the P25DMA-based RFID Three Sensor Array .....	276
Table H.10: Factor Coordinates of Cases for the P25DMA-based RFID Three Sensor Array ...	277
Table H.11: Factor Coordinates of Variables for the P25DMA-based RFID Three Sensor Array.....	277
Table H.12: Eigenvalues for the P25DMA-based RFID Three Sensor Array.....	278
Table I.1: Sensing Mechanisms for Polymer Functional Groups .....	279
Table I.2: Potential Polymeric Sensing Materials and their Functional Groups.....	280
Table J.1: Safety Precautions for Various Chemicals.....	289

# **1. Outline and Objectives**

## **1.1 Introduction and Motivation**

Drinking and driving is still a major problem, despite strict laws for blood alcohol content (BAC) when driving. In 2009, “1,074 Canadians were killed and more than 63,000 were injured in impairment-related crashes”. The current system of random alcohol testing, through roadside checks, does not deter people from driving while intoxicated (Solomon et al., 2012).

The best way to reduce drinking and driving is to install an ignition interlock system in every vehicle. Currently, ignition interlock systems are only placed in a vehicle by court order. Ignition interlock systems work by locking the gear shift in park, preventing the vehicle from moving when alcohol is detected using a breathalyzer (Webster and Gabler, 2007).

The current ignition interlock systems are very bulky and there is a stigma associated with a person having one in their vehicle. In addition, these systems do not monitor the driver throughout a journey. Therefore, a small and discreet ethanol sensor that is able to monitor the driver periodically throughout a journey without diverting his/her attention from the road would be beneficial.

One way to do this would be to create a transdermal ethanol sensor that was tied to a vehicle’s ignition interlock system that was designed to check the driver before starting the vehicle, as well as periodically while the vehicle was in motion. A discreet sensor that is easily reached by the driver could provide this solution (Kanable, 2006). An alternative solution could be a wearable ethanol sensor (Chen et al., 2015a).

The most important part of a sensor is the sensing material(s). By changing the sensing materials on a sensor, the sensor is able to detect different analytes. For an ethanol gas sensor, it is important to design sensing materials that are both sensitive and selective.

## **1.2 Objectives**

There were three main objectives for this thesis. The first was to design sensitive and selective polymeric sensing materials for ethanol as the target analyte ethanol. The second objective was to take the knowledge gained from evaluating potential polymeric sensing materials for ethanol and other common interferents and identify the main sensing mechanisms by which the analytes interact with the sensing material. The third objective was to use this knowledge to come up with general prescriptions to guide selection of a polymeric sensing material for a target analyte (design stage).



Designing potential sensing materials is typically done through a trial and error approach. Instead, a more direct approach was taken targeting specific analytes (e.g. ethanol). Initially, the polymeric sensing materials were chosen based on previous experience and literature. From here, this first set of sensing materials was evaluated and then new potential sensing materials were chosen based on the trends observed. It was important to find sensing materials that were both highly sensitive to ethanol, as well as selective to common interferents (other gas analytes present).

Analytes and sensing materials interact through sensing mechanisms. These sensing mechanisms are based on the chemical nature of both the sensing material and the analyte. This thesis focuses on the interactions between polymeric sensing materials and volatile organic compounds (VOCs). By comparing polymeric sensing materials for multiple VOCs evaluated or presented in the literature, trends were found that suggested specific sensing mechanisms.

These trends and sensing mechanisms were evaluated using specifically designed case studies. Based on this additional information, the sensing mechanisms were categorized and organized to produce a set of prescriptions that could be followed when designing new potential sensing materials for a target analyte. These prescriptions also take into account any constraints due to the sensor application. This approach is a more direct route to designing polymeric sensing materials for a target analyte and sensor application than typically used trial and error procedures.

### **1.3 Outline**

The first chapter is an introduction to the thesis. It discusses the motivation and objectives of this work. In addition, the first chapter outlines what is presented in subsequent chapters.

The second chapter covers relevant literature background. In the second chapter, gas sensors for volatile organic compounds (VOCs) and, specifically, ethanol are discussed. In addition, sensing characteristics, including sensitivity and selectivity, are defined as well as types of sensing materials and sensors. Chapter 2 wraps up with sensing materials and sensors that have been designed for ethanol.

The third chapter explains the experimental procedures that were used. An experimental test system was designed to evaluate both sensing materials and complete sensors (sensors with sensing materials) that contain a highly specialized gas chromatograph (GC) with a photon discharge helium ionization detector (PDHID). This chapter also includes the synthesis of the polymers and polymeric nanocomposites, as well as the deposition onto the various sensors used. Both the polymeric materials and sensors were evaluated using the experimental test system and the results were examined using various methods of statistical analysis.

There are four results and discussion chapters. The results and discussion have been broken down into four parts: Sensing Material Analysis (Chapter 4), Sensors and Further Analysis (Chapter 5), Mechanistic Explanations (Chapter 6), and Selecting a Sensing Material (Chapter 7). This was done for ease of reading.

The fourth chapter covers the experimental results pertaining to the transdermal gas emission studies that were performed to determine the concentration of ethanol, and other interferents, emitted from a person's skin. This gave a basis for the concentrations used to evaluate the various sensing materials and sensors. In addition, this chapter contains the characterization results and sorption studies of all the polymeric sensing materials. This includes both ethanol and up to five other interferent gases (acetaldehyde, acetone, benzene, formaldehyde, and methanol), if the sensing materials were promising. Based on these results, the best sensing materials were then deposited onto various sensors and further evaluated.

The fifth chapter contains the experimental results pertaining to the evaluation of different sensor and sensing material combinations, as well as other comparisons including backbone and functional group analysis, and the reproducibility of the polymer synthesis. Two different types of sensors were evaluated, a microelectromechanical systems (MEMS) microcantilever mass-based sensor and a radio frequency identification (RFID) capacitive sensor. In addition, different backbones and functional groups were evaluated to determine if any trends could be observed. Finally, comparisons such as those between batches and operators were analyzed to confirm the reproducibility of the polymerization process as well as the reliability of the experimental test system.

The sixth chapter discusses the sensing mechanisms that occur when polymeric sensing materials and gas analytes, specifically VOCs, interact. These mechanisms are broken down into primary and secondary effects. In addition, this chapter includes the dominant mechanisms for different VOC classes, based on their functional groups.

The seventh chapter begins by looking at the requirements or constraints a target application may have. By combining this with the dominant sensing mechanisms of the target analyte, potential sensing materials can be efficiently identified. This idea was tested using various case studies, which ultimately led to practical prescriptions that can be followed when designing a new sensing material for a target analyte and application.

Finally, the eighth chapter contains the concluding remarks and main contributions to the field of sensors and sensing materials. The chapter also includes both short term and long term future goals.

Note that all of the references used in this thesis are listed in the Reference Section. The references are listed alphabetically by the first author's last name.

In addition, ten appendices are attached at the end of the thesis. These appendices provide extensive overview tables for VOCs emitted from a person (Appendix A), and sensing materials for VOCs (Appendix B and C). Additional information including typical chromatograms (Appendix D), experimental data (Appendix E), statistical analysis (Appendix F), polymeric and other material characterization data (Appendix G), and principal component analysis (Appendix H) are listed in the respective appendices. A table of potential polymeric sensing materials for ethanol has been compiled (Appendix I). Finally, some safety considerations are briefly cited in Appendix J.

## **2. Literature Background**

### **2.1 Volatile Organic Compound (VOC) Detection**

#### ***2.1.1 Gas Sensors***

It is important to detect toxic gas analytes in a variety of applications, including ethanol detection to prevent a person from driving while intoxicated (Winther-Jensen et al., 2014); acetone detection in disease diagnosis such as diabetes (Choi et al., 2013); and formaldehyde and benzene detection for indoor air quality (González-Chavarri et al., 2015). Therefore, highly sensitive and selective sensing materials are required.

#### ***2.2.2 Ethanol Sensors***

Driving under the influence of alcohol (ethanol) is a major problem and results in numerous casualties and deaths each year (Solomon et al., 2012). In addition, these crashes cost the economy billions of dollars every year (Sullivan, 2015). Therefore, reliable monitoring of blood alcohol content (BAC) is needed.

Currently, breathalyzers, which measure ethanol in the breath, are used; however, their frequency of use (typically sporadic spot checks) is limited. Ignition interlock systems are available, which do not allow a person to put the car into gear if a person's BAC is above a threshold value. These are only placed into vehicles by court order once a person has been convicted of driving under the influence of alcohol (Sullivan, 2015). Also, current interlock ignition systems are cumbersome and a distraction to the driver (Sawyer and Hancock, 2014).

Therefore, the goal is to create a reliable method of continuous or frequent monitoring of a person's BAC. A transdermal ethanol sensor mounted conveniently close to the driver would be less distracting to the driver and could autolock the vehicle's ignition or slow a vehicle to a stop when ethanol is detected from the driver.

### **2.2 Sensing Characteristics**

Sensors are evaluated based on their sensing characteristics. The desired sensing characteristics with which to evaluate different sensors are based on the target application. The two most important sensing characteristics are sensitivity and selectivity. These two characteristics dictate how low a concentration of an analyte can be detected (sensitivity) and how well only the target analyte is detected when other interferents are present (selectivity).

In addition, other sensing characteristics are also important, such as response and recovery times and operational temperature. The response and recovery times are the times required for the sensor to produce a response when exposed to a target analyte and the time it takes for the sensor to return back to its baseline after exposure (recover). The operational temperature is the temperature at which the sensor typically operates.

### 2.2.1 Sensitivity

Sensitivity is related to the lowest concentration detectable (limit of detection) by a sensor or sensing material. The lower the concentration a sensor can detect, the more sensitive that sensor is. The morphology of sensing materials affects sensing properties (see Figure 2.1). Singh et al. (2008) compared nanorods and nanoparticles made of ZnO as sensing materials for ethanol. It was found that the nanoparticles had higher sensitivity, which can be attributed to nanoparticles having a higher effective surface area (surface to volume ratio), and thus more available sensing (or active) sites for the ethanol to sorb to. Therefore, sensing materials with higher surface areas, and thus more sensing sites for analytes, have increased sensitivity (Nair and Alam, 2007).

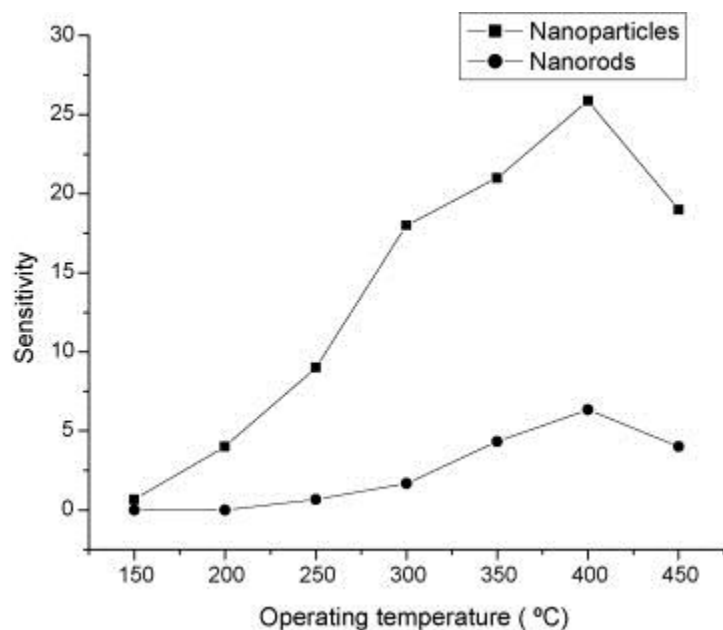


Figure 2.1: Comparison of ethanol sensitivity ( $R-R_0/R_0$ , where  $R$  is the response to ethanol and  $R_0$  is the response to air) of ZnO nanoparticles and nanorods (Singh et al., 2008).

The limit of detection (LoD), or detection limit, is the lowest signal that can be detected, which is not buried in the noise of the baseline, and is calculated from the signal-to-noise ratio. Generally, a signal-to-noise ratio of 3 is used to find the limit of detection, where the LoD is equal to 3 times the noise response, where the response corresponding to noise is converted to a concentration (see Equation 2.1). This ensures that the signal is not lost within the noise of the baseline exhibited by

the sensor; however, the signal may still be present and detectable (discernible) but is considered buried within the noise (see Figure 2.2).

$$\text{Detection Limit} = 3 \times [\text{Response}]_{\text{Noise}} \quad (\text{Equation 2.1})$$

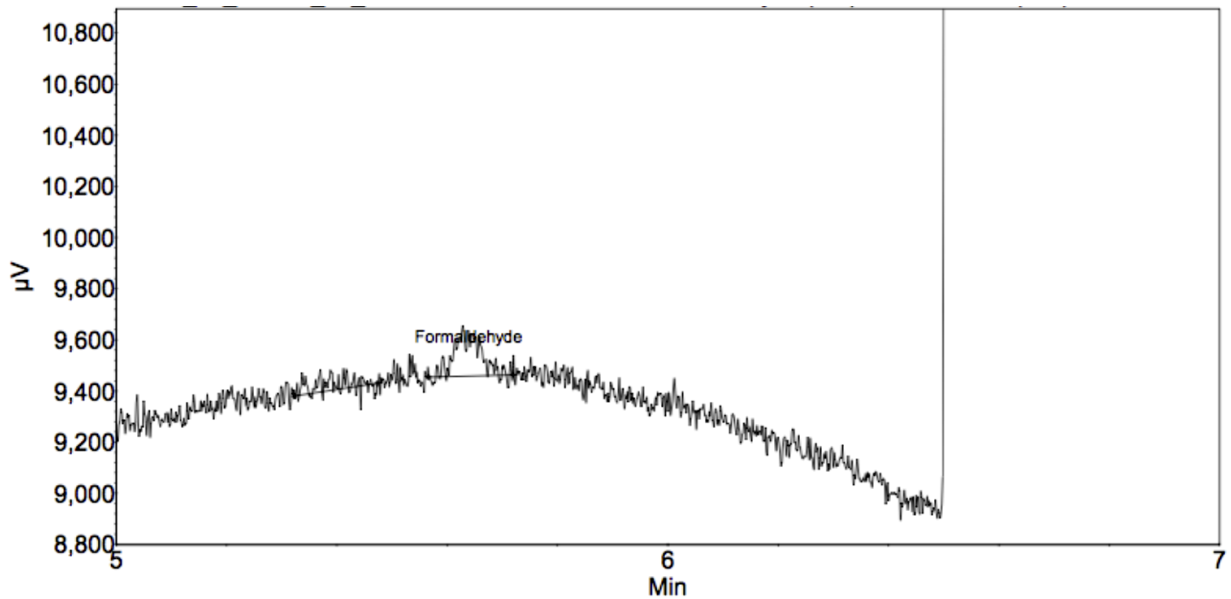


Figure 2.2: Chromatogram of 0.05 ppm formaldehyde.

Although Figure 2.2 shows a signal (response) that is discernible, the signal is considered buried within the noise of the baseline. The signal itself is only 2 times the noise and thus, considered buried within the noise.

### 2.2.2 Selectivity

Selectivity is a unitless measurement of how much the target analyte is favoured over interferent analytes. Ideally, the response from the target analyte should be much higher than the response from an interferent. Figure 2.3 shows a highly selective sensor for formaldehyde. At 250 ppm, formaldehyde produced a response that was five times greater than methanol did (Wang et al., 2009a).

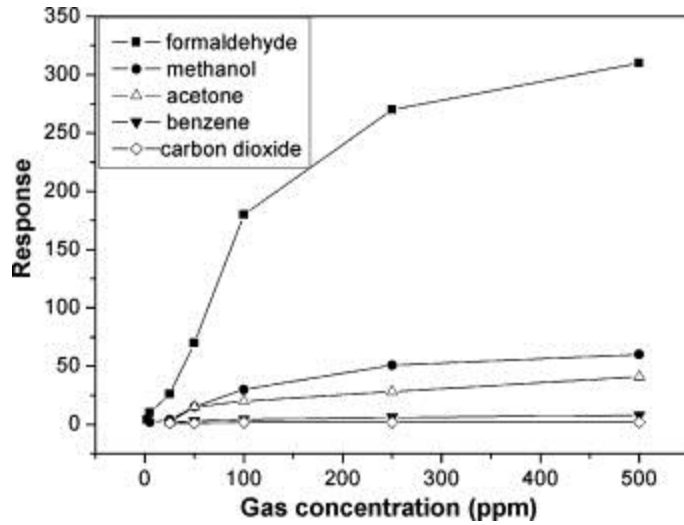


Figure 2.3: Selectivity of Ag doped  $In_2O_3$  gas sensor (Wang et al., 2009a).

Selectivity can be measured in two ways. Either the same concentration of two different gases is tested to determine the ratio of the magnitude of the two responses or the same response is measured for two gases at different concentrations. In both cases, the ratio between the two gases (response or concentration) is the selectivity (see Equations 2.2 and 2.3).

$$Selectivity = \frac{Target\ Analyte_{Sorbed}}{Interferent_{Sorbed}} \quad (Equation\ 2.2)$$

$$Selectivity = \frac{[Target\ Analyte]_{Tested}}{[Interferent]_{Tested}} \quad (Equation\ 2.3)$$

The larger the ratio between the target analyte and an interferent, the better the selectivity. It should be noted that a sensing material or sensor may be highly selective to some interferents but not to others.

### 2.2.3 Response and Recovery Times

Sensing (or response) time is the time needed to reach 90% of the maximum signal, whereas recovery time is the time the response takes to return within 10% of the original baseline (Virji et al., 2004). These times are not always mentioned in publications; however, estimates may be taken in some cases based on cited response graphs, such as Figure 2.4. Note that for the response shown in Figure 2.4, the response time was recorded by the authors as 3 seconds. If the response and recovery time were only shown by graphical representation, it would be impossible to tell that the response time was 3 seconds due to the timescale of the graph (Jia et al., 2014).

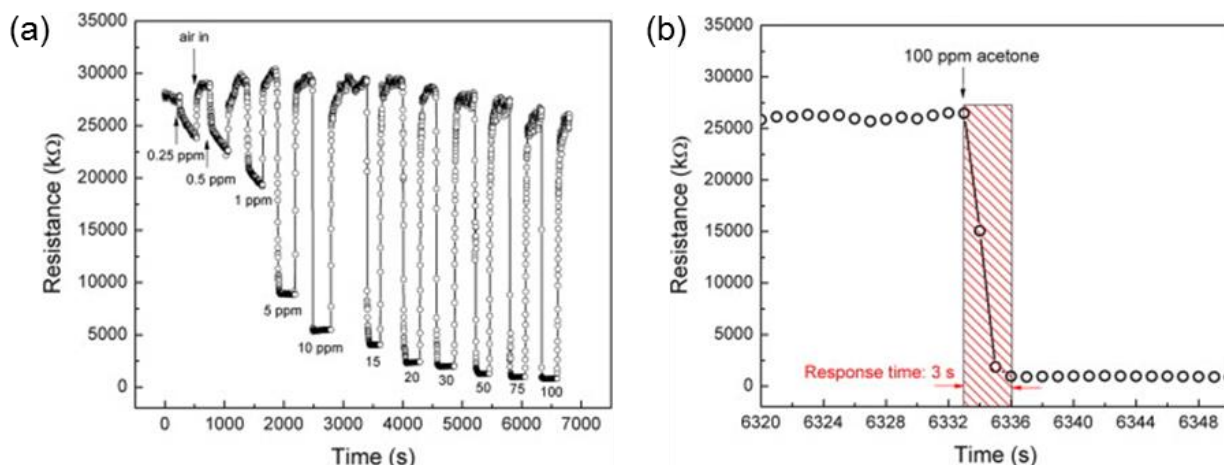


Figure 2.4: Response and recovery times of ZnO gas sensor for acetone at (a) multiple concentrations and (b) 100 ppm (Jia et al., 2014).

### 2.2.4 Operational Temperature

Operational temperature is the typical temperature at which the sensor operates while sensing. Different sensing materials work best at different temperatures for a given analyte. It is possible to change both the sensitivity and/or selectivity of a sensing material depending on the operational temperature (see Figure 2.5).

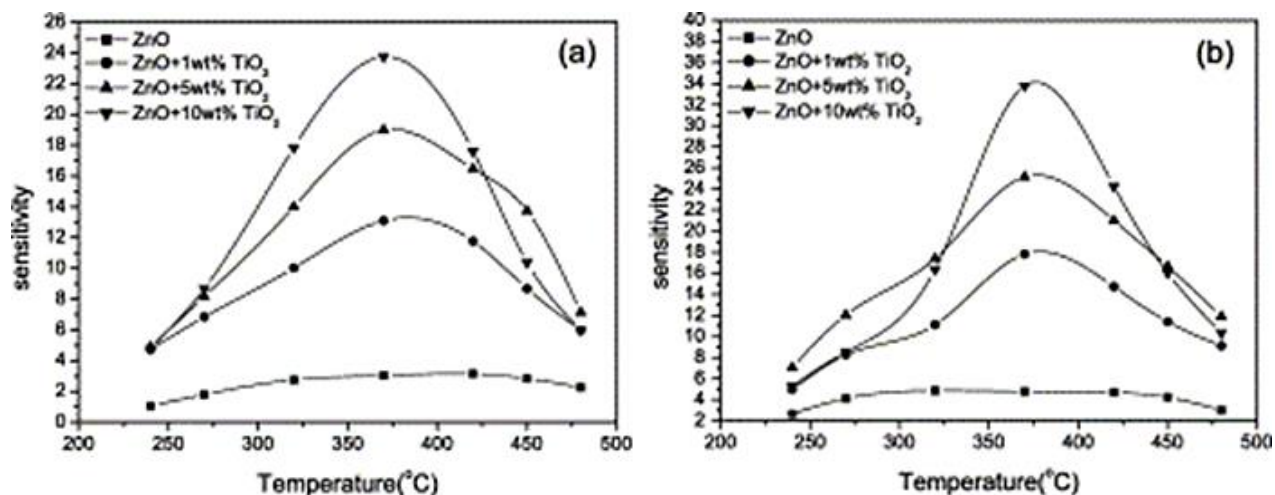


Figure 2.5: Sensitivity versus operational temperature for various doped ZnO sensing materials for (a) benzene and (b) toluene (Zhu et al., 2004).

Note that in Figure 2.5a, at 350°C, ZnO-10 wt. % TiO<sub>2</sub> has a higher sensitivity than ZnO-5 wt. % TiO<sub>2</sub>, but at 450°C, this is reversed. As well, at 325°C, the sensitivity of ZnO-10 wt. % TiO<sub>2</sub> is ~18 for benzene (Figure 2.5a) and ~16 for toluene (Figure 2.5b); however, at 375°C, the sensitivity of ZnO-10 wt. % TiO<sub>2</sub> is ~24 for benzene (Figure 2.5a) and ~34 for toluene (Figure 2.5b).



Therefore, in some cases, it is even possible to change which analyte a sensing material is more selective towards based on operational temperature (Zhu et al., 2004).

The majority of metal and metal oxide sensors operate at these high temperatures; however, not all applications require sensors that operate at such high temperatures. If the application is to detect a gas analyte at room temperature, then sensing materials that are able to detect at room temperature are better than sensing materials that detect at much higher temperatures since the latter require a heater (Sun et al., 2012).

### 2.3 Transdermal Ethanol

Humans emit a multitude of volatile organic compounds (VOCs), which vary with age, sex, diet, state of health, genetic background, environmental exposure, climatic conditions, and medication (Shirasu and Touhara, 2011, Acevedo et al., 2007, and Ruzsanyi et al., 2012). Appendix A lists a selection of chemical compounds that have been identified in blood, in breath and emitted from the skin of human beings with their possible concentrations, when available, and literature sources for each particular piece of information. VOCs enter the body through inhalation and transdermal sorption or they are the result of metabolic pathways. After entering the blood stream, these VOCs are transported through the body for final removal. The body removes unwanted VOCs through breath, sweat, skin, and urine (and other bodily secretions). Some VOCs are also produced from the metabolism of symbiotic bacteria that live on the skin (Shirasu and Touhara, 2011), as well as residues that are left on the skin from various substances such as soaps, deodorants, colognes, perfumes, lotions, and tobacco smoke (Soini et al., 2006).

Soini et al. (2006) sampled the inner arm of five volunteers and detected around 400 compounds using a gas chromatograph/mass spectrometer (GC/MS). Of those 400 compounds, approximately 100 compounds could be identified. These compounds included aldehydes, ketones, fatty acids, and alcohols. It should be noted that there was a large variation between the individuals studied; however, the results from a single person were repeatable (Ruzsanyi et al., 2012) (see Table 2.1).

Table 2.1: Mean Concentration of Compounds from Three Different Volunteers

Compound	Mean Concentration Detected from GC/MS (ppb)		
	Volunteer 5	Volunteer 6	Volunteer 7
Benzaldehyde	0	10.1	3.8
6-methyl-5-hepten-2-one	5.2	2	11.5
Octanal	5.3	0	11.4

(Ruzsanyi et al., 2012)

A larger study conducted by Mochalski et al. (2014), with 60 participants, also noted an abundance of aldehyde and ketones emitted from the skin. In addition, there was a large variance in the amount of analyte emitted (see Figure 2.6). The emission rates ( $\text{fmol cm}^{-2} \text{min}^{-1}$ ) were calculated as a normalized flux observed. Figure 2.6 shows many gas analytes, colour coded by compound classes, and the broad range of emission rates at which these compounds were emitted. Note, however, that the majority of these emission rates translate to the ppb range and thus would not likely produce a response for a sensor designed to detect ethanol in the ppm range.

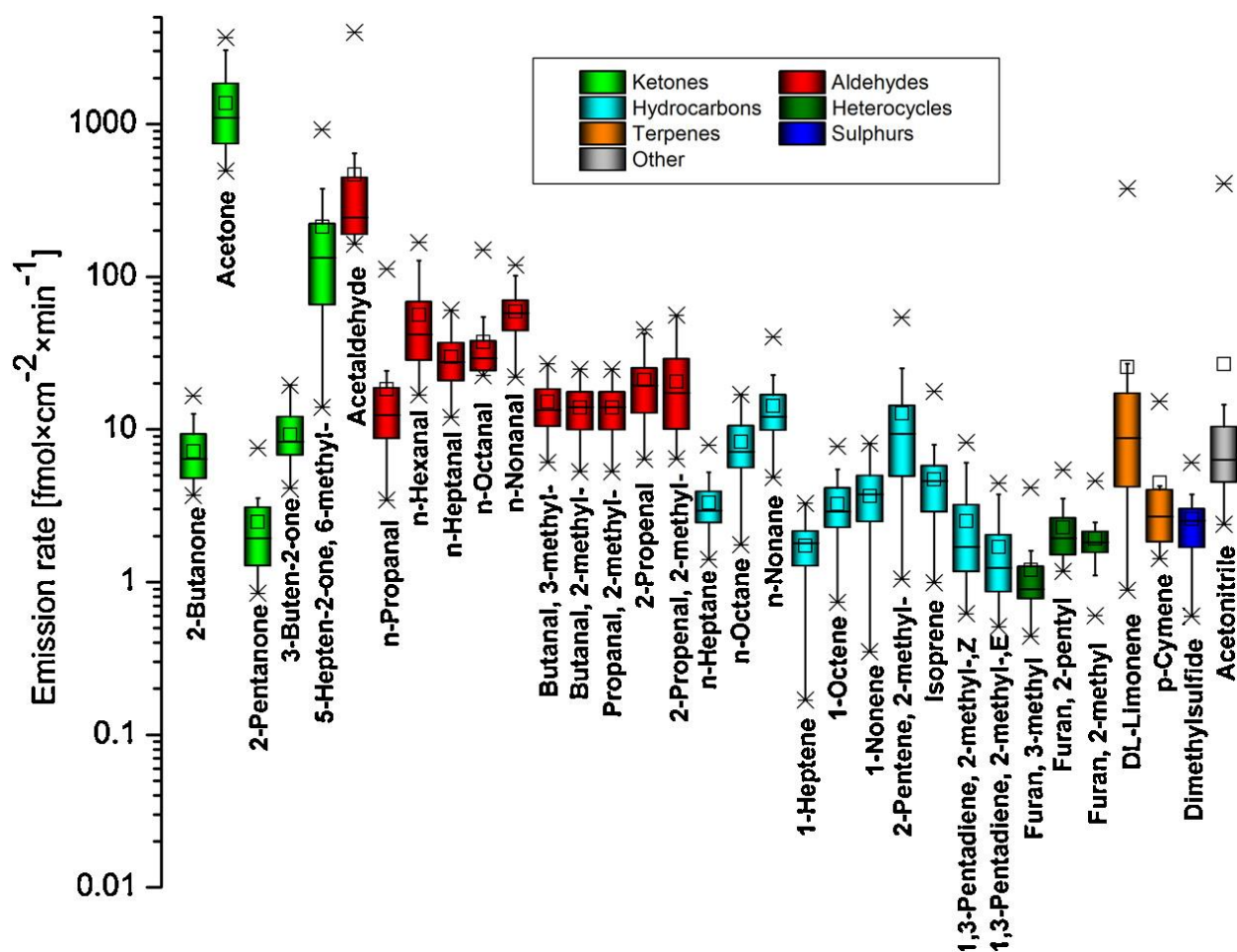


Figure 2.6: Emission rate of gas analytes emitted from the skin. Note the compounds (analytes) are colour coded by compound class (Mochalski et al., 2014).

## 2.4 Sensing Materials

The sensing material is the ‘heart’ of the sensor, since it is the material that interacts with the target gas (e.g. ethanol) through “sorption” (adsorption and/or absorption). Adsorption is defined as a gas sticking to the surface of the sensing material, whereas absorption is defined as a gas entering (diffusing) into the interstitial spaces between the sensing material layers (see Figure 2.7).

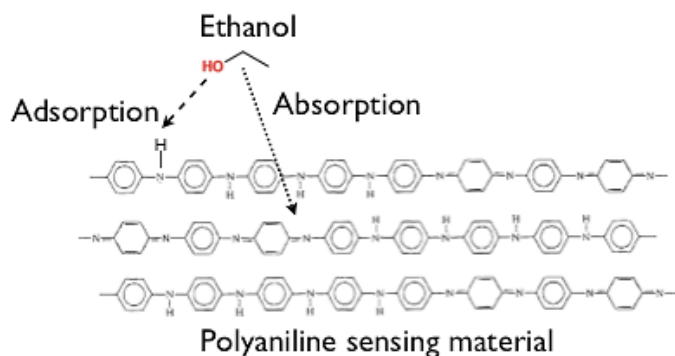


Figure 2.7: Adsorption and absorption of ethanol.

By just changing the sensor material the same sensor is able to detect different analytes. Many different materials can be used as sensing materials to target specific analytes. The two main classes of sensing materials, currently used, are polymers and metals and metal oxides. In addition, these sensing materials can be doped by adding a small amount of a desired compound (essentially an impurity), which can significantly change some of the sensing materials' properties. Due to the extent with which sensing materials can be combined and modified, there are a near endless number of compounds that can be used as sensing materials to target specific analytes.

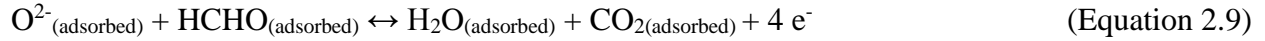
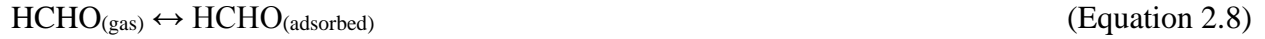
#### 2.4.1 Polymeric Materials

Polymeric sensing materials are ideal because they can be tailor-made to attract a specific gas and thus, can have high selectivity (Talwar et al., 2014). This can be done by adding one or more side chains, a dopant (small amount of another material such as a metal oxide), or creating a copolymer (Rochat and Swager, 2013). Polymeric sensors work mainly at low temperatures (below 100°C) and are relatively inexpensive (Mabrook and Hawkins, 2001).

Polymers are generally used in the form of thin films because thin films have a high surface area to volume ratio. Since analytes are more likely to interact with active (or sorption) sites on the surface of a sensing material, a higher surface to volume ratio provides more readily available sensing sites for the target gas. These thin films can be used in a variety of sensor types including resistive sensors, mechanical sensors, and optical sensors (Fink, 2012).

#### 2.4.2 Metals and Metal Oxides

Metal and metal oxide sensing materials are widely used in resistive type sensors due to their high thermal and mechanical stability, ease of processability, and low cost (Sun et al., 2012). The catalytic nature of both metals and metal oxides is exploited, such as the oxidation of formaldehyde (see Equations 2.4 – 2.9). A similar mechanism occurs for the oxidation of any small organic molecule (Wang et al., 2009b).



This process is a redox reaction. The oxidation utilizes the partial pressure of oxygen in the atmosphere. Small amounts of other metals and metal oxides can be added to the sensing material to increase the amount of adsorbed oxygen on the surface, thereby improving the sensitivity of the sensor. As the oxidation takes place, electrons ( $e^-$ ) are created that reduce the resistance of the sensor, which is monitored (Lee et al., 2006).

### **2.4.3 Dopants**

A dopant is usually a small amount of a desired additive used to improve the properties of a material. In sensing materials, dopants are generally used to improve the sensitivity and/or selectivity, although they can also be used to improve other properties such as thermal or chemical stability or electrical conductivity. Compounds used as dopants include metals and metal oxides, acids, and surfactants (Talwar et al., 2014).

The addition of metal and metal oxide dopants to polymeric sensing materials generally improves the thermal and mechanical properties of the polymers (Chen et al., 2009). Metal and metal oxide dopants can also increase the electrical conductivity of conductive polymers (Dirksen et al., 2001).

The catalytic nature of metals and metal oxides, in small amounts, can be used to improve the sensing properties. When a dopant coordinates with a polymer, a conformational change occurs, which can result in larger interstitial spaces and less order amongst the polymer chains (Han et al., 2006). If too much of a dopant is added, the polymer chains become too disordered and/or the chains are pushed too far apart, which can result in a decrease of sensitivity and selectivity. This can also negatively affect other properties, such as mechanical stability (Arsuaga et al., 2013).

Any compound can be used as a dopant. For example, acids are added to polyaniline (PANI) to make it conductive. PANI is unique in that it is nonconductive unless it has been doped. The addition of protons to PANI creates positively charged nitrogen ( $\text{N}^+$ ) atoms, creating holes along

the polymer chain (see Figure 2.8). These holes allow valence electrons to travel along the polymer chain by jumping from one hole to another, thereby making PANI conductive (Kukla et al., 1996).

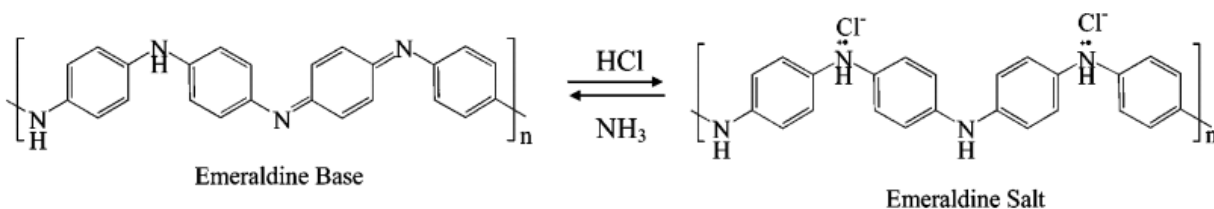


Figure 2.8: Schematic of PANI-acid doping mechanism (Virji et al., 2004). Note that this figure shows HCl as the acid, but the mechanism can be extended to all other acids.

#### 2.4.4 Polymeric Nanocomposites

Polymeric nanocomposites (polymers doped with metal and metal oxide nanoparticles) are ideal sensing materials because they can be tailored towards specific target analytes (Pandey and Thostenson, 2012). In addition, polymeric nanocomposites can have improved sensitivity and selectivity (Vaddiraju and Gleason, 2010) towards specific analytes and operate at room temperature (Zhan et al., 2013). The addition of metal oxide nanoparticles into a polymer can also improve the material's mechanical and electrical properties (Nehete et al., 2012).

#### 2.4.5 Sensing Materials for Volatile Organic Compounds (VOCs)

Many sensors and sensing materials have been developed for a variety of volatile organic compounds (VOCs). These sensing materials include both metal oxide-based sensing materials and polymeric-based sensing materials. In both cases, dopants were sometimes added to improve the sensing characteristics of the sensing materials. Appendix B includes multiple tables of sensing materials for various VOCs.

The tables of sensing materials in Appendix B are divided by the target gas analyte. These tables include the sensing materials and dopants (if used), as well as the detection limit, operational temperature, and response and recovery times. If an entry in the table is missing, it is because the author(s) did not include the specific information in their paper. Given that this thesis focuses on sensing materials for ethanol, Appendix C contains selectivity data presented in the literature.

### 2.5 Types of Sensors

There are many different types of sensors onto which a sensing material can be placed. Each type of sensor has its own advantages and disadvantages. In addition, some types of sensors have constraints on the type of sensing material that can be used.

It should be noted that the type of sensor, not just the sensing material, can also affect the sensitivity of a sensor. Shen et al. (2012) tested the same sensing material on three different sensor types (see Figure 2.9). Sensor A was an indirect heated sensor; Sensor B was a microsensor with interdigitated fingers; and Sensor C was a plane sensor with a large sensing area. All three sensors exhibited the same trend over the temperature range tested; however, sensor C produced the largest response. The larger surface area created more active sites for the analyte, thereby increasing sensor sensitivity.

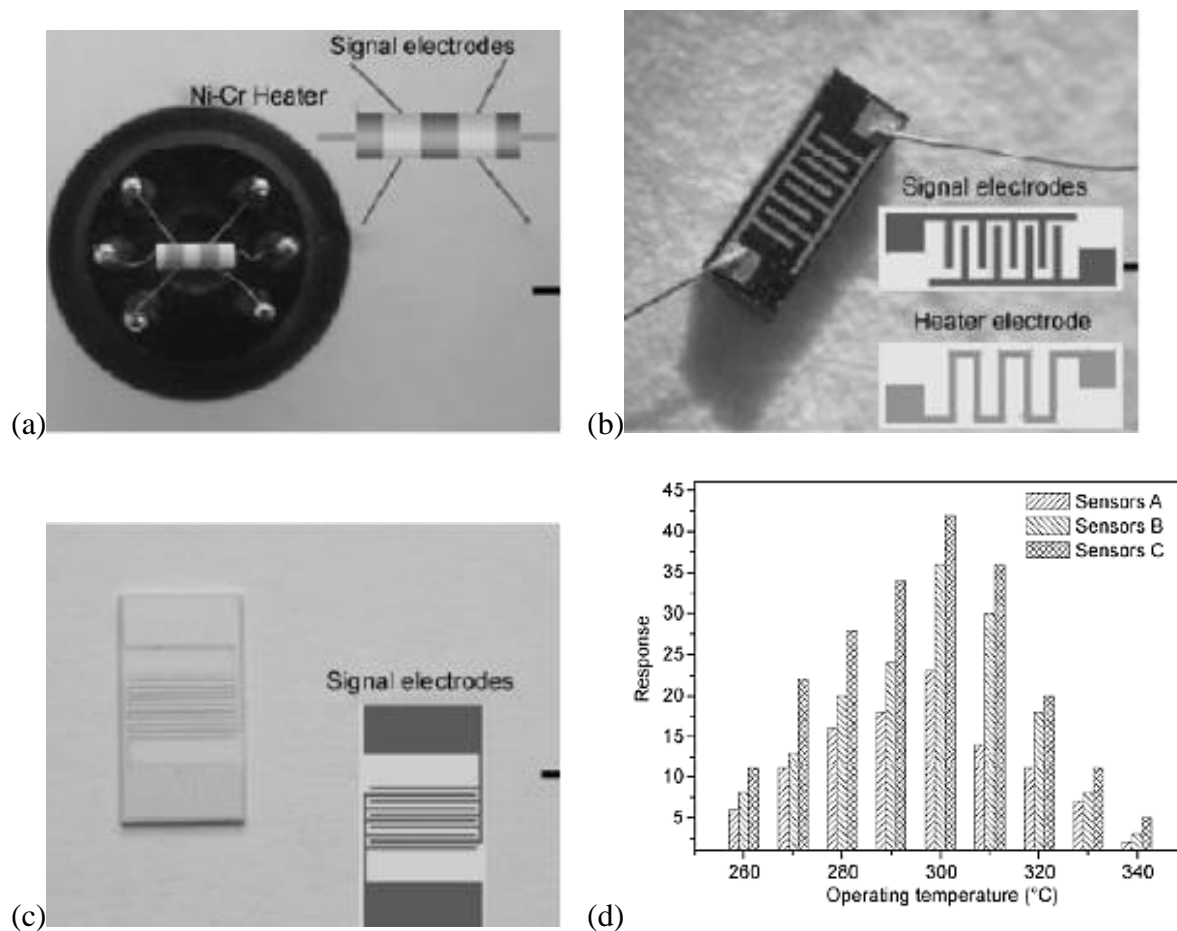


Figure 2.9: (a) Sensor A, (b) Sensor B, (c) Sensor C, and (d) response of all three sensors to 100 ppm of ethanol at different temperatures (Shen et al., 2012).

### 2.5.1 Resistive Sensors

Conductive sensing materials are needed in resistive type sensors where the conductivity is exploited. The sensing materials become chemiresistors in the circuit and the resistivity of the sensing material is measured. The change in resistivity caused by the adsorption or absorption of a target analyte onto the sensing material is then detected/monitored (Agbor et al., 1995).

Resistive sensors have many advantages including low power, low cost, and fast response times (Righettoni et al., 2015). Traditionally, metals and metal oxides were used as sensing materials in resistive type sensors; however, conducting polymeric materials can also be used in resistive sensors (Nicolas-Debarnot and Poncin-Epaillard, 2003). Conducting polymers have some advantages in resistive sensors including high sensitivity and selectivity and low operating temperatures, near room temperature (Chiang et al., 2013).

### 2.5.2 Capacitive Sensors

Capacitance is the charge-storing ability of a capacitor and is defined as the amount of charge stored on one plate divided by the applied voltage (Callister, 2005). Capacitive sensors usually work in two ways. Either the swelling of the sensing material when a target analyte is absorbed causes the capacitance to change, or a change in dielectric permittivity is caused by the adsorption of the target analyte to the sensing material, which subsequently results in a change in capacitance (Mlsna et al., 2006; Pich et al., 2004).

Capacitive sensors can have a variety of structures in which a capacitor is formed. For example a sensor may consist of parallel plates (Mlsna et al., 2006) or interdigitated fingers (Chen et al., 2013). In both cases, the sensing material is deposited between the capacitor elements (plates or fingers) and a change in dielectric constant or swelling of the sensing material produces a response.

Chen et al. (2015b) designed a capacitive sensor that operated in the radio frequency (RF) range. By using RFs, the electronic field (E-field) distribution was narrowed as it passed across the capacitor (see Figure 2.10). This narrow distribution allowed more field lines to pass through the sensing material, thereby increasing the sensitivity of the sensor.

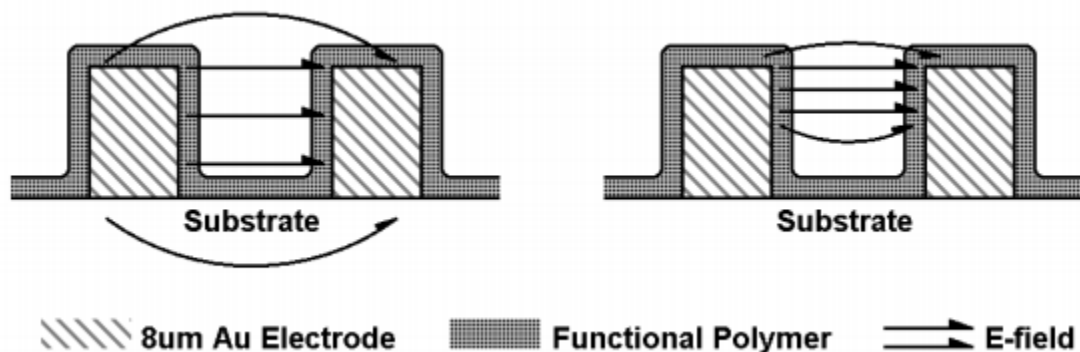


Figure 2.10: E-field distribution across a capacitor using low frequencies (left) and RF frequencies (right) (Chen et al., 2015b).

### 2.5.3 Mass-based Sensors

Mass-based sensors measure a change in mass that occurs when an analyte sorbs onto the sensing material of a sensor. Commonly used mass-based sensors are quartz crystal microbalances (QCMs). QCMs exploit the piezoelectric properties of quartz that convert mechanical energy into electrical energy. A QCM with a sensing material vibrates at an initial frequency. When an analyte sorbs onto the sensing material, mass is added and the frequency at which the QCM vibrates shifts. This shift in frequency is measured and can be calibrated to the amount of mass added and thus, the concentration of the analyte (Nguyen et al., 2011). The more mass (and thus analyte) sorbed, the greater the frequency shift (Chen et al., 1997).

Another type of mass-based sensor is the microelectromechanical systems (MEMS) microcantilever that is displaced when a gas sorbs onto the sensing material (see Figure 2.11). This displacement produces an electrical signal that represents the sensor's response to the gas sorbed. These sensors can be calibrated such that the response from the displacement of the microcantilever can be used to determine the concentration of the gas that sorbed. The sensing material is chosen for a target analyte, but cannot weigh too much (causing the microcantilever to stick to its housing); otherwise the sensor is rendered useless (Khater et al., 2009).

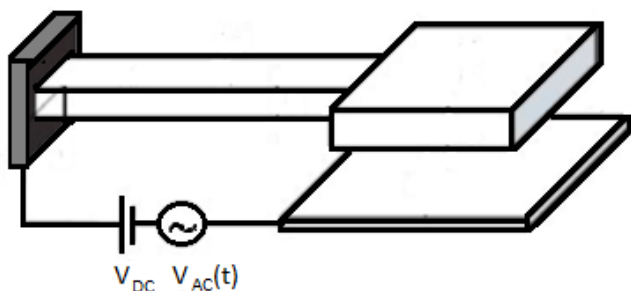


Figure 2.11: Schematic of microcantilever sensor (Khater et al., 2009).

### 2.5.4 Optical and Spectroscopic Sensors

Optical sensors or spectroscopic techniques use part of the electromagnetic spectrum (specific wavelengths) to identify a target analyte. A light (such as a laser or LED) is shone on the sensing material (and sorbed analyte), then deflected to a detector, which measures the intensity of the light across a range of wavelengths. When the light reaches a compound, different bonds (at specific bond energies) absorb at specific wavelengths. This results in characteristic peaks for different analytes (Mondin et al., 2014). By selecting a small number of peaks characteristic to a target analyte (typically one to three), a target analyte can be identified. In addition, the intensity of the wavelengths can be used to determine the concentration of analyte present (Tavoli and Alizadeh, 2013). Note that it is important that the sensing material not absorb in that range of light (Yebo et al., 2010).



### 2.5.5 Sensor Arrays and Electronic Noses

Electronic noses are designed to mimic the mammalian nose and combine multiple partially selective sensing materials (mimicking the nose) with a sophisticated software and reference database (mimicking the brain). Electronic noses are generally non-specific sensors used to identify multiple gas components simultaneously (see Figure 2.12). When gases interact with the partially selective sensing materials, the data obtained are analyzed using multivariate (pattern recognition) statistical techniques such as principal component analysis (PCA). This analysis produces a response pattern that is compared to the database for identification. The larger the reference database, the better the electronic nose (De Wit et al., 1998; Beltrán et al., 2006).

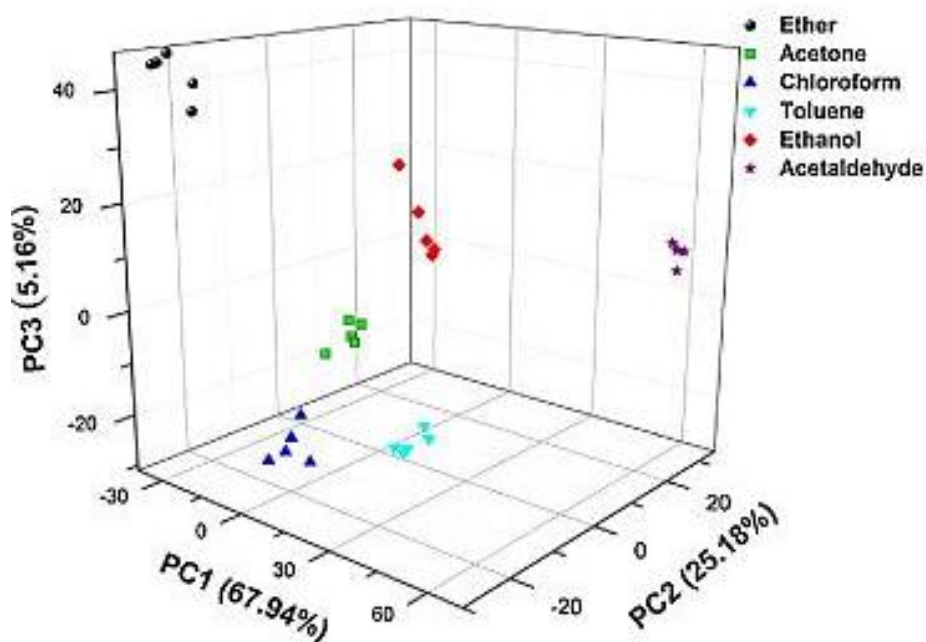


Figure 2.12: Three dimensional PCA plot for six different VOCs (Li et al., 2013a).

### 2.5.6 Other Sensors

The sensors discussed in the previous sections are the most commonly used; however, there are other types of sensors in use. Other types of sensors include biosensors and chemical reaction-based sensors.

Biosensors use some form of biological agent, such as enzymes or antibodies, as their sensing material (Mitsubayashi et al., 1994). Biosensors have high selectivity; however, they have a very short shelf-life (usually only a few days) because the biological agents require controlled environments to survive (Putzbach and Ronkainen, 2013). These controlled environments are liquid in nature and therefore, the target gas must first dissolve into the liquid before it can be tested (Mitsubayashi and Hashimoto, 2002).

Reaction-based sensing materials produce a response when the analyte chemically binds to the sensing material. This reaction is typically not reversible and thus, the sensing materials are not reusable. This results in consumable sensing materials, such as filters that are replaced for each test (Kawamura et al., 2005). Many of these reaction-based sensors are colourimetric in nature, with the reaction occurring between the analyte and a dye (Meng et al., 2014).

## 2.6 Sensing Materials and Sensors for Ethanol

### 2.6.1 Polymeric Sensing Materials

#### 2.6.1.1 Polyaniline (PANI)

Polyaniline (PANI) (see Figure 2.13) is a widely used sensing material for resistive type sensors due to its conductivity; however, polyaniline may also be non-conductive, as in its basic form (Kukla et al., 1996). This widens the types of potential sensors onto which PANI can be used. PANI, like other polymeric sensing materials, has the advantage of sensing at room temperature or other low temperatures (below 100°C). In addition, PANI can be doped with different acids and/or metal oxides to improve the sensing properties (Virji et al., 2004).

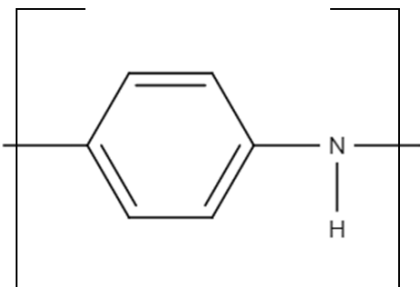


Figure 2.13: Chemical structure of polyaniline (PANI).

PANI has been used as a sensing material for ethanol in multiple sensors (see Table 2.2). Ethanol is able to bind to PANI through hydrogen bonding (see Chapter 6). When the OH group of ethanol hydrogen bonds to the NH of PANI, a conformation change of PANI results, which increases the resistance of the sensing material, which is then measured in a resistive type sensor (Choudhury, 2009).

Table 2.2: Summary of Sensing Characteristics for Various PANI Sensors for Ethanol

Dopant	Detection Limit	Selectivity	Operational Temperature	Response/Recovery Time	Reference
Ag 2.5 mol %	100 ppm	-	Room Temperature	102 seconds/ 20 minutes	Choudhury (2009)
NiO 10 wt. %	1 ppm	Benzene (6.2) Methanol (1.2) Formaldehyde (1.1)	21°C	-	Stewart et al. (2012)
Dinonyl- naphthalene- sulfonic acid	764 ppm	-	Room Temperature	5 minutes/ 2 minutes	Svetlicic et al. (1998)
TiO <sub>2</sub> 10 wt. %	150 ppm	Acetaldehyde (1.8) Formaldehyde (1.3)	-	58 seconds/ 300 seconds	Zheng et al. (2008)

In Table 2.2, and in the tables to follow in Chapter 2, a summary of sensing characteristics are shown. The two most important characteristics are the detection limit and selectivity. The detection limit recorded in the tables is either the lower measured concentration or the detection limit calculated by the authors from the noise measured. The selectivity is the ratio between the response of the target analyte ethanol and the response from an interferent. The higher the ratio, the more selective the sensor and sensing material are to ethanol. In Table 2.2, the interferents are listed followed by the selectivity in brackets. For example, for PANI doped with 10 wt. % NiO (second entry in Table 2.2) with benzene as the interferent, the selectivity is 6.2. This means that PANI 10 wt. % NiO is 6.2 times more sensitive to ethanol than to benzene (i.e. ethanol produced a response 6.2 times larger than benzene).

#### 2.6.1.2 Poly (*o*-anisidine) (PoANI)

Poly (*o*-anisidine) (PoANI), also known as poly (methoxyaniline), is both chemically and environmentally stable, conductive, and more readily processable than polyaniline due to its greater solubility (Valentini et al., 2004); see Figure 2.14. Note that PoANI is soluble in ethanol (Rawat et al., 2015). The processability of PoANI is also increased due to the decreased rigidity of the polymer chains (Wang et al., 2012). Torsion is created along the chain due to the steric repulsion between hydrogen and the methoxy group. This steric repulsion, or hindrance, reduces the chains' crystallinity (Gupta and Umare, 1992). Despite the reduction in crystallinity, PoANI's

thermal and chemical stability and processability are why it is still used as a sensing material (see Table 2.3).

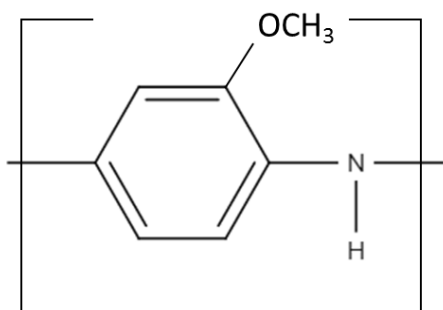


Figure 2.14: Chemical Structure of PoANI.

Table 2.3: Summary of Sensing Characteristics for Various PoANI Sensors for Ethanol

Dopant/ Copolymer	Detection Limit	Selectivity	Operational Temperature	Response/ Recovery Times	Reference
None	3000 ppm	Propanol (2.0) Butanol (1.9) <sup>1</sup>	Room Temperature	1 minute/ 4 minutes	Athawale and Kulkarni (2000)
Polystyrene	3850 ppm	Water (2.1)	25°C	30 minutes/ 30 minutes	Aussawasathien et al. (2011)
Silver- Multiwall Carbon Nanotubes	0.1 μM <sup>2</sup>	<i>n</i> -hexane (5.6) Dichloro- methane (3.8) Acetaldehyde (2.0) Methanol (1.3) Acetone (1.1) <sup>3</sup>	-	10 seconds/ Not given	Rahman et al. (2015)

<sup>1</sup>Note that PoANI was more selective to methanol than ethanol.

<sup>2</sup>In solution, with phosphate buffer.

<sup>3</sup>More selective to tetrahydrofuran, pyridine, phenol, and 3-methoxyphenol.

### 2.6.1.3 Poly (2,5-dimethyl aniline) (P25DMA)

Poly (2,5-dimethyl aniline) (P25DMA) (see Figure 2.15) has many of the same desirable sensing material traits as PANI; however, P25DMA is more processable than PANI since its chains are

not packed as closely. The steric hindrance produced by the two methyl groups reduces the ability of the polymer to pack closely, which thereby increases the size of the interstitial spaces in the polymer. This improves its sensitivity, by allowing easier access to more active sites. P25DMA is less stable when doped with an acid since the chain has a restricted ability to make conformational changes caused by steric hindrance (Bavastrello et al., 2004).

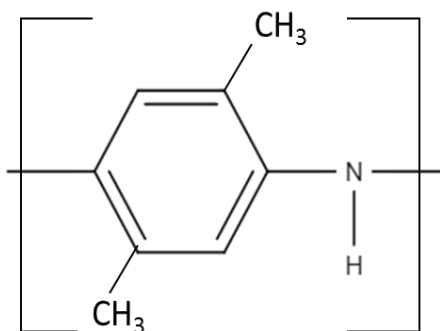


Figure 2.15: Chemical Structure of P25DMA.

P25DMA had previously only been used as a sensing material for ethanol in one instance, where Athawale and Kulkarni (2000) evaluated PANI and many of its derivatives as sensing materials for aliphatic alcohols. P25DMA had the highest selectivity towards ethanol with respect to larger alcohols; however, P25DMA was more selective to methanol than ethanol (see Table 2.4). Note that ethanol was used as an interferent for P25DMA intercalated with MoO<sub>3</sub> where the target analyte was formaldehyde (Itoh et al., 2007a). Ethanol showed very little response when P25DMA was used intercalated with MoO<sub>3</sub>, and this was likely due to MoO<sub>3</sub>'s poor affinity to ethanol. Other polymers (such as polyaniline (Itoh et al., 2008), poly (*o*-anisidine) (Itoh et al., 2008), poly (*N*-methylaniline) (Itoh et al., 2007c), and polypyrrole (Hosono et al., 2005) intercalated with MoO<sub>3</sub> proved to be good sensing materials for aldehydes. This suggests that the affinity and selectivity for aldehydes were due to the MoO<sub>3</sub> and not the polymers used.

Table 2.4: Summary of Sensing Characteristics for Various P25DMA Sensors for Ethanol

Dopant/ Copolymer	Detection Limit	Selectivity	Operational Temperature	Response/ Recovery Times	Reference
None	-	3.6 <sup>1</sup>	Room Temperature	1 minute/ 4 minutes	Athawale and Kulkarni (2000)

<sup>1</sup>Towards larger alcohols; however, methanol produced a stronger signal.

## 2.6.2 Metal Oxide Sensing Materials and Dopants

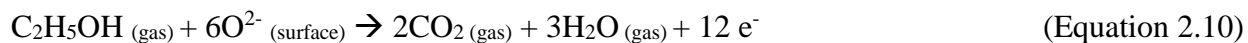
### 2.6.2.1 Aluminum Oxide ( $Al_2O_3$ )

Aluminum oxide ( $Al_2O_3$ ) is typically used as a dopant in other sensing materials such as ZnO (Ruchika et al., 2016) and graphene (Jiang et al., 2011), although  $Al_2O_3$  has been used doped with dysprosium ( $Dy^{3+}$ ) (Okabayashi et al., 2000). Table 2.5 lists a variety of sensors in which  $Al_2O_3$  was employed for the detection of ethanol.

Table 2.5: Summary of Sensing Characteristics for Various  $Al_2O_3$  Sensors

Material	Dopant	Detection Limit	Selectivity	Operational Temperature	Sensing/ Recovery Time	Reference
$\gamma$ - $Al_2O_3$	$Dy^{3+}$ (1 mol %)	500 ppm	-	450 °C	-	Okabayashi et al. (2000)
Graphene	$Al_2O_3$	1225 ppm	-	200 °C	10/ 100 seconds	Jiang et al. (2011)
ZnO	$Al_2O_3$ (1 wt. %)	400 ppm	-	300 °C	6 / 20 seconds	Ruchika et al. (2016)
ZnO	$Al_2O_3$ (1 wt. %)	500 ppm	Carbon Monoxide (34.5) Ammonia (12.0) Hydrogen Gas (90.1) LPG (6.1) Hydrogen Gas (2.9)	400 °C	10 / 40 seconds	Deore and Jain (2014)
ZnO	$Al_2O_3$ (1 wt. %)	100 ppm	Carbon Dioxide (5.1) Ammonia (6.4) Chlorine Gas (15.1)	300 °C	18 / 40 seconds	Patil et al. (2007)
ZnO	$Al_2O_3$ (2 at. %)	1000 ppm	-	290 °C	8 / 10 seconds	Yang et al. (2009b)

When ethanol interacts with Al<sub>2</sub>O<sub>3</sub>, ethanol is catalytically decomposed into formaldehyde, resulting in some type of response detectable by the sensor (Okabayashi et al., 2000). For a resistive type sensor, this catalytic activity produces electrons (see Equation 2.10), which results in an increase in conductivity on the sensor (Patil et al., 2007).



The addition of a small amount of Al<sub>2</sub>O<sub>3</sub> to ZnO improved the sensitivity to ethanol. Yang et al. (2009b) found that an optimal amount of Al<sub>2</sub>O<sub>3</sub> was 2 at. % and increasing the amount of Al<sub>2</sub>O<sub>3</sub> further resulted in a poorer response (sensitivity) than ZnO alone (see Figure 2.16).

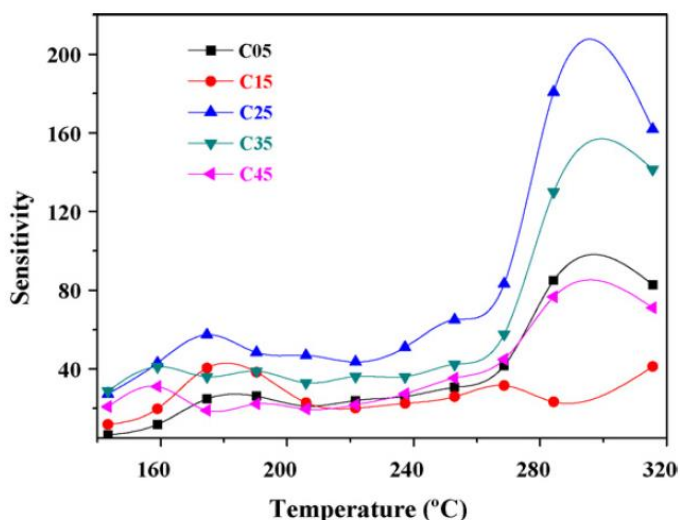


Figure 2.16: Sensitivity to ethanol versus temperature for ZnO doped with 0 atomic (at.) % (C05), 1 at. % (C15), 2 at. % (C25), 3 at. % (C35), and 4 at. % (C45) (Yang et al., 2009b).

#### 2.6.2.2 Copper Oxide (CuO)

Copper oxide (CuO) has been used as a sensing material for ethanol since it is catalytically active towards ethanol (Zhou et al., 2006). In addition, cuprous oxide (Cu<sub>2</sub>O) has also been used as a sensing material for ethanol (see Table 2.6).

Table 2.6: Summary of Sensing Characteristics for Various CuO Sensors

Material	Dopant	Detection Limit	Selectivity	Operational Temperature	Sensing/ Recovery Time	Reference
CuO	-	100 ppm	-	240 °C	110 / 120 seconds	Raksa et al. (2009)
CuO	Pt	5 ppm	* <sup>1</sup>	200 °C	4 / 7 seconds	Gou et al. (2008)
CuO	Au	5 ppm	* <sup>1</sup>	200 °C	4 / 7 seconds	Gou et al. (2008)
Cu <sub>2</sub> O	-	10 ppm	Acetone (1.1)	200 °C	170 / 180 seconds	Barreca et al. (2009)
Cu <sub>2</sub> O	-	10 ppm	-	210 °C	15 / - seconds	Zhang et al. (2006)

<sup>1</sup>More sensitive to formaldehyde than ethanol

Cuprous oxide (Cu<sub>2</sub>O) and copper oxide (CuO) were compared as sensing materials for ethanol. Barreca et al. (2009) found that while the CuO produced a larger response to ethanol, Cu<sub>2</sub>O was slightly more selective towards ethanol with respect to acetone. Zhang et al. (2006) found that Cu<sub>2</sub>O was more sensitive to ethanol than CuO. It should be noted that the morphology and structure were different for these comparisons.

Various morphologies have been used including nanowires (Raksa et al., 2009), nanospheres (Zhang et al., 2006), nanoribbons (Gou et al., 2008), and nanoplates (Gou et al., 2008). Gou et al. (2008) evaluated the effect of morphology on the response of CuO to ethanol and found that the nanoribbons were much more responsive (i.e. sensitive) to ethanol than the nanoplates.

CuO has also been doped to improve its sensing properties towards ethanol. CuO doped with Pt was shown to be more sensitive (produced a larger response to the same concentration) to ethanol than CuO doped with Au; however, both of these sensing materials produced a larger response when exposed to formaldehyde than to ethanol (Gou et al., 2008).

### 2.6.2.3 Nickel Oxide (NiO)

NiO has been used as both the sensing material and dopant in a variety of ethanol sensors (see Table 2.7). Although many metal oxide sensors operate at high temperatures (above 100°C), NiO is able to detect ethanol at room temperature (Li, 2016). This demonstrates that despite the need to operate at high temperatures for catalytic activity, NiO is able to sense at both high and low temperatures.



Table 2.7: Summary of Sensing Characteristics for Various NiO Sensors

Material	Dopant	Detection Limit	Selectivity	Oper. Temp.	Sensing/ Recovery Time	Reference
NiO	-	5 ppm	Acetone (1.5) Carbon Monoxide (3) <sup>1</sup>	300 °C	-	Kaur et al. (2016)
NiO	-	10 ppm	-	Room Temp.	-	Li (2016)
NiO	TiO <sub>2</sub> (25 wt. %)	2000 ppm	Methanol (2.8) <sup>2</sup>	Room Temp.	9 / 16 seconds	Arshak et al. (2004)
SnO <sub>2</sub>	NiO (5 mol %)	5 ppm	Acetone (3.2) Hydrogen Gas (6.8) Methane (10.2) Ethyne (12.6) Benzene (18.7) Carbon Monoxide (21.8)	300 °C	2 / 3 seconds	Liu et al. (2011a)
SnO <sub>2</sub>	NiO	6.7 ppm	Formaldehyde (3.4) Carbon Monoxide (6.9) Water Vapour (8.1) Ethene (8.7) Nitrogen Monoxide (9.2) Carbon Dioxide(8.7) Chlorine Gas (5.8) Methane (8.1) Nitrogen Dioxide (8.1) Hydrogen Sulfide (8.7)	280°C	0.6 / 10 seconds	Lou et al. (2012)
Polyaniline (PANI)	NiO (10 wt. %)	0.31 ppm	Formaldehyde (1.1) Acetaldehyde (1.2) Benzene (6.2)	21 °C	-	Stewart et al. (2012)

<sup>1</sup> More selective to hydrogen gas.

<sup>2</sup> More selective to toluene and propanol.

The addition of NiO to SnO<sub>2</sub> nanofibers significantly increased the sensitivity towards ethanol (see Figure 2.17) (Liu et al., 2011a). Furthermore, Zheng et al. (2012) noted that adding NiO as a dopant to SnO<sub>2</sub> polyhedra also increased the selectivity to ethanol (see Figure 2.18). Therefore, both sensitivity and selectivity are improved by the addition of NiO. It should be noted that the structures of the sensing materials in both these cases are different.

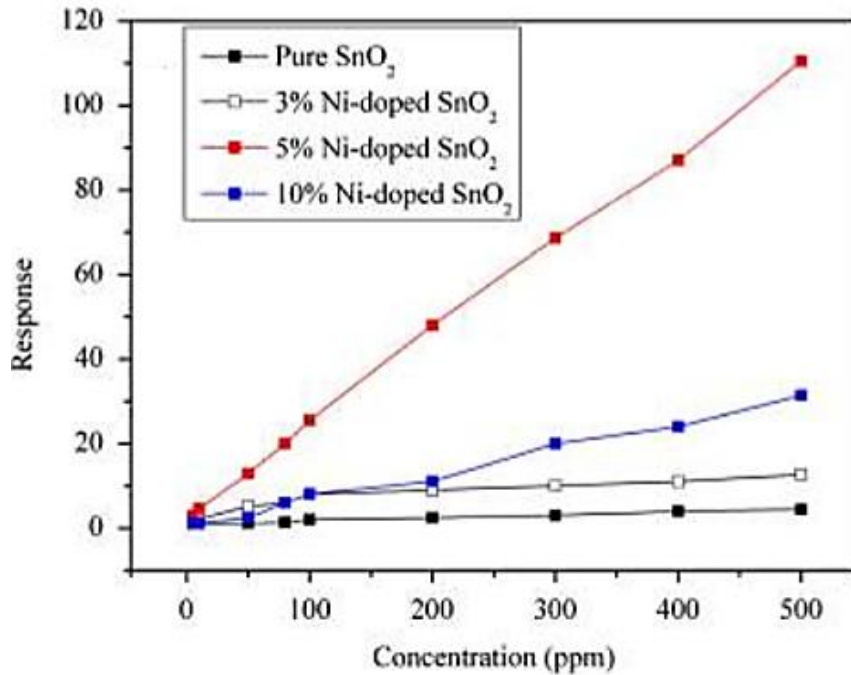


Figure 2.17: Effect of NiO dopant concentrations on the sensitivity of SnO<sub>2</sub> to ethanol (Liu et al., 2011a).

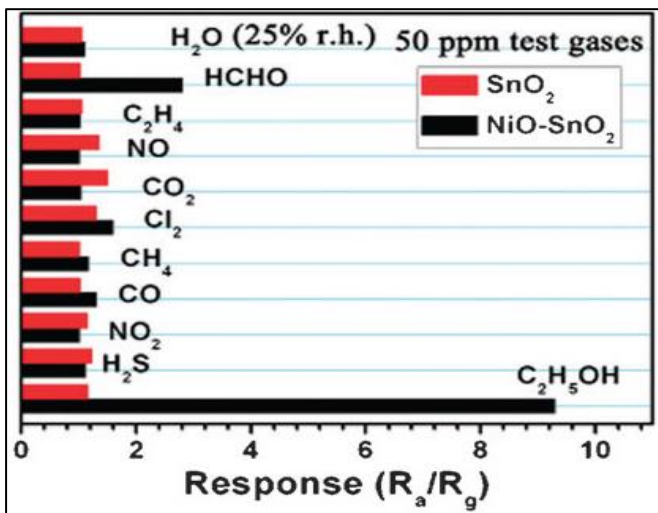


Figure 2.18: Effects of NiO addition on sensitivity and selectivity (Zheng et al., 2012).

#### 2.6.2.4 Titanium Dioxide (TiO<sub>2</sub>)

Titanium dioxide (TiO<sub>2</sub>) is a relatively sensitive sensing material for ethanol; however, not much work has been done on the selectivity of TiO<sub>2</sub> with respect to ethanol (see Table 2.8). In addition, TiO<sub>2</sub> has been used as a dopant in a ZnO sensor (Zhu et al., 2004) and a polyaniline (PANI) sensor (Zheng et al. 2008).

Table 2.8: Summary of Sensing Characteristics for Various TiO<sub>2</sub> Sensors

Material	Dopant	Detection Limit	Selectivity	Oper. Temp.	Sensing/ Recovery Time	Reference
TiO <sub>2</sub>	-	20 ppm	-	350 °C	12 / 9 seconds	Wang et al. (2010a)
TiO <sub>2</sub>	-	40 ppm	Hydrogen Gas (7.2)	400 °C	1 / 10 seconds	Tang et al. (1995)
TiO <sub>2</sub>	Ag	5 ppm	-	250 °C	1 / 2 seconds	Hu et al. (2010)
ZnO	TiO <sub>2</sub> (10 wt. %)	100 ppm	Acetone (1.9)	370 °C	10 / 5 seconds	Zhu et al. (2004)
Polyaniline (PANI)	TiO <sub>2</sub>	150 ppm	Formaldehyde (1.3) Acetaldehyde (1.8) <sup>1</sup>	Room Temp.	280 / - seconds	Zheng et al. (2008)

<sup>1</sup>More selective towards trimethylamine and trimethylamine.

It is important to note that for PANI doped with TiO<sub>2</sub>, the detection limit listed in Table 2.8 is likely much higher than the actual detection limit for ethanol due to the large response Zheng et al. (2008) observed for ethanol. Ethanol was only evaluated at 150 ppm since the paper focused on sensing materials for trimethylamine and triethylamine.

#### 2.6.2.5 Zinc Oxide (ZnO)

ZnO was one of the first and is still widely used as a sensing material in a variety of sensors (see Table 2.9) (Xu et al., 2000). It is a desirable sensing material due to its high chemical stability, non-toxicity, and low cost (Liu, 2010). In addition, ZnO can be doped with other metal oxides to improve both its sensitivity and selectivity. Note that Table 2.5 also contains some ZnO sensing materials which were doped with Al<sub>2</sub>O<sub>3</sub>.

Table 2.9: Summary of Sensing Characteristics for Various ZnO Sensors

Material	Dopant	Detection Limit	Selectivity	Oper. Temp.	Sensing/ Recovery Time	Reference
ZnO	-	10 ppm	-	400 °C	5 / 10 seconds	Singh et al. (2008)
ZnO	-	25 ppm	-	400°C	1 / many minutes	Liewhiran et al. (2007)
ZnO	-	50 ppm	-	220 °C	25 / 50 seconds	Choopun et al. (2007)
ZnO-Graphene	-	5 ppm	Acetone (1.5) Formaldehyde (3.3) Hydrogen Sulfide (3.7) Nitrogen Dioxide (6.5) Ammonia (6.8) Hydrogen Gas (7.0) Carbon Monoxide (7.6)		10 / 10 seconds	Zou et al. (2013)
ZnO	NiO	0.3 ppm	Formaldehyde (3.1) Acetone (7.3) Carbon Monoxide (7.3) Benzene (9.7)	450 °C	~ 60 / 60 seconds	Na et al. (2012)
ZnO	Ti (1.86 at %)	50 ppm	-	250 °C	~ 200 / 60 seconds	Hsu et al. (2014)

ZnO has high sensitivity to ethanol. The high sensitivity can be attributed to both its catalytic activity and small grain size. By reducing the grain size, the specific area is increased, and thus more active sites are available (Xu et al., 2000). Nanoparticles have a high surface area to volume ratio and therefore have more active sites available than larger particles.



## 3. Experimental

### 3.1 Gas Test System

#### 3.1.1 Experimental Set-up

To evaluate the potential sensing materials, gas sorption tests were performed. Each sensing material was exposed to a known concentration of analyte (e.g. 5 ppm ethanol gas in a balance of nitrogen) and the amount of analyte that sorbed onto the sample was measured. The more analyte that sorbed onto the sensing material, the more sensitive the sensing material was to that analyte. Measurements were conducted at room temperature (21°C) and slightly above atmospheric pressure (15 psi).

The gas test system was designed to be able to evaluate both sensing materials and complete sensors at room temperature (see Figure 3.1). Gas analytes were mixed, if necessary, using an inline passive mixer, after which the gas line was split using an MKS RS-485 mass flow controller on one side and an MKS 640A pressure controller and MKS 1179A flow meter on the other to ensure a 50:50 volumetric split. Both the sensing materials and sensors were tested using a flow rate of 200 sccm. When splitting the gas stream, a total initial flow rate of 400 sccm was used. Half of the gas stream (200 sccm) was directed into a test chamber that contained the full sensor (sensor with the sensing material). The other half (200 sccm) passed through a 100 mL round bottom flask (with or without a sensing material) into a specialized Varian 450 gas chromatograph (GC) with a photon discharge helium ionization detector (PDHID), capable of measuring down to the ppb level for different compounds. The flask could be removed from the system so that the gas stream ran directly into the GC. This allowed for simultaneous parallel measurement of the concentration of gas analyte(s) while a sensor was being tested (Stewart and Penlidis, 2013), for reference purposes.

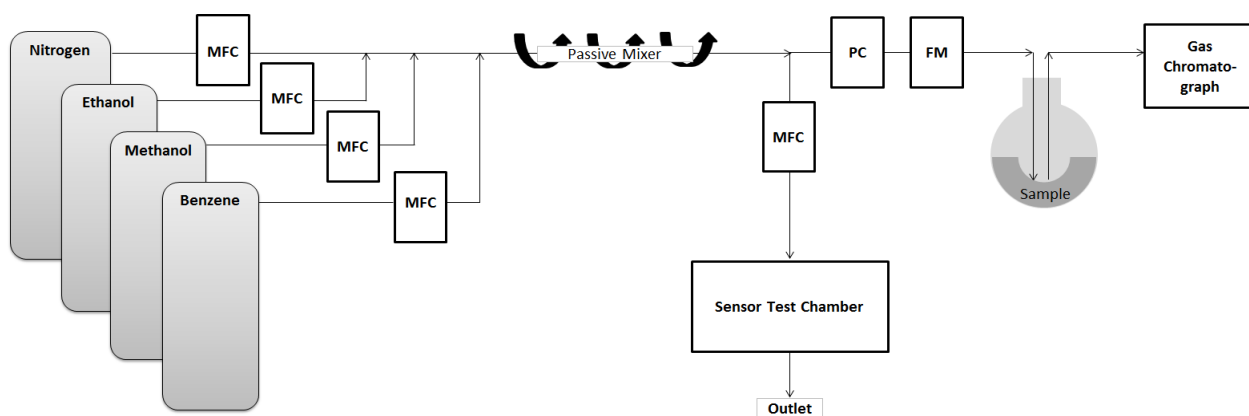


Figure 3.1. Schematic of the test system, where MFC, PC, and FM are mass flow controller, pressure controller, and flow meter, respectively. Note that the analytes shown are ethanol, methanol, and benzene, but represent the individual tanks of all the different analytes used.

### 3.1.2 Specialized Gas Chromatograph

A very sensitive, specialized gas chromatograph (GC) was used to qualitatively and quantitatively identify components in either a liquid or a gas sample. The components of a sample were separated as they flowed through a column, which contained a suitable packing material (see paragraph that follows). The packing material was chosen based on what components were known to be in the sample. As the components of a sample passed through the column, they sorbed (adsorbed or absorbed) onto the packing material at different rates, resulting in each component having its own retention time. Hence, the components of the sample were separated based on their retention times. The retention time indicated qualitatively which components were present in a sample. The data from the GC appeared as peaks on a voltage versus time graph. The areas under the peaks were integrated, and compared to those of a standard with a known concentration, to determine quantitatively the concentration of each component in the sample (Grob and Barry, 2004).

The specialized (highly sensitive) GC needed to be able to separate very chemically similar compounds (see Figure 3.2) and detect very low concentrations (see Figures 3.3). Additional chromatograms appear in Appendix D. For example, the separation was achieved using a Varian CP-Sil 5 CB (column packing identifier) for formaldehyde with a capillary column of dimensions 60m x 0.32mm x 8 $\mu$ m.

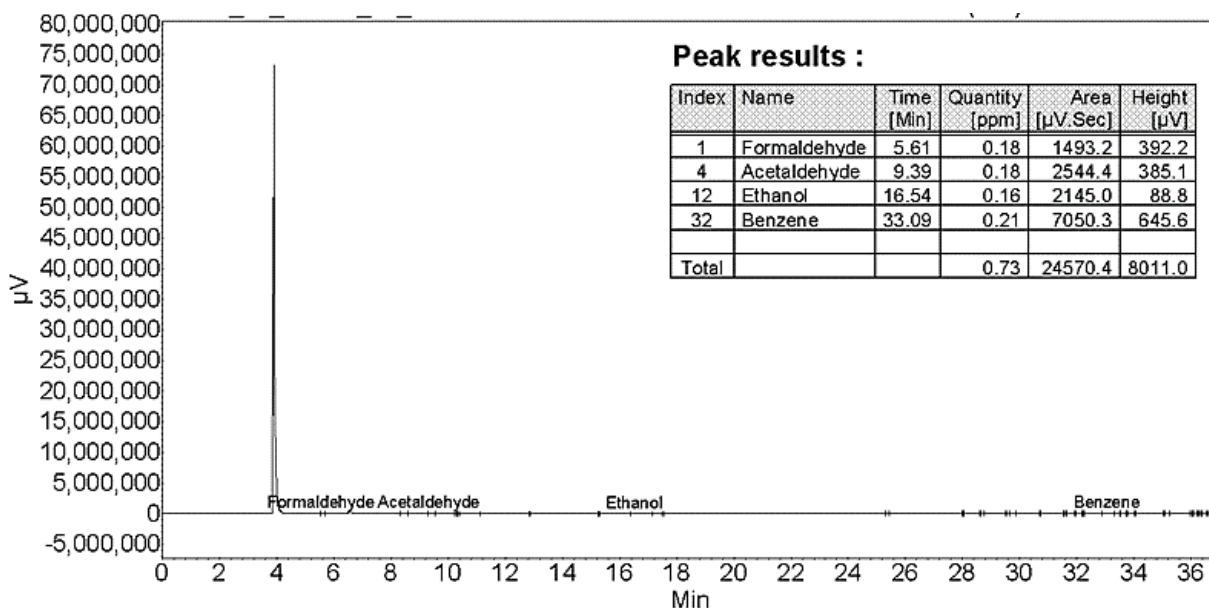


Figure 3.2: Chromatogram of four different gas analytes (formaldehyde, acetaldehyde, ethanol, and benzene), eluting out at different times.

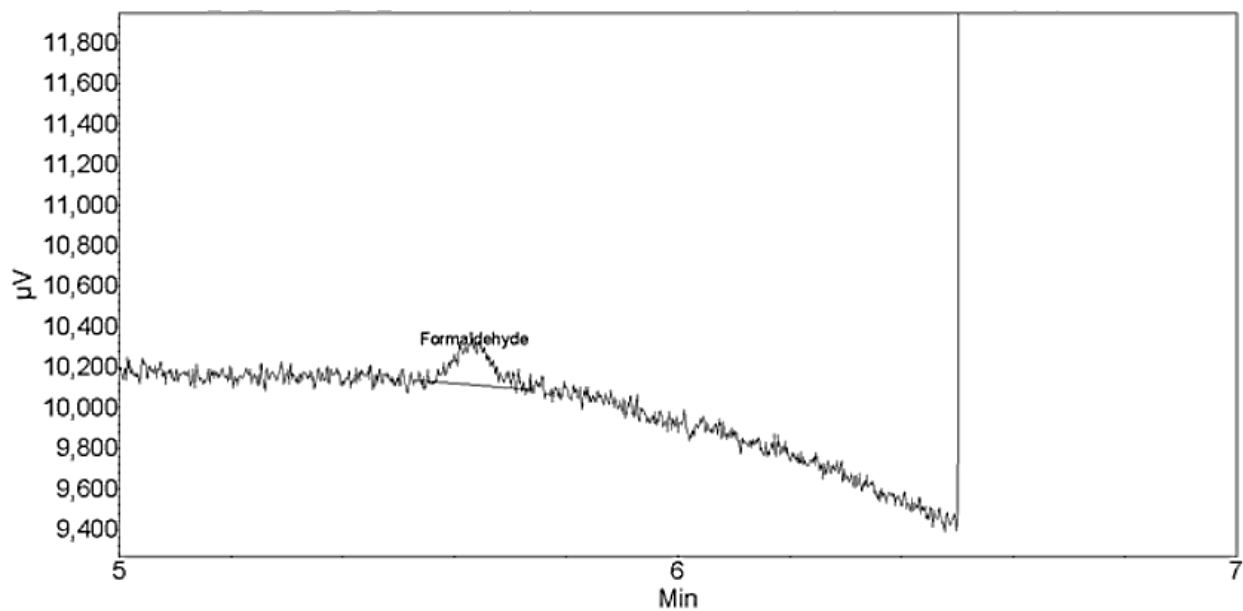


Figure 3.3: Chromatogram of formaldehyde at 0.09 ppm.

The GC used a pulsed discharge helium ionization detector (PDHID) which was very sensitive and could detect in the parts per billion (ppb) range. Pulsed direct current (DC) discharge caused the helium to ionize. As the helium returned to its natural state, photons were released and ionized the sample as it flowed down the column, producing electrons. These electrons were forced towards the detector and generated a response. This detector was virtually non-destructive to the sample and very sensitive. Because of the sensitivity of the detector, the detector was encased in helium to limit interference from the atmosphere (Agilent Technologies, 2006).

### 3.1.3 Gas Analytes Tested

Six gas analytes (ethanol, methanol, acetone, benzene, formaldehyde, and acetaldehyde) were available to use in the gas test system (see Table 3.1 for the concentrations of each gas analyte available). All of these gases were specialty gas mixtures (standard grade) in a balance of nitrogen gas (Praxair, California, USA). In addition, other concentrations of each of these gases could be achieved by dilution with 5.0 grade nitrogen (Praxair, Mississauga, Ontario, Canada). Note that dilutions were limited by the accuracy of the mass flow controllers and were done down to 12.5% (1/8) of the original concentration in the tank.



Table 3.1: Gas Analytes and Concentrations Used

Gas Analyte	Concentration (ppm)
Ethanol	5.00, 9.41, 20.03, 101, 1000, 5000
Methanol	4.66, 4895
Acetone	5.50, 5030
Benzene	5.10, 5040
Formaldehyde	5.05
Acetaldehyde	5.08

## 3.2 Transdermal Gas Determination

### 3.2.1 Transdermal Volatile Organic Compounds (VOCs)

To determine which gases are emitted from a person's hand, the GC was first calibrated using 13 different gases: ethanol, methanol, isopropyl alcohol, acetone, acetic acid, benzene, toluene, formaldehyde, acetaldehyde, pentane, chloroform, methylene chloride, and 1-butanol. Some of these gases came from gas mixtures in tanks and the rest came (as vapours) from a head space over their liquid counterpart. The gases in the tanks were calibrated standards and hence their concentration could be used directly to calibrate the GC. The concentrations of the other vapours from the head spaces were approximated using the corresponding vapour pressure at a given temperature.

Once the GC was calibrated, a gas-tight 5 mL syringe was used to take samples. A 5 mL sample ensured that any previous sample was plunged out of the sampling chamber in the GC with enough remaining for the 1 mL sample needed. The 5 mL volume was slowly injected into the inlet port of the GC over 30 seconds.

The lab air was tested first to determine the background. Only nitrogen, helium (carrier gas), water, and a peak from the plastic tubing used, were observed (see Figure 3.4). This ensured that the peaks observed from the hand were in fact from the skin and not from the surrounding environment.

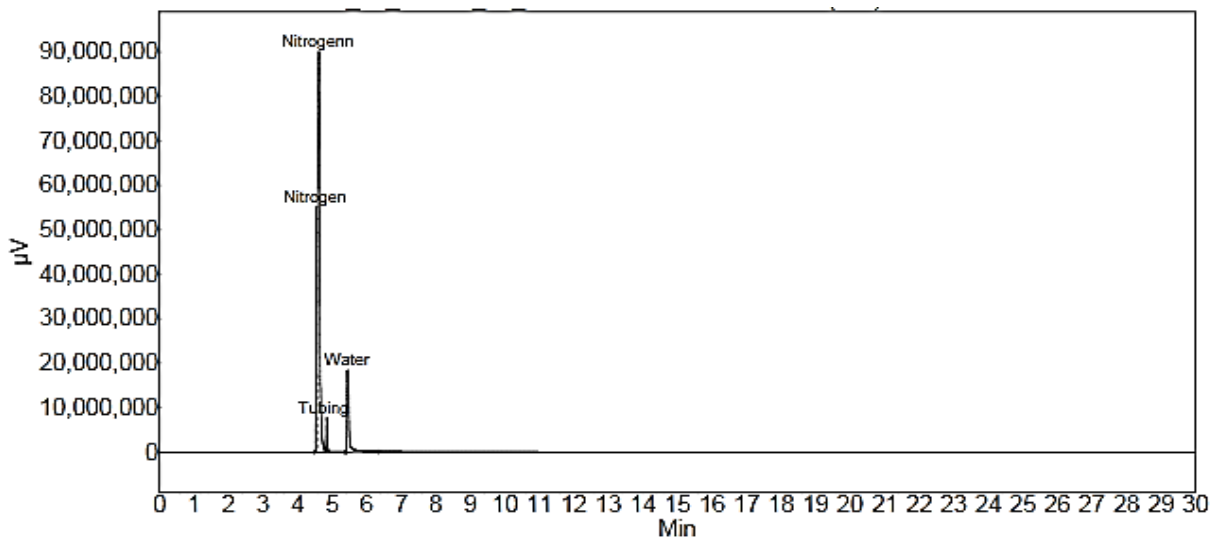


Figure 3.4: Chromatogram of lab air (reference point for further determinations).

A sample from the palm of a hand was then taken. The hand was cupped, while the sample was taken from the head space just above the palm. This was done with unwashed hands to determine what gases are present from both transdermally emitted gases and residues from various items a person comes into contact with. The sample was then injected into the GC to identify the gases emitted from a person's hand (see Figure 3.5).

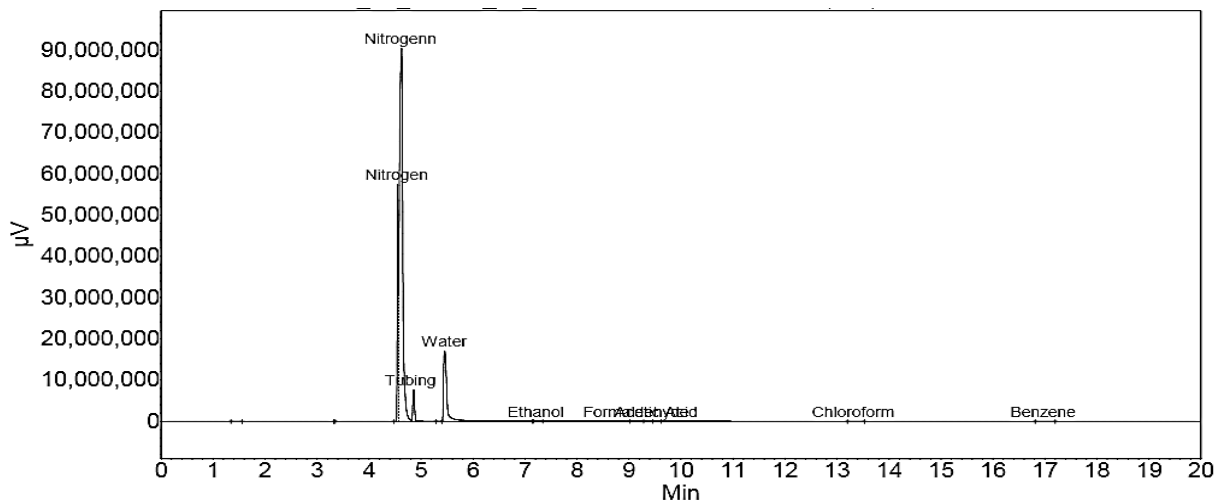


Figure 3.5: Chromatogram from the palm of a hand. Note formaldehyde and acetic acid labels are overlapping.

### 3.2.2 Transdermal Ethanol Concentration

This experimentation was conducted to assess whether or not a target of 5 ppm was reasonable for transdermal ethanol. The transdermal ethanol concentration (in ppm) was compared to the blood alcohol content (BAC) measured using a commercially available (BACtrack) breathalyzer. The

goal was to determine what the concentration of transdermal ethanol was in relation to a BAC of 0.05. Since only one person was used for the study, these results can be used to show qualitative trends and give an idea about transdermal ethanol concentration levels, but cannot be used as a definitive concentration comparison as the sample size was too small.

One test was performed per day. Each test consisted of one shot (1.5 oz of 40% v/v vodka). Vodka was chosen since it has little flavour, and thus fewer organic compounds that may have interfered with the test. The tests were conducted on an empty stomach (no food for 12+ hours prior to the tests). A single shot was consumed and measurements commenced at time zero.

Prior to the sample being consumed, the lab air was sampled and at least one sample was taken from the hand as a baseline. Taking two consecutive samples from the hand allowed replication of the process.

Samples were taken using a gas tight syringe (without a needle). The tip of the syringe was placed in the palm of the hand (with the hand cupped) and a 5 mL sample of air was drawn. This procedure was designed to mimic a hand cupping the steering wheel, with a pump drawing a sample from the palm of the hand. The sample was immediately injected into the sensitive gas chromatograph. A sample from the hand was taken every 10 minutes, up to 90 minutes per test.

A breathalyzer was used to measure the blood alcohol content (BAC) from the breath. Measurements from the breath were conducted 15 seconds before the sample was taken from the hand. This allowed the response from the hand to be correlated to the BAC.

A double shot (3 oz of vodka) was taken once as a comparison to the single shots. After the double shot was consumed, the same procedure was followed as for the single shots. The only difference was that the response was measured over 4 hours.

### **3.3 Sensing Material Preparation**

Polyaniline (PANI) was synthesized by mixing aniline, ammonium persulfate, and, if present, the dopants, in deionized water. 0.39 mL of aniline (A.C.S. reagent, Sigma-Aldrich, Oakville, Ontario, Canada) was added to 20 mL of deionized water and then mixed using a sonicator for 30 minutes. This solution was then cooled to  $-1^{\circ}\text{C}$  before the addition of a solution containing 1.0 g of ammonium persulfate (A.C.S. Reagent, Sigma-Aldrich, Oakville, Ontario, Canada) in 5 mL of deionized water. The solution was shaken for one minute to ensure thorough mixing. The mixture was subsequently left to react at  $-1^{\circ}\text{C}$  for 6 hours (Stewart et al., 2012). The polymer was filtered out using a funnel and Wattman #5 filter paper and left overnight. The polymer was then washed with acetone until the liquid ran clear. Finally, the polymer was scraped into a glass vial for storage under atmospheric conditions.

To obtain the doped polymer, the monomer was polymerized with the dopant suspended in the starting solution. The dopant was added up to 20% by weight with respect to the monomer, before the solution was initially cooled prior to the addition of the ammonium persulfate. Other than the addition of the dopant, which was aluminum oxide ( $\text{Al}_2\text{O}_3$ ) (particle size < 50 nm, 10 wt. % dispersion in water, Sigma-Aldrich, Oakville, Ontario, Canada), copper (II) oxide ( $\text{CuO}$ ) (particle size <50 nm, Sigma-Aldrich, Oakville, Ontario, Canada), nickel (II) oxide ( $\text{NiO}$ ) (particle size <50 nm, concentration of 99.8%, Sigma-Aldrich, Oakville, Ontario, Canada), titanium (IV) oxide ( $\text{TiO}_2$ ) (particle size 21 nm, concentration of 99.5%, Sigma-Aldrich, Oakville, Ontario, Canada), or zinc oxide ( $\text{ZnO}$ ) (particle size <100 nm, 50 wt. % in water, Sigma-Aldrich, Oakville, Ontario, Canada), the polymerization procedure was the same as described above for PANI without any dopant.

Poly (*o*-anisidine) (PoANI) was prepared in the same manner as PANI, except *o*-anisidine (A.C.S. reagent, Sigma-Aldrich, Oakville, Ontario, Canada) was used as the monomer instead of aniline. Similarly, poly (2,5-dimethyl aniline) (P25DMA) was prepared using its monomer, 2,5-dimethyl aniline (A.C.S. reagent, Sigma-Aldrich, Oakville, Ontario, Canada).

PANI, PoANI, and P25DMA were initially doped with 10 wt. % and 20 wt. % NiO or ZnO, giving rise to a total of fifteen polymeric nanocomposites, and subsequently evaluated for their effectiveness as sensing materials for ethanol. Since P25DMA performed significantly better, P25DMA was further doped with 5 wt. %, 10 wt. %, and 20 wt. % of  $\text{Al}_2\text{O}_3$ ,  $\text{CuO}$ ,  $\text{NiO}$ ,  $\text{TiO}_2$ , or  $\text{ZnO}$ , resulting in an additional 11 polymer nanocomposites evaluated as sensing materials for ethanol. Note that for ease of naming, the polymer nanocomposites will be referred to as polymer wt. % dopant (i.e. PANI doped with 10 wt. % NiO will be named PANI 10% NiO).

The sensing materials were evaluated using gaseous ethanol in tanks from Praxair (California, USA). The 5 ppm of standard grade gaseous ethanol in nitrogen was used. Nitrogen (5.0 grade, Praxair, Mississauga, Ontario, Canada) was used to purge the sensing materials prior to evaluation using ethanol. The potential polymeric sensing materials were evaluated using the gas test system described in Section 3.1.

Note that other commercially available polymers were also evaluated. These polymers were used as obtained, except poly (ethylene imine), which was dried first before use. These include specialty polymers such as OV 225, OV 275, and SXFA from Seacoast Sciences, Inc. (Carlsbad, California, USA), and other polymers such as poly (methyl methacrylate) (PMMA) (Average  $M_w = 15,000$ , Sigma-Aldrich, Oakville, Ontario, Canada), poly (ethylene imine) (PEI) (Average  $M_n = 60,000$ , 50 wt. % in water, Sigma-Aldrich, Oakville, Ontario, Canada), polypyrrole (PPy) (Conductivity 10 – 50 S/cm, pressed pellet, Sigma-Aldrich, Oakville, Ontario, Canada), poly (vinyl pyrrolidone) (PVP) (Average  $M_w = 40,000$ , Sigma-Aldrich, Oakville, Ontario, Canada), and

poly (2,6-dimethyl-1,4-phenylene oxide) (PPO) (Average  $M_w = 30,000$ , Sigma-Aldrich, Oakville, Ontario, Canada).

### **3.4 Deposition onto Sensors**

#### ***3.4.1 Radio Frequency Identification (RFID) Sensor***

Each of the polymeric sensing materials was suspended/dissolved into a solvent at a concentration of 0.1 wt. %. The OV 225, OV 275, and SXFA were suspended in diethyl ether and the polyaniline (PANI) derivatives and nanocomposites were suspended in *N*-methylpyrrolidone (NMP). The suspension was deposited using a microplotter (30  $\mu\text{m}$  tip) onto the RFID sensors. The solvent was evaporated off at 120°C for the OV 225, OV 275, and SXFA, and at 60°C for the PANI derivatives and nanocomposites. The temperatures were selected based on the degradation temperatures of polymeric sensing materials so as to avoid degradation. Multiple applications (or coats) were applied to ensure full coverage was achieved and a deposition thickness of 5  $\mu\text{m} \pm 0.5 \mu\text{m}$ , which was measured using an optical microscope (Chen et al., 2015b).

#### ***3.4.2 Microelectromechanical Systems (MEMS) Microcantilever Sensor***

Two polymers were deposited onto the MEMS microcantilever sensor: polyaniline (PANI) doped with 10% NiO and poly (2,5-dimethyl aniline) (P25DMA). 0.1 g of the polymeric sensing material was mixed with approximately 1 mL of ethylene glycol to form a paste. This paste was spread onto the end plate on the microcantilever and the ethylene glycol was allowed to dry in atmosphere (Khater et al., 2014). Because the sensor plate was on the micron scale, the deposition was done under a microscope.

### **3.5 Evaluation of Sensing Materials and Sensors**

#### ***3.5.1 Evaluation of Sensing Materials***

All potential polymeric sensing materials were evaluated based on the amount of gas analyte they sorbed. 0.120 g of polymer was weighed into a 100 mL round bottom flask. 5 mL of ethanol was added to the flask and the flask was swirled for 30 seconds to disperse the polymer and coat the flask. This was done to increase the surface area of the polymer exposed to the analyte. The flask was then placed in a 50 °C oven for 18 hours to evaporate off the ethanol and dry the polymer samples. The samples were cooled to room temperature (21°C) prior to testing.

As described in Section 3.1.1, the polymer samples were purged with dry nitrogen for 30 minutes before being exposed to the gas analyte. This ensured any residual analyte sorbed onto the polymer was released. The polymer samples were exposed to gas analytes individually and the highly

specialized gas chromatograph (GC) was used to measure the amount of gas that did not sorb (residual gas). By subtracting the residual analyte concentration ( $[Analyte]_{residual}$ ) from the initial concentration of analyte ( $[Analyte]_{initial}$ ) exposed to the polymer sample, the amount sorbed could be obtained (see Equation 3.1).

$$[Analyte]_{sorbed} = [Analyte]_{initial} - [Analyte]_{residual} \quad (\text{Equation 3.1})$$

The amount of analyte sorbed was measured at equilibrium. To ensure equilibrium had been reached, two consecutive samples were measured by the GC, typically 12 minutes apart. The time between samples run by the GC was limited by the amount of time it took for the gas analyte to elute out of the GC column.

### **3.5.2 Evaluation of Sensors**

#### *3.5.2.1 RFID Sensors*

The RFID sensors were placed inside the sensor chamber described in Section 3.1.1. The chamber contained an inlet where the gas analytes entered, two holes for the cables connecting the sensors and the sensor readout, and an outlet hole. Two RFID sensors could be evaluated simultaneously.

The output signal from the RFID sensors were recorded using a Hewlett Packard 8722E5 S-parameter network analyzer, which measured amplitude versus frequency. Specific peaks (in the GHz range) and the frequency shifts of these peaks, which resulted from the analyte sorbing onto the sensing material, were monitored and recorded.

Both the transient (real time) and equilibrium responses were measured for the RFID sensors. The equilibrium responses were used to determine the sensitivity and selectivity of the sensor, while the transient response was used to determine the response and recovery times of the sensor. Due to equipment limitations, the transient responses were measured every 15 seconds over an 8 minute period (4 minutes of analyte exposure, followed by 4 minutes of dry nitrogen purge).

#### *3.5.2.2 MEMS-based Sensors*

The MEMS sensors were evaluated in a specially designed test chamber (see Figure 3.6). The test chamber contained an inlet, outlet, and ports for electrical wires. The test chamber was large enough to accommodate a microscope that was used to visually monitor the MEMS sensor. A pressurized canister of standard grade gas analyte was used to fill the chamber with analyte at a specific concentration. The chamber was purged between runs.

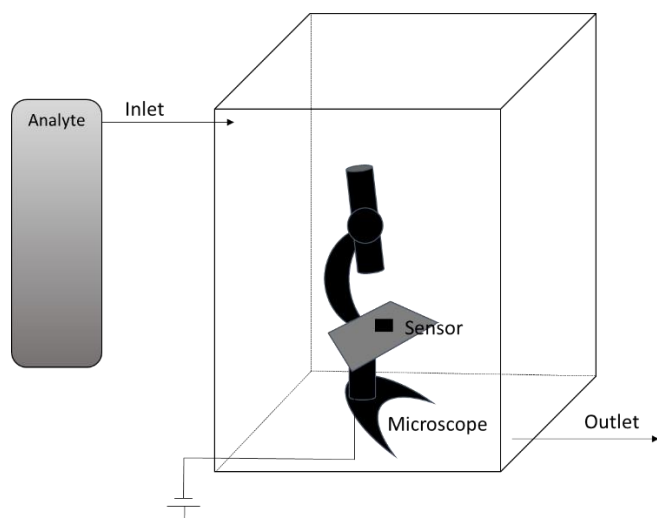


Figure 3.6: Schematic of the test chamber used for evaluation of the MEMS-based sensor.

The MEMS sensor was a binary cantilever sensor that “switched on” when a threshold concentration of analyte was reached. The cantilever response was mass-based; therefore, when enough analyte sorbed onto the sensing material, the added weight caused the cantilever to bend. When enough mass was added (a threshold concentration was reached), the sensor “switched on”. This “switch” was observed visually using a microscope. Note that the amount of mass sorbed onto the sensor was correlated to the analyte concentration in the chamber.

### 3.6 Statistical Analysis

The experiments were run using a full factorial design with three independent replicates each. Therefore, all levels of one factor were combined with all levels of the other factors. For example, all the gas analytes (one factor) were evaluated against all of the sensing materials (the other factor). Note that the samples were randomly ordered before testing to minimize any bias that may have been present day to day.

Not every possible dopant and polymer combination was run. Screening experiments were used to determine the best sensing materials in terms of ethanol sorption. Based on these results, specific polymers and dopants were chosen to be evaluated further. For example, the sensing materials which sorbed more ethanol were the ones further evaluated using other interferents.

The data collected (see Appendix E) were analyzed using analysis of variance (ANOVA), which determines if there is a significant difference between the means ( $\mu$ ) of two or more samples. ANOVA begins with a null hypothesis ( $H_0$ ) that states there is no difference between the means of all samples evaluated (see Equation 3.2) under a multiple comparison scenario.

$$H_0: \mu_i - \mu_j = 0 \quad \text{for all } i, j \quad \text{(Equation 3.2)}$$

The sum of squares (SS), degrees of freedom (df), and the mean square (MS) are all calculated for the data and summarized in an ANOVA table (see Appendix F for the ANOVA tables pertaining to the results discussed in Chapters 4 and 6). In addition, an  $F_{\text{observed}}$  value was calculated from the MS and  $MS_{\text{error}}$ . The equations used for the ANOVA are listed in Appendix F (see Equations F.1 - F.10). If the  $F_{\text{observed}}$  is larger than the  $F_{\text{critical}}$  (from an F-table at a given confidence level, typically 95%,  $\alpha = 0.05$ ), then the null hypothesis is rejected. Otherwise, there is not sufficient evidence to reject the null hypothesis.

If the null hypothesis is rejected, it means at least two of the sample means are significantly different at a confidence level (typically 95%,  $\alpha = 0.05$ ) for a given number of samples evaluated. ANOVA does not distinguish which pairs of means show a difference, just whether there is a difference between at least two means. If the null hypothesis cannot be rejected, then there is no significant difference between the means. Therefore, the response from all the polymer samples evaluated is effectively the same.

For special cases, where one factor may affect another factor being evaluated, ANOVA with blocking was used. This was the case for evaluating different sensors using different sensing materials, where lurking differences in the sensing material structure could affect the comparison between the types of sensors. By blocking one factor (the sensing materials), the effects of the blocks could be separated from the effects of the treatment (the sensors). The equations used for the ANOVA with blocking are also listed in Appendix F (see Equations F.11 - F.17)

To determine which polymers/analytes are significantly different, a multiple comparisons test must be done, since the ANOVA only determines if at least one sample mean is different from the others. ANOVA does not identify which samples mean(s) are different. Two multiple comparisons tests were carried out: the Bonferroni t-test and Fisher's Least Significant Difference (LSD). Both of these tests are paired comparison tests, used to evaluate whether two sample means are significantly different from one another. Both the Bonferroni t-test and the Fisher's LSD were done at 95% confidence levels ( $\alpha = 0.05$ ,  $\alpha/2 = 0.025$ ). The equations used for both the Bonferroni t-test (see Equations F.18 - F.20) and Fisher's LSD (see Equations F.20 - F.22) are listed in Appendix F.

In addition to calculating whether the responses were significantly different from each other, the error was also calculated from the three independent replicates. The percent error was calculated by dividing the sample mean by the standard deviation. The equations used to calculate the error are listed in Appendix F (see Equations F.23 - F.27). The percent error for each of the cases analyzed is listed in the tables in Appendix F. Note that the error measured was less than 10% for all cases and typically below 5%. These are very reasonable error estimates.



### 3.7 Polymerization Kinetics of Aniline

After detailed scrutiny of the literature, kinetic information on the polymerization characteristics of aniline is scarce or non-existent. Many literature sources mention a (relatively common) recipe, which is employed to produce polyaniline (PANI) for further investigations, with qualitative statements such as “very high molecular weight PANI was synthesized” (Steiskal and Gilbert, 2002). Several publications discuss postulated mechanisms for the polymerization of aniline, which are useful in visualizing the polymerization steps, but do not include any estimates of propagation or termination rate constants. Some sources offer estimates of activation energies for propagation or termination, which are within a reasonable range of expected values based on typical polymerization understanding (Mu et al., 1997). Table 3.2 includes the most useful references located with some relevant information about polymerization kinetic aspects of aniline.

Based on the information from the references in Table 3.2, it seems that PANI below a molecular weight of 50,000 Da is usually referred to as “low molecular weight PANI” (Yang and Mattes, 2002). Molecular weight estimates in the literature range from 50,000 to 1,500,000. Typical information about molecular weight ranges comes either from solution viscometry, which is useful for qualitative comparisons at best, or gel permeation chromatography (GPC). GPC is usually carried out in exotic solvents such as *N*-methyl-2-pyrrolidone (NMP), since PANI is not readily soluble in many solvents (Brandrup et al., 1999). Unfortunately, not a lot of useful and reliable information is given in terms of calibration, replication, error estimates, refractive index determination, etc.

From this, it is evident that a more quantitative description of polymerization kinetics of aniline is rather elusive. The best that can be done is to resort to an order of magnitude analysis based on the poor information given by the references in Table 3.2, and/or on typical polymerization theory and understanding.

Note that in Table 3.2, individual rate constants are denoted by a subscripted  $k$ , whereas a simple  $k$  denotes a pseudo (overall) rate constant. The initiator decomposition rate constant is denoted by  $k_d$ , and the polymerization (propagation) rate constant is denoted by  $k_p$ . In addition, the estimate of the activation energy of the overall polymerization is denoted by  $E_A$ . Table 3.2 also includes molecular weight estimates for polyaniline measured by either gel permeation chromatography (GPC) or dynamic light scattering (DLS).

Table 3.2: Polymerization Kinetic Aspects of Aniline from the Literature

Initial Conditions	Rate Constants/ Activation Energy	Temperature	Molecular Weight	Reference
0.05 M ANI 1 M H <sub>2</sub> SO <sub>4</sub>	$k = 0.48 (\pm 13\%) \text{ s}^{-1}$	-	-	Shim and Park (1989)
0.082 M ANI 0.110 M DBSA 0.017 APS	$k_d = 5 (\pm 1) \times 10^{-4} \text{ M}^{-1} \text{ min}^{-1}$ $k_p = 3 (\pm 1) \times 10^{-1} \text{ M}^{-1} \text{ min}^{-1}$	-10 °C	-	Gomes de Souza et al. (2009)
0.2 M ANI 0.8 M HCl	$E_A = 20.9 \text{ kJ/mol}$ $E_A = 5.4 \text{ kJ/mol}$	1 – 20 °C 20 – 35 °C	-	Mu et al. (1997)
0.5 M ANI 0.5 M APS 1 M HCl 6 M LiCl	-	- 30 °C	$M_w = 127,866$ (GPC) $M_w = 911,737$ (DLS)	Ramamurthy et al. (2012)
0.2 M ANI 0.25 M APS 0.1 M H <sub>2</sub> SO <sub>4</sub>	-	21 °C	$M_w \approx 40,000$	Sapurina and Shishov (2012)
0.2 M ANI 0.25 M APS 0.2 M Acetic Acid	-	21 °C	$M_w = 44,600$	Sapurina and Shishov (2012)
0.04 M ANI 1 M HCl 0.4 M APS	-	5 °C	-	Wei et al. (1989)

Where ANI is aniline, APS ammonium persulfate, H<sub>2</sub>SO<sub>4</sub> is sulfuric acid, DBSA isododecylbenzene sulfonic acid, HCl is hydrochloric acid, LiCl is lithium chloride.

Our exact recipe and rather straight forward polymerization procedure are described in Table 3.3. Based on the recipe shown in Table 3.3, an order of magnitude analysis was conducted. As part of the order of magnitude analysis, some rounding was done on the numbers representing initial concentrations of the ingredients. Note that the temperature used for the calculations was 0 °C, since the temperature varied between -2 °C and +2 °C during the polymerization (aniline polymerization is highly exothermic and hence it is difficult to control the polymerization temperature at such low temperature levels).

Table 3.3: Recipe used to Synthesize Polyaniline

Monomer	Initiator	Solvent	Temperature	Time
Aniline 0.4 g	Ammonium persulfate 1.0 g	Deionized Water 25 mL	-1 °C	6 hours
93.13 g/mol	228.18 g/mol			
[M] = 0.2 mol/L	[I] = 0.2 mol/L			

The excess of ammonium persulfate used for the polymerization is indicative of oxidative mechanisms, which have been proposed for the aniline polymerization (see Figure 3.7). Note that this mechanism has not been extensively studied and is not well understood. For example, it is unknown why this polymerization results in 95% on the aniline adding in the *para* position (Sapurina and Stejskal, 2008).

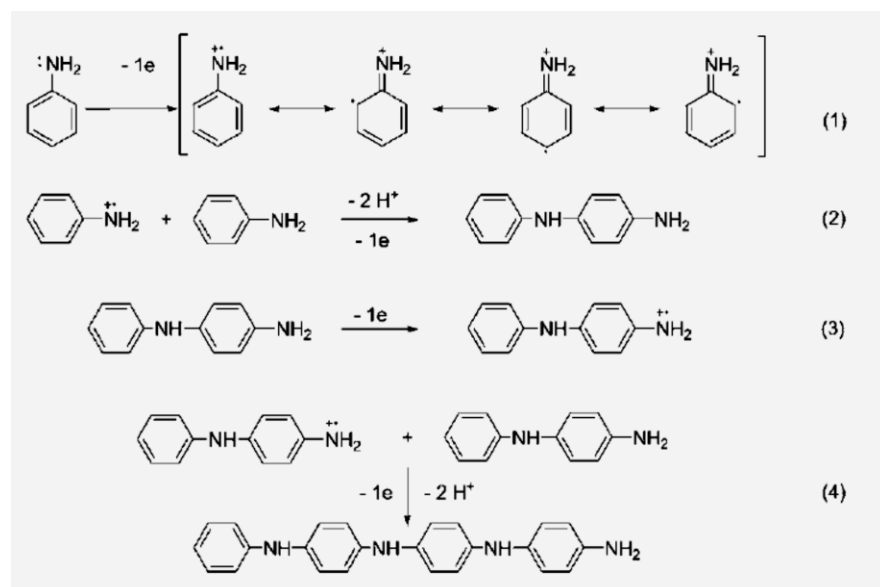


Figure 3.7: Proposed oxidation mechanism for the polymerization of aniline (Bocchini et al., 2013).

Typical rate constant,  $k_d$ , values for a decomposition of ammonium persulfate are seen in Table 3.4.

Table 3.4: Rates Constant Values for Ammonium Persulfate (APS)

Rate Constant	Temperature	Reference
$k_d = 5 \times 10^{-6} \text{ s}^{-1}$	50 °C	Gao and Penlidis
$k_d = 1.6 \times 10^{-7} \text{ s}^{-1}$	0 °C	(2002)

Conversion versus time data were collected for the synthesis of polyaniline (see Figure 3.8). The procedure was the same as described in Section 3.3, except that the polymerization was carried out

in test tubes with  $\frac{1}{4}$  of all ingredients (such that the concentrations remained the same), and the polymerization was stopped by dropping the test tube into liquid nitrogen. The samples were filtered and weighed.

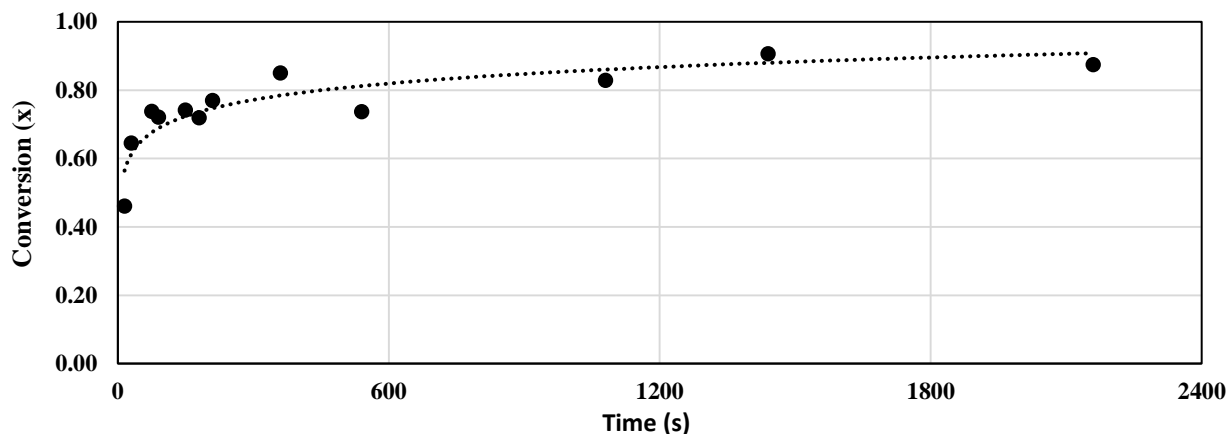


Figure 3.8: Typical conversion versus time graph for the polymerization of polyaniline.

Given the uncertainty surrounding the values of the kinetic rate constants involved in aniline polymerization, a typical molecular weight range at our polymerization conditions (and recipe) would be:

$$M_n \approx 200,000 - 500,000$$

The estimated range above is in agreement with the reported molecular weight values in the literature for a similar recipe and conditions (see Table 3.2). Note that the range of molecular weights shown in Table 3.2 is from 40,000 Da (for room temperature polymerization) to about 1,000,000 Da (for very low temperature polymerization).

The molecular weight of PANI in DMSO was measured using a Viscotek TDA 305 GPC. Given that no  $dn/dc$  value for PANI in DMSO could be found in the literature, two reasonable estimates of 0.4 and 0.2 were used to calculate the molecular weight (see Table 3.5). Note that these  $dn/dc$  values are estimated from PANI in other solvents (see Appendix D.2).

Table 3.5: Molecular Weight of PANI

Sample	$dn/dc$ (estimate)	$M_w$ (Da)	$M_n$ (Da)	PDI
PANI 1	0.4	386,866	<b>176,975</b>	2.186
PANI 2	0.4	407,761	<b>204,403</b>	1.995
PANI 1	0.2	773,733	<b>353,950</b>	2.186
PANI 2	0.2	815,521	<b>408,807</b>	1.995



## 4. Results and Discussion: Sensing Material Analysis

### 4.1 Transdermal Gas Studies

#### 4.1.1 Transdermal Volatile Organic Compounds (VOCs)

Identification of compounds (or gases) using a gas chromatograph (GC) is based on elution (retention) time. It is possible for multiple compounds to have the same (or very close, essentially indistinguishable) elution times. Therefore, there is potential for misidentification of the gases emitted from a person's hand when using a GC due to some gases having similar elution times. As well, some peaks on the chromatogram, such as the peak for water, which have a long tail, may obscure very small response peaks from other analytes that happen to elute out within the same range.

It is worth noting that the majority of gases emitted from the human body are in the sub ppb range, and therefore not detectable by GC. This is a good sign for sensors that are designed to detect analytes in the ppm to high ppb range, because the sensor would not have the appropriate sensitivity for all these interferents, and thus selectivity towards the target analyte, ethanol, would be very good.

When designing a sensor for a target analyte (i.e. ethanol), the interferents of concern are those which are in the same (or higher) concentration range than the target analyte. For example, if acetone were to come off a subject's hand at a concentration of 10 ppb, it would not likely result in a false positive from a sensor designed to detect analytes around 1 ppm; however, if acetone came off a subject's hand at 10 ppm, then it would be possible for acetone to give a false positive. Therefore, the VOCs that come off a subject's hand in concentrations of (high) ppb – (low) ppm are the interferents of interest, as they may affect the selectivity of a sensor.

The results from the study of the gases that are emitted from one particular person's hand are summarized in Figure 4.1. These results show that there is a large variability of gases emitted from one person's hand over time. They also show, for this particular person, that most of the gases emitted from the hand are in the 1 - 2 ppm range, and therefore, are less likely to produce a false positive when testing for ethanol.

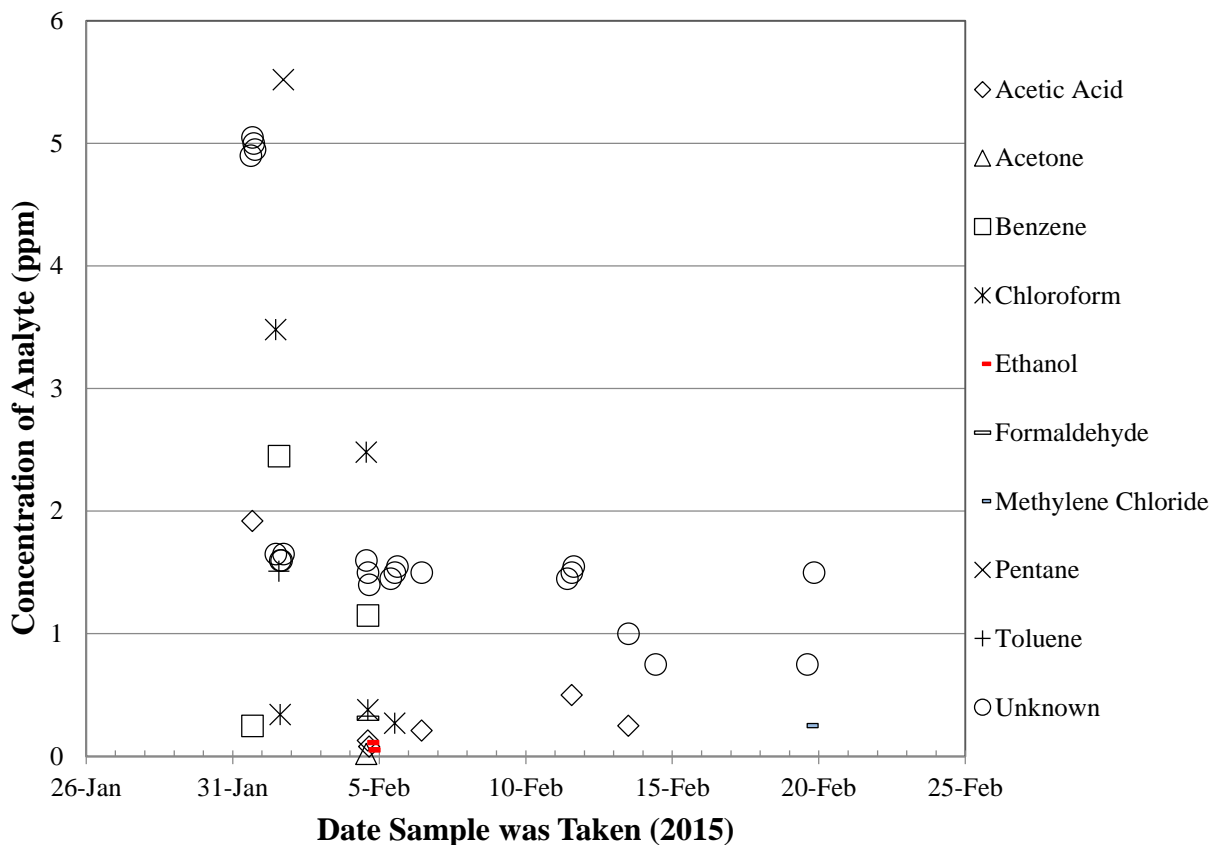


Figure 4.1: Gases emitted from one individual's hand over time.

It should be noted that there were a number of unidentified gases in the 1-5 ppm range that appeared on the chromatograms (see Figure 4.2). Also, the presence of ethanol (seen on February 5<sup>th</sup> in Figure 4.1) was observed after the person tested had consumed less than one ounce of alcohol within one hour prior to testing.

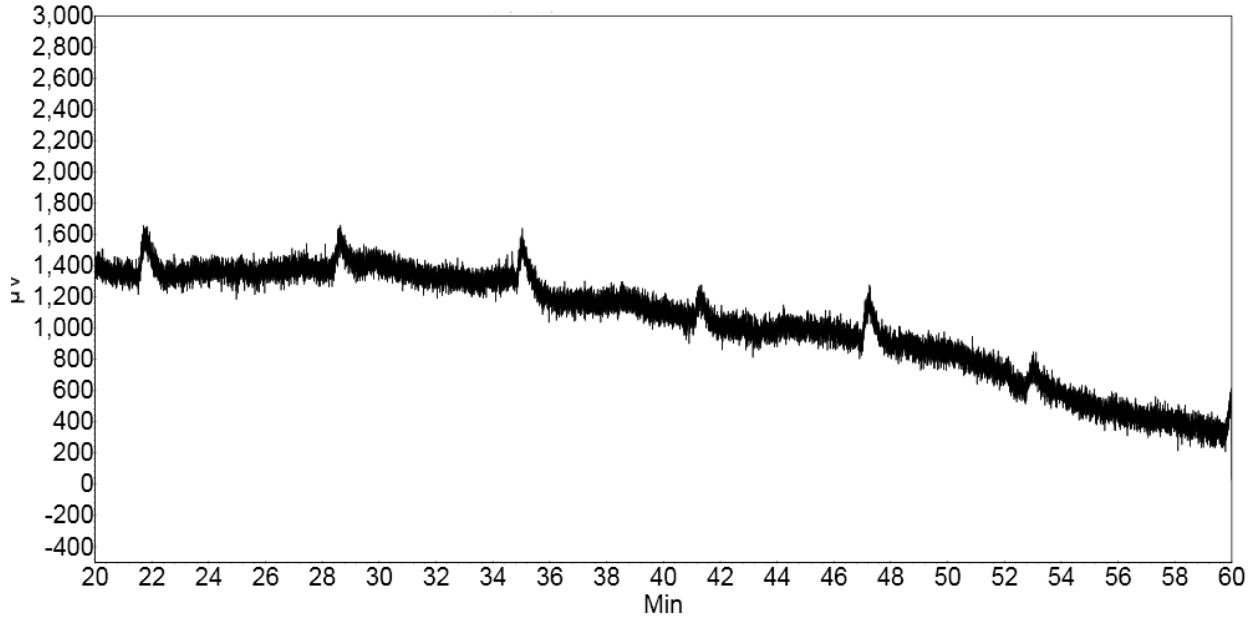


Figure 4.2: Gas chromatogram of unidentified (unknown) compounds emitted from the person's hand.

#### 4.1.2 Transdermal Ethanol Concentration

At time equal to zero, the amount of ethanol from both the hand and the mouth was zero (0 ppm from the hand and 0.00 BAC from the breathalyzer) for every test. These samples were measured just before the shot was taken to give a true baseline. Samples taken immediately after the shot resulted in excessively high concentrations of ethanol from both the mouth and hand. When the BAC was measured using a breathalyzer immediately after taking a shot, the breathalyzer maxed out (at 0.50 BAC) due to the alcohol in the mouth. It took a few minutes for the residual ethanol to be absorbed through the mouth or washed away with saliva. When a sample was taken from the hand immediately after consuming the vodka shot, the concentration of ethanol measured was approximately 10 times higher than the highest concentration measured around 20 or 30 minutes. This was due to ethanol vapour from the shot collecting on the palm of the hand while lifting the filled shot glass (to take the shot) due to ethanol's high vapour pressure.

The amount of ethanol from subsequent samples, taken every 10 minutes, was plotted. Figures 4.3 through 4.5 show the amount of ethanol measured from both the hand and mouth. Note that the amount of ethanol measured is very similar for all three days. In each case, the amount of ethanol measured from the hand initially peaked around 30 minutes, with a second spike around 80 minutes. The breathalyzer, which was used to measure BAC from the mouth, steadily decreased after 20 minutes. A sharper drop was observed between 10 and 20 minutes, which may have been due to residual alcohol in the mouth after the shot. This likely produced a higher reading from the breathalyzer at 10 minutes than the actual BAC.



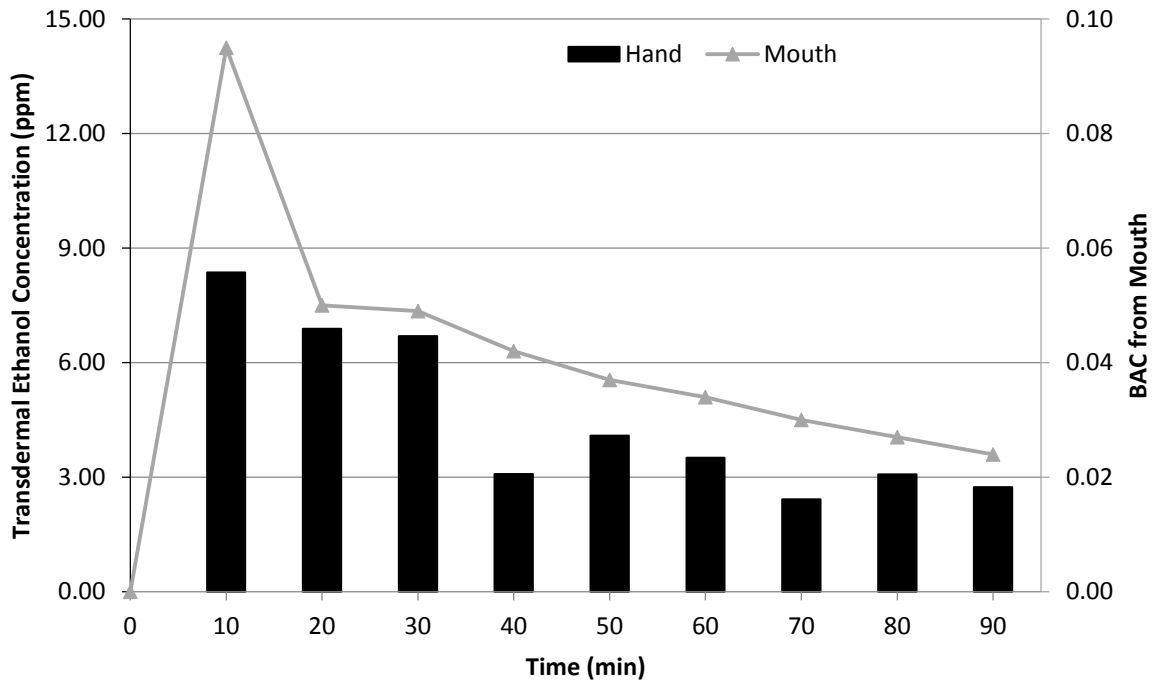


Figure 4.3: Comparison of the transdermal ethanol concentration and BAC measured from the mouth, March 25, 2015.

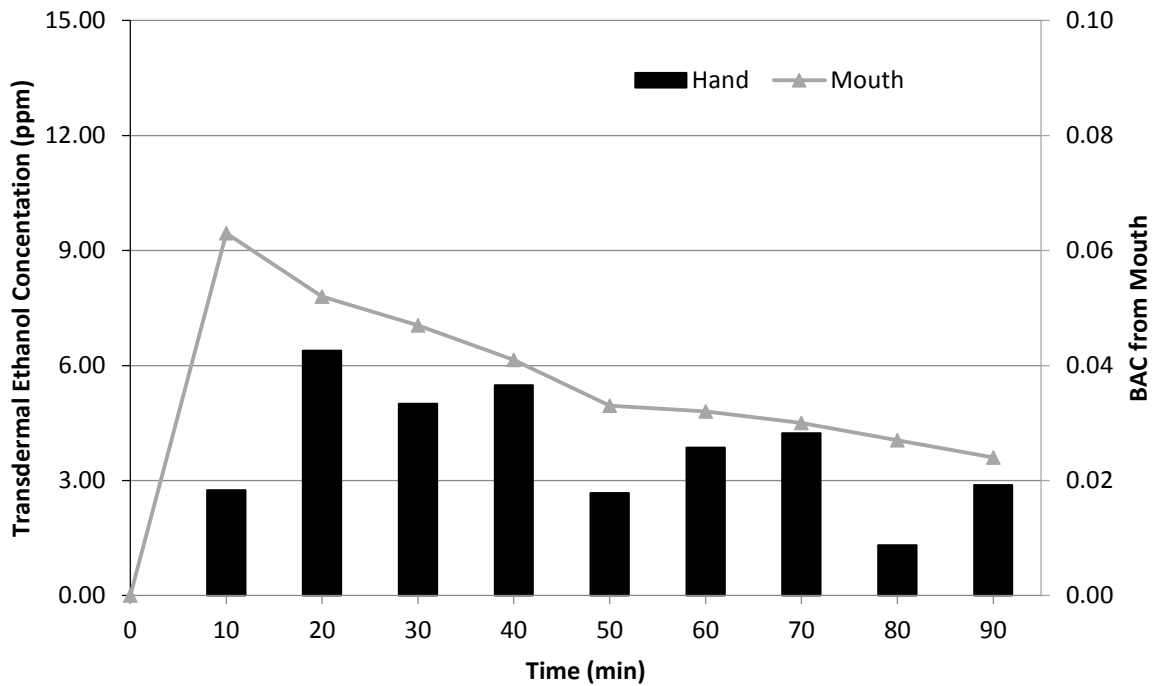


Figure 4.4: Comparison of the transdermal ethanol concentration and BAC measured from the mouth, April 1, 2015.

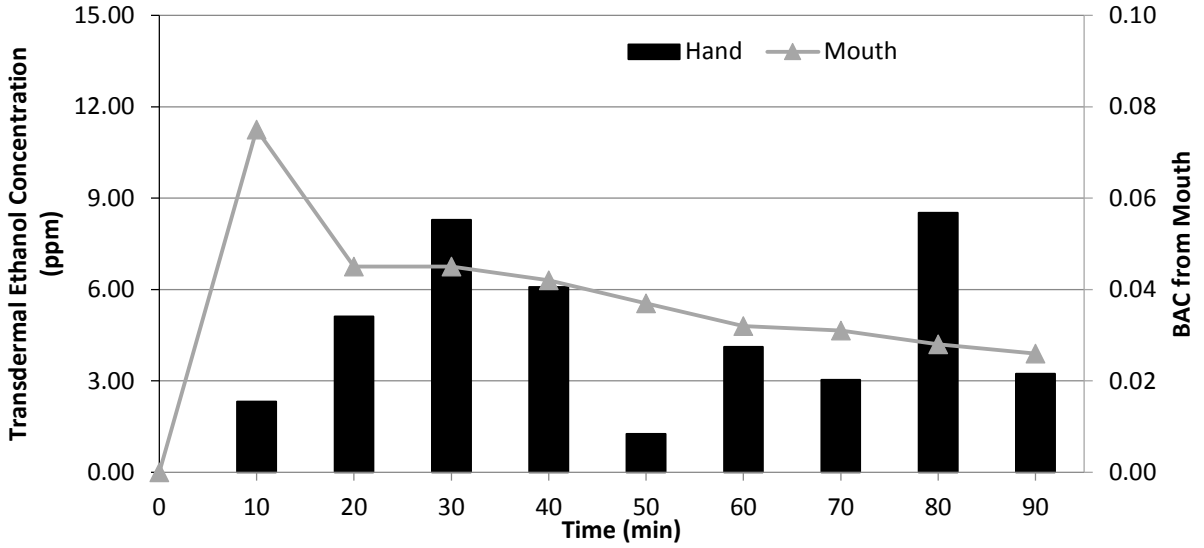


Figure 4.5: Comparison of the transdermal ethanol concentration and BAC measured from the mouth, April 14, 2015.

Due to possible fluctuations in metabolism, there are some variations in both the magnitude of the amount of ethanol emitted from the skin and the time at which the peaks occur. Note that the initial peak appears between 20 and 30 minutes for all of the samples, see Figure 4.6. Figure 4.6 shows the amount of ethanol that is emitted transdermally on six different days. These tests were conducted over three months, at different times in the month (beginning, middle, and end), but all tests were conducted in the morning on an empty stomach. Despite the fluctuations shown, trends are still visible. Note that the first few experiments (including those on Feb. 3 and 4, 2015) were not conducted for a full 90 minutes. The experiments were initially run for 60 minutes, but were later extended to 90 minutes.

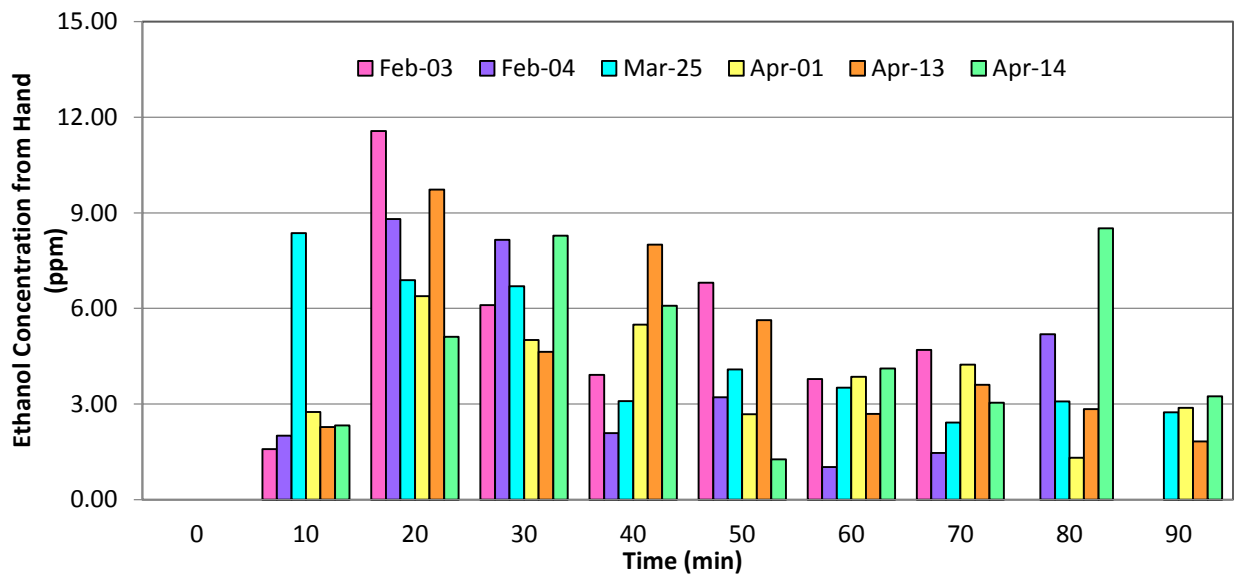


Figure 4.6: Transdermal ethanol concentration shown for different days over three months in 2015.

The average of the measurements shown in Figure 4.6 at both 20 minutes and 30 minutes is shown in Table 4.1. The breathalyzer concentrations were also averaged and are shown in Table 4.1. Comparing the average concentration from the hand to the BAC from the breathalyzer, it is found that the transdermal concentration from the hand is between 5 and 10 ppm at a BAC of 0.05. Therefore, qualitatively, a value of 7.5 ppm (since it is in the middle of the 5 and 10 range) is roughly equivalent to 0.05 BAC. This means that the target value of 5 ppm is appropriate as a threshold, but the lower the detection limit of a sensor, the better.

Table 4.1: Ethanol Concentration for both Hand and Mouth at 20 and 30 Minutes

Time of Peak	20 Minutes	30 Minutes
Average from Hand (ppm)	$8.08 \pm 1.95$	$6.48 \pm 1.26$
Average from Mouth (BAC)	$0.049 \pm 0.003$	$0.047 \pm 0.002$

Note: The error is for a 95.44% confidence interval.

In terms of error, the breathalyzer had a much lower error. Results from the BAC from the mouth are shown in Figure 4.7. Note that at 10 minutes, there was a higher concentration measured on March 25, 2015. This was probably due to residual ethanol in the mouth; however, after 20 minutes, the results are in close agreement with one another.

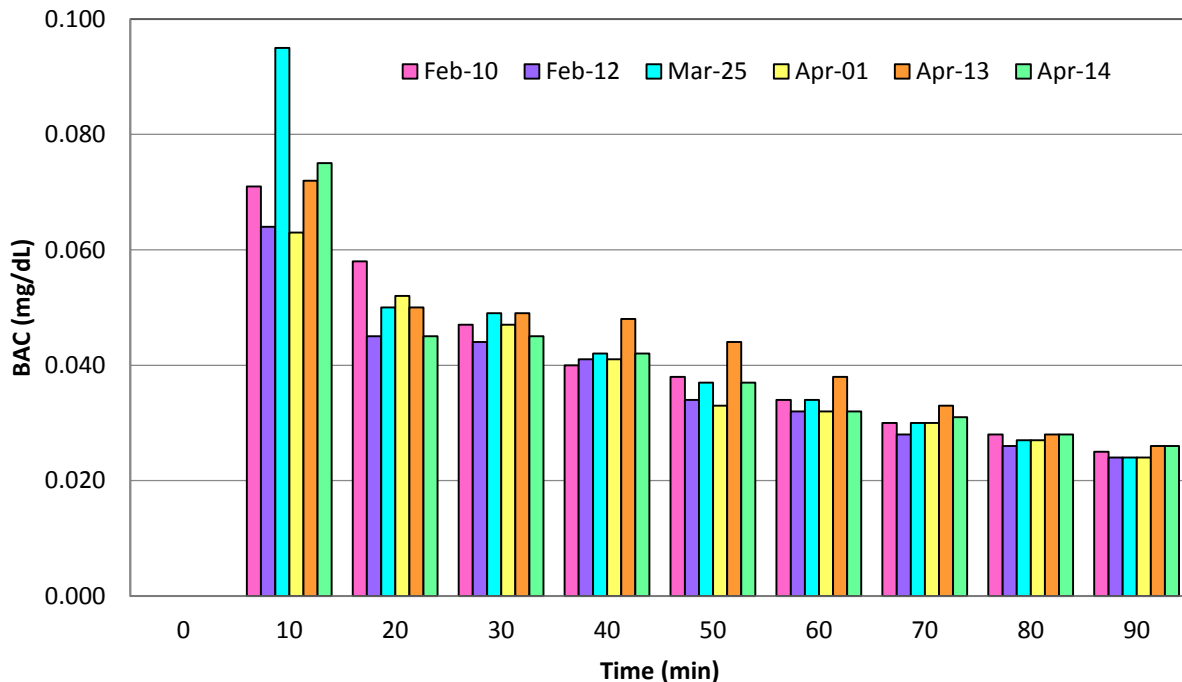


Figure 4.7: BAC from the breathalyzer shown for different days over three months in 2015.

A double shot was taken one day to compare the transdermal ethanol concentration between one shot and two (see Figure 4.8). Note that there was no sample taken at 220 minutes. This was due to the fact that the experiment proceeded longer than anticipated and the person sampled needed to eat. However, it is worth noting that the consumption of food hours after the consumption of ethanol did not affect the rate at which ethanol was metabolized in the body.

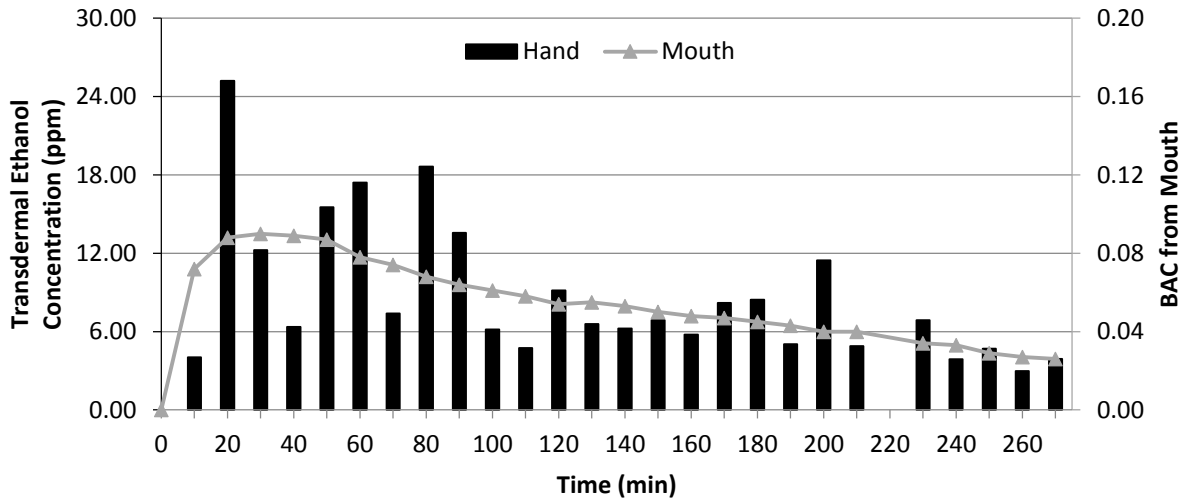


Figure 4.8: Transdermal ethanol concentration and BAC from the breathalyzer for the double shot (3 oz.), February 19, 2015.

Overall, the concentration of transdermal ethanol from the double shot was approximately triple that of the single shots (see Figure 4.9). This means that transdermal ethanol concentration does not likely scale linearly with the amount of alcohol consumed. Note that the six days shown in Figure 4.9 are the same as in Figure 4.6.

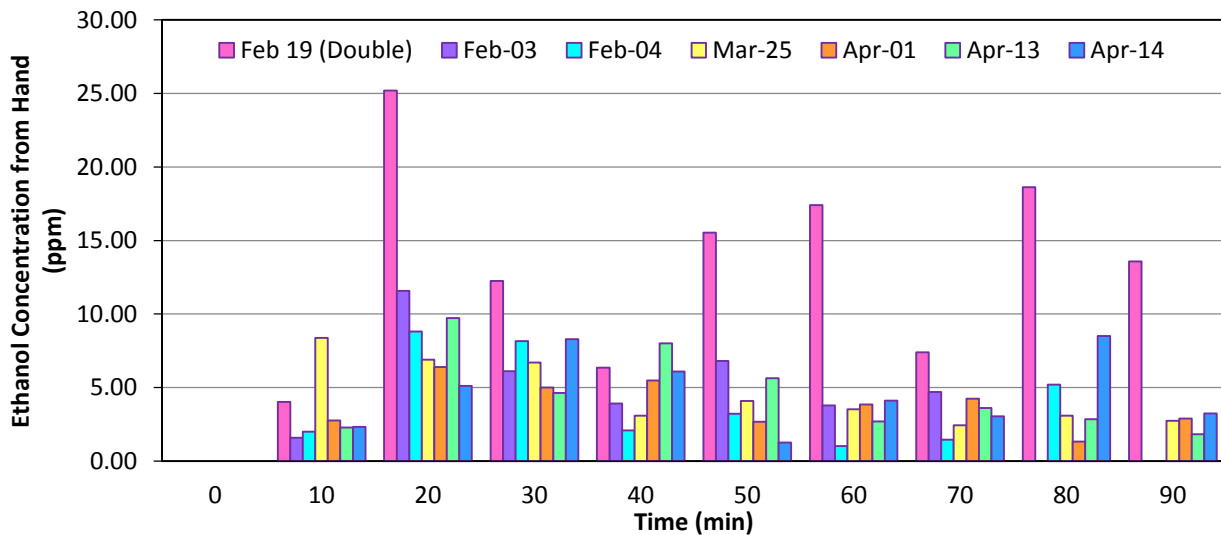


Figure 4.9: Transdermal ethanol concentration measurements for six days plus the double shot (shown as the first bar, February 19) for comparison.

The goal of these experiments was to determine whether a target of 5 ppm for the transdermal ethanol concentration was appropriate. The transdermal ethanol concentration was compared to the BAC that was measured from the mouth using a commercially available breathalyzer. It was found that the transdermal ethanol concentration peaked between 20 and 30 minutes after a single 1.5 oz. shot of vodka was taken. The average concentration at 20 and 30 minutes was between 5 and 10 ppm, given typical experimental fluctuations due to various metabolic processes. Therefore, the transdermal concentration was about 7.5 ppm, which corresponded to a 0.05 BAC. Hence, the target of 5 ppm is appropriate.

Note that since only one person was used for the study, these results can be used to show trends and give an idea about transdermal ethanol concentration, but cannot be used as a definitive concentration comparison as the sample size was too small. These tests were not meant to be a detailed comparison; they were meant to establish a feasible target for the ethanol sensing materials.

## **4.2 Characterization of Polymer Nanocomposites**

The poly (2,5-dimethyl aniline) (P25DMA) nanocomposites (P25DMA doped with  $\text{Al}_2\text{O}_3$ , CuO, NiO,  $\text{TiO}_2$ , and ZnO) were characterized using multiple techniques. The amount of dopant incorporated was measured using energy dispersive X-rays (EDX), the morphology was imaged using scanning electron microscopy (SEM), and the crystallinity of the polymer nanocomposites was analyzed using X-ray diffraction (XRD). Appendix G contains additional characterization data and plots.

### ***4.2.1 Dopant Concentration (EDX) and Morphology (SEM)***

Poly (2,5-dimethyl aniline) (P25DMA) was doped with five different metal oxides at three different concentrations (5, 10 and 20 wt. %). These concentrations of dopant were added during synthesis of the polymer (e.g. 5 wt. %  $\text{Al}_2\text{O}_3$  to 95% P25DMA). The actual amount of metal oxide dopant that was incorporated into the P25DMA was measured using energy dispersive X-rays (EDX, Ametek EDAX, New Jersey, USA). This was used to confirm if the amount of metal oxide dopant (e.g. 5 wt. %) added during synthesis was actually incorporated into the polymer nanocomposite (see Table 4.2). In addition, the morphology of the polymer nanocomposites was imaged using scanning electron microscopy (SEM, Zeiss Merlin, Oberkochen, Germany). Note that additional EDX data appears in Appendix G.

Table 4.2: Weight Percent of Metal in Each Polymer Nanocomposite at Different Concentrations

Polymeric Nanocomposite	Weight Percent of Each Metal (M)				
	Al	Cu	Ni	Ti	Zn
P25DMA 5% MO <sub>x</sub>	0.61	0.16	5.58	3.68	0.34
P25DMA 10% MO <sub>x</sub>	0.57	0.07	8.11	12.37	0.86
P25DMA 20% MO <sub>x</sub>	0.49	0.11	19.14	17.09	46.89

No CuO was incorporated into the P25DMA matrix, which means Cu is unable to coordinate with the P25DMA. Only a small amount of Al<sub>2</sub>O<sub>3</sub> was incorporated into the P25DMA; however, it was the same amount regardless of how much Al<sub>2</sub>O<sub>3</sub> was available during synthesis. Both NiO and TiO<sub>2</sub> were incorporated at roughly the same concentration (within error) as available during synthesis. ZnO showed an odd trend, with very little being incorporated at lower concentrations available (5 and 10 wt. %) and more than double ZnO present in the P25DMA matrix than what was available during synthesis at 20 wt. %. This was due to less polymer being formed around the ZnO nanoparticles, resulting in a higher weight percent of ZnO.

The amount and type of metal oxide present during synthesis affected the resulting P25DMA polymer nanocomposite. Not all of the metal oxides incorporated well into the P25DMA matrix. In addition, the morphology of the P25DMA nanocomposites varied when different metal oxides were present. The following subsections (4.2.1.1 - 4.2.1.5) discuss how including the metal oxides in the synthesis affected the resulting polymer nanocomposite, for each metal oxide. The polymer nanocomposites were compared to the undoped P25DMA.

#### 4.2.1.1 P25DMA doped with CuO

P25DMA was doped with 5 wt. %, 10 wt. %, and 20 wt. % of copper oxide (CuO), denoted as P25DMA 5% CuO, P25DMA 10% CuO, and P25DMA 20% CuO. These concentrations reflect the amount of CuO added during synthesis, with respect to the total polymer weight (i.e. 5% CuO and 95% P25DMA). EDX was used to confirm whether the amount of CuO added during synthesis was actually incorporated into the polymer matrix. It was found that for all three P25DMA nanocomposites, less than 0.20 wt. % of copper was in each sample. This effectively means that no Cu was actually incorporated into the P25DMA (see Table 4.2).

Images from scanning electron microscopy (SEM) show very similar morphology for all three samples that “contain” CuO (see Figure 4.10). The morphologies of P25DMA and the P25DMA made with CuO in Figure 4.10 are different. It is likely that the CuO acted as a “catalyst” and “shaped” the P25DMA by inducing conformational changes or “kinks” in the polymer chain. In essence, the 2,5-dimethyl aniline (the monomer) is able to coordinate with the CuO; however, the strain between the growing polymer chains and CuO is too large to be compensated by a conformational change. This temporary coordination (similar to how a molecule interacts with a

catalyst) would result in morphological changes in the polymer, which were observed (see Figure 4.10a (undoped P25DMA) and Fig. 4.10b-d (P25DMA doped with CuO)).

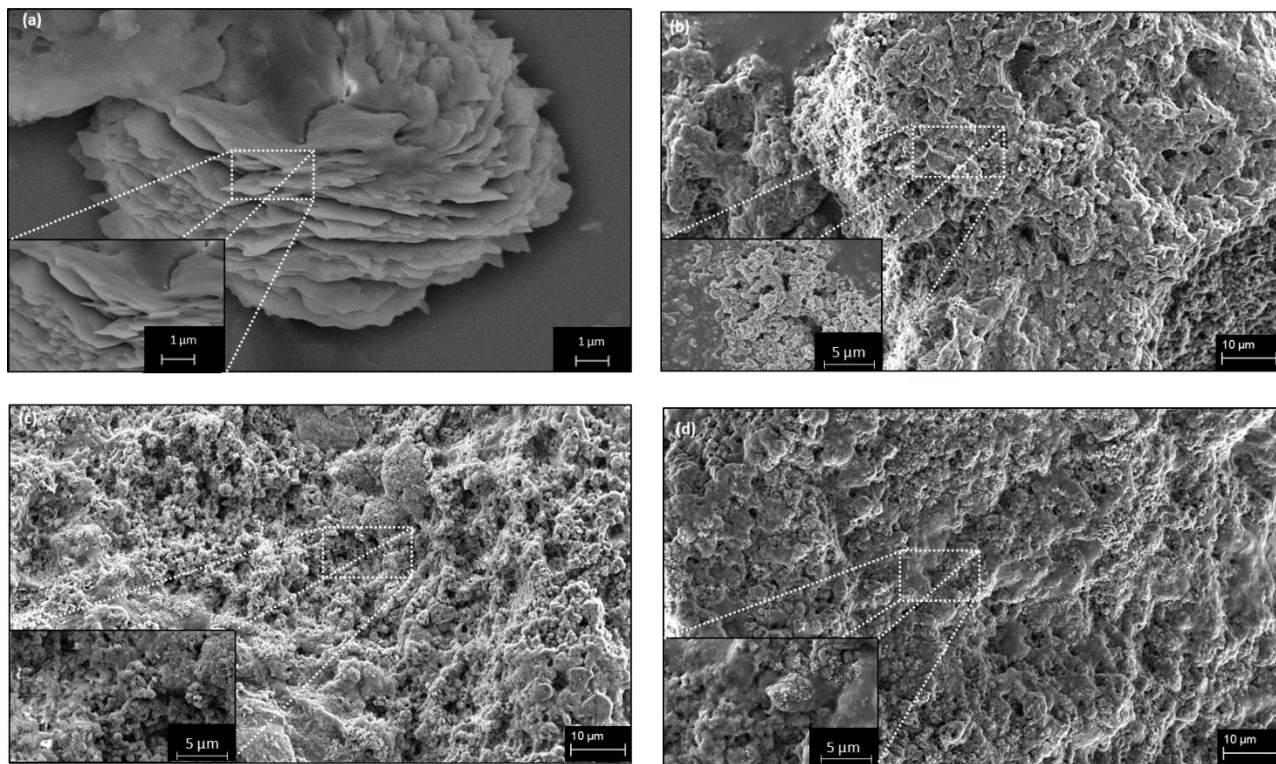


Figure 4.10: SEM of (a) P25DMA, (b) P25DMA 5% CuO, (c) P25DMA 10% CuO, and (d) P25DMA 20% CuO.

The morphology observed for the CuO-doped P25DMA had less surface area exposed than undoped P25DMA, thus reducing the amount of sensing sites available to the analytes. Note that P25DMA had thin layered sheets stacked as petals of a flower (see Figure 4.10 a) and thus, had a large surface area exposed. This large surface area meant that more sensing sites were available for the analytes to bond in P25DMA, which were not present in the P25DMA doped with CuO. Therefore, more analyte was able to sorb onto the undoped P25DMA.

#### 4.2.1.2 P25DMA doped with $Al_2O_3$

P25DMA was doped with 5 wt. %, 10 wt. %, and 20 wt. % of aluminum oxide ( $Al_2O_3$ ), denoted as P25DMA 5%  $Al_2O_3$ , P25DMA 10%  $Al_2O_3$ , and P25DMA 20%  $Al_2O_3$ . These concentrations represent the amount of  $Al_2O_3$  added during synthesis, based on the total polymer weight (i.e. 5%  $Al_2O_3$  and 95% P25DMA). EDX was used to confirm the amount of  $Al_2O_3$  that was actually incorporated into the polymer matrix. It was found that for all three P25DMA nanocomposites, only a small amount of  $Al_2O_3$  (approximately 0.5 wt. %) was actually incorporated (see Table 4.2). Despite increasing the amount of  $Al_2O_3$  available during synthesis from 5 wt. % to 20 wt. %,

roughly the same amount of  $\text{Al}_2\text{O}_3$  was incorporated. Therefore, it is likely that P25DMA can only support a small amount of  $\text{Al}_2\text{O}_3$  without incurring too much strain on the polymer.

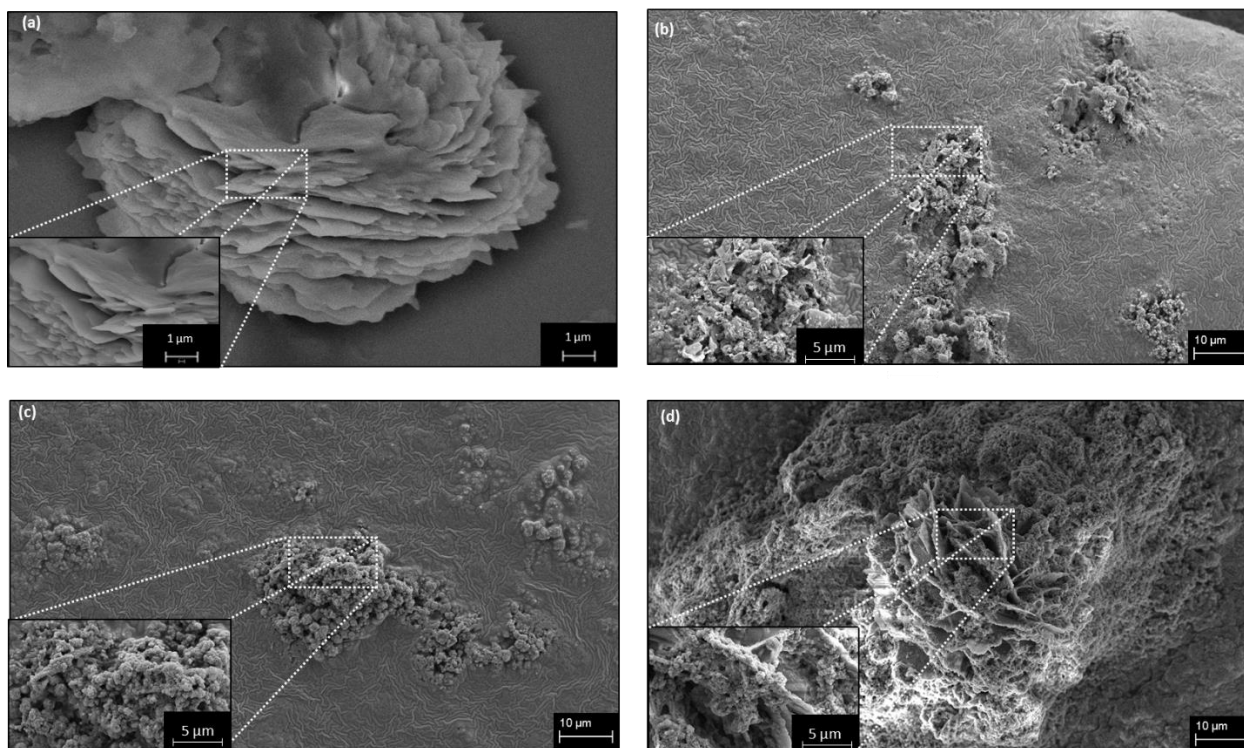


Figure 4.11: SEM images of (a) P25DMA, (b) P25DMA 5%  $\text{Al}_2\text{O}_3$ , (c) P25DMA 10%  $\text{Al}_2\text{O}_3$ , and (d) P25DMA 20%  $\text{Al}_2\text{O}_3$ .

The three  $\text{Al}_2\text{O}_3$  polymeric nanocomposites had similar morphology (see Figure 4.11) and contained approximately the same amount of  $\text{Al}_2\text{O}_3$  (see Table 4.2). The addition of  $\text{Al}_2\text{O}_3$  gave rise to a porous polymer when compared to the undoped P25DMA, and also kept some of the thin layered structure of the undoped P25DMA. This is especially apparent when comparing Fig. 4.11a (undoped P25DMA) to Figure 4.11d (P25DMA 20%  $\text{Al}_2\text{O}_3$ ). The morphology of the P25DMA doped with  $\text{Al}_2\text{O}_3$  had increased surface area and thus more sensing sites available to the analytes. In addition, some  $\text{Al}_2\text{O}_3$  was incorporated into the P25DMA matrix (see Table 4.2). Therefore, with the increased surface area and the incorporation of  $\text{Al}_2\text{O}_3$ , P25DMA doped with  $\text{Al}_2\text{O}_3$  should have improved sensitivity and/or selectivity to ethanol.

#### 4.2.1.3 P25DMA Doped with ZnO

Very little zinc oxide (ZnO) was incorporated into P25DMA when 5 wt. % and 10 wt. % were present during synthesis (see Table 4.2). A significantly higher amount of ZnO was observed when 20 wt. % was used during synthesis. According to the EDX, double the amount of ZnO was incorporated, than initially present, which means much less polymer (P25DMA) was polymerized when so much ZnO was present.



From the SEM images (see Figure 4.12d), it appears that the synthesis of P25DMA 20% ZnO resulted in ZnO nanoparticles (or aggregated ZnO nanoparticles) coated in P25DMA, rather than ZnO nanoparticles dispersed within the P25DMA matrix (for instance, contrast Figure 4.12d with Figure 4.12c). Following this observation, this would mean that less 2,5-dimethyl aniline monomer was able to polymerize in the presence of ZnO, resulting in a lower conversion to P25DMA (in other words, it appears that the presence of ZnO effectively inhibits the polymerization of 2,5-dimethyl aniline). Hence, a smaller amount of P25DMA is produced. This reduced amount of P25DMA would explain the 47 wt. % of ZnO observed within the P25DMA 20% ZnO sample. Given the evidence from both the SEM (Figure 4.12d) and EDX (Table 4.2), this is likely the case.

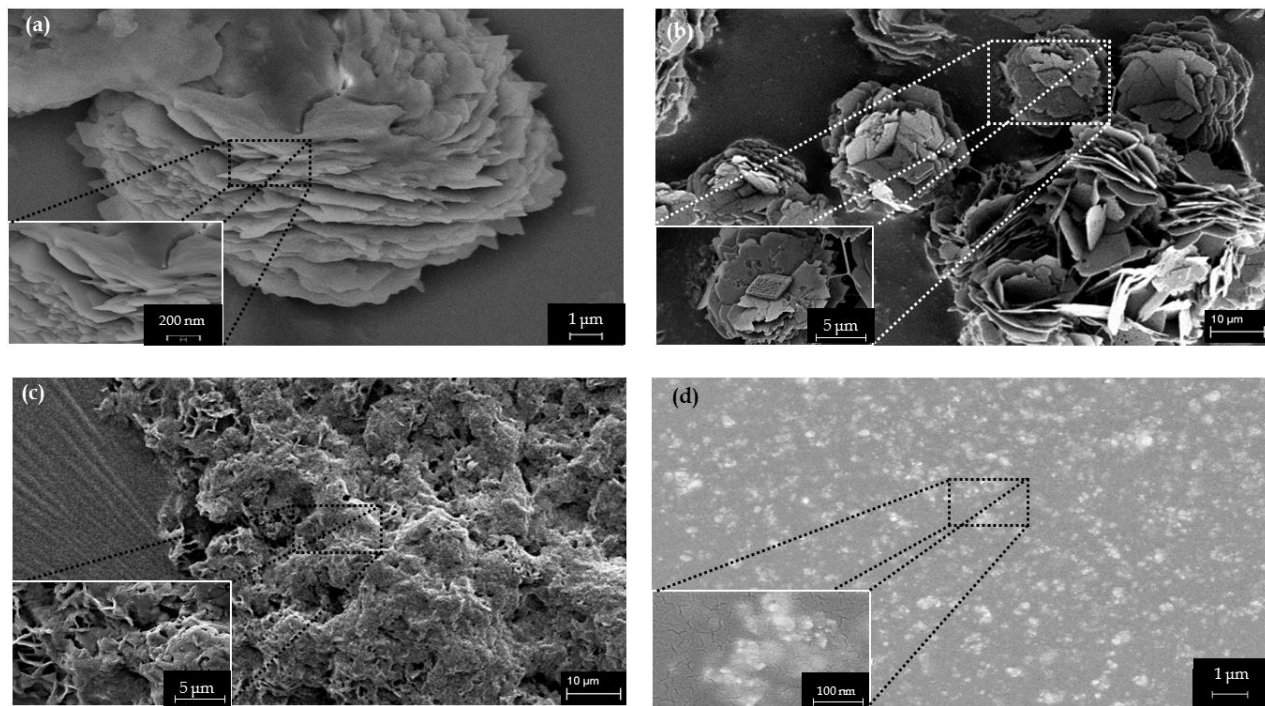


Figure 4.12: SEM images of (a) P25DMA, (b) P25DMA 5% ZnO, (c) P25DMA 10% ZnO, and (d) P25DMA 20% ZnO.

Only a small amount of ZnO was incorporated when 5% ZnO was available during synthesis and it appears that the ZnO did not affect the structure; in fact, it may have increased the spacing between the P25DMA layers (see Figure 4.12b). The particles that appear in the center of the “flowers” are ZnO nanoparticles coated in P25DMA. As more ZnO was available, the morphology deteriorated; however, some of the P25DMA sheets can still be seen in the 10% ZnO sample (see Figure 4.12c). Therefore, not much ZnO can be incorporated into the P25DMA matrix.

#### 4.2.1.4 P25DMA doped with NiO

NiO was incorporated at roughly the amount added during the polymerization (see Table 4.2). This means that Ni is able to coordinate with the P25DMA, by binding to the nitrogen in the amine groups (Han et al., 2006), without causing too much strain on the polymer chain. This is ideal for incorporating nanoparticles into a polymer matrix, where the polymer remains almost intact and is able to bind to the nanoparticles.

Increasing the amount of NiO incorporated into the P25DMA changed the morphology of the polymeric nanocomposite (see Figure 4.13). As more NiO was incorporated, the thin sheets of P25DMA (Figure 4.13 a) changed into more porous and globular structures (Figures 4.13 b-d). This is due to the Ni-N bonds causing “kinks” along the polymer chain where the ring in P25DMA changes conformation, to reduce strain caused by the NiO binding. More “kinks” result in a more porous structure, since the P25DMA chains are no longer able to stack as compactly.

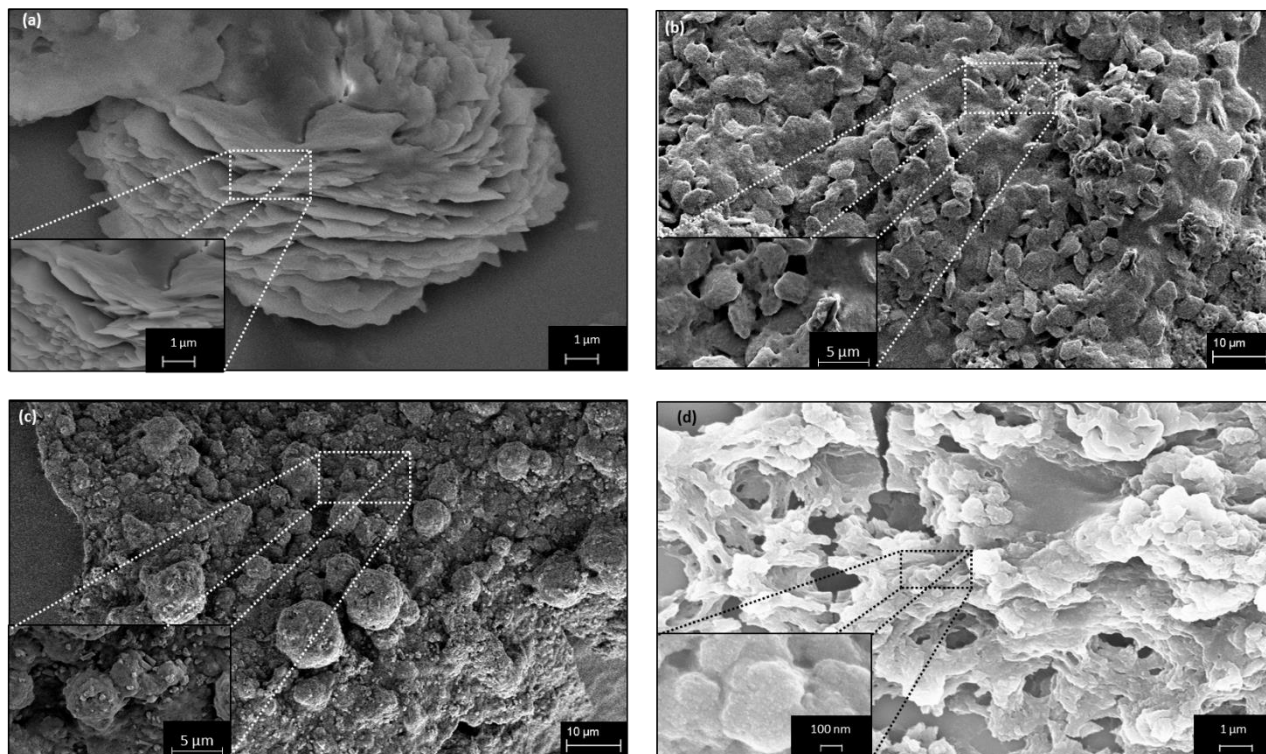


Figure 4.13: SEM images of (a) P25DMA, (b) P25DMA 5% NiO, (c) P25DMA 10% NiO, and (d) P25DMA 20% NiO.

#### 4.2.1.5 P25DMA doped with TiO<sub>2</sub>

The incorporation of TiO<sub>2</sub> to P25DMA was effective and the amount added during polymerization (5%, 10%, and 20%) was approximately the amount of TiO<sub>2</sub> incorporated into the P25DMA, by weight (see Table 4.2). NiO and TiO<sub>2</sub> have energy bands (or levels) where their electrons sit, that

are close in energy to one another (Ibupoto et al., 2014). Given this, it is likely that some of the energy levels for P25DMA are similar to those of NiO and TiO<sub>2</sub>, given how well both metal oxides were able to coordinate to P25DMA.

In addition, the morphology of the P25DMA doped with TiO<sub>2</sub> was similar for all three concentrations of TiO<sub>2</sub> but different from that of P25DMA (see Figure 4.14). This suggests that as TiO<sub>2</sub> is incorporated into the P25DMA, the morphology also is changed due to “kinks” that form along the polymer chains, similar to what was described earlier for NiO.

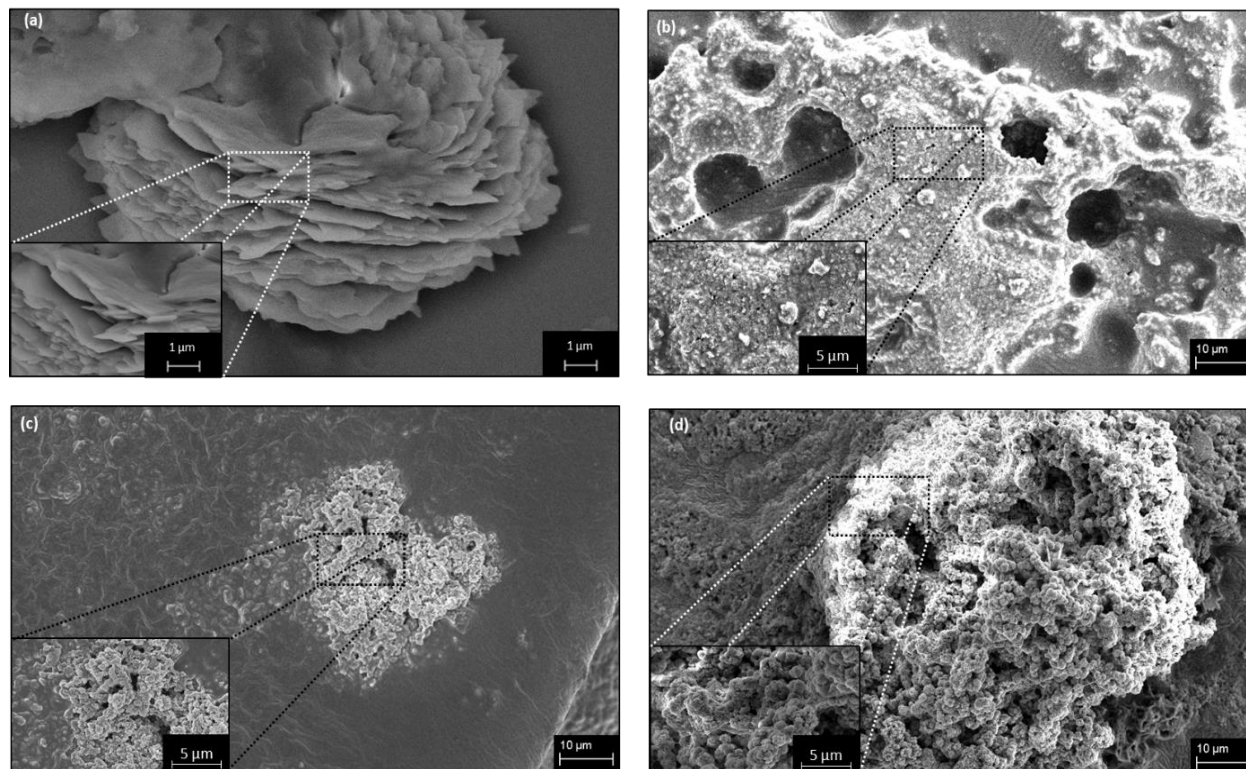


Figure 4.14: SEM images of (a) P25DMA, (b) P25DMA 5% TiO<sub>2</sub>, (c) P25DMA 10% TiO<sub>2</sub>, and (d) P25DMA 20% TiO<sub>2</sub>.

#### 4.2.2 Crystallinity (XRD)

The polymer nanocomposites were also characterized using X-ray diffraction (XRD, X'Pert PRO PANalytical Material Powder Diffractometer (MPD), source: CuK-alpha radiation, wavelength: 0.154 nm, Almelo, The Netherlands) to determine their crystallinity. As seen in Figure 4.15, all of the polymeric nanocomposites are semi-crystalline, with the least crystalline material (no distinct crystalline peaks) being P25DMA doped with 5% CuO (see Figure 4.15b). Since the peaks in XRD are additive, the additional peaks observed (when compared to the undoped P25DMA) are from the addition of the metal oxide or a change in the morphology (resulting in more

crystallinity) caused by the metal oxide (see Figure 4.16). Additional XRD information is available in Appendix G.

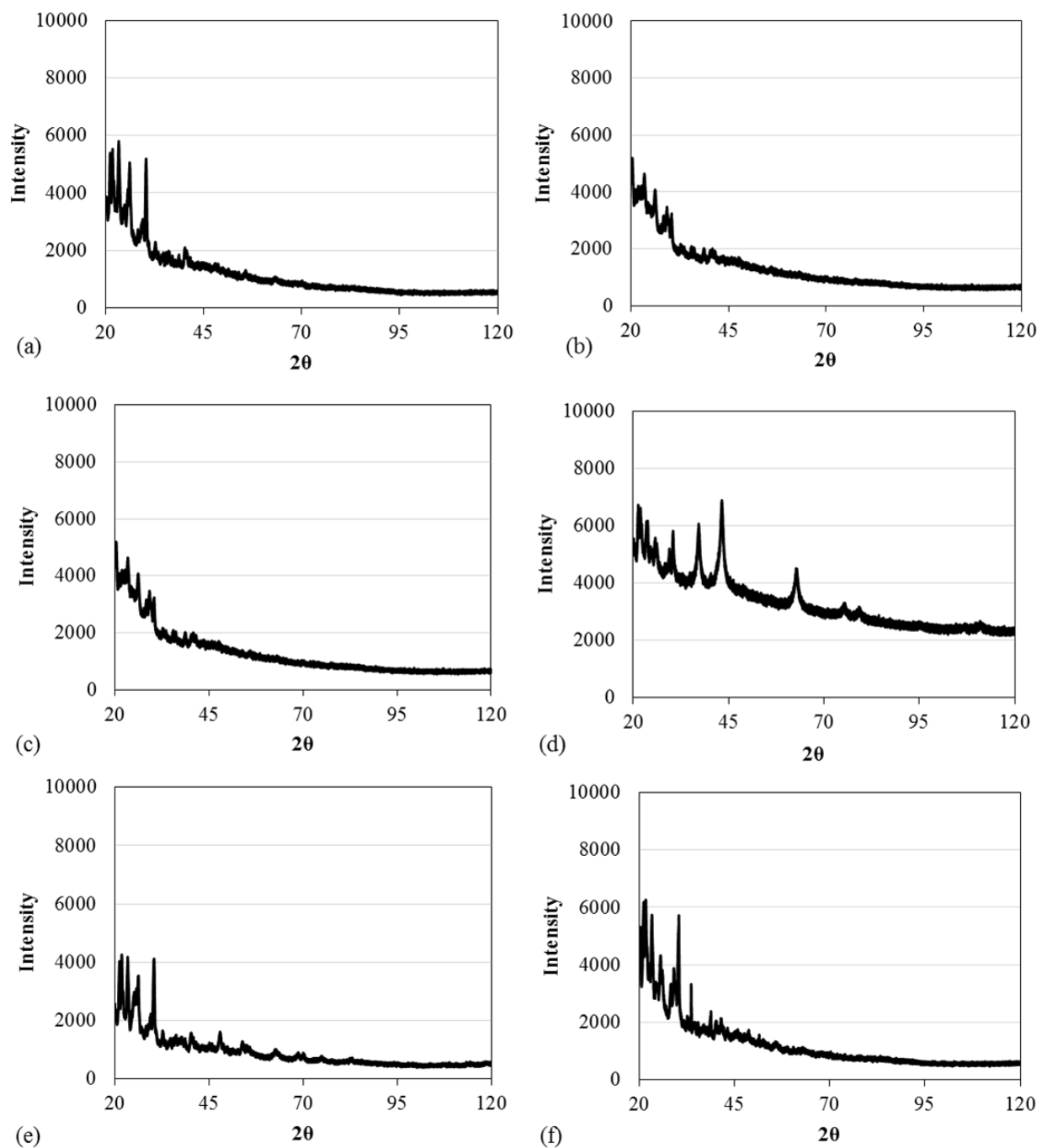


Figure 4.15: XRD of (a) P25DMA, (b) P25DMA 5% CuO, (c) P25DMA 5% Al<sub>2</sub>O<sub>3</sub>, (d) P25DMA 5% NiO, (e) P25DMA 5% TiO<sub>2</sub>, and (f) P25DMA 5% ZnO

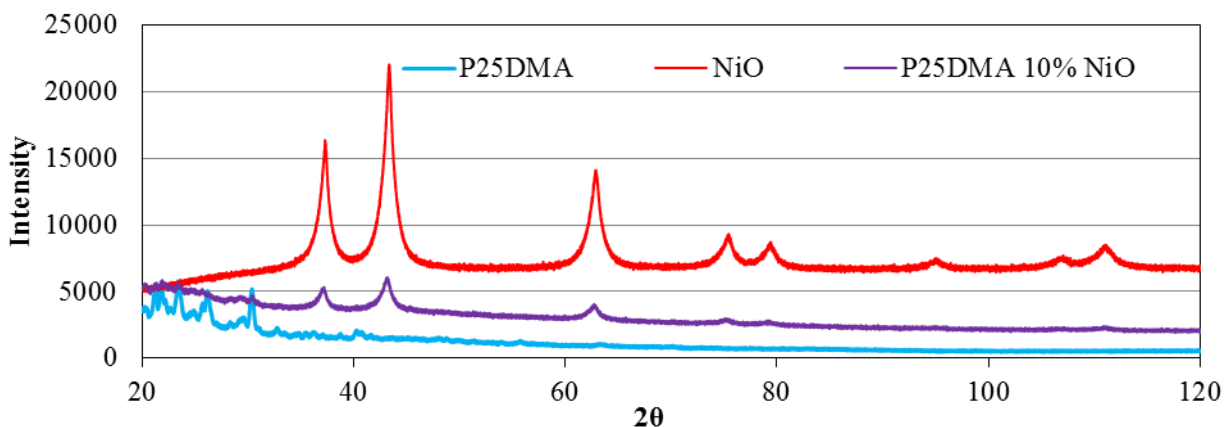


Figure 4.16: XRD of P25DMA, NiO nanoparticles, P25DMA, and P25DMA 10% NiO.

### 4.3 Ethanol Sorption Studies

#### 4.3.1 Polyaniline (PANI) and its Derivatives

Initially, polyaniline (PANI) and two of its derivatives, poly (*o*-anisidine) (PoANI) and poly (2,5-dimethyl aniline) (P25DMA), were evaluated as potential sensing materials for ethanol. Each polymer sample was exposed to 5 ppm of ethanol and the amount of ethanol sorbed was measured (see Figure 4.17).

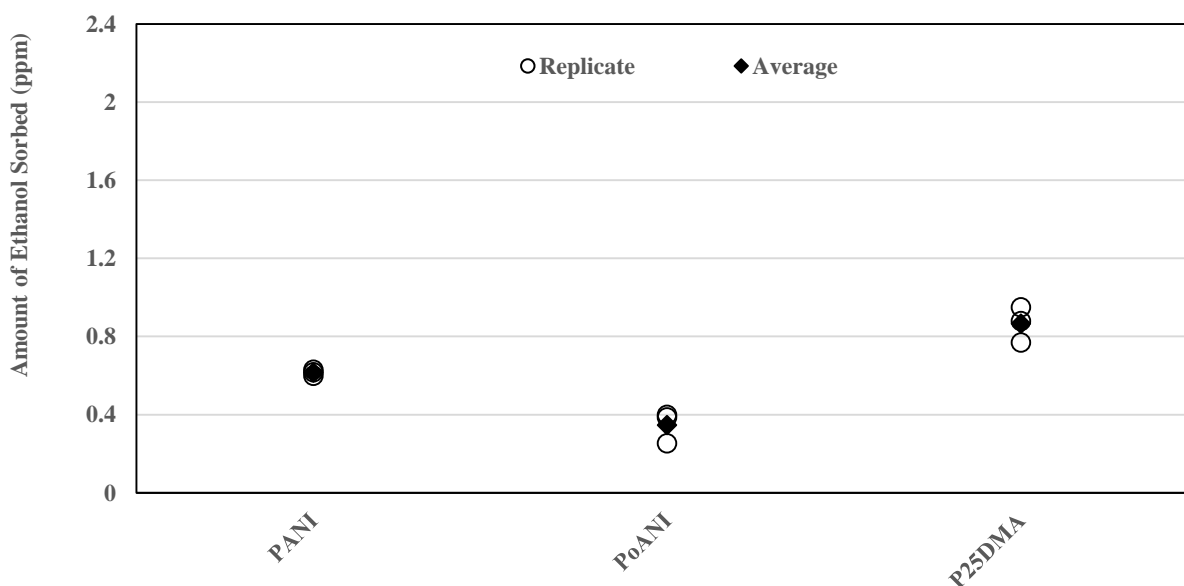


Figure 4.17: Amount of ethanol sorbed onto PANI, PoANI, and P25DMA.

Analysis of variance (ANOVA) found that there was a statistically significant difference between the average amount of ethanol sorbed (see Section F.1.1 in Appendix F). Further analysis (the

Bonferonni t-test and the Fisher's least significant difference (LSD)) found that PoANI and P25DMA sorbed significantly different amounts of ethanol; however, the amount of ethanol PANI sorbed was not significantly different from either PoANI or P25DMA (see Section F.1.1 in Appendix F). Therefore, P25DMA was more sensitive to ethanol than PoANI; however, neither P25DMA nor PoANI were significantly better or worse (respectively) than PANI at sorbing ethanol.

The addition of a methoxy group to PANI (e.g. PoANI) reduced the sensitivity to ethanol. This may be due to the amine in PoANI binding to the methoxy group and reducing the number of sensing sites available to ethanol. The two methyl side groups on P25DMA, on the other hand, improved the sorption of ethanol which was likely due to the reduced packing efficiency of P25DMA versus PANI. The methyl groups provided steric hindrance that created larger interstitial spaces in the polymer chains of P25DMA, compared to PANI, allowing ethanol to diffuse more easily into the P25DMA matrix.

#### 4.3.2 Doped Polyaniline (PANI) and Poly (o-anisidine) (PoANI)

In an attempt to improve the sensitivity of polyaniline (PANI) and poly (o-anisidine) (PoANI), both polymers were doped with 10 wt. % and 20 wt. % NiO or ZnO. Note that each doped polymer will be referred to by the amount of dopant added during synthesis (e.g. PANI doped with 10 wt. % NiO will be referred to as PANI 10% NiO, and so on). These four polymer nanocomposites were also exposed to 5 ppm of ethanol and the amount sorbed was measured (see Figure 4.18). These results were compared to those with the undoped polymers.

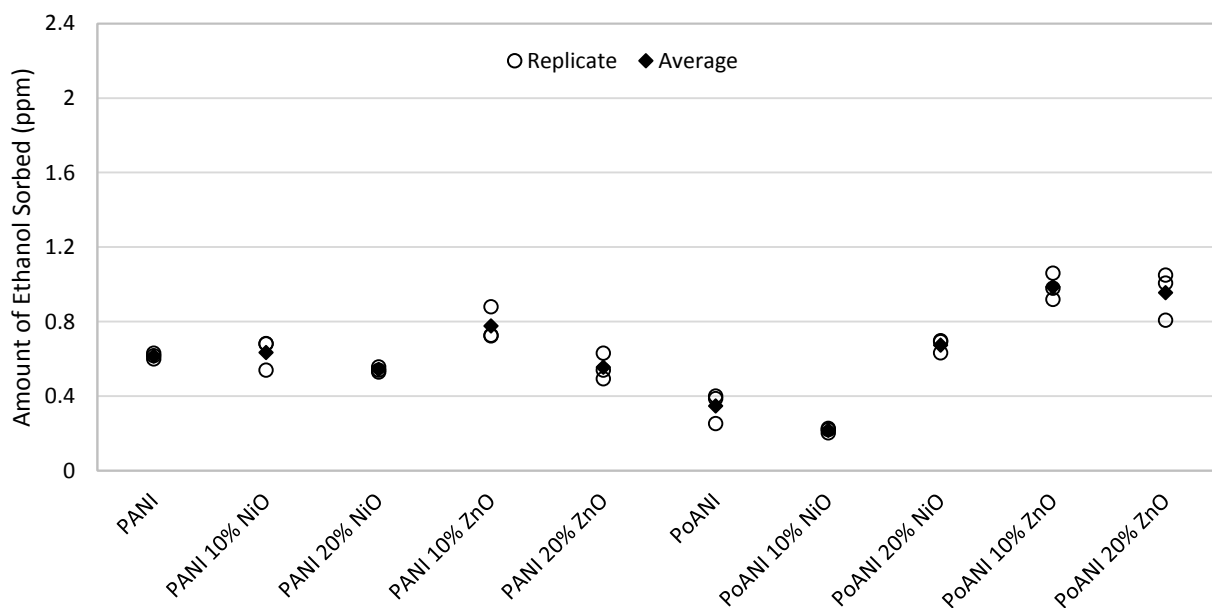


Figure 4.18: Ethanol sorption onto undoped and doped PANI and PoANI.

The addition of either NiO or ZnO did not significantly change the amount of ethanol that sorbed onto PANI; however, the addition of NiO and, especially ZnO, did significantly affect the amount of ethanol sorbed onto PoANI. See Section F.1.2 in Appendix F for the summary of the statistical analysis.

The apparent reduction in ethanol sorption when 10 wt. % NiO was incorporated into PoANI (seen in Figure 4.18) was not actually significantly different (at a 95% confidence level). Therefore, the addition of 10 wt. % NiO did not significantly affect the sensitivity of PoANI to ethanol. This is likely to be a result of competing sensing mechanisms (hydrogen bonding with PoANI vs. metal coordination with the NiO) caused by the addition of NiO (see Section 6.1). Note that ethanol and NiO compete for the amine groups on PoANI, since the NiO coordinates with PoANI by binding to the amine groups on PoANI, which removes sensing sites for analytes like ethanol. There is, however, a significant (at a 95% confidence level) increase in ethanol sorption for PoANI 20% NiO when compared to undoped PoANI, which means that the sensing mechanisms related to NiO have become dominant (i.e. the metal coordination with NiO has overcome the reduction in sensing sites caused by NiO coordinating with PoANI).

The addition of both 10 wt. % and 20 wt. % ZnO did improve the sorption of ethanol to PoANI; however, there was no significant difference between the amounts of ethanol sorbed for PoANI 10% ZnO compared to PoANI 20% ZnO. This means that adding more ZnO during synthesis (20% vs. 10%) did not improve the sorption. Therefore, any further testing should be done on the material with 10% ZnO, since PoANI 10% ZnO is more cost effective to produce because the nanoparticles are more expensive than the polymer.

#### ***4.3.3 Doped Poly (2,5-dimethyl aniline) (P25DMA)***

Since P25DMA performed the best out of the PANI and PANI derivatives, P25DMA was doped with five different metal oxide dopants ( $\text{Al}_2\text{O}_3$ , CuO, NiO,  $\text{TiO}_2$ , and ZnO) at three different concentrations (5 wt. %, 10 wt. %, and 20 wt. %). Note that each doped polymer will be referred to by the amount of dopant added during synthesis (e.g. P25DMA doped with 5 wt. %  $\text{Al}_2\text{O}_3$  will be referred to as P25DMA 5%  $\text{Al}_2\text{O}_3$ , and so on). This resulted in a total of 16 sensing materials, including undoped P25DMA. Each sensing material was exposed to 5 ppm of ethanol and the amounts sorbed are shown in Figure 4.19.

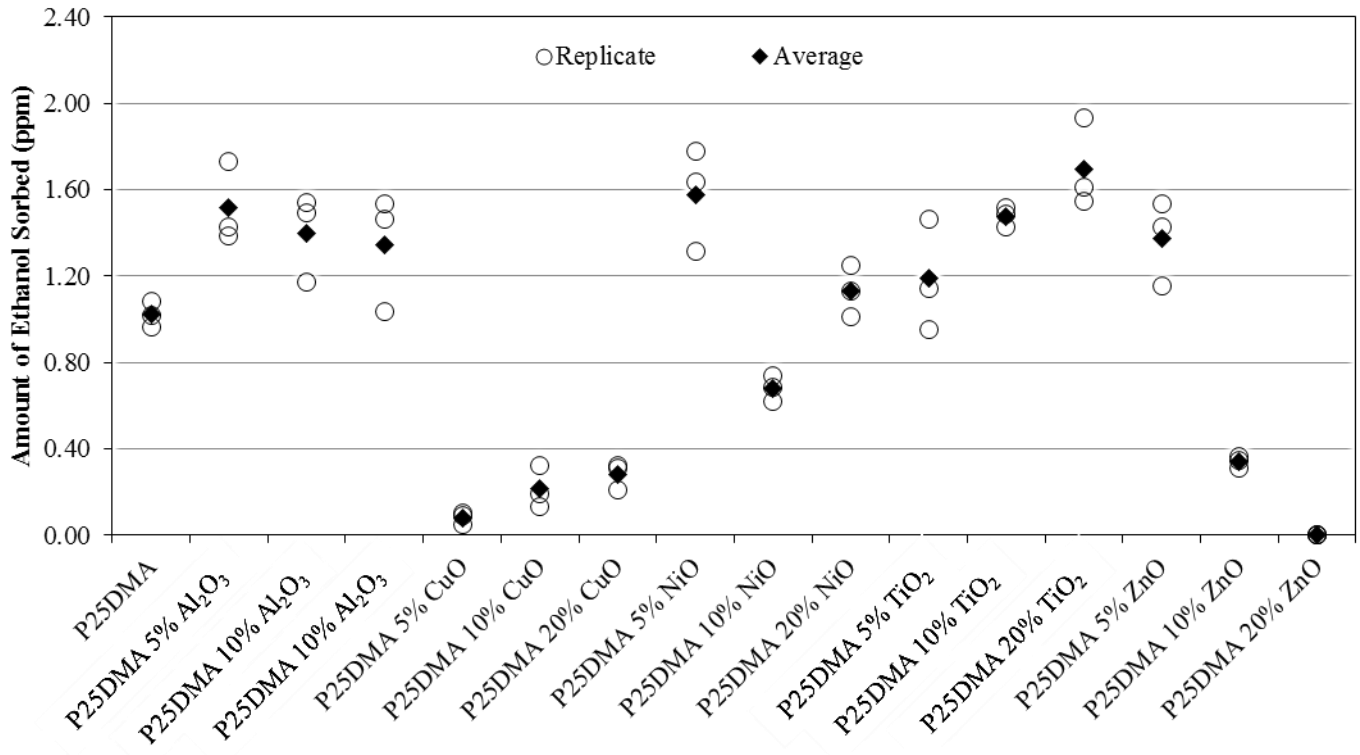


Figure 4.19: Ethanol sorption onto undoped and doped P25DMA.

#### 4.3.3.1 P25DMA Doped with Al<sub>2</sub>O<sub>3</sub>

A comparison of the three Al<sub>2</sub>O<sub>3</sub> polymer nanocomposites showed that the amounts of ethanol sorbed onto the polymer nanocomposites were not significantly different (at a 95% confidence level) despite the addition of more Al<sub>2</sub>O<sub>3</sub> during synthesis (see Figure 4.20). This is further support that only a small percentage of Al<sub>2</sub>O<sub>3</sub> can be incorporated into P25DMA (see Table 4.2 in Section 4.2.1).



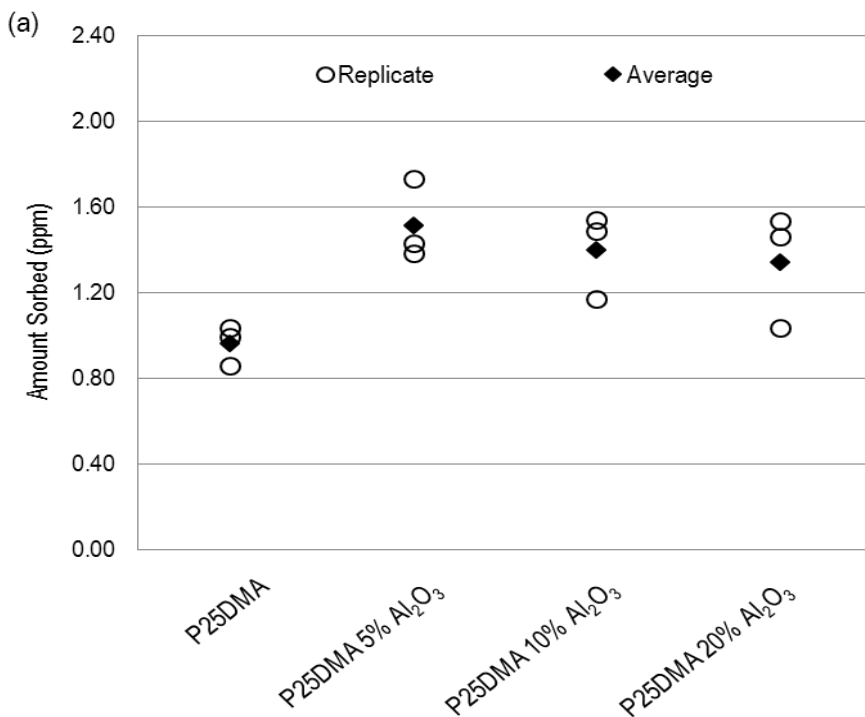


Figure 4.20: Ethanol sorption of P25DMA and P25DMA doped with 5%, 10%, and 20% Al<sub>2</sub>O<sub>3</sub>.

By incorporating only 5% Al<sub>2</sub>O<sub>3</sub> into P25DMA, the sensitivity to ethanol significantly increased (the amount sorbed almost doubled). Since the addition of more Al<sub>2</sub>O<sub>3</sub> during synthesis did not improve the sorption, only 5 wt. % of Al<sub>2</sub>O<sub>3</sub> is needed to significantly improve the sorption of ethanol on P25DMA.

#### 4.3.3.2 P25DMA Doped with CuO

P25DMA doped with 5% CuO, 10% CuO, and 20% CuO were individually evaluated using 5 ppm ethanol. The amount of ethanol sorbed onto the P25DMA doped with CuO was the same (a low level, close to zero) for all three CuO samples (see Figure 4.21). The amounts of ethanol sorbed onto each CuO nanocomposite were not significantly different, at a confidence level of 95%. Therefore, adding more CuO to P25DMA during polymerization did not affect the sorption of ethanol (see Figure 4.21); however, the addition of CuO did significantly decrease the amount of ethanol sorbed compared to the undoped P25DMA. The CuO doped P25DMA sorbed approximately five times less than the amount of ethanol sorbed onto the undoped P25DMA.

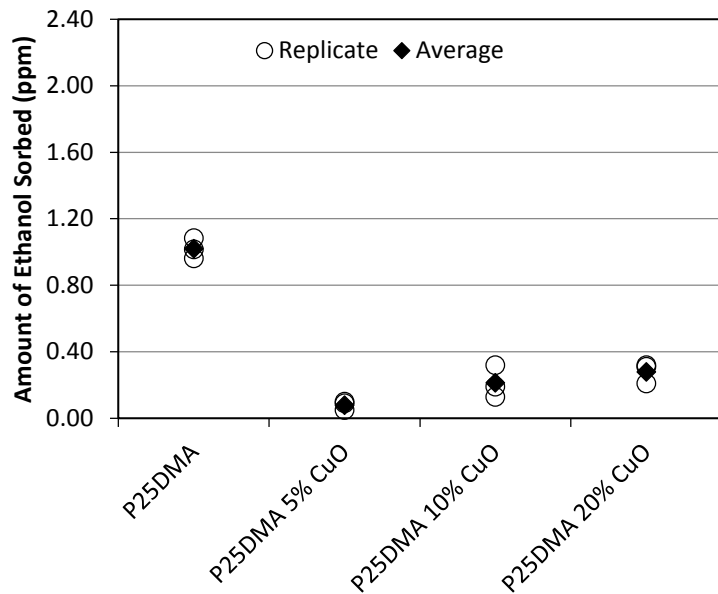


Figure 4.21: Ethanol sorption of P25DMA doped with CuO.

#### 4.3.3.3 P25DMA Doped with NiO

The addition of 5 wt. % NiO increased the amount of ethanol sorbed; however, increasing the concentration of NiO to 10 wt. % significantly reduced the amount of ethanol sorbed. The trend then reversed itself when more NiO (20 wt. %) was added (see Figure 4.22). This trend can be explained by the dominant mechanism at different concentrations of NiO (see Section 6.1).

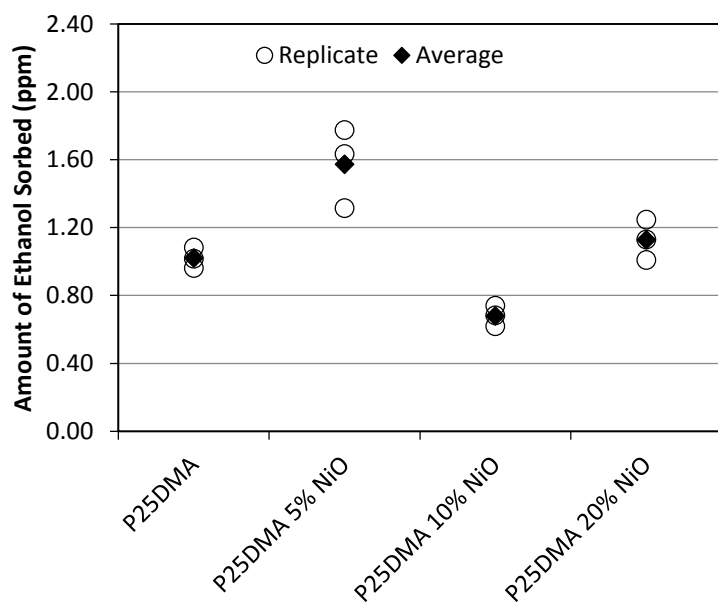


Figure 4.22: Amount of sorbed analyte for P25DMA, P25DMA 5% NiO, P25DMA 10% NiO, and P25DMA 20% NiO.

For both P25DMA and P25DMA 5% NiO, the dominant mechanism was hydrogen bonding between the amine group of P25DMA and the oxygen on ethanol. However, as more NiO was added, the amines in P25DMA were less available to the analytes because the Ni bound to the amine instead. At a certain point, somewhere between 5 wt. % and 10 wt. %, metal coordination took over as the dominant mechanism, where the gas analytes were more likely to bond with the Ni than hydrogen bond with the amine. This resulted in a significantly reduced amount of sorption because coordinating with the Ni was limited (by less access to the NiO nanoparticles) through diffusion. As more NiO was added (increasing to 20 wt. %), more Ni was available for the analyte to coordinate to and thus, sorption was increased (Stewart and Penlidis, 2016).

#### 4.3.3.4 P25DMA Doped with TiO<sub>2</sub>

Overall, it was found that adding more TiO<sub>2</sub> improved the amount of each analyte sorbed, with P25DMA 20% TiO<sub>2</sub> sorbing the most ethanol (see Figure 4.23). Note that the addition of 5% TiO<sub>2</sub> did not significantly affect the sorption of ethanol (at a 95% confidence level), whereas the addition of 10% and 20% TiO<sub>2</sub> did significantly improve the amount of ethanol sorbed onto the polymer nanocomposite, compared to the undoped P25DMA. This is likely due to the P25DMA doped with TiO<sub>2</sub> having more “kinks” along the polymer chains where the TiO<sub>2</sub> is bound and thus, larger interstitial spaces are formed, allowing easier diffusion of the analytes.

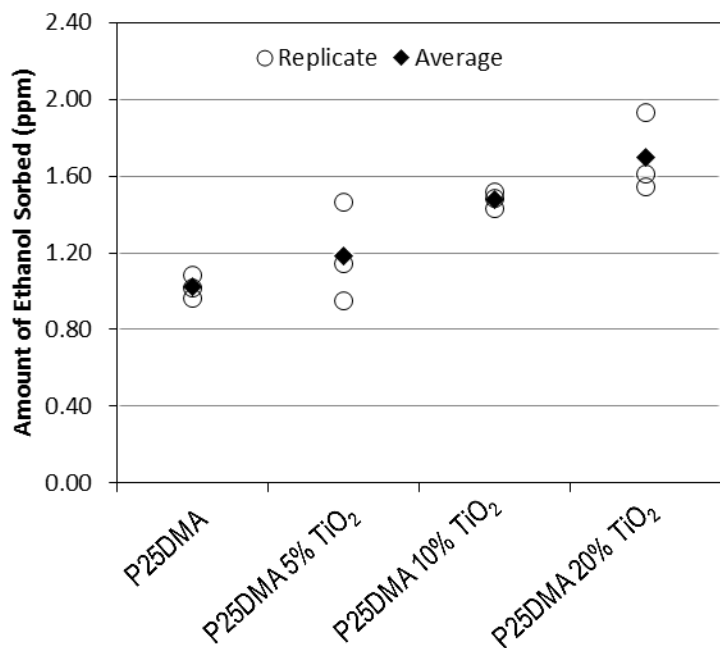


Figure 4.23: Amount of sorbed analyte for P25DMA, P25DMA 5% TiO<sub>2</sub>, P25DMA 10% TiO<sub>2</sub>, and P25DMA 20% TiO<sub>2</sub>.

#### 4.3.3.5 P25DMA Doped with ZnO

ZnO did not incorporate well into P25DMA, as seen in Table 4.2. A tiny amount of ZnO (0.34 wt. %) that incorporated in the P25DMA 5% ZnO did appear to improve the sorption of ethanol (see Figure 4.24); however, both the Bonferroni t-test and the Fisher's LSD determined that there was no significant difference between P25DMA and P25DMA 5% ZnO (see Section F.1.3 in Appendix F). On the other hand, the amount of ethanol sorbed by both P25DMA 10% ZnO and P25DMA 20% ZnO was significantly less than the amount that sorbed onto the undoped P25DMA (at a 95% confidence level). Therefore, in general, as more ZnO was added during synthesis, the amount of ethanol sorbed significantly decreased (see Figure 4.24).

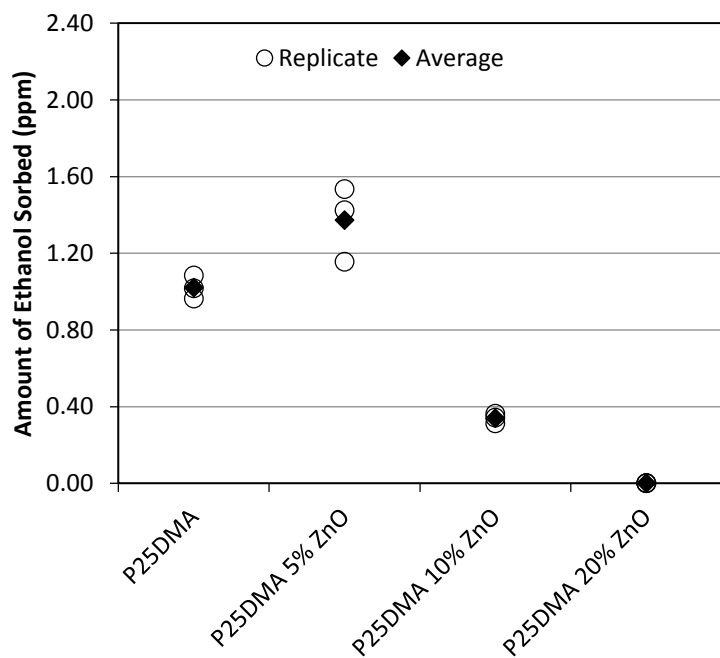


Figure 4.24: Amount of sorbed analyte for P25DMA, P25DMA 5% ZnO, P25DMA 10% ZnO, and P25DMA 20% ZnO.

P25DMA 20% ZnO actually sorbed no ethanol, when exposed to 5 ppm. This is likely due to the ZnO nanoparticles being coated with a thin layer of P25DMA that “pacified” the ZnO. In addition, ethanol could not bind to P25DMA due to the amine groups on P25DMA binding to the ZnO.

## 4.4 Selectivity Studies

Based on the sorption tests shown in Section 4.3, the most promising sensing materials for ethanol were P25DMA doped with 5% Al<sub>2</sub>O<sub>3</sub>, 5% ZnO, 5% and 20% NiO, and 5%, 10%, and 20% TiO<sub>2</sub>. These materials were further evaluated for selectivity along with undoped P25DMA and P25DMA10% NiO (for completeness of the NiO trends). Five interferent gases (formaldehyde,

methanol, acetaldehyde, acetone, and benzene) were used to evaluate the selectivity towards ethanol.

While P25DMA sorbed significantly less ethanol than when doped with various metal oxides at certain concentrations, undoped P25DMA was evaluated for its selectivity to ethanol and used as a reference with which to compare the doped P25DMA sensing materials. Note that undoped P25DMA is more selective to formaldehyde and methanol than to ethanol. In addition, the values reported for each gas (to compare selectivity) represent an average of three independent replicates.

#### 4.4.1 P25DMA Doped with $Al_2O_3$

A comparison of the three  $Al_2O_3$  polymer nanocomposites showed that the amounts of ethanol sorbed onto the polymer nanocomposites were not significantly different (at a 95% confidence level, see Section F.1.3 in Appendix F), despite the addition of more  $Al_2O_3$  during synthesis (see Figure 4.25 a). Due to the similar morphologies (see Figure 4.11 in Section 4.2.1.2), uptake of  $Al_2O_3$  (see Table 4.2), and sorption of ethanol, only P25DMA 5%  $Al_2O_3$  was used to evaluate further the nanocomposite's effectiveness as a sensing material for different toxic analytes (Figure 4.25 b).

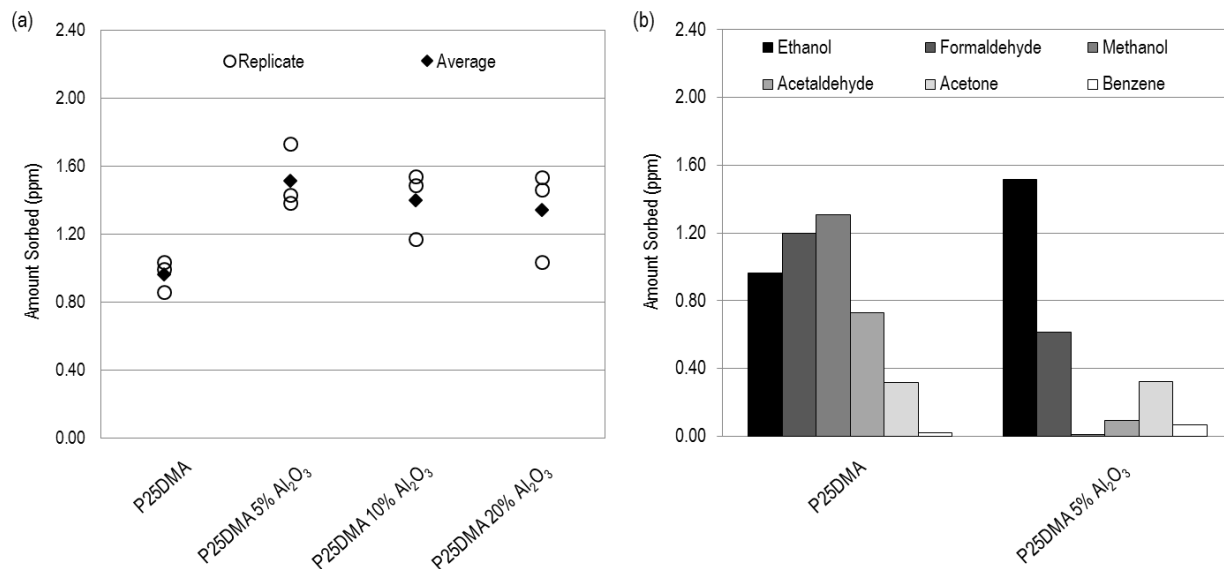


Figure 4.25: (a) Ethanol sorption of P25DMA and P25DMA doped with 5%, 10%, and 20%  $Al_2O_3$  and (b) Amount of sorbed analyte for P25DMA and P25DMA 5%  $Al_2O_3$ . Note that for (b), the gases, from left to right (black to white), are ethanol, formaldehyde, methanol, acetaldehyde, acetone, and benzene.

By incorporating only 5%  $Al_2O_3$  into P25DMA, the sensitivity to ethanol significantly increased (the amount sorbed almost doubled) and the selectivity with respect to five typical interferents was significantly improved (see Figure 4.25 b). The addition of  $Al_2O_3$  did not affect the amount of

acetone sorbed; however, the amount of acetone sorbed was still significantly less than that of ethanol. Overall, P25DMA 5% Al<sub>2</sub>O<sub>3</sub> is a highly selective sensing material for ethanol.

#### 4.4.2 P25DMA Doped with ZnO

Since P25DMA 10% ZnO and P25DMA 20% ZnO sorbed significantly less ethanol than P25DMA, only P25DMA 5% ZnO was evaluated for selectivity with five different interferents (see Figure 4.26). The addition of 5% ZnO improved the selectivity of undoped P25DMA towards ethanol, especially towards formaldehyde and methanol.

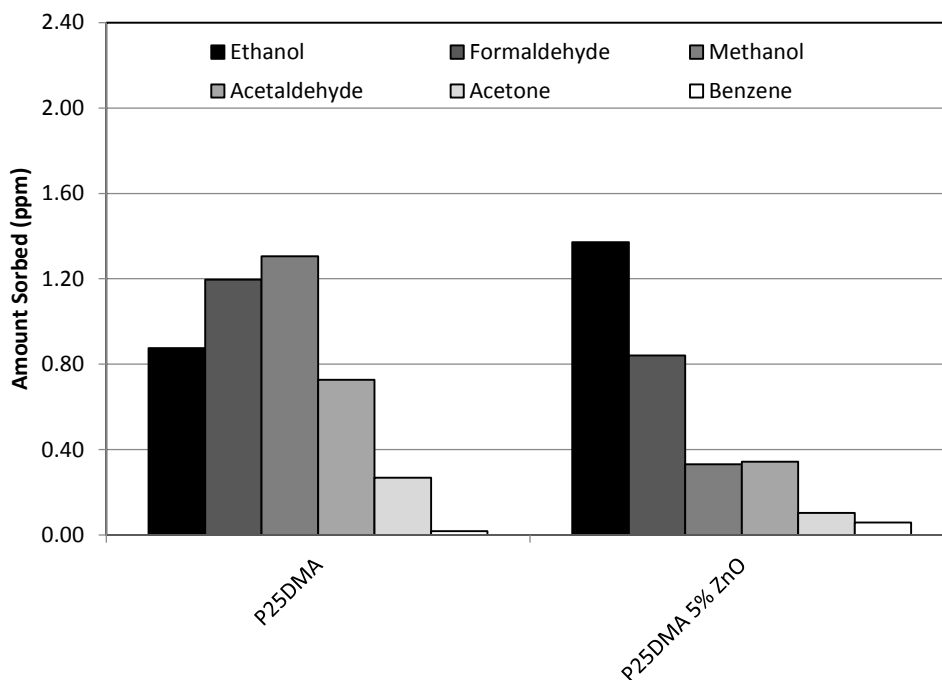


Figure 4.26: Amount of sorbed analyte for P25DMA and P25DMA 5% ZnO. Note that from left to right (black to white), the gases are ethanol, formaldehyde, methanol, acetaldehyde, acetone, and benzene.

#### 4.4.3 P25DMA Doped with NiO

All three concentrations (5%, 10%, and 20%) of P25DMA doped with NiO were evaluated for selectivity to ethanol (see Figure 4.27), despite P25DMA 10% NiO showing poorer ethanol sorption than undoped P25DMA. This was done to assess any trends observed as the amount of NiO incorporated into the P25DMA increased.

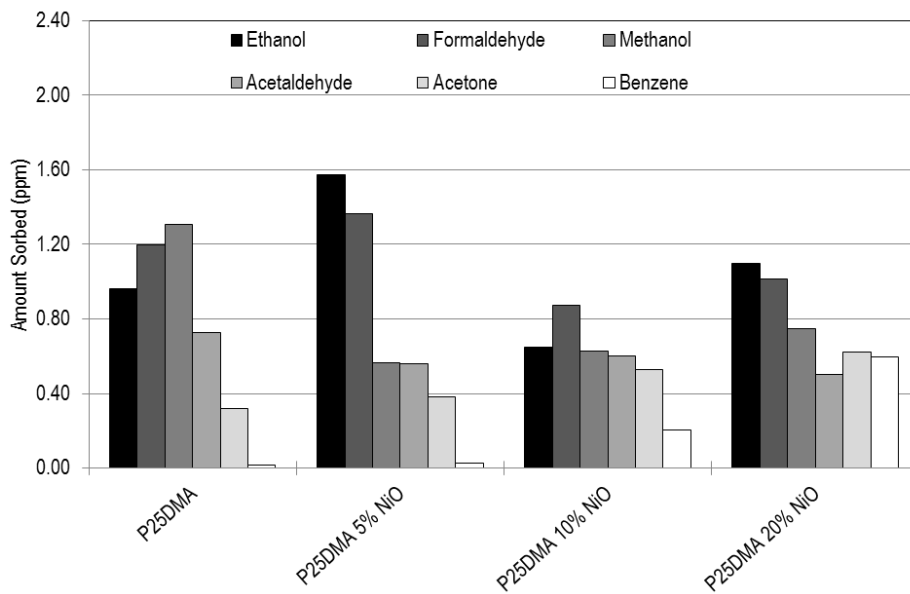


Figure 4.27: Amount of sorbed analyte for P25DMA, P25DMA 5% NiO, P25DMA 10% NiO, and P25DMA 20% NiO.

The amount of methanol, acetaldehyde, and acetone that sorbed remained roughly the same (not significantly different) despite the increased concentration of NiO. It should be noted that a significant drop in the amount of methanol sorbed occurred with the addition of NiO compared to the undoped P25DMA. This is likely due to methanol readily desorbing from NiO at room temperature (Natile and Glisenti, 2002).

As the concentration of NiO increased, so did the concentration of benzene (see Figure 4.27). This is likely due to the larger interstitial spaces created in the polymer matrix as more NiO is incorporated, since a benzene molecule is significantly larger in size than the other analytes tested.

An interesting trend is observed for both ethanol and formaldehyde (see Figure 4.27). The addition of 5 wt. % NiO increases the amount of both analytes sorbed, especially for ethanol; however, increasing the concentration of NiO to 10%, significantly reduces the amount of both ethanol and formaldehyde being sorbed. The trend then reverses itself again with more NiO (20 wt. %). This trend can be explained by the dominant mechanism at the different concentrations of NiO (see Section 6.1).

#### 4.4.4 P25DMA Doped with TiO<sub>2</sub>

The three TiO<sub>2</sub> polymeric nanocomposites (5 wt. %, 10 wt. %, 20wt. %) were all evaluated for their selectivity towards ethanol. It was found that adding more TiO<sub>2</sub>, overall, improved the amount of each analyte sorbed (see Figure 4.28). This is likely due to TiO<sub>2</sub> producing more

“kinks” along the polymer chains as more TiO<sub>2</sub> was incorporated into the P25DMA. These “kinks” would reduce the polymer chains’ ability to pack closely and thus, create larger interstitial spaces allowing for easier diffusion of the analytes.

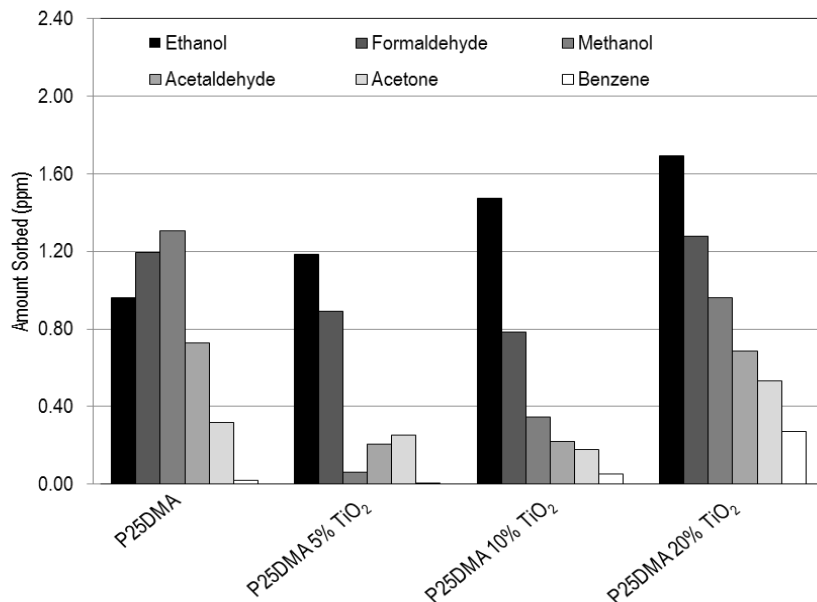


Figure 4.28: Amount of sorbed analyte for P25DMA, P25DMA 5% TiO<sub>2</sub>, P25DMA 10% TiO<sub>2</sub>, and P25DMA 20% TiO<sub>2</sub>.

Overall, incorporating more TiO<sub>2</sub> into P25DMA resulted in better sorption of all the analytes evaluated. P25DMA 20% TiO<sub>2</sub> sorbed the most ethanol of all the polymeric nanocomposites evaluated; however, P25DMA had better methanol sorption. Therefore, TiO<sub>2</sub> more selectively attracts ethanol than methanol, especially below 10 wt. %. With the exception of formaldehyde, P25DMA 5% TiO<sub>2</sub> and P25DMA 10% TiO<sub>2</sub> had good selectivity with respect to ethanol.

#### 4.5 Optimal Sensing Materials for Ethanol

The selectivity ratios towards ethanol (ratio of ethanol sorption to interferent gas sorption), are listed in Table 4.3. If the selectivity is below 1, then the sensing material is more selective to the interferent rather than ethanol, which is the case for P25DMA for formaldehyde and methanol. The higher the selectivity, the better. Table 4.3 is colour coded: the darker the red, the poorer the selectivity; the darker the green, the better the selectivity. For reference, poor selectivity is below 1.5, moderate selectivity is round 3 and good selectivity is above 5.



Table 4.3: Selectivity of Doped and Undoped P25DMA towards Ethanol

Sensing Material	Formaldehyde	Methanol	Acetaldehyde	Acetone	Benzene
P25DMA	0.73	0.67	1.20	3.26	47.73
<b>P25DMA 5% Al<sub>2</sub>O<sub>3</sub></b>	<b>2.48</b>	<b>151.50</b>	<b>15.95</b>	<b>6.27</b>	<b>22.17</b>
P25DMA 5% ZnO	1.63	4.14	4.00	13.27	23.51
P25DMA 5% NiO	1.16	2.78	2.81	4.14	55.59
P25DMA 10% NiO	0.74	1.03	1.08	1.23	3.21
P25DMA 20% NiO	1.08	1.47	2.19	1.76	1.84
P25DMA 5% TiO <sub>2</sub>	1.05	19.78	5.79	4.72	178.00
<b>P25DMA 10% TiO<sub>2</sub></b>	<b>1.89</b>	<b>4.28</b>	<b>6.76</b>	<b>8.20</b>	<b>26.85</b>
P25DMA 20% TiO <sub>2</sub>	1.33	1.77	2.46	3.18	6.28

None of the sensing materials evaluated were very selective towards ethanol with respect to formaldehyde. This may be due to the fact that ethanol is readily catalytically decomposed into formaldehyde and thus, both ethanol and formaldehyde are able to coordinate well to the metal oxides used to catalyze the oxidation of ethanol into formaldehyde (Okabayashi et al., 2000). Overall, P25DMA 5% Al<sub>2</sub>O<sub>3</sub> and P25DMA 10% TiO<sub>2</sub> had the best selectivity towards ethanol. In addition, P25DMA 5% ZnO and P25DMA 5% TiO<sub>2</sub> were also acceptable, although formaldehyde as an interferent will pose a problem.

## 4.6 Sensor Array

To improve the selectivity of a sensor, multiple sensing materials can be used in an array. By combining the responses on multiple sensing materials, different gas analytes can be separated using a statistical algorithm. These algorithms compare the different responses from different analytes on different sensing materials and capture the basic trends of the underlying correlation structure of the whole data set.

A common algorithm used is principal component analysis (PCA). PCA is a multivariate statistical method that converts an array of data into principal components that are a linear combination of the original variables. The goal is to reduce the number of principal components (the maximum number of principal components is equal to the total number of variables), while capturing/retaining the maximum amount of variability/basic underlying information from the whole data set. Therefore, only the first few principal components are typically used, where the first principal component contains the most variance and the  $n^{\text{th}}$  principal component contains the least (Scott and Penlidis, 2013).

For the sensor array of the current investigation, only the first two principal components (Factor 1 and Factor 2) were employed in the plots that follow, since these two principals contain the most variance (they captured 95% of the variability). In this case, the variables were the sensing

materials and the data were grouped by gas analyte. This correlated the data (amounts sorbed) with the corresponding gas analyte, resulting in gas analytes being separated into clusters when Factor 1 was plotted against Factor 2.

The five sensing materials used in this sensor array were P25DMA, P25DMA 5% Al<sub>2</sub>O<sub>3</sub>, P25DMA 5% NiO, P25DMA 5% TiO<sub>2</sub>, and P25DMA 5% ZnO. Each of the five sensing materials was initially evaluated for selectivity, individually. Each sensing material was exposed to approximately 5 ppm of each of six gas analytes (acetaldehyde, acetone, benzene, ethanol, formaldehyde, and methanol). The amount of gas analyte that sorbed onto each sensing material is shown in Figure 4.29 (effectively, a sensitivity indicator).

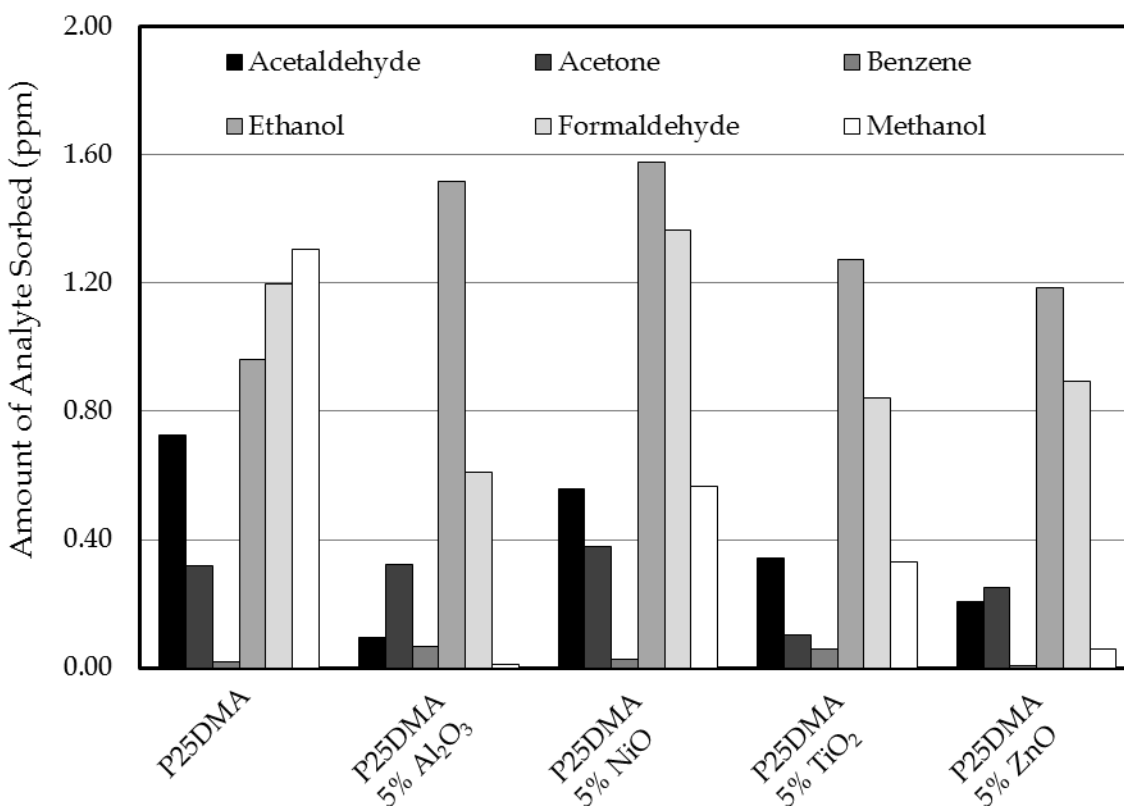


Figure 4.29: Amount of gas analyte sorbed onto each sensing material. Note that from left to right, the bars represent acetaldehyde, acetone, benzene, ethanol, formaldehyde, and methanol, respectively.

From Figure 4.29, one can see that high concentrations of both ethanol and formaldehyde sorbed onto each sensing material. Therefore, none of the sensing materials is particularly selective to any of the gas analytes evaluated. However, it should be noted that all of these sensing materials are very sensitive to the six gas analytes evaluated since gas sorption (i.e. a response) was observed when these sensing materials were exposed to 5 ppm of gas analyte, which is a very low concentration to detect.

The most selective sensing material was P25DMA 5% Al<sub>2</sub>O<sub>3</sub>, which is fairly selective towards ethanol. For comparison, P25DMA had the worst selectivity towards any of the gas analytes. Therefore, as a single sensing material on a gas sensor, none of these sensing materials, with the possible exception of P25DMA 5% Al<sub>2</sub>O<sub>3</sub>, would have the required selectivity. However, their partial selectivity could be exploited on a sensor array.

The data collected from the sorption tests in the previous section were entered into the algorithm (using Statistica). Four replicates for each sensing material-gas analyte combination were used. The resulting bi-plots (Factor 2 vs Factor 1, i.e., the first two principal components) are shown below, starting with Figure 4.30, which is essentially the reference or calibration graph with which unknown gases are compared. See Appendix H for additional information on the PCA results.

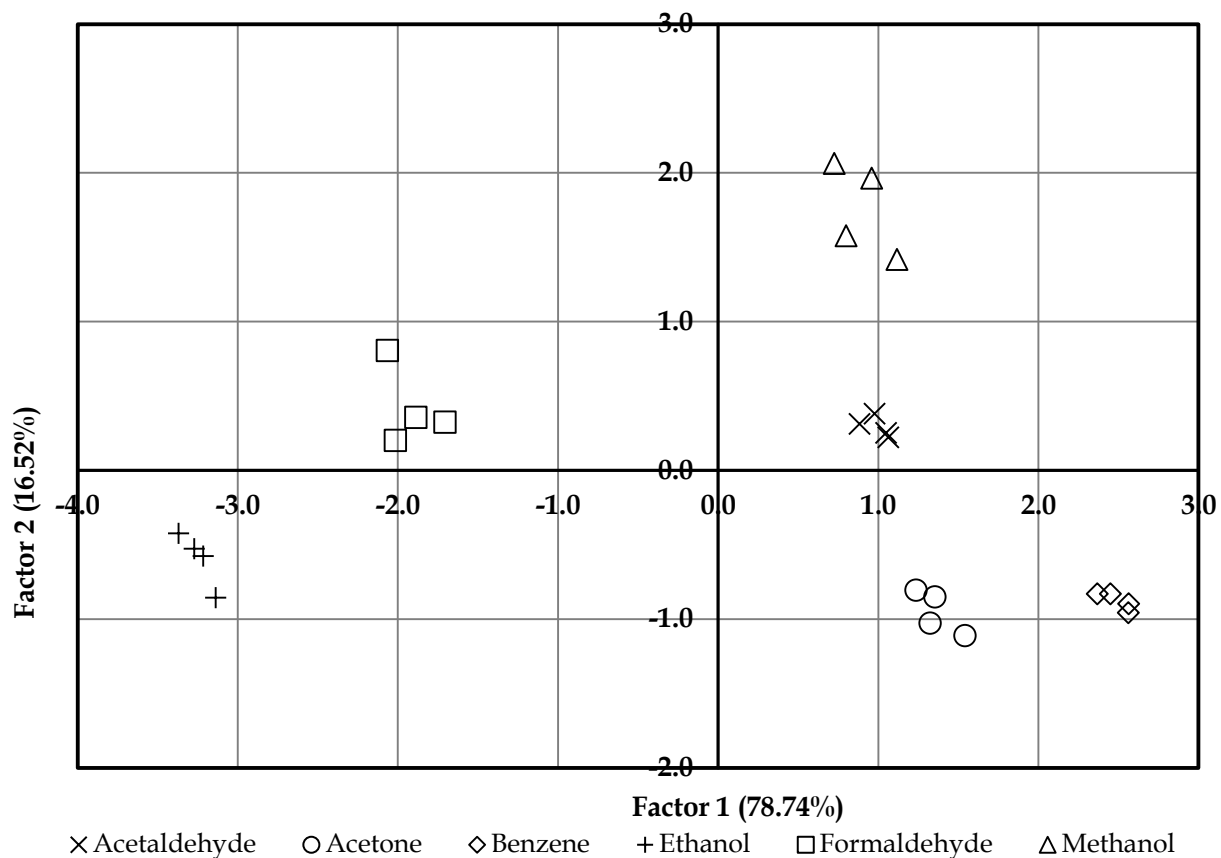


Figure 4.30: PCA reference plot.

Note that Factor 1 includes 78.74% of the variability and Factor 2 includes 16.52% of the variability (the scree plot in Figure 4.31 shows the variability of each Factor). This means that plotting Factor 2 versus Factor 1 accounts for 95.26% of the total variability, which is quite high.

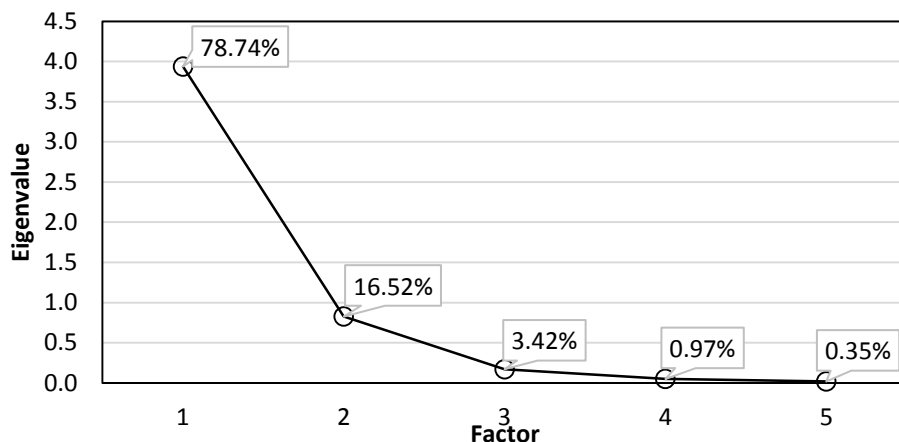


Figure 4.31: Scree plot showing the percent of variability for each Factor.

Using the plot in Figure 4.30 as a reference, six unknown gases were subsequently evaluated. Each of these gases was singular in nature (i.e. only one gas analyte was measured at a time). The resulting points for each unknown, after being analyzed using PCA, were plotted on top of the reference graph (Figure 4.32). In all cases, the unknown (single gas) could easily be identified since the response on the unknown landed very close to the previously identified gas clusters.

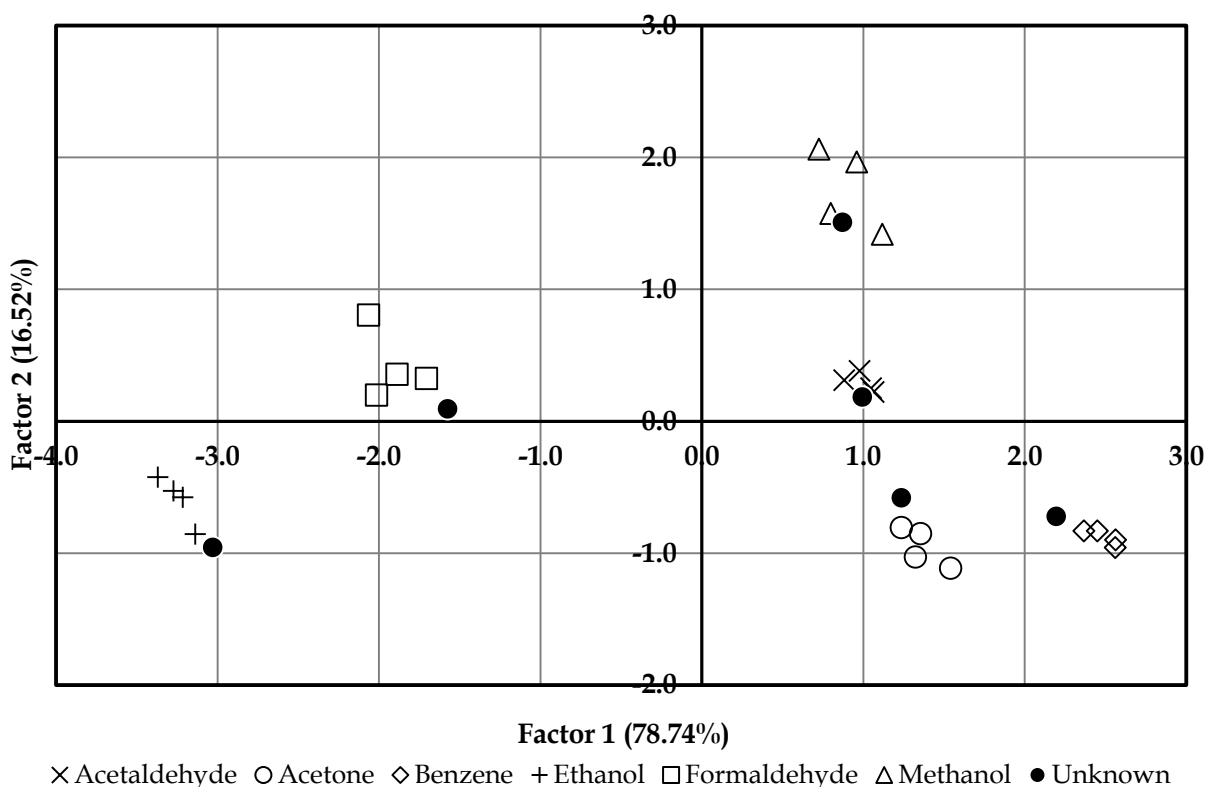


Figure 4.32: PCA plot with unknowns (single gases).

A gas mixture was also evaluated (again for initial proof-of-concept), using ethanol and acetaldehyde in a 2:1 ratio. Two replicates were run, which produced four points (two for ethanol and two for acetaldehyde). These points landed partway between ethanol and acetaldehyde on the reference plot (Figure 4.33). In addition, these points did not overlap with any of the other gas clusters. This was promising.

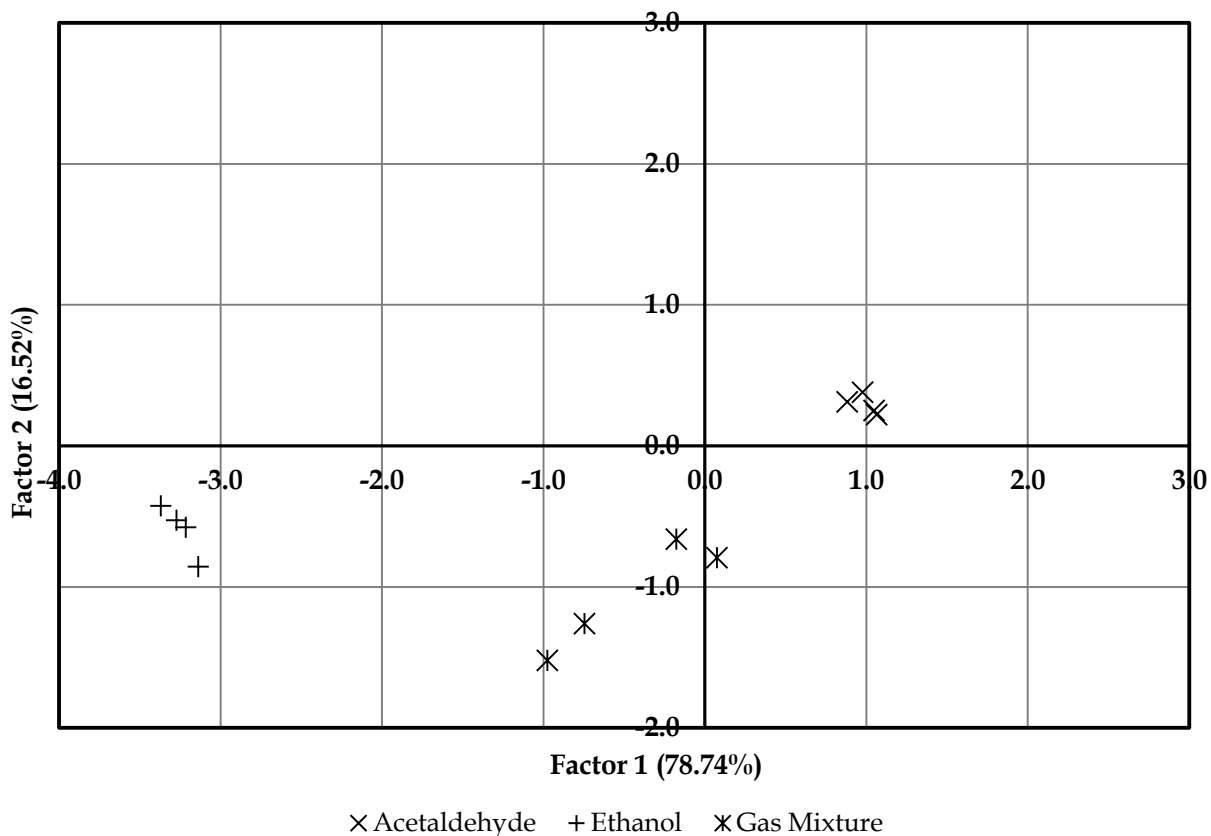


Figure 4.33: Unknown gas mixture.

It should be noted that an interaction between acetaldehyde and ethanol did occur (i.e. the presence of acetaldehyde did affect how much ethanol sorbed and vice versa). In this case, ethanol facilitated the sorption of acetaldehyde resulting in acetaldehyde more readily sorbing than ethanol. Therefore, these interactions in binary, ternary, etc. gas mixtures should be further evaluated to improve the discriminating capabilities of the algorithm in better separating gas analytes in mixtures. However, for single gas analytes, a sensor array consisting of these five sensing materials (P25DMA, P25DMA 5% Al<sub>2</sub>O<sub>3</sub>, P25DMA 5% NiO, P25DMA 5% TiO<sub>2</sub>, and P25DMA 5% ZnO) is able to distinguish quite reliably between six different gas analytes (acetaldehyde, acetone, benzene, ethanol, formaldehyde, and methanol).

Note that this is a first attempt (proof-of-concept) and seems quite promising. Of course, the more data points PCA uses, the better the data correlation structure will be identified.

## 5. Results and Discussion: Sensors and Further Analysis

The more promising potential polymeric sensing materials that were evaluated in Chapter 4 were subsequently deposited onto different sensors for further evaluation in this chapter. In addition, some other studies were conducted on these polymeric nanocomposites to assess any other trends and obtain a reproducibility measure for the polymer nanocomposites.

### 5.1 Sensor Evaluation

Two different types of sensors were evaluated using multiple sensing materials: a radio frequency identification (RFID) sensor that measured a change in capacitance and a microelectromechanical systems (MEMS) microcantilever that measured a change in mass. Note that the data presented in Section 5.1 were collected in collaboration with other graduate students. The RFID sensors (Section 5.1.1) were done in collaboration with Wei Ting (Scott) Chen, who designed the RFID sensors that were used to evaluate the sensing materials (Chen et al., 2015a; Chen et al., 2015b; Chen et al., 2015c; Stewart et al., 2015). The MEMS-based microcantilever sensors (Section 5.1.2) were done in collaboration with Mahmoud Khater who designed the MEMS sensors that were used to evaluate the sensing materials (Khater et al., 2014).

#### 5.1.1 Radio Frequency Identification (RFID)

The RFID sensor is a capacitive sensor that was designed with interdigitated fingers. Six different sensing materials were deposited onto various RFID sensors. Two substrates onto which the RFID sensors were made, rigid and flexible, were evaluated (see Section 5.1.1.1). Further analysis for selectivity was done on the rigid RFID sensor (See Section 5.1.1.2). In addition, a three sensor array, using two different sets of polymeric sensing materials was also evaluated on the rigid RFID (see Section 5.1.1.3).

##### 5.1.1.1 Rigid versus Flexible RFID Sensor

These radio frequency identification (RFID) sensors were composed of an interdigital chemi-capacitor and operated at RF frequencies. The sensing material was deposited on top of the interdigitated capacitor, which interacted with the gaseous analytes resulting in a change in the dielectric constant. The change in capacitance shifted the resonant frequency, which could subsequently be observed as a change in the response amplitude (Ampl) at a specific frequency ( $f$ ) (see Figure 5.1). Note that each sensing material resonates at its own unique resonant frequency (Chen et al., 2013).

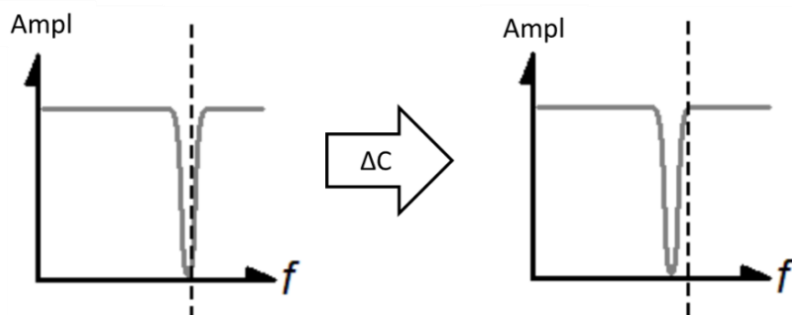


Figure 5.1: Response schematic of RFID sensor. A change in capacitance ( $\Delta C$ ) results in a change in response amplitude as the resonant frequency shifts (Stewart et al., 2015).

Two different types of RFID sensors (rigid and flexible) were compared using six different sensing materials (OV 275, OV 225, SXFA, P25DMA, P25DMA 20% NiO, and P25DMA 20% ZnO) to determine if there was a significant difference in the responses of the two types of sensors. The rigid sensor was made on a rigid, unbending substrate, whereas the flexible sensor was made on a flexible substrate that could bend up to  $90^\circ$  (Chen et al., 2015a). For this comparison, the rigid sensor had a flat configuration and the flexible sensor was bent at a  $90^\circ$  angle, fixed by an L-shaped acrylic form (see Figure 5.2).

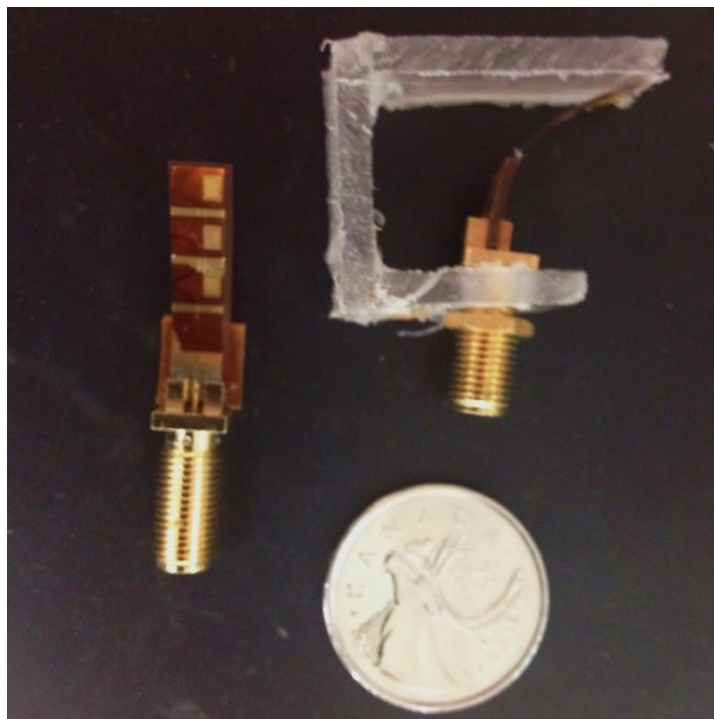


Figure 5.2: Rigid RFID sensor (left) and flexible RFID (right) sensors, with a Canadian quarter for scale. The flexible RFID sensor is bent at  $90^\circ$  in an acrylic form.

Two different sets of sensing materials were evaluated: OV 225, OV 275, and SXFA (all from Seacoast Sciences, Inc.), which will be denoted as the siloxane-based sensing materials, and

P25DMA, P25DMA 20% NiO, and P25DMA 20% ZnO, which will be denoted as the P25DMA-based sensing materials. Four gas analytes (ethanol, methanol, acetone, and benzene) were tested at a concentration of 1250 ppm. Note that a higher concentration was used to show proof-of-concept for this newly designed sensor. A change in the response amplitude at specific frequencies was measured. Note that the frequency at which the responses were measured was dependent on the sensing material.

Ethanol (1250 ppm) was used to determine whether there was a significant difference between these two types of sensors. Note that each of these sensing materials (OV 275, OV 225, SXFA, P25DMA, P25DMA 20% NiO, and P25DMA 20% ZnO) responded differently to ethanol, with some sensing materials responding with greater amplitude than others. Because of these different responses, analysis of variance (ANOVA) with blocking was done. The blocking was used to minimize the differences (and thus error) observed between the sensing materials on the same sensor. It was found that the  $F_{\text{observed}}$  was less than  $F_{\text{critical}}$ ; therefore, the response to ethanol on both the rigid and flexible sensors was not significantly different from one another. In addition, this analysis confirmed that there was a significant difference between at least two of the responses of the sensing materials on one sensor. Further analysis using the Bonferroni t-test and the Fisher's Least Significant Difference (LSD) was done on the responses for each sensing material on both sensors, individually. The summary of this analysis is listed in Section F.2.1 in Appendix F.

Each of these six sensing materials was evaluated for selectivity towards ethanol at 1250 ppm, using three different interferents (methanol, benzene, and acetone), with each interferent also evaluated at 1250 ppm. In addition, combinations of two, three, and four gases flowed over the sensor and the response was recorded. Ethanol was always included and the concentration of the gases was initially equal. Then, only the concentration of ethanol was halved, while the interferent gases remained at the initial concentration (i.e. initially all the gases were at 1250 ppm; then ethanol was halved to 625 ppm, while the rest remained at 1250 ppm). Nitrogen gas was used to balance the concentrations to keep the flow rate at 200 sccm. For a perfectly selective sensor, by halving the concentration of ethanol, the response should also be halved; however, this was not the case.

In general, a sensing material will sorb many analytes that have a similar chemical nature. For example, methanol and ethanol are likely to interact similarly because they both contain an alcohol (OH) functional group. Therefore, it is expected that when either ethanol or methanol interact with a sensing material, they will both produce a response; however, since mechanisms are complex and multiple mechanisms occur simultaneously, it is possible for one analyte (ethanol or methanol) to interact more preferentially (see Chapters 6 and 7). Therefore, it is possible that one analyte, such as ethanol, will produce a larger response than methanol despite their similar chemical nature. When both ethanol and methanol are exposed to a sensing material simultaneously, the response produced is due to the interaction between the sensing material and both analytes;



however, it is impossible to separate which percentage of the response is due to ethanol (and which is due to methanol) with a single sensing material.

The first test for selectivity (see Figure 5.3), and the only test for selectivity often performed in the literature, is individually testing multiple gases (target analyte and interferents) to determine how a sensor and sensing material respond. This shows the response of the sensor and sensing material to a specific analyte; however, it does not show how analytes interact. In most cases, analytes do interact with one another. For instance, two molecules may bind to the same sensing site on the sensing material with one analyte binding to a second analyte that is already bound to the sensing material.

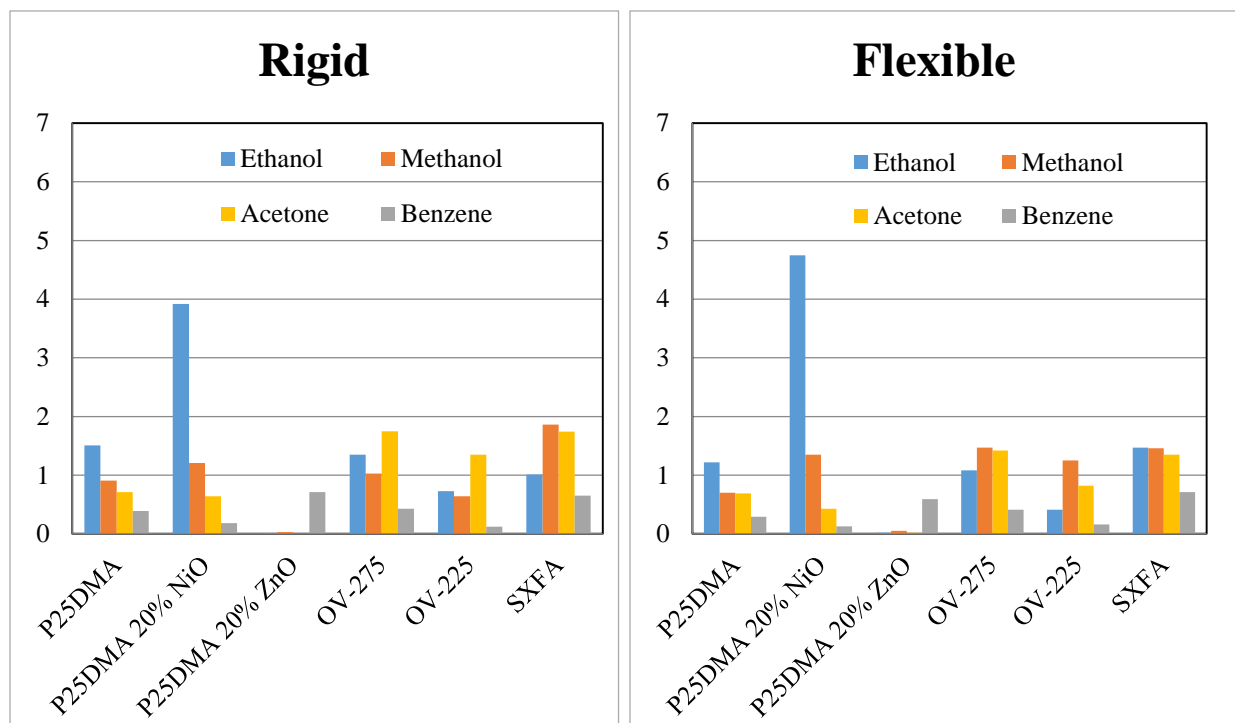


Figure 5.3: The response amplitude (unitless) for all six sensing materials for both the rigid and flexible sensor. Each analyte (ethanol, blue; methanol, green; acetone, orange; benzene, yellow) was individually exposed to the sensing materials at 1250 ppm.

Each sensing material was exposed to pure ethanol at 1250 ppm and then halved to 625 ppm. This provided a reference point to which the various combinations of multiple gases were compared. The percent change of the responses is shown in Table 5.1. Ideally, the response should drop by 50% when reducing the concentration of ethanol by half; however, mechanisms are complex and sometimes the affinity between a sensing material and analyte is strong. This means that if the sensing material was exposed to the higher concentration first, then at the lower concentration, a strong affinity for an analyte would result in the sensing material retaining more analyte, and thus eventually result in a lower percentage drop than 50%.

Table 5.1: Percentage by which the Response Dropped when Ethanol Concentration was Halved for Both Sensors

<b>Sensing Material</b>	<b>P25DMA</b>	<b>P25DMA 20% NiO</b>	<b>P25DMA 20% ZnO</b>	<b>OV 275</b>	<b>OV 225</b>	<b>SXFA</b>
<b>Rigid</b>	50	53	100 <sup>1</sup>	44	77	57
<b>Flexible</b>	44	62	100 <sup>1</sup>	51	15	48

<sup>1</sup>Response in both cases went from 0.01 to 0, which is essentially no change (negligible), within error.

Overall, the response drops were around 50%, assuming a 10% error of the response (not response drop). P25DMA with 20% ZnO had a response drop of 100%; however, the initial response (to 1250 ppm) was 0.01 in both cases and dropped to 0. Therefore, within error, no response was measured for ethanol at 1250 ppm, and thus the drop of 100% should be considered a drop of 0% or no change. The response change for OV 225 was an anomaly that should be re-evaluated to determine why there is such a difference in responses between the two types of sensors, when none of the other sensing materials showed such a wide variation in response.

The individually tested gases were all run at 1250 ppm to compare the response when additional gases were simultaneously exposed. If a sensing material is perfectly selective towards ethanol, then the response to ethanol when tested by itself and the response of ethanol with another analyte would be equal. Generally, as more analytes are exposed to the sensing material, the response from the sensing material increases.

Further selectivity analysis was done by exposing the six sensing materials to mixtures of two gases (ethanol with one of the interferent gas analytes). Both gases had a concentration of 1250 ppm and the concentration of ethanol was halved to 625 ppm to determine how the response varied with the ethanol concentration (see Figure 5.3). Both the rigid and flexible RFID sensors had similar responses for the same sensing material.

In general, when ethanol was halved, there was a significant drop in response for all sensing materials (see Figure 5.4). Tables 5.2 and 5.3 show the amount the response dropped for each sensing material when the concentration of ethanol was halved, for the rigid and flexible sensors, respectively. The closer the drop in response to halving the ethanol concentration was to 50%, the more selective the sensing material was to ethanol with respect to the interferent (acetone, methanol, or benzene).

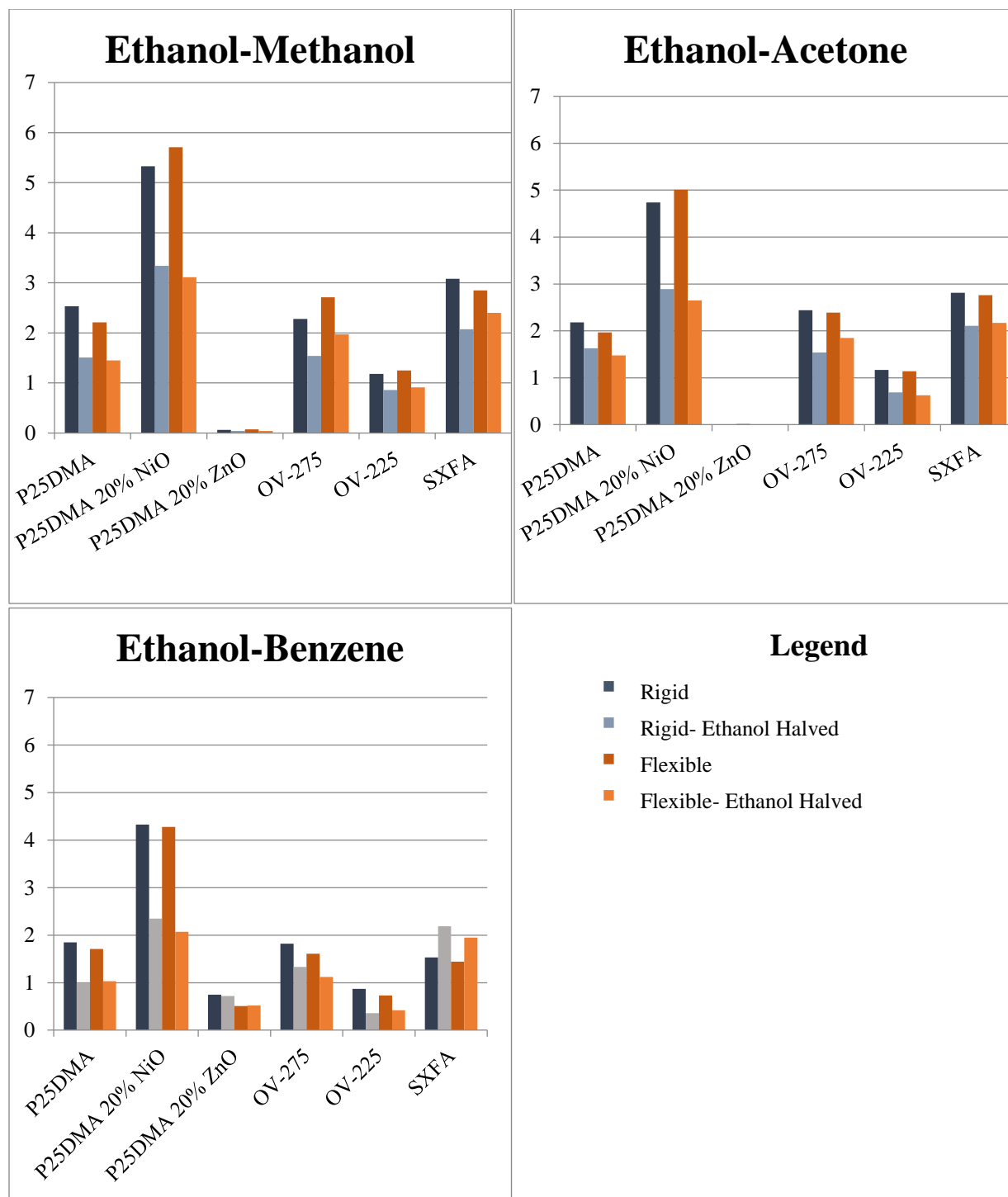


Figure 5.4: Response Amplitude (unitless) of all six sensing materials when exposed to ethanol and one other interferent simultaneously at 1250 ppm for both the rigid (grey) and flexible (orange) sensors. The second and fourth column for each sensing material show the response amplitude when the concentration of ethanol was halved to 625 ppm (lighter columns).

Table 5.2: Percentage by which the Response Dropped when Ethanol Concentration was Halved for the Rigid Sensor

<b>Sensing Material</b>	<b>P25DMA</b>	<b>P25DMA 20% NiO</b>	<b>P25DMA 20% ZnO</b>	<b>OV 275</b>	<b>OV 225</b>	<b>SXFA</b>
Ethanol-Methanol	40	37	33	32	27	33
Ethanol-Acetone	25	39	25	37	41	0
Ethanol-Benzene	46	46	4	27	59	-43 <sup>1</sup>

<sup>1</sup>The negative denotes that the response increased instead of decreasing when the concentration of ethanol was halved.

Table 5.3: Percentage by which the Response Dropped when Ethanol Concentration was Halved for the Flexible Sensor

<b>Sensing Material</b>	<b>P25DMA</b>	<b>P25DMA 20% NiO</b>	<b>P25DMA 20% ZnO</b>	<b>OV 275</b>	<b>OV 225</b>	<b>SXFA</b>
Ethanol-Methanol	34	46	43	27	27	16
Ethanol-Acetone	25	47	0	23	45	21
Ethanol-Benzene	40	52	-2 <sup>3</sup>	30	42	-35 <sup>1</sup>

<sup>1</sup>The negative denotes that the response increased instead of decreasing when the concentration of ethanol was halved.

P25DMA had the best selectivity towards ethanol with respect to benzene, at 46% (rigid) and 40% (flexible). High selectivity with respect to benzene was expected since P25DMA had a much lower response to benzene than ethanol when the gases were individually exposed (see Figure 5.3). When the methanol and acetone were individually exposed to P25DMA, methanol produced a larger response than acetone; however, the combination of ethanol and acetone produced a smaller change in response when the concentration of ethanol was halved than the combination of ethanol and methanol (see Tables 5.2 and 5.3). This difference between the individually and simultaneously exposed gases shows that there is some interaction between ethanol and acetone.

P25DMA 20% NiO also had high selectivity towards ethanol with respect to benzene, with responses of 46% (rigid) and 52% (flexible). Error within the response accounts for the slightly above 50% drop in response when the concentration of ethanol was halved. P25DMA 20% NiO had similar percent drops for acetone and methanol, which were still close to 50%, especially for the flexible sensor. Overall, P25DMA 20% NiO had the best selectivity towards ethanol with respect to all three interferents, when two gases were exposed to the sensing materials simultaneously.

P25DMA 20% ZnO had a very small to no response for most of the gases. Because the responses were so small, the percent change appears better, in some cases, than was actually the case. For example, when the concentration of ethanol was halved (on the rigid sensor) the response went from 0.03 to 0.02, a 33% drop; however, a 0.01 drop in response is negligible. Overall, P25DMA 20% ZnO had a poor response to ethanol and the selectivity towards ethanol was also poor.

OV 275 had similar and moderate selectivity towards ethanol with respect to all three interferents. All three mixtures, on both the rigid and flexible sensors, had a percent drop of approximately 30%. Given the difference in responses to ethanol and benzene when the gases were individually exposed to OV 275, it is surprising that the percent drop for ethanol and benzene was only ~30%.

OV 225 had a large percent drop (over 40% for both the rigid and flexible sensors) when the concentration of ethanol was halved for both the acetone and benzene mixtures. While this was expected for benzene due to the large difference in responses when the gases were individually exposed, acetone produced a larger response to OV 225 than ethanol. Therefore, it was expected that very little drop in the response would have occurred when the concentration of ethanol was halved. Methanol also had either a very similar response or larger response than ethanol when the gases were individually tested. However, the percent drop was lower at 27% (for both rigid and flexible sensors), which still seems high, especially since the response to methanol was more than double that of ethanol when the gases were individually tested. It is possible that the larger drop is due to two analytes binding to a sensing site (i.e. methanol binding to ethanol that is already bound). When the concentration of ethanol is halved, both analytes are ejected from the sensing site which results in a greater drop in response. It is important to note that the response is not likely linearly correlated with the number of sensing sites; therefore, two analytes at one sensing site would have an unpredictable response.

SXFA produced larger signals for acetone and methanol than ethanol on the rigid sensor and all three gases produced a similar response on the flexible sensor. Benzene produced a response that was about half that of ethanol's on both the rigid and flexible sensors. When exposed to two gases simultaneously, the results were very strange. On the rigid sensor, ethanol and methanol produced a moderate percent drop in response at 33%, which seems high since methanol produced a much larger response than ethanol when the gases were tested individually; however, no change was observed when the ethanol concentration was halved and the concentration of acetone remained the same. Given that the response of the individually tested gases on the rigid sensor was much higher for acetone and methanol, than ethanol, the percent drop probably should have been similar. As for the flexible sensor, the results seem more in line with what was expected. The percent drop in response when the concentration of ethanol was halved was low at 16% (methanol) and 20% (acetone). The drop in ethanol concentration should have resulted in some change, but

since all three (ethanol, methanol, and acetone) were equally competing for sites, the selectivity towards ethanol was low, and thus a small drop was expected.

An anomaly for benzene occurred for both the rigid and flexible sensors with SXFA as the sensing material. For some reason, the response increased when the concentration of the analytes decreased. It is possible that by lowering the concentration for ethanol, the ratio of benzene in the mixture increased (from 1:1 to 2:1), which allowed more benzene to bind due to less competition for sites from ethanol; however, further evaluation is needed to test this theory.

The selectivity evaluation was furthered using three gases (ethanol with two interferents). All three gases were simultaneously exposed to the sensing materials on both the rigid and flexible sensor. By introducing more types of analytes, there was more competition for sensing sites and more ability for multiple analytes to bond to the same sensing site. Because of this, generally, selectivity is decreased as more analytes are available, especially when analytes are chemically similar, as ethanol, methanol, and even acetone, are. Overall, the responses to the three gas mixtures produced a smaller percent drop when the concentration was halved (see Figure 5.5 and Tables 5.4 and 5.5); however, P25DMA 20% NiO still had very good selectivity with percent drops near 50%.

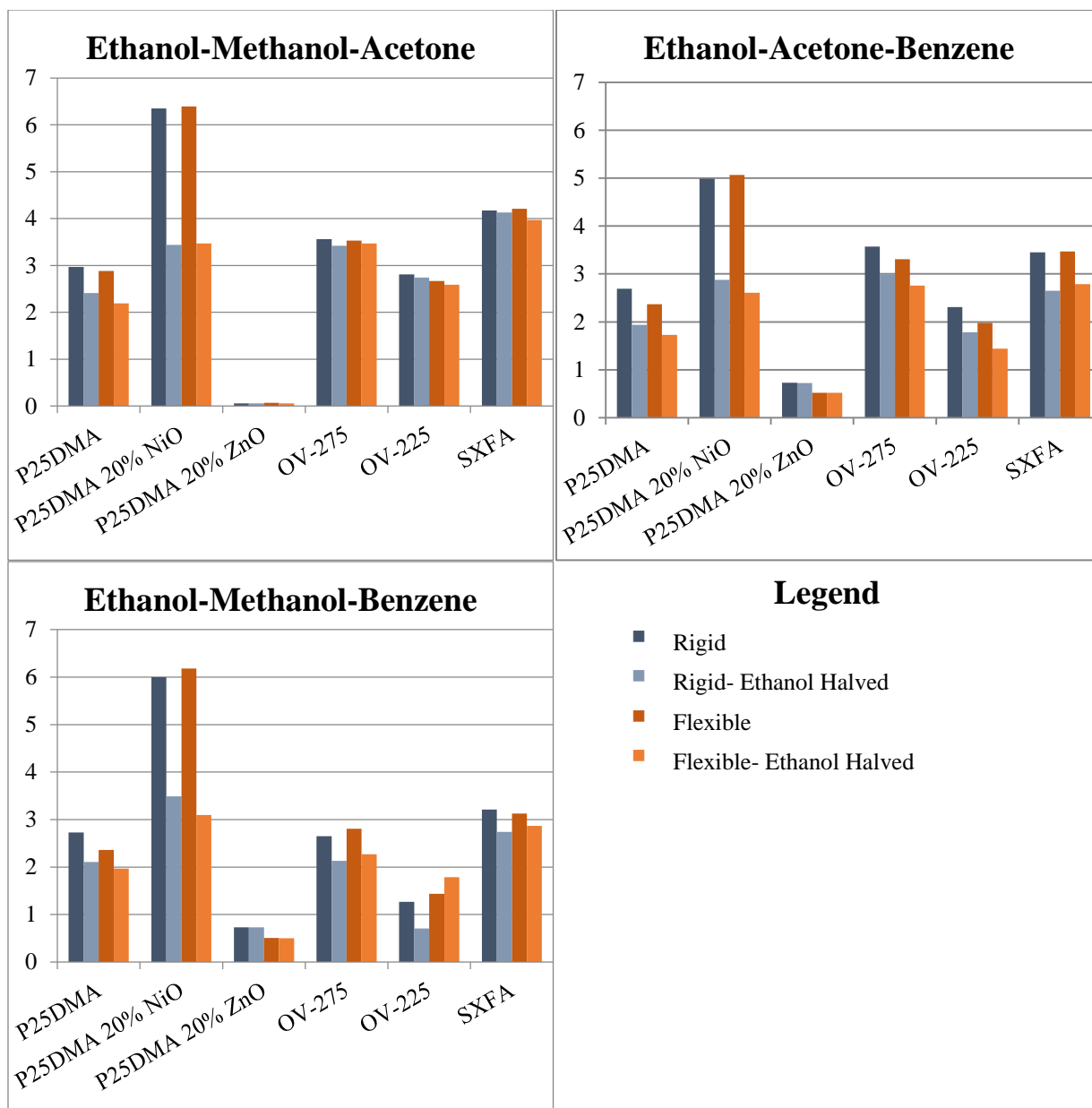


Figure 5.5: Response Amplitude (unitless) of all six sensing materials when exposed to ethanol and two interferences simultaneously at 1250 ppm for both the rigid (grey) and flexible (orange) sensors. The second and fourth column for each sensing material show the response amplitude when the concentration of ethanol was halved to 625 ppm (lighter columns).

Table 5.4: Percentage by which the Response Dropped when Ethanol Concentration was Halved for the Rigid Sensor

<b>Sensing Material</b>	<b>P25DMA</b>	<b>P25DMA 20% NiO</b>	<b>P25DMA 20% ZnO</b>	<b>OV 275</b>	<b>OV 225</b>	<b>SXFA</b>
Ethanol-Methanol-Acetone	19	46	0	4	2	1
Ethanol-Acetone-Benzene	23	42	0	20	44	15
Ethanol-Methanol-Benzene	28	42	1	16	23	23

Table 5.5: Percentage by which the Response Dropped when Ethanol Concentration was Halved for the Flexible Sensor

<b>Sensing Material</b>	<b>P25DMA</b>	<b>P25DMA 20% NiO</b>	<b>P25DMA 20% ZnO</b>	<b>OV 275</b>	<b>OV 225</b>	<b>SXFA</b>
Ethanol-Methanol-Acetone	24	46	14	2	3	6
Ethanol-Acetone-Benzene	17	50	2	19	-24 <sup>1</sup>	8
Ethanol-Methanol-Benzene	27	49	0	17	27	20

<sup>1</sup>The negative denotes that the response increased instead of decreasing when the concentration of ethanol was halved.

P25DMA had moderate selectivity with percent drops around 20% to 30% when the concentration of ethanol was halved. A higher percent drop was observed when acetone was not present in the gas mixture (ethanol, methanol, and benzene). Therefore, it is possible to conclude that ethanol and acetone competed more for sensing sites than ethanol did with the other interferents.

P25DMA 20% NiO had a percent drop for both types of sensors of around 50% when the concentration of ethanol was halved for each mixture of three gases. This shows that P25DMA 20% NiO had very good selectivity even when more interferents were present.

P25DMA 20% ZnO had really low responses to all mixtures of the analytes. Because of this, a small drop in response could amount to a larger drop in percent (i.e. 14% decrease for the ethanol, methanol, and acetone mixture in Table 5.5). Overall, the P25DMA 20% ZnO had a poor response



to ethanol and poor selectivity, given that almost no change in response was observed when the concentration of ethanol was halved.

OV 275 had moderate selectivity when only one of acetone or methanol was present and poor selectivity when exposed to ethanol, methanol, and acetone. This was expected since the individual gas tests showed that acetone produced a greater response to ethanol, whereas methanol produced a very similar response to ethanol. Because OV 275 was more selective towards acetone (and possibly methanol) than ethanol, it is not surprising that in a mixture of these three gases, ethanol likely lost when competing with acetone and methanol for sensing sites on OV 275. Therefore, when the concentration of ethanol was halved, there wasn't much ethanol to be removed from OV 275 and thus, the response only dropped slightly. When only one of acetone or methanol was present, a larger drop was observed since ethanol had less competition for sensing sites and benzene (the third gas) did not offer much competition.

OV 225 behaved very similarly to OV 275; however, the mixture of ethanol, acetone, and benzene produced odd results. Generally, the rigid and flexible sensors showed similar results and trends; however, the mixture of ethanol, acetone, and benzene did not. Given that acetone produced a larger response than ethanol on OV 225 when the gases were tested individually, it is strange that a percent drop of 44% was observed for the rigid sensor and an increase of 24% (hence the negative entry in Table 5.5) was observed for the flexible sensor. An increase should not occur when the total number of analytes decreases, thus leaving fewer analyte molecules to bind to the sensing material; however, the reduction in ethanol could mean less competition for the available sensing sites (that ethanol just vacated), allowing the interferents to bind and ultimately increase the response. More tests should be conducted to evaluate this further.

SXFA also had a larger (or at least equal) response to acetone and methanol than ethanol when the gases were tested individually. Therefore, when the gas mixture of ethanol, methanol, and acetone was exposed to SXFA, almost no percent drop was expected when the concentration of ethanol was halved. This was observed. It appears that acetone competed more with ethanol than methanol based on the larger percent drop observed when acetone was not present (ethanol, methanol, and benzene), than when methanol was present (ethanol, acetone, and benzene). This was also observed for P25DMA.

Finally, all four gases (ethanol, methanol, acetone, and benzene) were tested simultaneously (see Figure 5.6). For four of the sensing materials, poor selectivity was observed, with very little percent drop (see Table 5.6) when the concentration of ethanol was halved. P25DMA had moderate selectivity and P25DMA 20% NiO had good selectivity. As more interferents are present, the selectivity tends to decrease since there are more analytes competing for the same sensing sites and more interactions between the analytes occur.

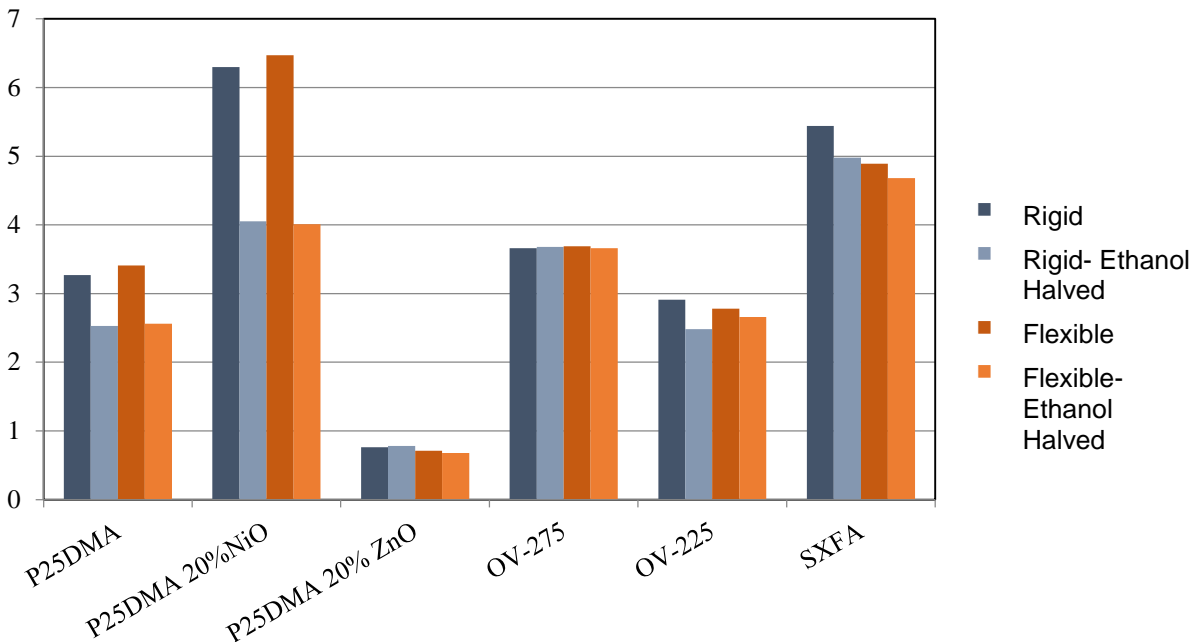


Figure 5.6: Response Amplitude (unitless) of all six sensing materials when exposed to all four gases simultaneously at 1250 ppm for both the rigid (grey) and flexible (orange) sensors. The second and fourth column for each sensing material show the response amplitude when the concentration of ethanol was halved to 625 ppm (lighter columns).

Table 5.6: Percentage by which the Response Dropped when Ethanol Concentration was Halved for Both Sensors

Sensing Material	P25DMA	P25DMA 20% NiO	P25DMA 20% ZnO	OV 275	OV 225	SXFA
Rigid	23	36	-3 <sup>1</sup>	-1 <sup>1</sup>	15	8
Flexible	25	38	4	1	4	4

<sup>1</sup>The negative denotes that the response increased instead of decreasing when the concentration of ethanol was halved.

A percent drop of ~25% (for both sensors) for P25DMA means that P25DMA had moderate selectivity when exposed to all four analytes simultaneously. As the number of analytes simultaneously exposed increased, the selectivity towards ethanol decreased; however, ethanol was still somewhat preferentially sorbed.

P25DMA 20% NiO showed a good percent drop when exposed to all four analytes. Similar to P25DMA, the percent drop was smaller as more analytes were added; however, to a much lesser degree. Overall, P25DMA 20% NiO still had good selectivity to ethanol despite three other interferences present.

The other four sensing materials all had really poor selectivity, below 10%, except OV 225 on the rigid sensor. The negative values, within error, are likely to indicate no change when the concentration of ethanol was halved since they are so close to zero. The increased response (larger percent drop) for the rigid sensor as opposed to the flexible sensor for OV 225 should be further investigated because the rigid and flexible sensors showed similar responses and trends.

After comparing the selectivity towards ethanol for six different sensing materials using three interferents (methanol, acetone, and benzene), it was found that there were interactions between the gas analytes that affected the selectivity of the sensing materials towards ethanol. As the number of analytes was increased, the percent drop got smaller indicating poorer selectivity. This is most likely due to increased competition between ethanol and the other interferents. P25DMA 20% NiO had the best selectivity to ethanol by far, with a percent drop near 50% for two and three analyte mixtures and almost 40% when exposed to all four analytes. This is near a perfectly selective sensor which would have dropped 50% when the concentration of ethanol was halved despite which and how many other analytes were present.

In addition to selectivity, the response and recovery times were also measured for the flexible sensor with each of the six sensing materials with each of the four analytes (ethanol and three interferents). The response time is the time it takes for the signal to reach 90% of the final signal (full response) and the recovery time is 90% of the time it takes the signal to return to the baseline. The response and recovery times were measured at 5000 ppm for each analyte. This is because response and recovery times tend to be proportional to concentration: the higher the concentration, the larger the response signal, and the longer the response and recovery times. Therefore, the response and recovery times are likely to be longer than the response and recovery times in this application.

The response and recovery times can be measured in two ways: amplitude and delay. A shift in resonant frequency is measured when ethanol sorbs onto the sensing material. This sorption causes a change in capacitance, which affects both the amplitude and time delay of the radio frequency (RF) pulse that is reflected back. A RF pulse is sent across the sensor, where most of the energy is stored, but a minimal amount is returned. Both the amplitude and time delay of the returning RF pulse are measured. The amplitude response is the same response measured for the selectivity measurements. In general, the amplitude and delay responses gave very similar responses; however, the delay response was generally much greater in magnitude.

Due to limitations of the equipment, the response was measured every 15 seconds. Therefore, the response and recovery times are a multiple of 15. The response and recovery times were more dependent on type of sensor than the interaction of the sensing material with the analytes. This can be seen in Figures 5.7 to 5.12 where the response times for all the sensing materials for all four analytes were ~90 seconds and the recovery times were ~120 seconds.

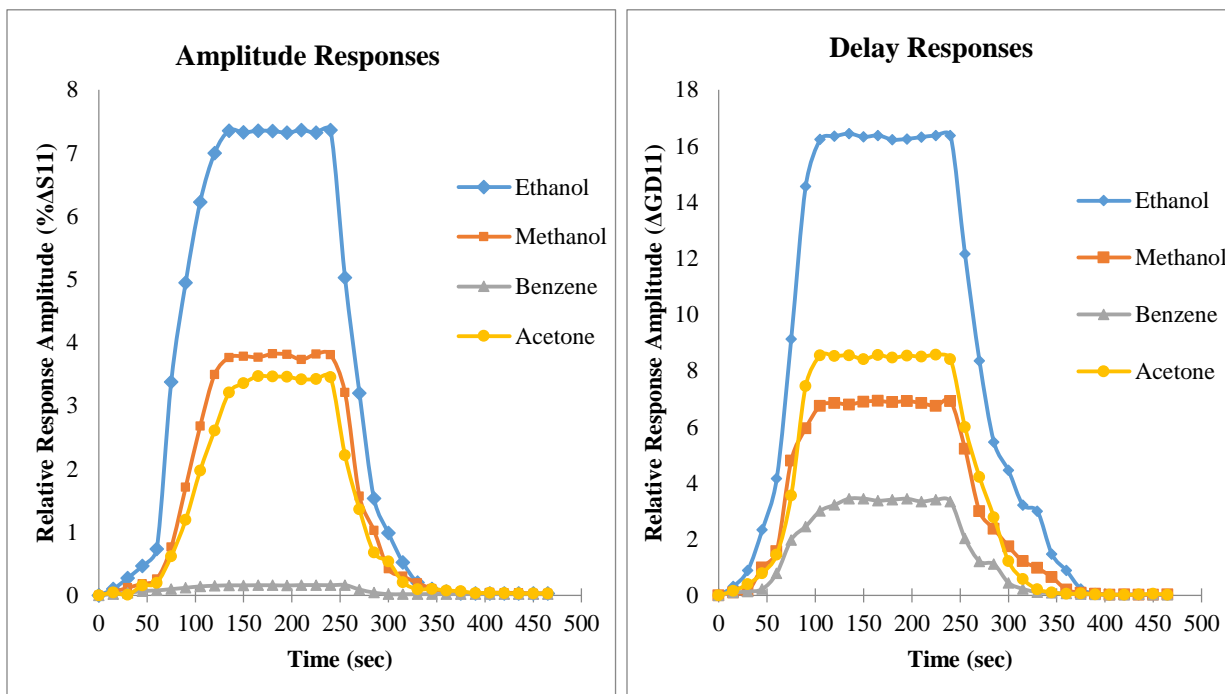


Figure 5.7: The amplitude and delay response and recovery curves for P25DMA for each analyte individually tested at 5000 ppm.

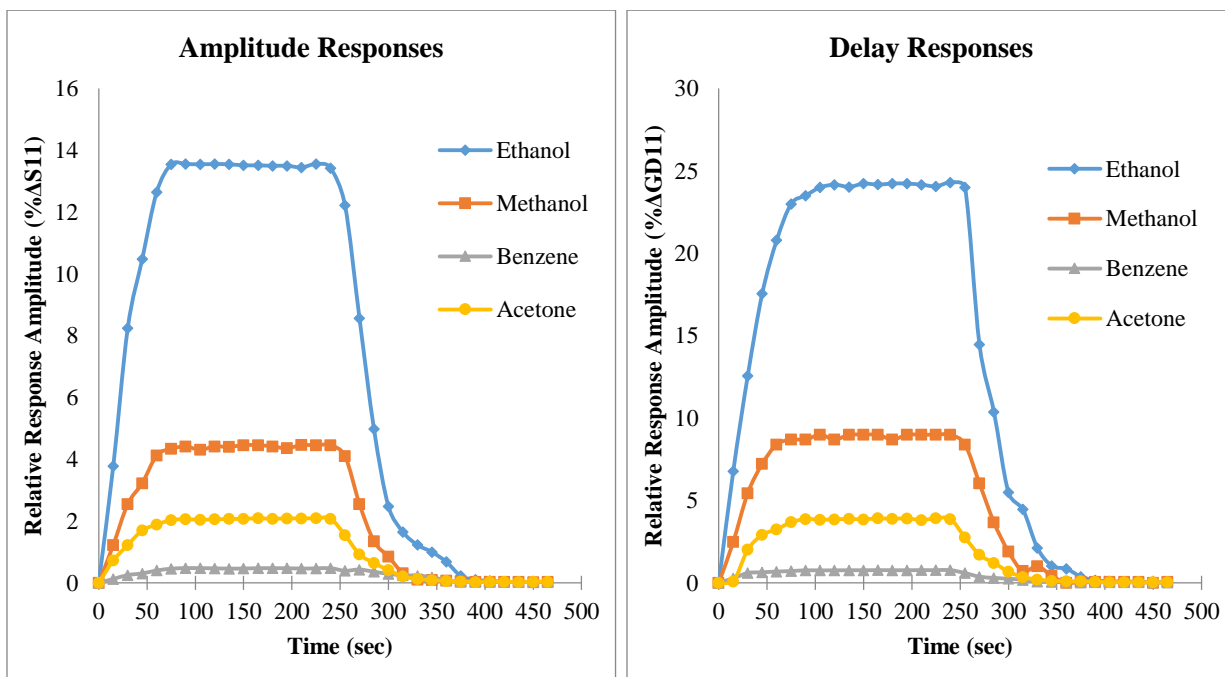


Figure 5.8: The amplitude and delay response and recovery curves for P25DMA 20% NiO for each analyte individually tested at 5000 ppm.

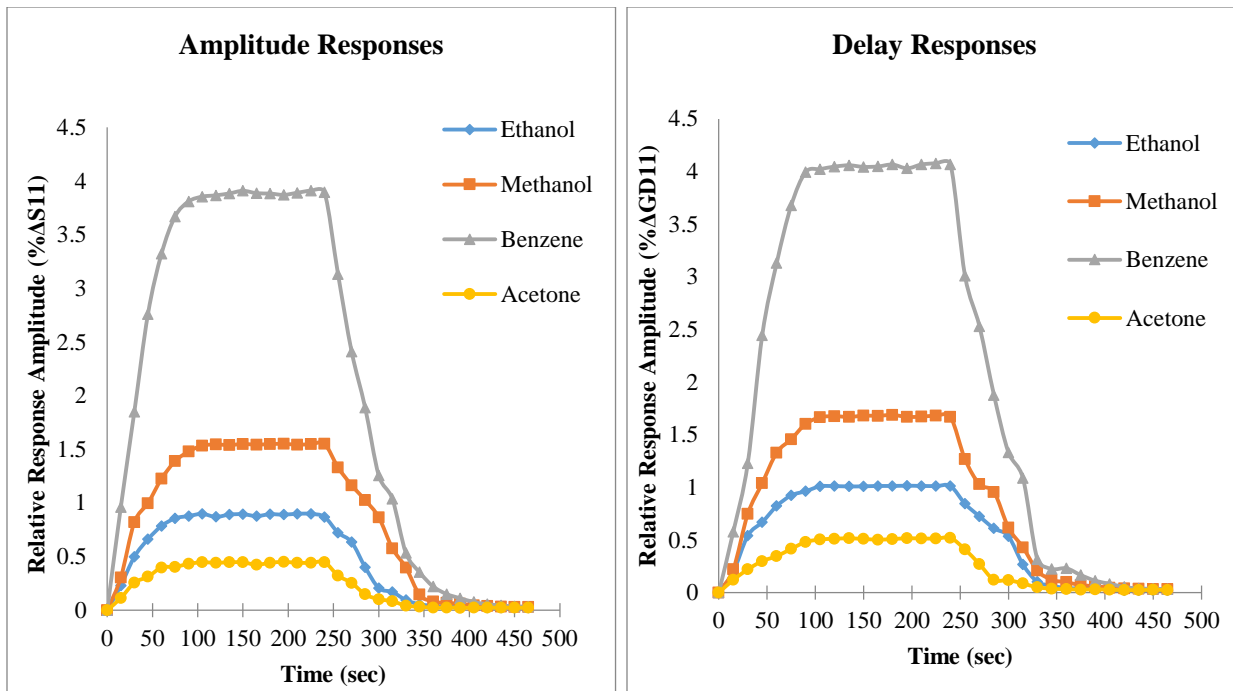


Figure 5.9: The amplitude and delay response and recovery curves for P25DMA 20% ZnO for each analyte individually tested at 5000 ppm.

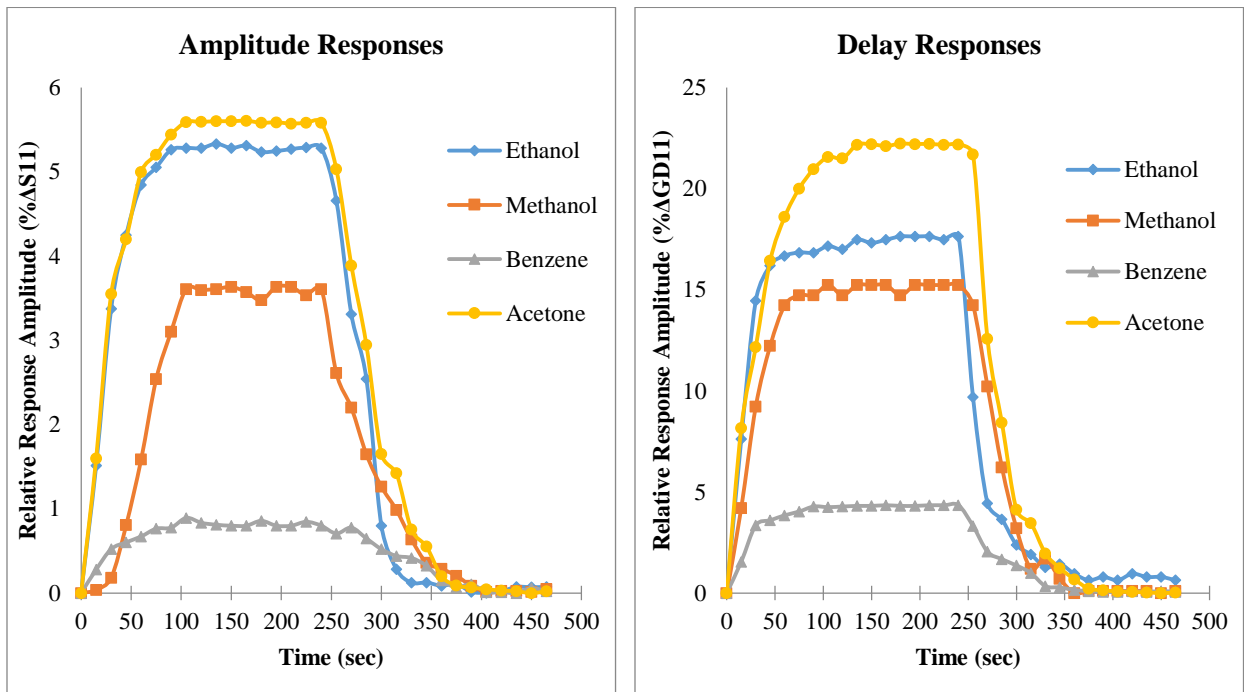


Figure 5.10: The amplitude and delay response and recovery curves for OV 275 for each analyte individually tested at 5000 ppm.

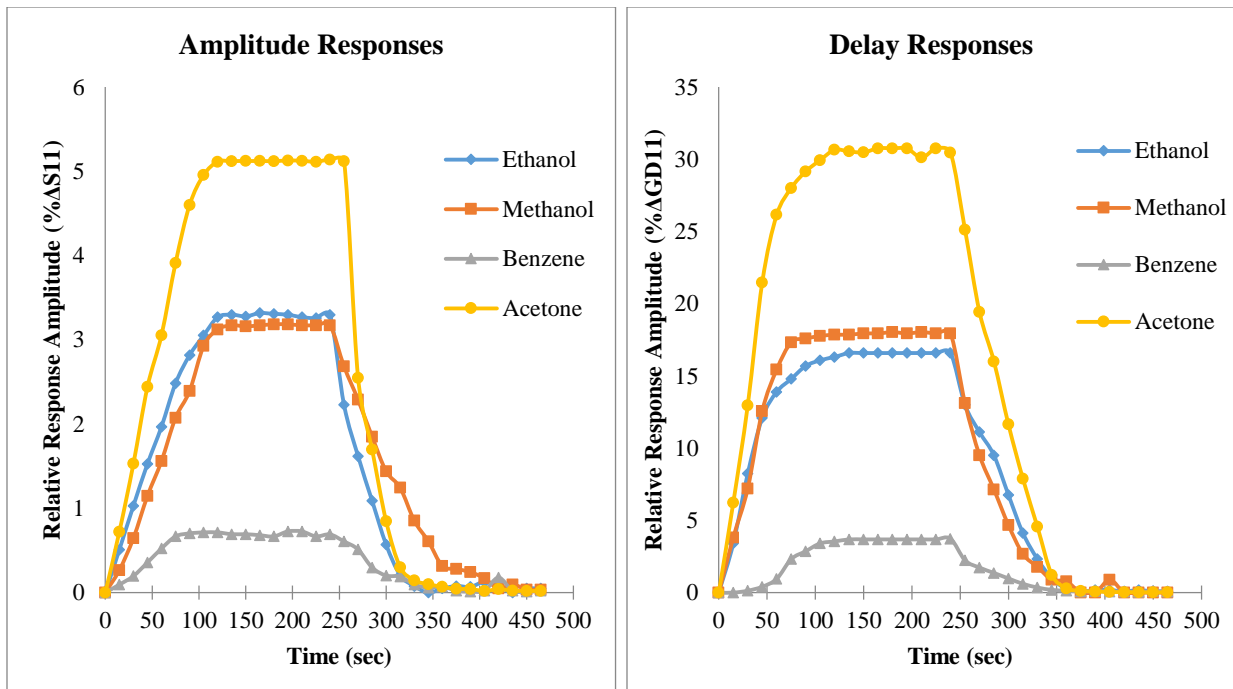


Figure 5.11: The amplitude and delay response and recovery curves for OV 225 for each analyte individually tested at 5000 ppm.

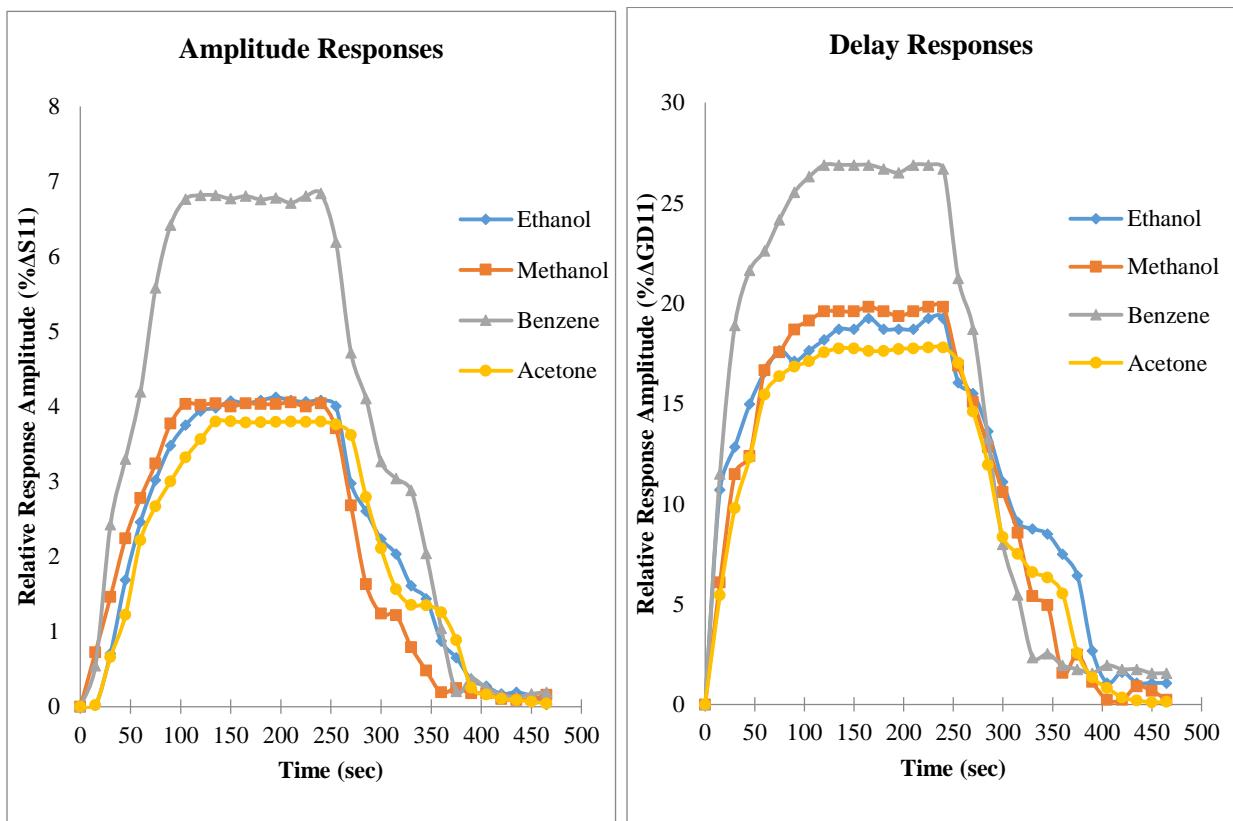


Figure 5.12: The amplitude and delay response and recovery curves for SXFA for each analyte individually tested at 5000 ppm.

### 5.1.1.2 RFID Rigid Sensor

Given that both the flexible and rigid radio frequency identification (RFID) sensor designs responded similarly, the RFID rigid sensor was further evaluated for sensitivity. Three sensing materials (poly (2,5-dimethyl aniline), poly (2,5-dimethyl aniline) doped with 20 wt. % NiO, and poly (2,5-dimethyl aniline) doped with 20 wt. % ZnO (denoted as P25DMA, P25DMA 20% NiO, and P25DMA 20% ZnO, respectively) were evaluated on the rigid RFID sensor. Each sensor was exposed to three different gas analytes (ethanol, methanol, and benzene) and their response recorded. Initially, ethanol was evaluated to determine the sensitivity and the limit of detection (LoD) to ethanol.

The twelve ethanol concentrations ranged from 2.5 to 5000 ppm of ethanol (in dry nitrogen). It should be noted that ethanol fully saturated P25DMA around 2500 ppm and P25DMA 20% ZnO around 1000 ppm (see Figure 5.13). When saturation occurred, increasing the concentration of analyte exposed to the sensing material no longer produced a change in response.

In these tests, ethanol was the single analyte to be detected. Responses could be detected at levels as low as 2.5 ppm; however, the LoD was calculated relative to the level of noise for each sensing material on the RFID sensor.

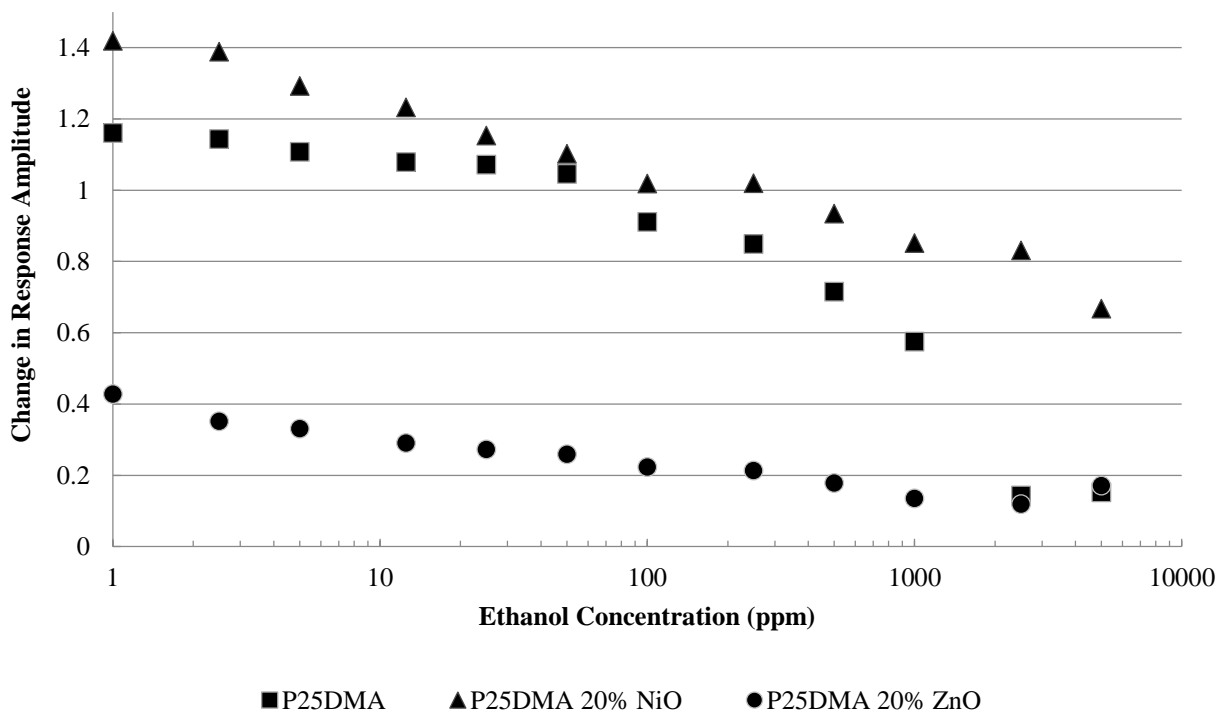


Figure 5.13: Change in sensor response amplitude for each sensing material at different concentrations of ethanol. Note that for clarity, the concentration has been placed on a log scale with a concentration of 0 ppm of ethanol equal to 1 on the scale.

The LoD was calculated from (baseline) noise measurements. The sensors were purged with nitrogen for 60 minutes while recording a measurement every 5 minutes. Noise was considered to be the standard deviation of the response signal to pure nitrogen. Ultimately, the LoD was calculated as three times the noise (by convention). Results from these calculations are cited in Table 5.7, where the noise response from the sensor was first converted into a concentration of ethanol based on a calibration curve produced from Figure 5.13, and then multiplied by 3 to get LoD.

Table 5.7: Noise and Limit of Detection for Ethanol for each Sensing Material on the RFID Sensor

<b>Sensing Material</b>	<b>Noise (response)</b>	<b>Noise (ppm)</b>	<b>LoD (ppm)</b>
<b>P25DMA</b>	0.0088	1	3
<b>P25DMA 20% NiO</b>	0.049	8	24
<b>P25DMA 20% ZnO</b>	0.069	140	420

Both P25DMA and P25DMA 20% NiO had similar responses to 2.5 ppm of ethanol (as seen from Figure 5.13); however, the noise for P25DMA 20% NiO was larger. The noise variation observed between sensing materials may have been due to interactions between the analytes and the sensing material or slight changes in the capacitive response of the sensing materials measured by the sensor. A high LoD was expected for P25DMA 20% ZnO based on the low ethanol sorption observed in the sorption studies (see Section 4.3.2).

Based on the LoD results shown in Table 5.7, P25DMA has the sensitivity needed for a transdermal ethanol sensor. By optimizing the sensing film thickness, it may be possible to reduce the noise observed for P25DMA 20% NiO and therefore reduce its LoD. While sensitivity is important, selectivity is equally important.

Selectivity towards ethanol was measured by exposing the sensing materials to ethanol and two typical interferent gases (benzene and methanol). The change in response amplitude was measured for three different analytes, for each sensing material. The gases were tested individually at four different concentrations (5000, 2500, 1250, and 625 ppm) and similar trends were seen at all four concentrations. Representative results are shown in Figure 5.14 a-b for 5000 and 625 ppm, respectively, i.e., at the two extremes of the concentration range. The response (change in response amplitude) for each gas is graphically displayed. The target analyte's response (ethanol, in this case) was much larger than the response to the interferents, thus indicating a highly selective sensor. This was the case for both P25DMA and P25DMA 20% NiO.



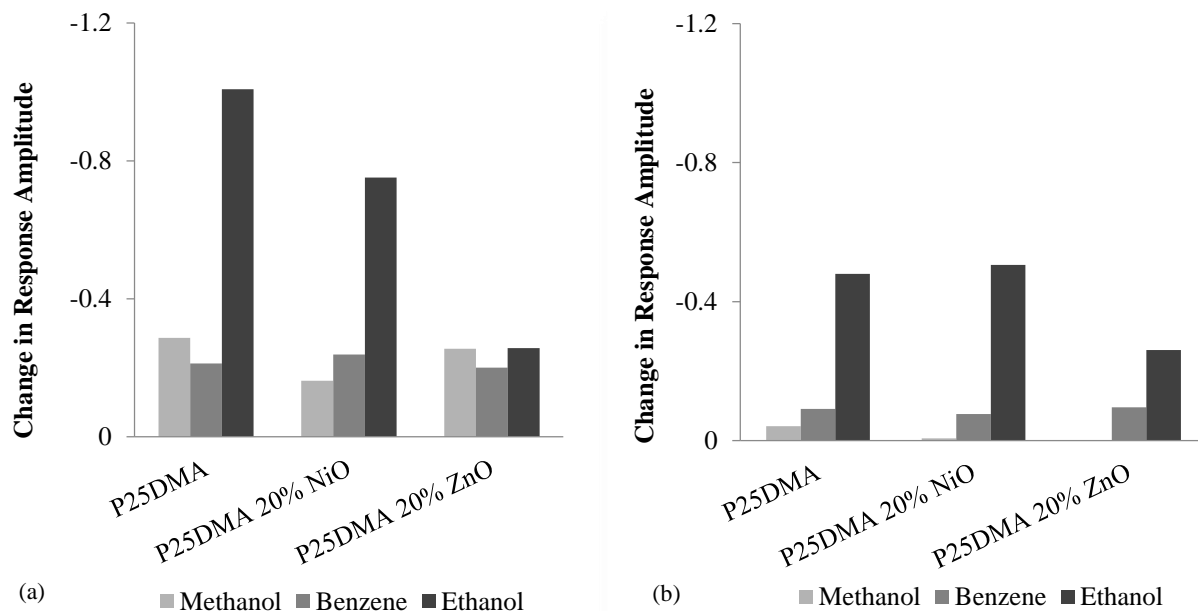


Figure 5.14: The change in resonant frequency measured at equilibrium for different analytes at (a) 5000 ppm and (b) 625 ppm for each sensing material.

Selectivity of the sensing materials was compared based on the same concentration of gas tested. At 5000 ppm, ethanol, benzene, and methanol had very similar responses with P25DMA 20% ZnO, which was due to the analytes saturating P25DMA 20% ZnO. However, at 625 ppm, P25DMA 20% ZnO's response was approximately twice as large for ethanol. Therefore, once saturation has been reached, the change in response amplitude will not increase, despite an increase in analyte concentration. Saturation of ethanol can be seen in Figure 5.13.

For P25DMA 20% NiO and P25DMA, similar trends were seen in Figure 5.3 at both 5000 ppm and 625 ppm, since saturation was much less of an issue. Both P25DMA 20% NiO and P25DMA produced a much higher response to ethanol, than the other two interferents, when exposed to the same concentration of each gas.

Therefore, both P25DMA and P25DMA 20% NiO exhibited high selectivity towards ethanol since ethanol produced a much larger response than the interferents. P25DMA 20% ZnO, on the other hand, had moderate selectivity at 625 ppm and poor selectivity at 5000 ppm.

In addition, the response and recovery times were measured at 5000 ppm of ethanol, since 5000 ppm produced the largest response signal. Generally, the larger the response, the slower the response and recovery times because the response time is measured as 90% of the full response and the recovery time is measured as 90% recovery with respect to the baseline (see Figure 5.15). Therefore, the response and recovery times for lower concentrations should be shorter, thus making the tests at 5000 ppm essentially 'worst case scenario' tests. The response and recovery

times were 35 and 100 seconds for P25DMA, 60 and 70 seconds for P25DMA 20% NiO, and 60 and 60 seconds for P25DMA 20% ZnO. These response and recovery times are acceptable for a transdermal ethanol sensor and are of the same time scale as current breathalyzers (Abdul Rahim and Syed Hassan, 2010); however, these times could be improved in the future with improvements to the sensor such as optimization of sensing material thickness and sensor electronics (improvements that are beyond the “proof-of-concept” scope of the current investigation).

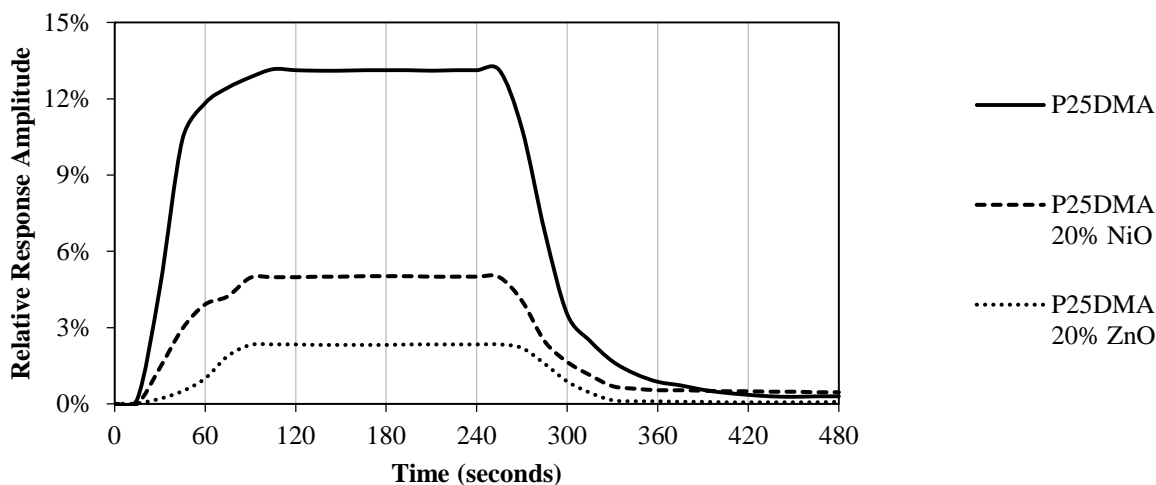


Figure 5.15: Response and recovery times for each sensing material measured for ethanol at 5000 ppm. Relative response amplitude is the percent change in the amplitude of the response from the baseline, when the sensing material is exposed to an analyte.

Overall, P25DMA and P25DMA 20% NiO are good sensing materials, on this RFID sensor, for ethanol with high selectivity and LoD of 3 and 24 ppm, respectively. P25DMA 20% ZnO had poor sensitivity and selectivity to ethanol; however, it may still be useful in a sensing array application as a way to avoid false positives. Response and recovery times were all acceptable in the order of a few tens of seconds.

### 5.1.1.3 RFID Sensor Array

Two rigid RFID sensor arrays were constructed and tested. Each sensor array contained three different sensing materials (see Figure 5.16). One sensor array contained the siloxane-based sensing materials (OV 225, OV 275, and SXFA) and the other sensor array contained the polyaniline-based sensing materials (P25DMA, P25DMA doped with 20 wt. % NiO, and P25DMA doped with 20 wt. % ZnO). These two sensor arrays will be referred to as the siloxane-based and the P25DMA-based sensor arrays.



Figure 5.16: The three sensor array on the rigid RFID platform. These RFID arrays are the same size as those shown in Figure 5.2.

The responses from each sensing material on the sensor array were able to be separated (see Figure 5.17) since all three sensing materials (in both cases) resonated at frequencies that were far enough from one another that peaks observed for each sensing material did not overlap. However, the magnitude of the peak for each additional sensing material is reduced. Note that for the P25DMA-based sensor array, P25DMA was the first sensing material sampled in the array, followed by P25DMA 20% NiO, and then P25DMA 20% ZnO. A similar response was observed for the siloxane-based sensing materials (Chen, 2015).

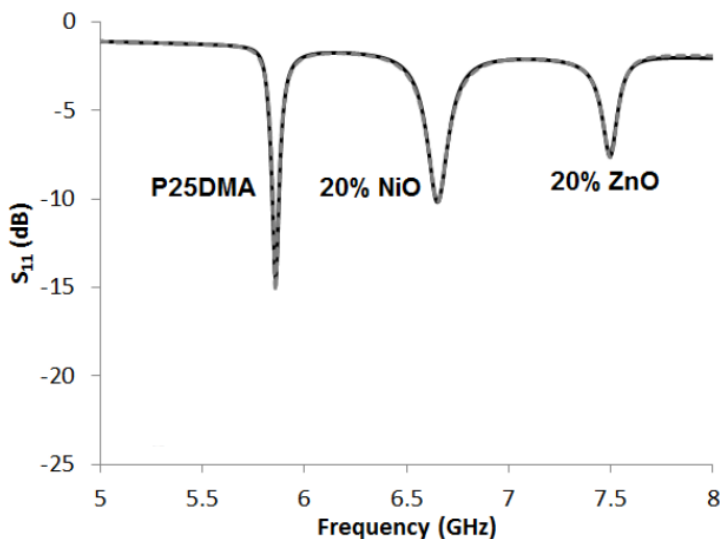


Figure 5.17: Sample readout of the RFID three sensor array for the P25DMA-based sensing materials. Note that the peaks for each sensing material are separate and distinct (Chen, 2015).

Each sensor array was exposed to four different gas analytes (ethanol, methanol, acetone, and benzene) at 1250 ppm (individually) and the responses were measured in terms of magnitude ( $S_{11}$ ) in decibels (dB). These responses were normalized as % change (see Figure 5.18).

Note that OV 225 had the highest response to ethanol out of all the sensing materials. Also note that for the single gas analytes, many of these sensing materials are much more selective towards the interferent gas analytes and not ethanol. For example, SXFA produced a much larger response to benzene than any of the other gases and all of the P25DMA-based polymers were more selective towards acetone than ethanol.

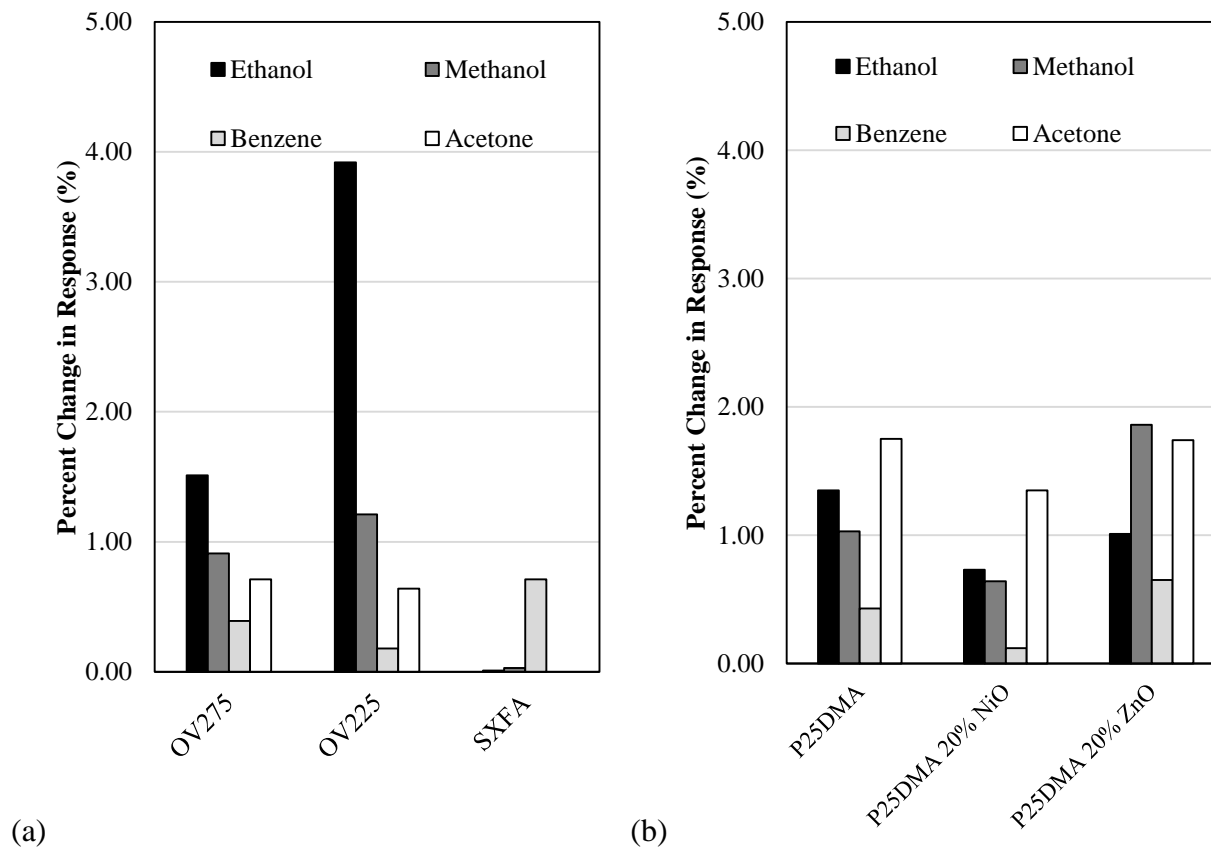


Figure 5.18: Single gas analytes for (a) the siloxane-based and (b) the P25DMA-based sensor arrays.

These sensors were then exposed to various gas mixtures, where all the gases were evaluated at 1250 ppm. Each gas mixture contained ethanol and at least one other of the interferents (methanol, acetone, and benzene). Initially two gas mixtures were prepared (see Figure 5.19), followed by three gas mixtures (see Figure 5.20), and finally all four gas analytes were evaluated simultaneously (see Figure 5.21). In each case, the concentration was initially measured at 1250 ppm, and then only the ethanol concentration was halved to 625 ppm, while all the other gas analytes (interferents) remained at a concentration of 1250 ppm. Nitrogen gas was used as the balance to ensure the flow rate and pressure remained the same throughout all measurements.

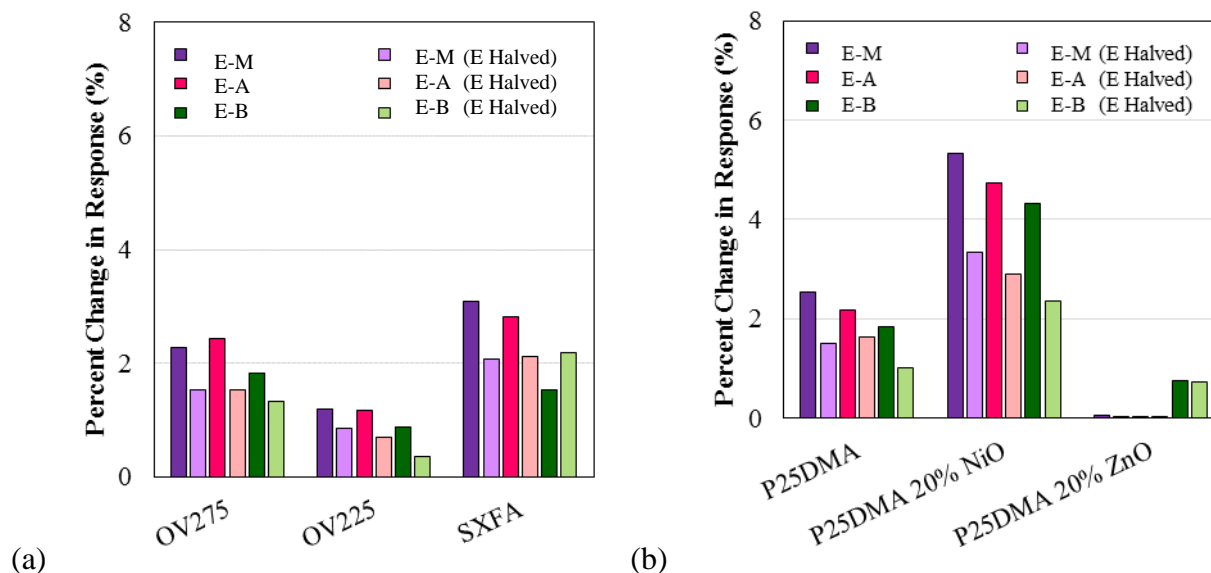


Figure 5.19: Two gas mixtures for (a) the siloxane-based and (b) the P25DMA-based sensor arrays. Note that E, M, A, and B denote ethanol, methanol, acetone, and benzene, respectively.

The two gas mixtures consisted of ethanol and methanol; ethanol and acetone; and ethanol and benzene. An ideal sensor for ethanol would halve its response when the concentration of ethanol was halved, despite the other interferent gas's concentration remaining the same. This, however, was not the case (see Table 5.8) since gas analytes interact with one another both in the environment while diffusing through the air and on the sensing materials when competing for sensing sites. Note that it is possible for two analyte molecules to sorb to the same sensing site, if one molecule binds to another that is already sorbed at the sensing site.

Table 5.8: Percent Drop of Response when the Ethanol Concentration was Halved

Gas Mixture <sup>1</sup>	Percent Drop of Response (%)					
	OV 275	OV 225	SXFA	P25DMA	P25DMA 20% NiO	P25DMA 20% ZnO
<b>E-M</b>	32	27	33	40	37	33
<b>E-A</b>	37	41	25	25	39	-100 <sup>2</sup>
<b>E-B</b>	27	59	-43 <sup>2</sup>	46	46	4

<sup>1</sup> E is ethanol, M is methanol, A is acetone, and B is benzene

<sup>2</sup> Negative numbers represent an increase in response

Overall, in the two gas mixtures, the responses dropped by about one third, when the concentration of ethanol was halved. The best sensing materials for selectivity towards ethanol would be P25DMA 20% NiO, P25DMA, and OV 225. These three sensing materials had the closest percent drops to the ideal 50%, for all three gas mixtures.

Note that the response for SXFA increased when the ethanol concentration was halved, in the presence of benzene. This is due to SXFA producing a large response to benzene (as already seen in Figure 5.18 for the individual gases). When benzene has less competition with ethanol (when the concentration of ethanol is halved), benzene is able to more readily bind to SXFA, thereby increasing the response. Also note the 100% increase in response for P25DMA 20% ZnO when exposed to the ethanol-acetone mixture. In this case, the large percent drop is misleading due to the small responses observed (0.01 to 0.02) and thus, the response would be considered the same, within error.

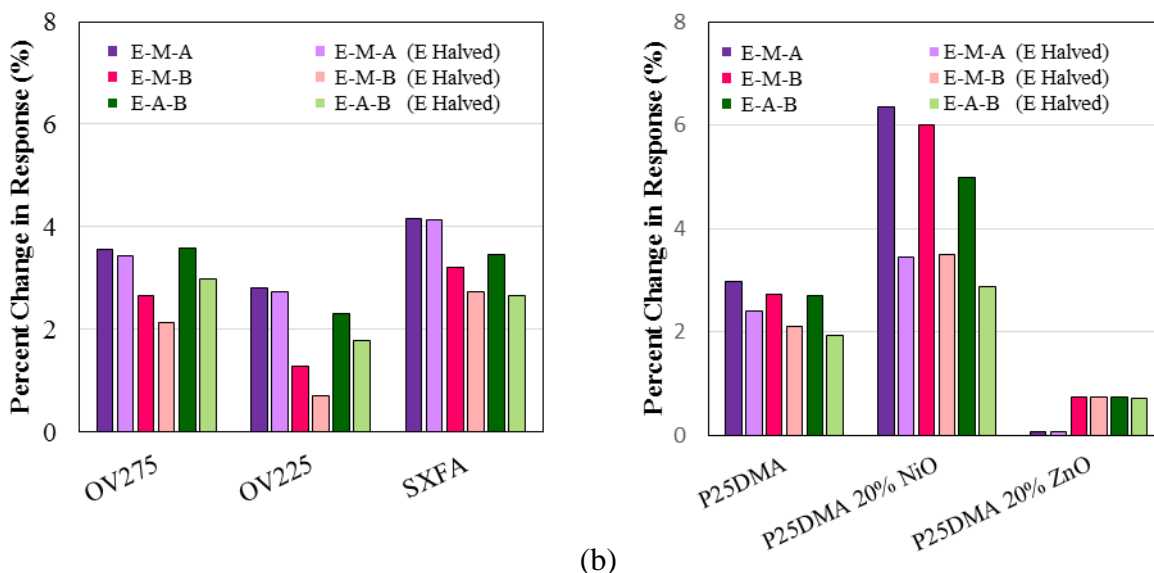


Figure 5.20: Three gas mixtures for (a) the siloxane-based and (b) the P25DMA-based sensor arrays. Note that E, M, A, and B denote ethanol, methanol, acetone, and benzene, respectively.

The three gas mixtures produced less of a percent drop, as expected. As more gas analytes were present, the more the analytes interacted. Again, the ideal case is a 50% drop when the concentration of ethanol is halved; however this was not observed for any of the sensing materials (see Table 5.9). Note that P25DMA 20% NiO produced close to a 50% drop when the concentration of ethanol was halved and therefore, had very good selectivity for all of the mixtures of the three gas analytes.

Table 5.9: Percent Drop of Response when the Ethanol Concentration was Halved

Gas Mixture <sup>1</sup>	Percent Drop of Response (%)					
	OV 275	OV 225	SXFA	P25DMA	P25DMA 20% NiO	P25DMA 20% ZnO
E-M-A	4	2	1	19	46	0
E-M-B	20	44	15	23	42	0
E-A-B	16	23	23	28	42	1

<sup>1</sup> E is ethanol, M is methanol, A is acetone, and B is benzene.

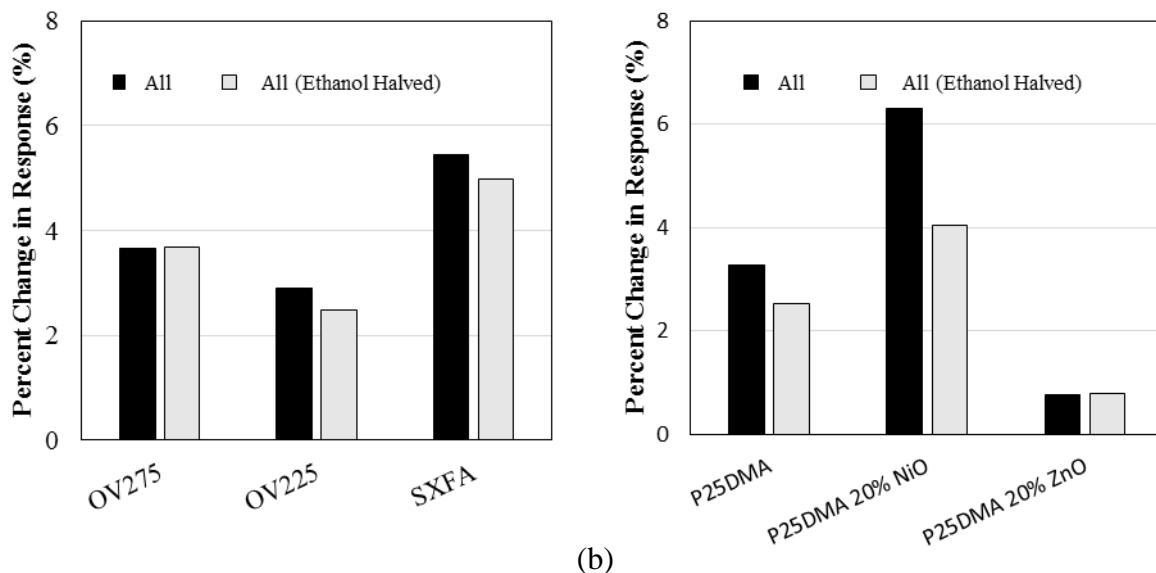


Figure 5.21: All four gases for (a) the siloxane-based and (b) the P25DMA-based sensor arrays.

The gas mixture containing all four gas analytes generated even lower selectivity, as expected (see Table 5.10). However, the best sensing material, in terms of selectivity towards ethanol, was P25DMA 20% NiO. It is interesting to note that P25DMA 20% NiO had the highest selectivity towards ethanol when interferences were present in the gas mixture, but produced a larger response to acetone than ethanol when single gases were used. Therefore, when acetone and ethanol are present together, ethanol seemed to bind more preferentially to the P25DMA 20% NiO, thereby effectively blocking (or significantly minimizing) the acetone's ability to bond to P25DMA 20% NiO. This again confirms that gas analytes do interact with one another.

Table 5.10: Percent Drop of Response when the Ethanol Concentration was Halved

Gas Mixture <sup>1</sup>	Percent Drop of Response (%)					
	OV 275	OV 225	SXFA	P25DMA	P25DMA 20% NiO	P25DMA 20% ZnO
<b>E-M-A-B</b>	-1 <sup>2</sup>	15	8	23	36	-3 <sup>2</sup>

<sup>1</sup> E is ethanol, M is methanol, A is acetone, and B is benzene.

<sup>2</sup> Negative numbers represent an increase in response.

All of the data collected for the various gas mixtures shown in Figures 5.16 – 5.19 were subsequently run through a filtering algorithm. Principal component analysis (PCA) was used to separate the responses of each of the gas analytes evaluated (ethanol, methanol, acetone, and benzene) on the two sensor arrays described above (siloxane-based and P25DMA-based).

The gas analytes interacted with one another, which in turn affected how the analytes interacted with the sensing materials. This can be seen from the responses observed when the gas analytes were mixed and exposed to the sensor array. If there was no interaction or competition between

sensing sites, the response of a sensing material/sensor to two analytes would be (more or less) additive. This, however, was not the case and is why poorer selectivity was observed as more gas analytes were mixed together and simultaneously tested. Because of the gas analyte interactions and poor selectivity, the gas mixtures were likely to appear as their own clusters on a PCA plot. In other words, each gas mixture (e.g. single gas analytes, two gas mixtures, three gas mixtures, etc.) was likely to present its own cluster. This was the case for the RFID three sensor array and the sensor array shown in Section 4.6 (see Figure 4.33). Note that for the data used in this PCA analysis, each gas mixture, except for the single gas analytes, contained some ethanol. Therefore, the separation of gas analytes was more noticeable for the three interferents (acetone, methanol, and benzene).

Figure 5.22 shows the PCA plot for the siloxane-based sensor array (see Appendix H for additional details on PCA). Overall, the four gas analytes are well separated. The two gas mixtures all fall close to the respective single gas mixture. For example, the benzene (green circle) and benzene and ethanol mixture (light green diamonds) are close together in the upper middle portion of the PCA plot. In addition, the three gas mixtures (triangles) fall between the two interferent gas mixtures (diamonds). For example, the ethanol, methanol, and benzene (E-M-B) (orange triangles) is between ethanol and benzene (E-B) (light green diamonds) and ethanol and methanol (E-M) (pink diamonds). Finally, the four component gas mixture (E-M-A-B) (black squares) is in the middle, which is between all the other gas analyte combinations.

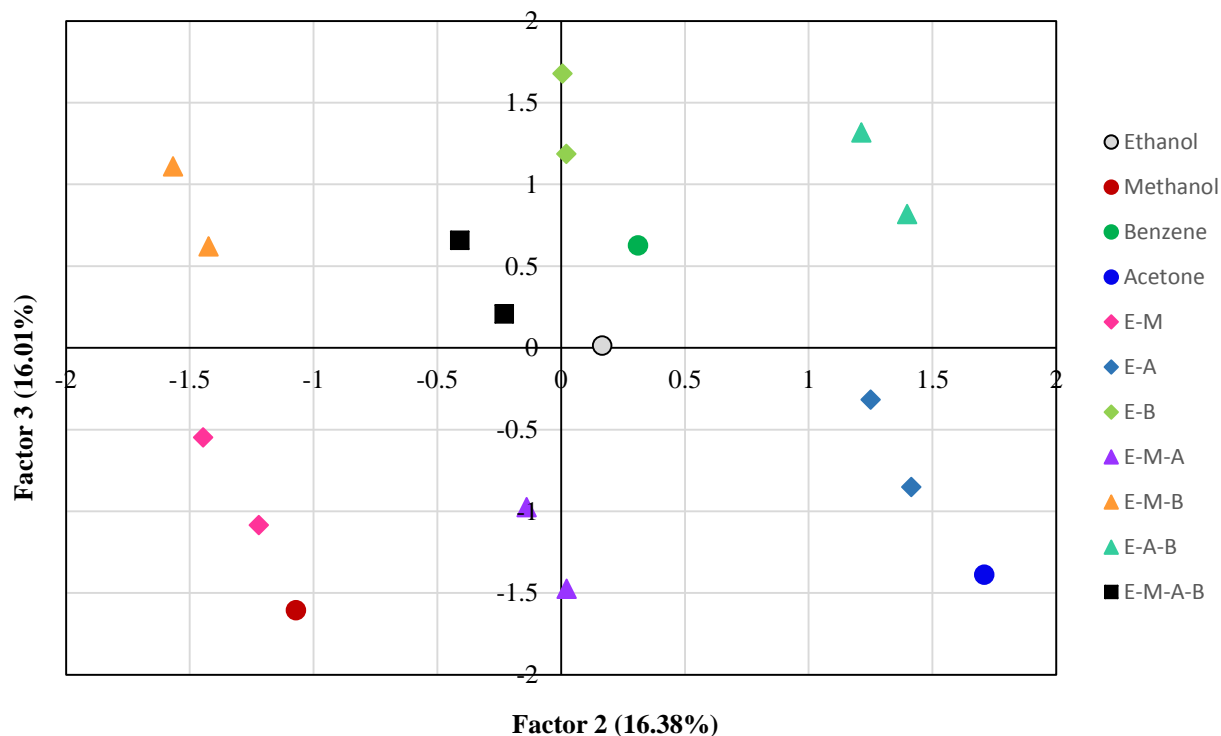


Figure 5.22: PCA plot for the siloxane-based RFID sensor array. Note that E is ethanol, M is methanol, A is acetone, and B is benzene in the gas mixtures.



Similarly, Figure 5.23 shows the PCA plot of Factor 3 vs Factor 2 for the P25DMA-based RFID sensor array. Again, the clusters for each single gas (ethanol (grey circle), methanol (red circle), benzene (green circle), and acetone (blue circle)) are well separated. In addition, the two gas mixtures of the analytes with ethanol are close to the single gas analytes and the three gas mixtures (triangles) are clustered between the two gas mixtures (diamonds). For example, the ethanol, methanol, and acetone three gas mixture (purple triangles, middle left) is about halfway between the two gas mixtures of ethanol and methanol (pink diamonds, lower left) and the acetone and ethanol mixture (lighter blue diamonds, upper left).

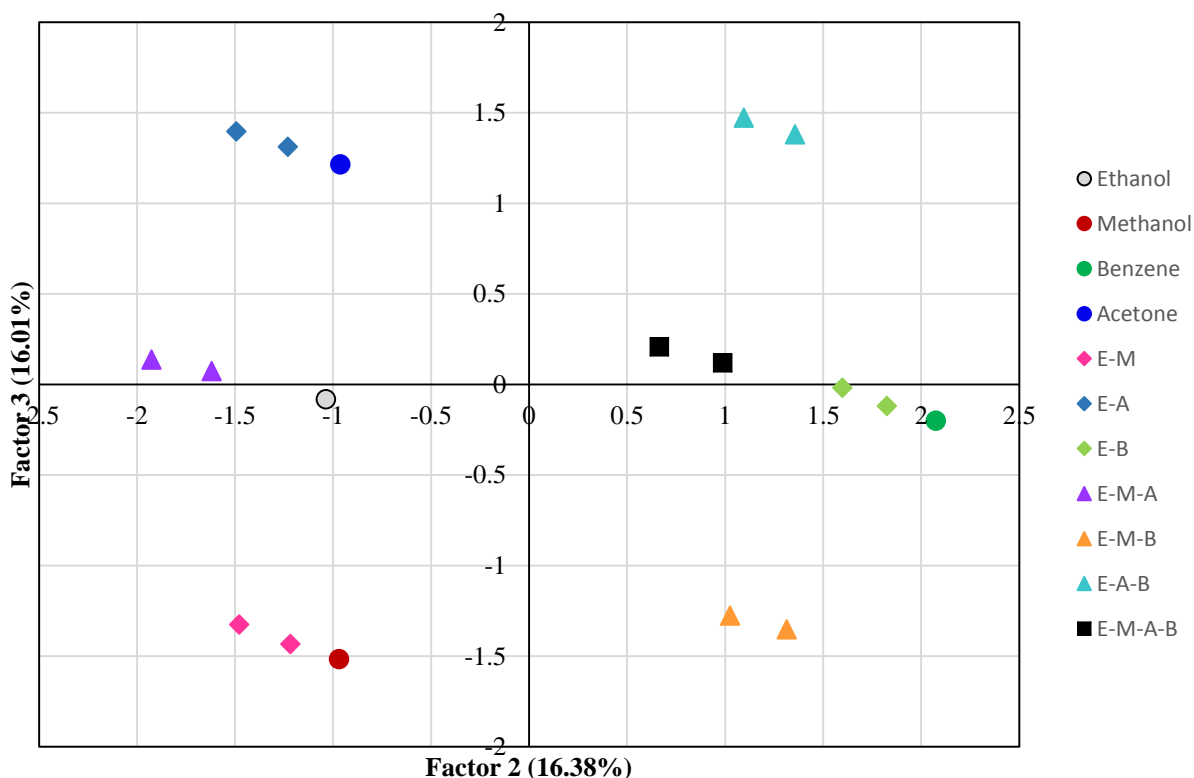


Figure 5.23: PCA plot for the P25DMA-based RFID sensor array. Note that E is ethanol, M is methanol, A is acetone, and B is benzene in the gas mixtures.

Note that the Factors used in both Figures 5.22 and 5.23 to separate the analytes were Factor 2 and 3, instead of Factors 1 and 2 (as seen in Figure 4.33 in Section 4.6). This was because Factors 2 and 3 were much more dependent on the type of gas analyte than Factors 1 and 2. When the projection of the variables (gas analytes and sensing materials) onto the Factor 2 x 3 plane was plotted (see Figure 5.24), the contribution of the gas analytes was more prevalent (larger), which translated into the type of gas analyte affecting the Factors. In essence, the longer the lines from the centre on the projection plot (Figure 5.24), the more that variable affected the clusters in the PCA plot for those two Factors. In this case, the four gas analytes (variables) had much longer lines from the centre of the plot than the sensing materials. Therefore, the gas analytes affected

the location of the clusters much more than the sensing materials. This resulted in clusters that were well separated by analyte.

It is important to understand that despite Factor 1 containing the majority of the variability for both of the RFID sensor arrays, the variability masked the effects of the type of gas analyte. In some cases, it is better to plot lower variability factors to separate the effects.

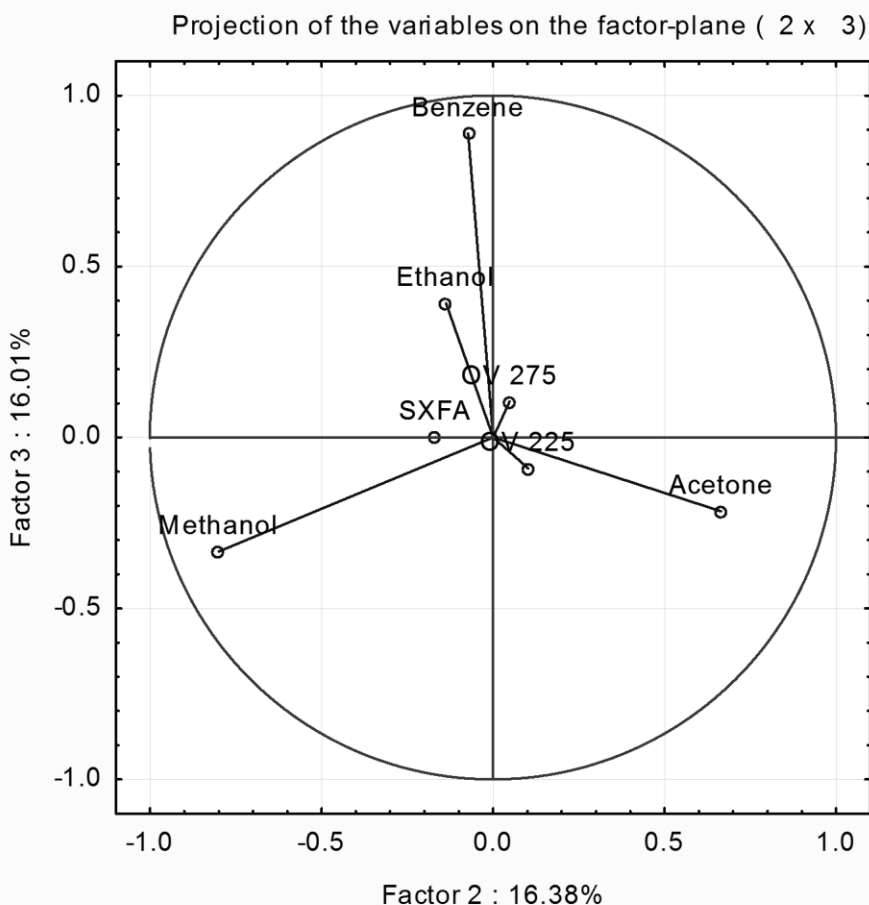


Figure 5.24: Factor 2 vs. Factor 3 projection of variables onto the 2 x 3 plane for the siloxane-based RFID sensor array.

Overall, both the siloxane-based and the P25DMA-based RFID sensor arrays were able to differentiate and identify three interferences for ethanol (acetone, methanol, and benzene). To distinguish between ethanol and benzene, Factor 1 vs. Factor 4 could be plotted which separated benzene and ethanol quite well (see Figure 5.25). Ethanol and benzene are represented by larger circles in Figure 5.25 for emphasis. In addition, the four component gas mixture (E-M-A-B) is clearly separated in the upper left quadrant.

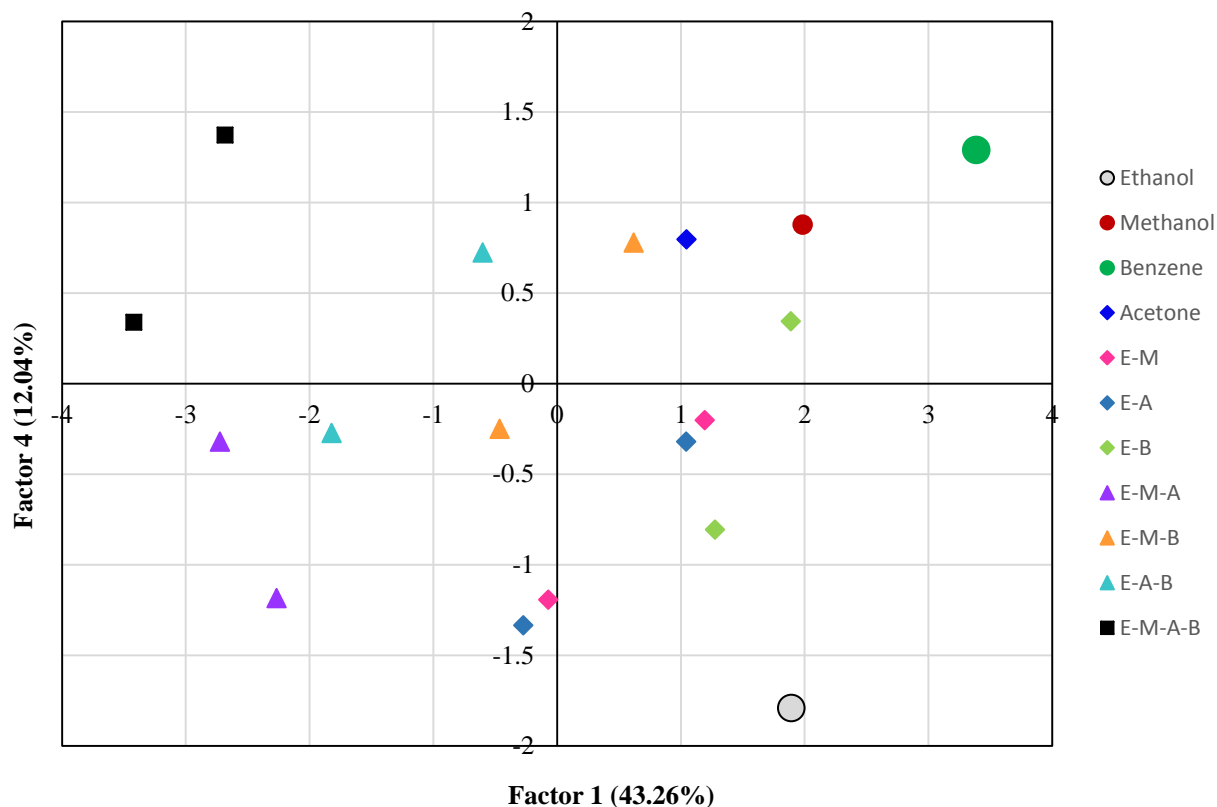


Figure 5.25: Factor 1 vs Factor 4 PCA plot for the siloxane-based RFID sensor array. The two squares emphasize ethanol and benzene. Note that E is ethanol, M is methanol, A is acetone, and B is benzene in the gas mixtures.

### 5.1.2 Microelectromechanical Systems (MEMS) Microcantilever

A small amount of polymer was deposited onto the sensing plate. The sensing plate is shown at the bottom of Figure 5.26 a-b, with a “blob” of polymer on it. A current was applied to the microcantilever such that the microcantilever was poised to “pull-in”. This is referred to as preloading the cantilever. Pull-in occurred when a gas analyte (ethanol, in this case) sorbed onto the sensing material. Figure 5.26 shows the microcantilever before (a) and after (b) ethanol was sorbed. Note the “fringe fields” in Figure 5.26b. This is a visual indication that the microcantilever experienced pull-in (Khater et al., 2014).

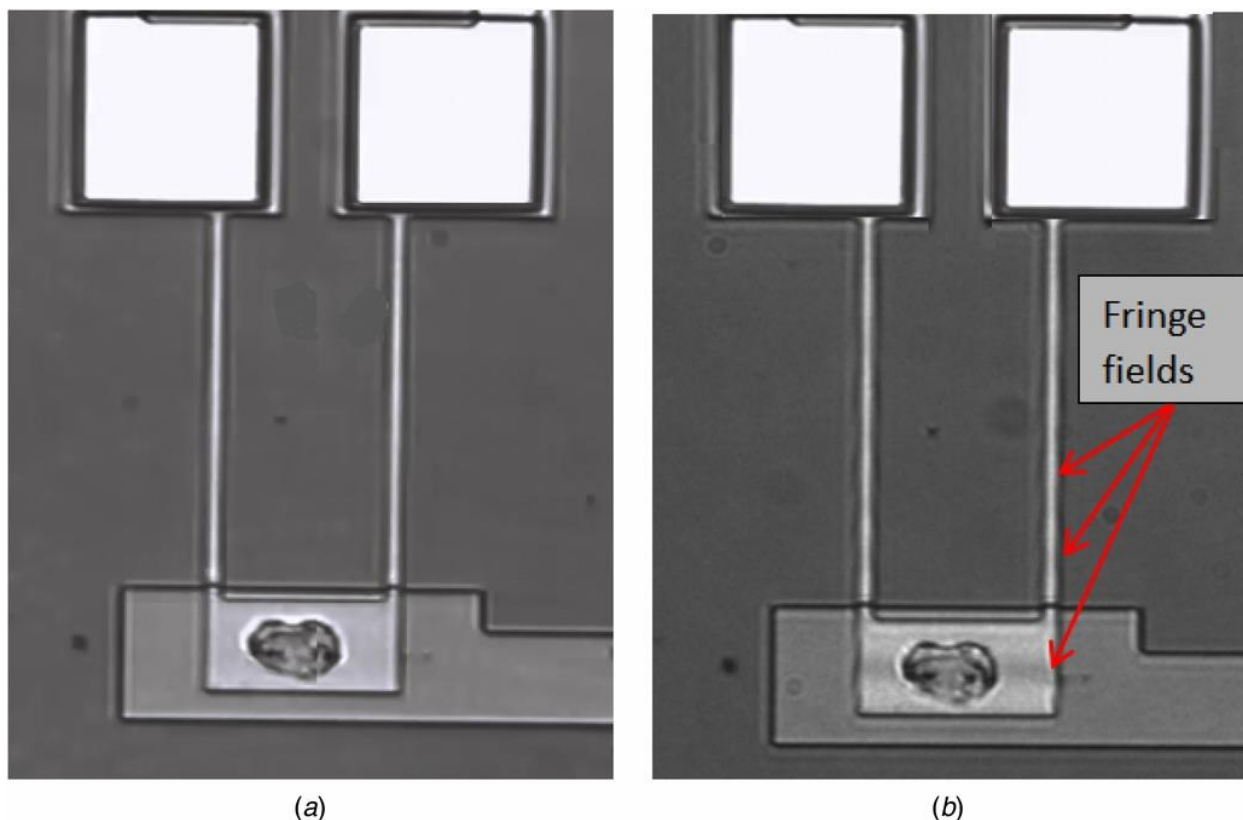


Figure 5.26: (a) before and (b) after ethanol sorption onto the MEMS microcantilever (Khater et al., 2014).

Two sensing materials were evaluated on this MEMS microcantilever: polyaniline doped with 10 wt. % NiO (PANI 10% NiO) and poly (2,5-dimethyl aniline) (P25DMA). Each sensing material was evaluated at different concentrations of ethanol (see Table 5.11). Note that the limit of detection for this sensor was equal to the concentration of analyte that corresponded to a set-off voltage of 1 mV. Therefore, PANI 10% NiO had a limit of detection of 50 ppm and P25DMA had a limit of detection of 5 ppm.

Table 5.11: Ethanol Response

Sensing Material	Set-off Voltage (mV)	Estimated Mass (pg)	Ethanol Concentration (ppm)
PANI 10% NiO	20	845	1000
PANI 10% NiO	15	727	100
PANI 10% NiO	1	165	50
P25DMA	5	407	50
P25DMA	1	165	5

## 5.2 Polymer Backbone Studies

Two cases were examined where the polymeric side chains or functional groups were identical, but polymer backbones were different. The amounts of gas analyte sorbed onto each polymeric material were compared to determine if the backbone of a polymeric sensing material significantly affected the sorption, and thus sensing properties, of a polymeric sensing material.

### 5.2.1 No Side Chains or Groups

Two polymers were chosen that were similar in nature, but that had no side chains or functional groups off of the polymeric backbone. These two polymers, polyaniline (PANI) and polypyrrole (PPy), are both aromatic in nature and have a secondary amine (see Figure 5.27). Both polymers were evaluated, using the test system described in Chapter 3, to determine if there was a significant difference between the amounts of ethanol that sorbed onto each polymer (see Figure 5.28). Analysis of variance (ANOVA) was used to evaluate the results to determine if there was a statistically significant difference (at the 95% confidence level) between the sorption of the polymers (see Section F.2.2 in Appendix F).

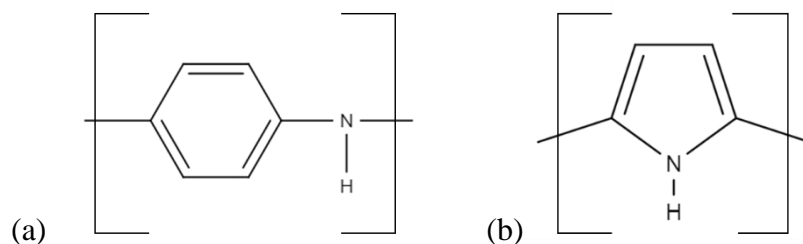


Figure 5.27: Chemical structure of (a) PANI and (b) PPy.

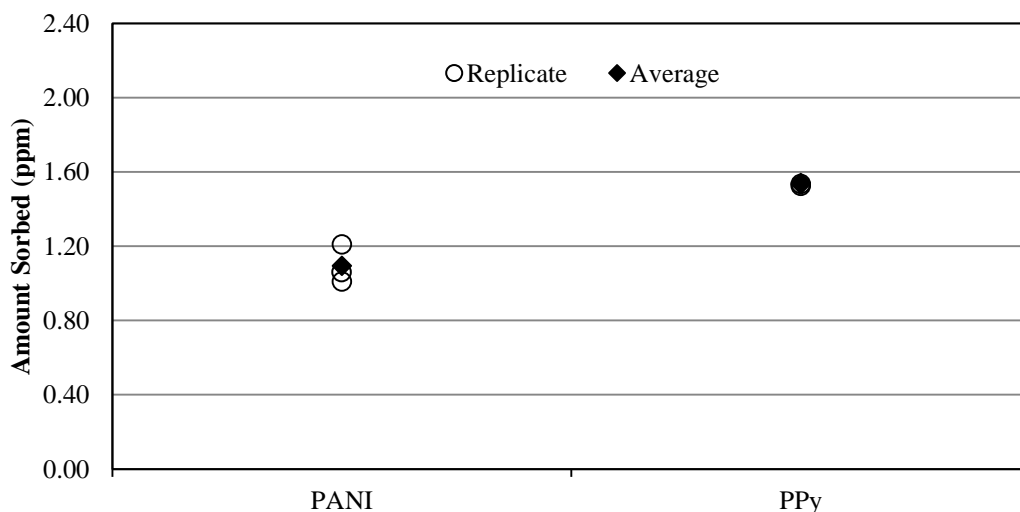


Figure 5.28: Amount of ethanol sorbed onto PANI and PPy.

It was found that there was a significant difference (at a 95% confidence level) between the amount of ethanol that sorbed onto PANI and PPy. Therefore, the backbone of a polymeric sensing material does affect the sensing properties. Thus, the backbone of a polymer must be considered when selecting potential polymeric sensing materials.

### 5.2.2 Dimethyl Side Groups

A further comparison was conducted to determine the effect the polymer backbone had on the sensing properties using two polymers that had identical side groups (functional groups), but different backbones. The polymers chosen were poly (2,5-dimethyl aniline) (P25DMA) and poly (2,6-dimethyl-1,4-phenylene oxide) (PPO), both of which contain an aromatic ring and two methyl functional groups (see Figure 5.29). Both of these polymers have a similar “bulkiness” and thus similar steric interactions (see Section 6.1.5). Therefore, the sensitivity (amount of analyte sorbed) should not be limited by steric considerations, but only by the other sensing mechanisms (see Chapter 6 for more details on sensing mechanisms).

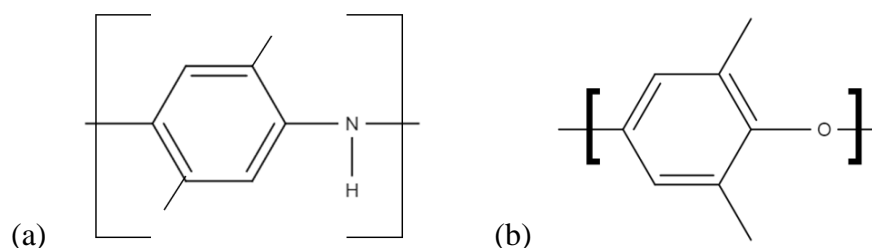


Figure 5.29: Chemical structure of (a) P25DMA and (b) PPO.

P25DMA and PPO were evaluated using 5 ppm of ethanol. The amount of ethanol sorbed onto each polymeric sensing material was measured using the test system described in Chapter 3 and these results are shown in Figure 5.30.

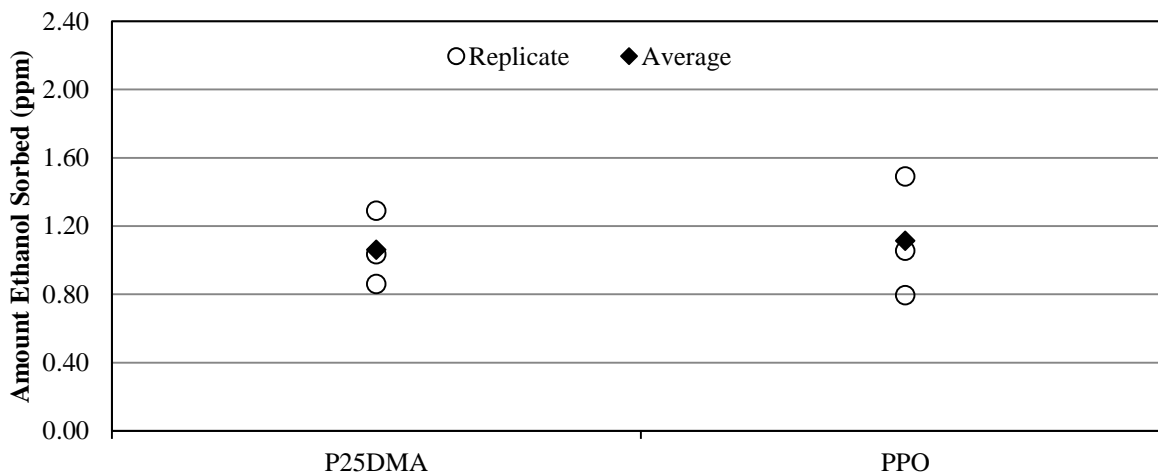


Figure 5.30: Amount of ethanol sorbed onto P25DMA and PPO.

Analysis of variance (ANOVA) was used to determine whether there were significant differences between the amounts of ethanol sorbed onto each polymeric sensing material. It was found that there was no significant difference (at a 95% confidence level) in the responses of the two polymers (see Section F.2. in Appendix F). This may be due to the similar backbone structures, both containing an aromatic ring, with the primary difference between P25DMA and PPO being an amine and an ether, respectively.

Given the previous results for PANI and PPy that showed a significant difference in the response, a further analysis was done using another analyte, methanol (see Figure 5.31). When methanol was used instead of ethanol to compare P25DMA and PPO (see Section F.1.1 in Appendix F), there was a significant difference (at a 95% confidence level) in the amount of analyte sorbed. In addition, the selectivity towards ethanol, with respect to methanol, was significantly different, especially since P25DMA was more selective to methanol than ethanol (see Table 5.12).

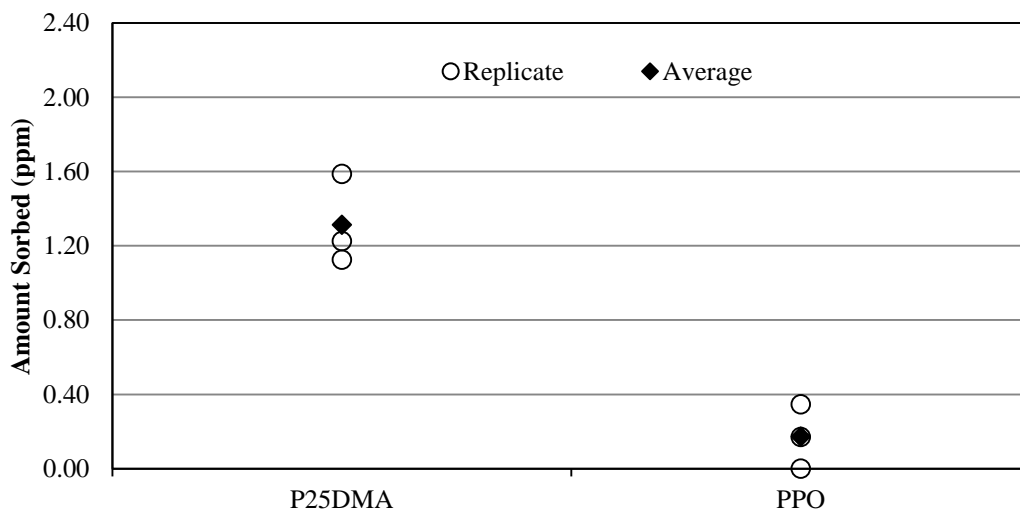


Figure 5.31: Amount of methanol sorbed onto P25DMA and PPO.

Table 5.12: Selectivity towards Ethanol with respect to methanol for P25DMA and PPO

Sensing Material	Selectivity to Methanol
P25DMA	0.67
PPO	6.60

Despite the not statistically significant difference in the amount of ethanol sorbed onto P25DMA and PPO, there was a statistically significant difference in the amount of methanol sorbed. In addition, there was a large difference in selectivity towards ethanol between P25DMA and PPO. This means that despite both polymers having the same dimethyl functional groups, P25DMA and PPO responded differently to methanol, which means that their difference in polymer backbone structure affected their response to methanol. Therefore, the backbone of a polymeric sensing

material does affect the sorption of different analytes and thus, must be considered when selecting potential sensing materials.

### 5.2.3 Effect of Polymeric Backbones

Two different cases (no functional groups and dimethyl functional groups) were evaluated to determine if the backbone of a polymer affected the sorption of an analyte. PANI and PPy sorbed statistically significant amounts of ethanol, whereas P25DMA and PPO sorbed significantly different amounts of methanol, despite sorbing similar amounts of ethanol. Therefore, the polymeric backbone does affect the sorption of analytes and polymer backbones must be taken into consideration when designing polymeric sensing materials towards a target analyte. In addition, how interferences interact with the polymer backbone must also be considered, since the analyte affects the sorption and response of a polymeric sensing material.

## 5.3 Polymer Functional Groups and Side Chain Studies

A similar study was conducted comparing different side chains or functional groups on polymers with the same backbone. Three different backbones were considered, an ethylene ( $\text{CH}_2\text{-CH}_2\text{-}$ ) backbone, a polyaniline ( $\text{C}_6\text{H}_6\text{-NH-}$ ) backbone, and a siloxane ( $\text{Si-O-}$ ) backbone.

### 5.3.1 Linear Polyethylene Backbone

Two polymers, poly (methyl methacrylate) (PMMA) and poly (vinyl pyrrolidone) (PVP), which both have a typical vinyl backbone ( $\text{CH}_2\text{-CH}_2\text{-}$ ) were considered for determining the effect of functional groups on a polymeric sensing material. PMMA contains an ester and a methyl group whereas PVP contains an amide and a five-member ring (see Figure 5.32).

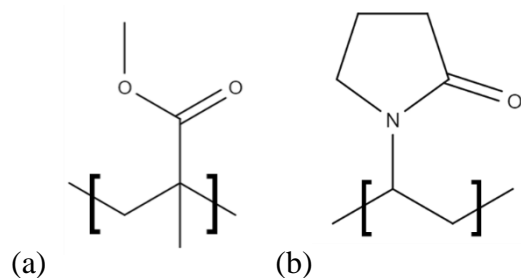


Figure 5.32: Chemical structure of (a) PMMA and (b) PVP.

The amounts of ethanol sorbed onto PMMA and PVP (see Figure 5.33) were compared using analysis of variance (ANOVA). It was found that there was no statistically significant difference in the amount of ethanol that sorbed onto PMMA versus PVP (see Section F.2.3 in Appendix F).



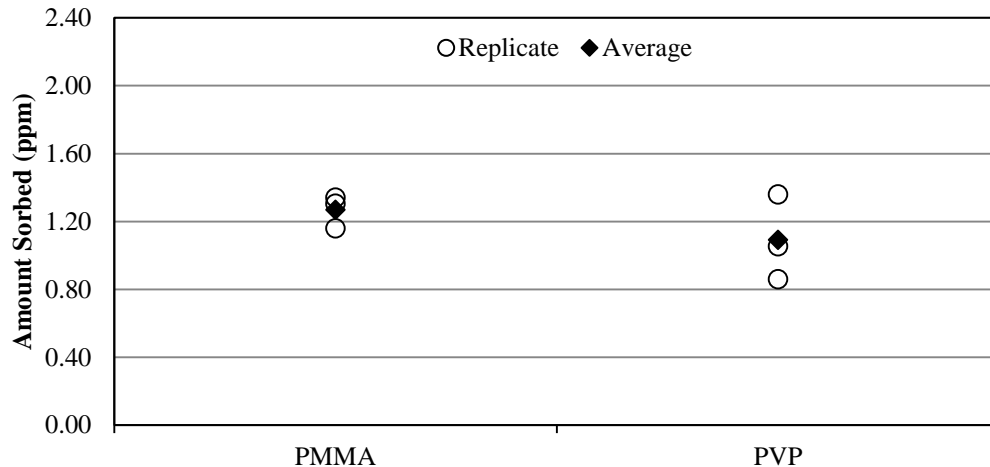


Figure 5.33: Amount of ethanol sorbed onto PMMA and PVP.

The ANOVA showed no significant difference (at a 95% confidence level) between the amount of ethanol sorbed onto PMMA and PVP. A further analysis of these two polymers using methanol and acetone (see Section F.2.3 in Appendix F) also showed no significant difference (at a 95% confidence level) between the amounts of each analyte sorbed onto the two polymers. This may be because the functional groups are somewhat similar (both containing double bonded oxygens and being of similar bulkiness, and hence, of similar steric hindrance (see Section 6.1)).

Therefore, it is possible that the functional groups may play a lesser role in affecting the amount of gas analytes sorbed onto the polymers. Two further analyses using different backbones were conducted to see if they followed the same trend.

### 5.3.2 Polyaniline Backbone

Three different polyaniline (PANI) derivatives, PANI, poly (*o*-anisidine) PoANI, and poly (2,5-dimethyl aniline) (P25DMA), were compared using ethanol to determine the effect of functional groups on sorption and sensing properties (see Figure 5.34). The amount of ethanol sorbed onto each polymeric material (see Figure 5.35) was analyzed using analysis of variance (ANOVA) and the Bonferroni t-test and the Fisher's least significant difference (LSD) (see Section F.2.3 in Appendix F). Note that these are the same sets of data as those compared in Section 4.3.1.

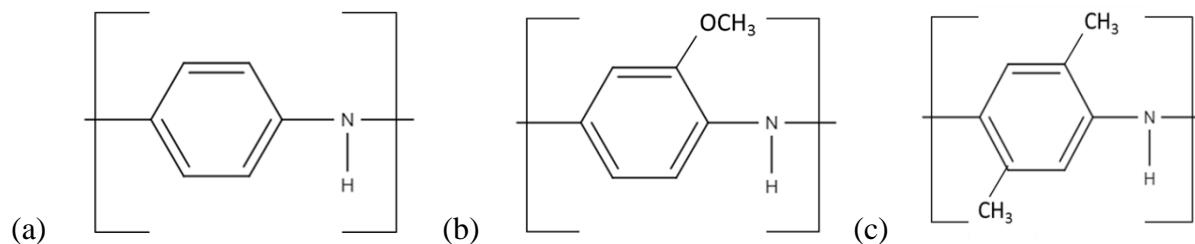


Figure 5.34: Chemical structure of (a) PANI, (b) PoANI, and (c) P25DMA.

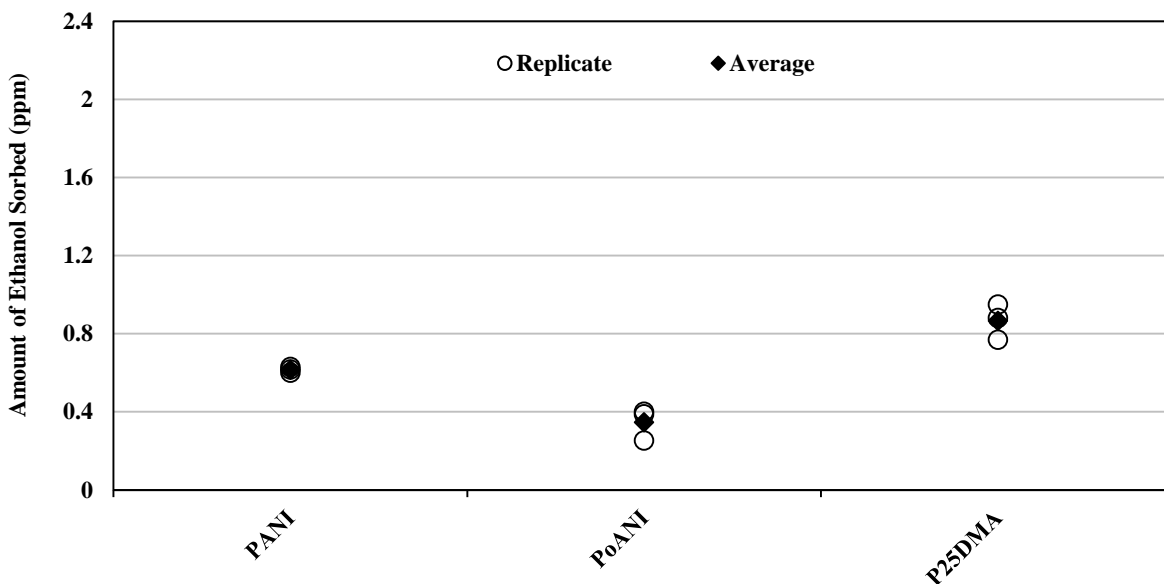


Figure 5.35: Amount of ethanol sorbed onto PANI, PoANI, and P25DMA.

As stated in Section 4.3.1, it was found that P25DMA and PoANI sorbed significantly different (at a 95% confidence level) amounts of ethanol; however, PANI did not sorb statistically significantly different amounts of ethanol compared to PoANI or P25DMA. Since P25DMA and PoANI have different functional groups off the same backbone and sorb significantly different amounts of ethanol, it can be suggested that the functional groups, and by extension side chains, do affect the sorption properties of a polymeric sensing material. Therefore, it is important to consider how the functional groups on a polymer will interact with the analytes.

### 5.3.3 Siloxane Backbone

Three polymers (OV 225, OV 275, and SXFA; Seacoast Sciences Inc., California, USA) were compared to determine the effect of functional groups. Each of these three polymers has a siloxane backbone (Si-O-), but different functional groups (see Figure 5.36). Note that OV 225 and OV 275 have very similar side chains, except OV 275 has two cyano ( $C\equiv N$ ) groups and OV 225 has one cyano group and one benzene group.

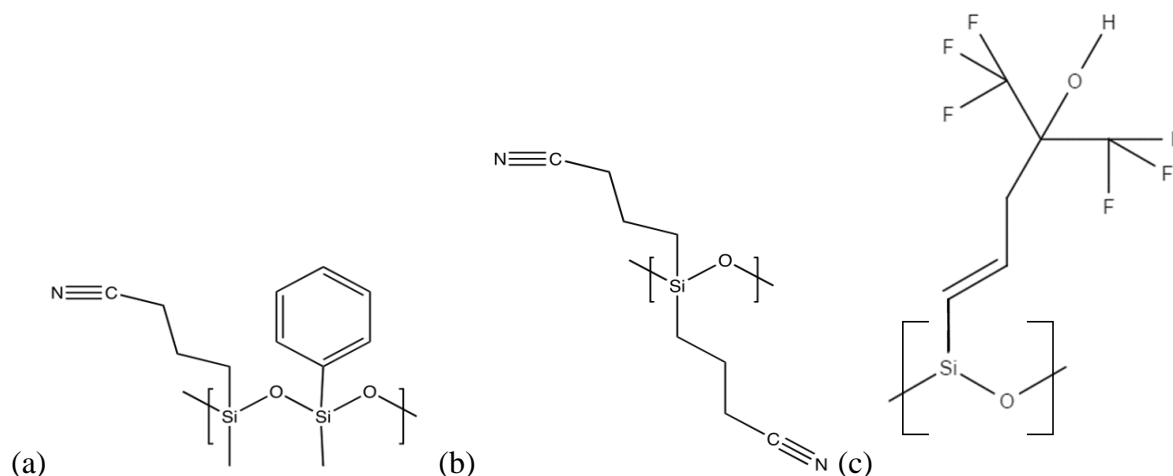


Figure 5.36: Chemical structure of (a) OV 225, (b) OV 275, and (c) SXFA.

These three polymers were evaluated on an RFID sensor (Chen et al., 2015b) and the response to ethanol gas was recorded (see Figure 5.37). These responses were compared using analysis of variance (ANOVA), the Bonferroni t-test, and the Fisher's least significant difference (LSD) (see Section F.2.3 in Appendix F). It was found that there was a significant difference (at the 95% confidence level) between the responses of all three polymeric sensing materials.

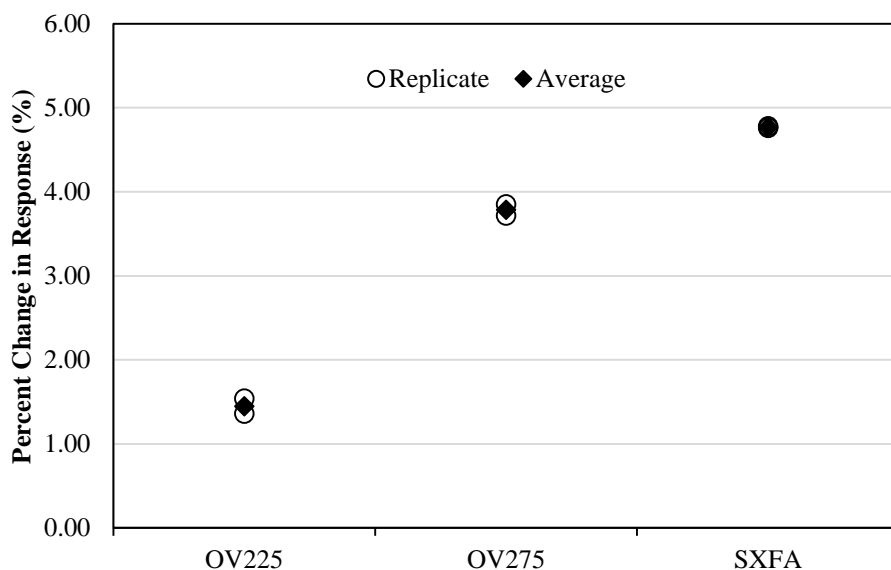


Figure 5.37: Response to ethanol for OV 225, OV 275, and SXFA.

Therefore, it can be concluded that the functional groups or side chains do have an effect on the sensing properties of a polymeric sensing material. Given that both the polyaniline derivatives and the siloxane-based polymers showed some difference (a significant difference between at least two polymers with the same backbone but different side groups), the similar responses between PMMA and PVP were likely a coincidence.

### 5.3.4 Effect of Functional Groups and Side Chains

Based on the results evaluated in the previous subsections of Section 5.3, the functional groups do have an effect on the amount of analyte sorbed onto the polymeric materials. Significant statistical differences between the responses to ethanol of the PANI backbones and the siloxane backbones show that the functional groups on the polymer do affect the interaction between the polymer and the analyte. PMMA and PVP, which have an ethylene backbone, sorbed similar amounts of ethanol, methanol, and acetone, despite having different functional groups. This is likely a coincidence. Therefore, by tailoring the functional groups on a polymer, one can target specific analytes.

## 5.4 Sample Stability

The environmental stability of polyaniline (PANI) was evaluated to determine if storage at atmospheric conditions (atmospheric pressure and room temperature, 21°C) caused degradation. Three samples that were five years old, two years old, and freshly made (zero years/months old) were evaluated based on the amount of ethanol sorbed. The older samples (five and two years old) were stored for their respective amounts of time in 20 mL scintillation vials in air at atmospheric pressure and room temperature (21°C).

Each sample was exposed to 10 ppm of ethanol and the amount of ethanol sorbed onto each polymer sample was measured (see Figure 5.38). The amount of ethanol sorbed by each sample was compared using analysis of variance (ANOVA). The  $F_{\text{observed}}$  was calculated to be 3.42, which is less than the  $F_{\text{critical}}$  (see Section F.2.4 in Appendix F). The null hypothesis could therefore not be rejected. Thus, there is no statistically significant difference between these polymer samples.

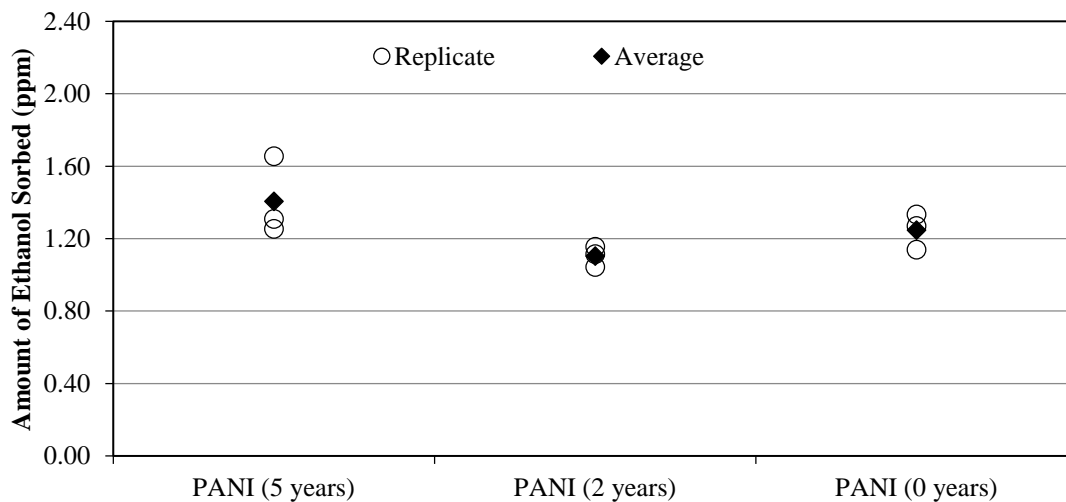


Figure 5.38: Amount of ethanol sorbed onto varying ages of PANI (five, two, and zero years old).

Since there was no significant difference between the three PANI samples, it can be assumed that PANI did not significantly degrade when stored at room temperature (21°C) in atmospheric conditions (i.e. no special storage considerations were used). Therefore, PANI is environmentally stable and storage up to five years will not affect the analyte sorption of PANI. This may or may not apply to other backbones; however, the comparison result is encouraging for the aniline-based sensing materials (PANI, PoANI, and P25DMA). Similar comparative investigations can be conducted for other polymeric sensing materials, if these experimental investigations are designed properly and for the long term.

## 5.5 Further Comparisons

Some other comparisons were conducted to determine the effect of batch to batch variability, different operators, day to day variability, and form (powder versus film) of the polymer. These comparisons were done to ensure the polymeric sensing materials could be reliably evaluated.

### 5.5.1 Batch to Batch Comparison

Two batches of the same polymer (poly (2,5-dimethyl aniline) doped with 5 wt. % NiO, denoted as P25DMA 5% NiO) were prepared by the same operator. The same recipe was followed and was prepared at the same time, under the same conditions. The resulting polymer batches were evaluated using 10 ppm ethanol (see Figure 5.39).

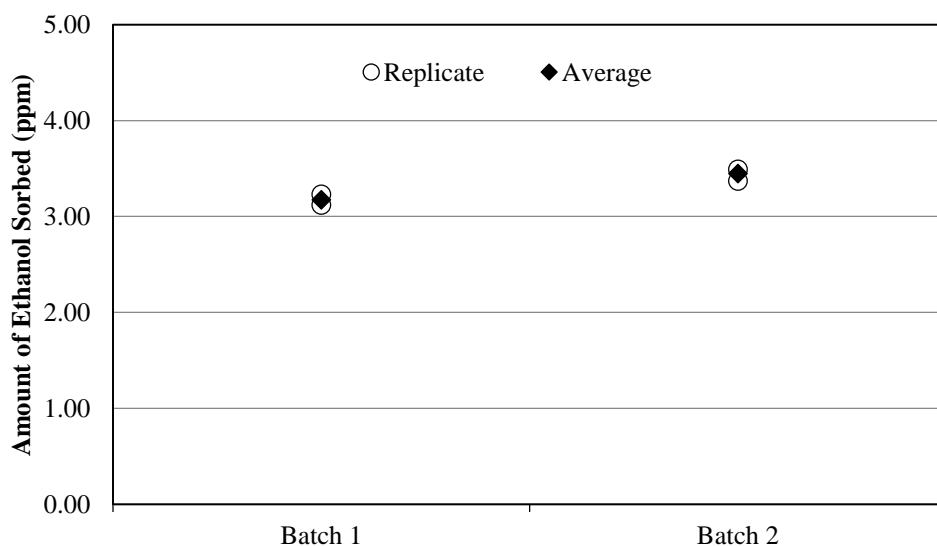


Figure 5.39: Amount of ethanol sorbed onto two different batches of P25DMA 5% NiO.

It was found that there was no difference, at a 95% confidence level, between the amount of ethanol that sorbed for both batches (Batch 1 and Batch 2) of P25DMA 5% NiO (see Section F.2.5 in Appendix F for the ANOVA table). Therefore, the recipe produced consistent polymer

nanocomposites. It is important that batch to batch variability is low so that the polymer nanocomposites can be reproduced for further sensing material production and sensor preparation.

### 5.5.2 Operator Comparison

Since there was no batch to batch difference by the same operator, a further comparison was done with two different batches of the same polymer made by two different operators (people). The recipe was the same for each batch and the only difference was the operator making and testing the sample. The operator made and tested (gas sorption study) his/her own sample. The same polymer nanocomposite was used (P25DMA 5% NiO) and was evaluated using 10 ppm ethanol (see Figure 5.40), a level higher than the previously employed 5 ppm.

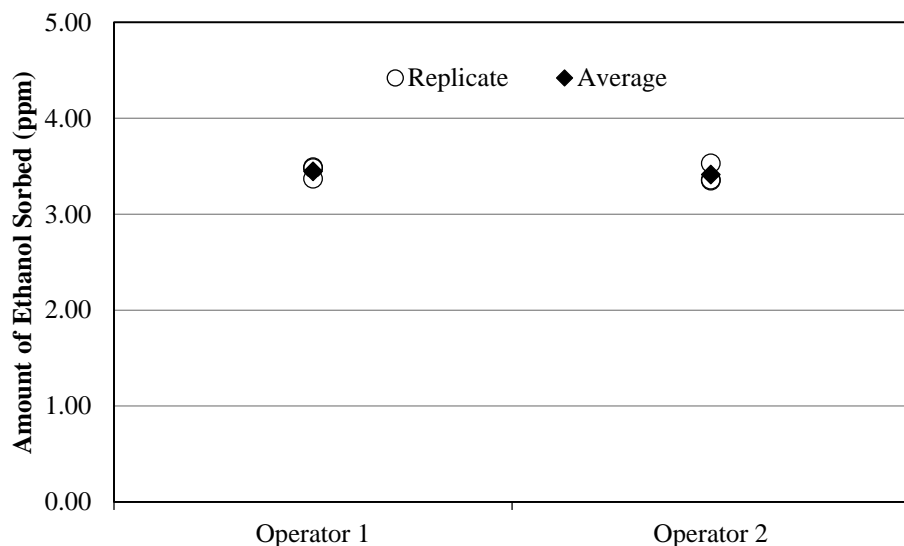


Figure 5.40: Amount of ethanol sorbed onto two different batches of P25DMA 5% NiO made by two different operators.

ANOVA was used to compare the average response of the polymers to each other (see Section F.2.6 in Appendix F). It was found that at a 95% confidence level no significant difference was observed between operators. Therefore, the operator did not affect the polymer nanocomposite and multiple batches of the polymer nanocomposite could be made using different (but suitably trained) operators, with reproducible results.

### 5.5.3 Day to Day Comparison

To ensure that there was no variability in both the test system and polymeric samples from day to day, the same polymer was evaluated on multiples days. P25DMA 5% NiO was evaluated using 10 ppm of ethanol and the amounts of ethanol sorbed on three different days were compared (see Figure 5.41). Note that three days were chosen at random over a two week period and the time of

day was also varied. ANOVA was used to compare the amount of ethanol sorbed on each day (see Section F.27 in Appendix F).

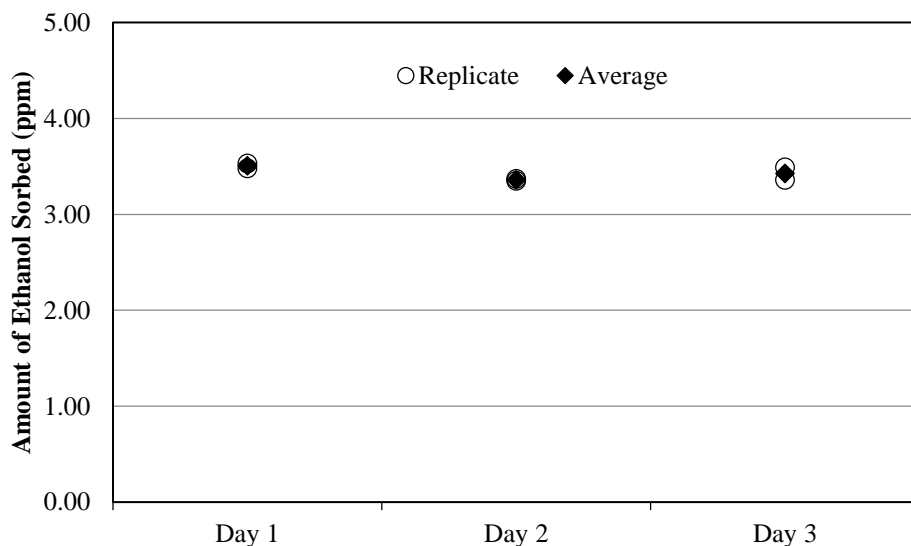


Figure 5.41: Amount of ethanol sorbed onto P25DMA 5% NiO on multiple days.

It was found that there was no significant difference (at a 95% confidence level) in the response of P25DMA 5% NiO. Therefore, there was no day to day variability. This allowed for measurements to be taken on multiple days and still be comparable. This also meant that the test system could be relied upon to evaluate and compare the effectiveness of multiple polymeric nanocomposites as sensing materials for gas analytes.

#### 5.5.4 Powder vs. Film

Two polymers, poly (vinyl pyrrolidone) (PVP) and poly (methyl methacrylate) (PMMA), were evaluated as both a powder and a film. The same amount of polymer was added to a round bottom flask as described in Section 3.1.1. The powder form was left to dry in air (atmospheric conditions) and the film form was left to dry in the oven at 60°C until a film had formed across the bottom of the round bottom flask (approximately 12 hours).

Both the powder and film were exposed to 5 ppm ethanol and the amount that sorbed was measured (see Figure 5.42). ANOVA was used to determine if there was a difference in response between the powder and film forms for each polymer (see Section F.2.8 in Appendix F). It was found that there was no significant difference (at a 95% confidence level) between the amount of ethanol that sorbed onto the powder and the film of the same polymer.

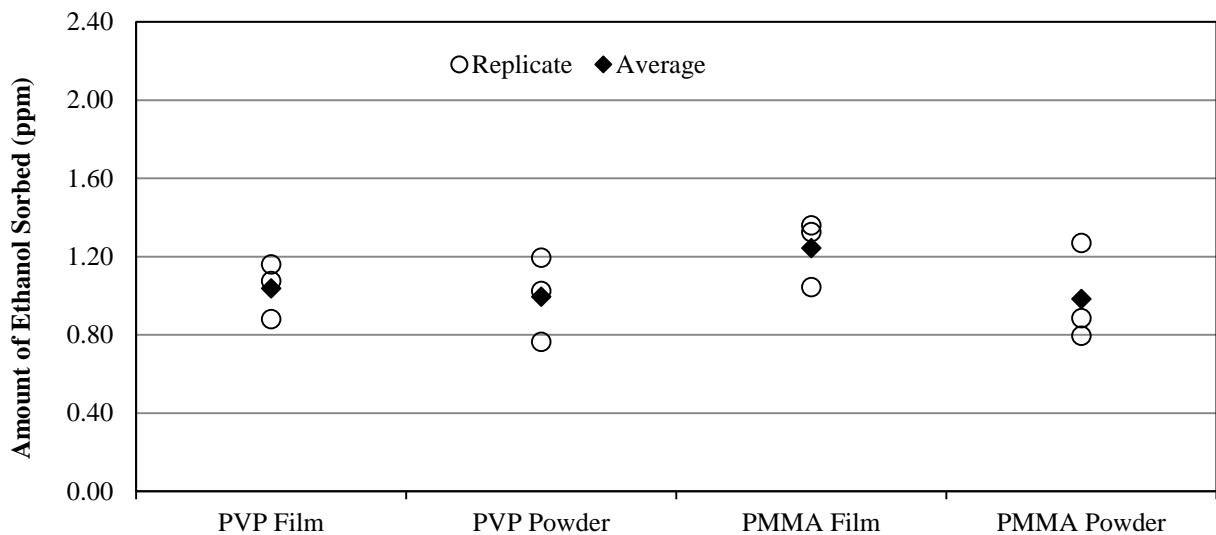


Figure 5.42: Ethanol sorption onto film and powder forms of PVP and PMMA.

The fact that both the film and powder are not significantly different is beneficial since a film may form during the deposition process on a sensor. While removing the solvent used to deposit the sensing material, it is possible that the sensing material may melt and form a film. Whether a film, or partial film, is formed is due to the temperature at which the “curing” process (solvent removal) occurs. Given that for two different polymeric sensing materials the sorption was not affected by the form (powder or film), it is likely this may be the case for many different polymeric materials as well.





## 6. Results and Discussion: Mechanistic Explanations

Sensing mechanisms describe how an analyte and a sensing material interact. Aspects may include what attracts/repels the analyte, as well as how the analyte sorbs onto the sensing material. An analyte may either adsorb onto the surface of a sensing material (at a sensing site) and weakly bind through electrostatic interactions, or absorb into the sensing material, by diffusing into the interstitial spaces created within the packed polymeric chains of a sensing material.

By examining the chemical nature of both the analyte and the sensing material, it is possible to determine the predominant mechanism(s) by which the analyte and sensing material will likely interact. However, multiple mechanisms are always at play and they may counteract one another. For example, polarity and Lewis acid-base mechanisms are attractive in nature, whereas steric hindrance is repulsive; the attractive and repulsive forces will counteract one another. Often, one mechanism may dominate (even if slightly), which results in the analyte sorbing or not sorbing onto the sensing material. Understanding potential mechanisms allows their identification given an analyte's chemical composition, and this allows in turn sensing materials to be designed to target specific analytes.

### 6.1 Primary Sensing Mechanisms

Primary sensing mechanisms are what attract or repel an analyte to a sensing material. All of these effects are electrostatic in nature. Polarity, Lewis acid-base interactions, and metal coordination all attract analytes based on electrostatic forces. Steric hindrance, on the other hand, is a repulsive force that pushes analytes away from a sensing material.

#### 6.1.1 Polarity and Hydrogen Bonding

A covalently bound compound may either be polar or non-polar (assuming a net charge of zero on the molecule). The polarity is based on whether some atoms within a molecule disproportionately draw electron density towards themselves. Atoms with high electro-negativities, such as nitrogen (3.0), oxygen (3.5), and fluorine (4.0), draw electron density from nearby atoms that are less electronegative, such as carbon (2.55) and hydrogen (2.1) towards themselves. If a disproportionate amount of electron density surrounds one or more atoms, then it results in the molecule having a slightly more negative charge on the electron dense atom(s) and a slightly positive charge on the electron deficient atoms, which results in an overall charge distribution (or dipole moment) on the molecule. This is known as a polar molecule (Stewart et al., 2016). For reference, Table 6.1 includes the dipole moments of common VOCs. The higher the dipole moment, the larger the charge difference on the molecule; and thus the more polar the molecule.

Table 6.1: Dipole Moment of Common Volatile Organic Compounds (VOCs)

Analyte	Dipole Moment (D) <sup>1</sup>
Methane	0.00
Ethane	0.00
Benzene	0.00
Toluene	0.36
Ethylbenzene	0.58
Xylene	0.64
Triethylamine	0.87
Dichloromethane	1.14
Chloroform	1.15
Phenol	1.22
Formic Acid	1.41
Ammonia	1.42
Tetrahydrofuran	1.63
Isopropanol	1.66
Ethanol	1.69
Methanol	1.70
Acetic Acid	1.74
Ethyl Acetate	1.78
Water	1.85
Ethylene Glycol	2.28
Formaldehyde	2.33
Acetaldehyde	2.70
Acetone	2.91
Acetonitrile	3.92

<sup>1</sup>Haynes (2016)

The geometry of a molecule is also important. A perfectly symmetric molecule, such as a tetrahedral shape where all four atoms/functional groups surrounding a central atom are identical, is non-polar since the overall charge on the molecule is zero. For example, carbon tetrachloride (CF<sub>4</sub>) has a charge distribution between the carbon (2.55) and each fluorine (4.0) atom, where the fluorine draws electron density away from the carbon. But since this occurs in four equally opposite directions, due to the tetrahedral shape, the net charge on CF<sub>4</sub> is zero (no dipole) and thus, CF<sub>4</sub> is non-polar. Other symmetric geometries include linear (CO<sub>2</sub>), trigonal planar (BF<sub>3</sub>), trigonal bipyramidal (PF<sub>5</sub>), and octahedral (SF<sub>6</sub>).

Non-polar molecules have a dipole moment of less than 0.4 D. This is why hydrocarbons, which contain only hydrogen and carbon, are non-polar, despite a small difference in electronegativities (2.55 for carbon and 2.2 for hydrogen). The dipole created between the hydrogen and carbon

atoms is considered negligible. In addition, many hydrocarbons are symmetric and have an overall net dipole of zero, as is the case for linear alkanes (Coulson, 1942).

Two polar molecules are attracted to one another through electrostatic forces. The more polar the molecules, the stronger the attraction. A special case of this is called hydrogen bonding. This occurs when a highly electronegative atom, nitrogen (3.0), oxygen (3.5), or fluorine (4.0), is bound to a hydrogen (2.2). This large electronegativity difference results in the nitrogen, oxygen, or fluorine atom stealing most of the electron density away from the hydrogen atom and thus, a large dipole is created. This results in electrostatic forces strong enough to create a weak (physical) bond between the hydrogen of one molecule and the nitrogen, oxygen, or fluorine of another molecule. For example, polyaniline (PANI) is able to hydrogen bond to alcohols, such as methanol. The amine (NH) in PANI is able to hydrogen bond to the alcohol (OH) in methanol (Tan and Blackwood, 2000).

### ***6.1.2 Lewis Acid-Base Interactions***

A Lewis acid-base interaction occurs when a Lewis acid binds to a Lewis base. A Lewis acid is characterized as an electron deficient atom, such as a positively charged hydrogen or carbon atom. A Lewis base contains at least one lone pair of electrons, such as on an oxygen or nitrogen atom. The Lewis base behaves as a nucleophile, and seeks out (attacks) an electron deficient atom with which to donate a lone pair of electrons. This donation is not “complete”, in that the electron density is shared between the two molecules and thus, a weak physical bond is formed.

For example, acetaldehyde contains a double bonded oxygen atom that has two pairs of lone electrons that are capable of behaving as a Lewis base. One pair of electrons is able to bond to a Lewis acid, such as an electron-deficient carbon. The electron deficient carbon must also be sterically unhindered (see Section 6.1.5), in that the Lewis base must be able to get close enough to bond. The electron deficient carbons in aldehydes and ketones, which have a trigonal planar geometry, are very susceptible to nucleophilic attack since there is little steric hindrance that repels the nucleophile. The carbon attached to a double bonded oxygen atom is electron-deficient (since the oxygen draws the carbon's electrons away from the carbon and towards itself), such as that in methyl methacrylate. Both aldehydes and ketones can behave as a Lewis acid (deficient carbon) and Lewis base (lone pairs on the double bonded oxygen). Similarly, methyl methacrylate can also behave as a Lewis acid or base. Therefore, the addition of methyl methacrylate to a sensing material for acetaldehyde may improve the sensitivity to acetaldehyde (Hirayama et al., 2002).

### ***6.1.3 p-orbitals and $\pi$ -bonds***

Volatile organic compounds (VOCs) and carbon-based polymers all contain p-orbitals since many of the atoms (i.e. carbon, nitrogen, and oxygen) covalently bond using p-orbitals. If a p-orbital is

covalently bound, the pair of electrons is shared between two atoms and cannot be further shared with another molecule. The p-orbitals of interest are those with a lone pair of electrons, as in the case of nitrogen (one pair) and oxygen (two pairs), assuming a neutral charge on the atom. These lone pairs can behave as Lewis-bases (as described in Section 6.1.2), but they can also become delocalized in certain cases. In addition, the p-orbitals that are shared in double bonds (e.g. C=C), can also become delocalized in specific cases such as in conjugated systems, discussed below.

Alternating single and double bonds in a molecule result in an overlap of p-orbitals (or  $\pi$ -bonds). This alternation of single and double bonds in a ring may produce an aromatic compound. Delocalization of electrons across  $\pi$ -bonds occurs due to this overlap of p-orbitals and allows electrons to travel freely between multiple atoms. This delocalization of electrons results in the formation of a so-called ‘conjugated system’. Aromatic rings, such as benzene, are a prime example of structures that can delocalize electrons; however, delocalization can also occur along linear chains. This delocalization results in lower energy, and therefore, more stable molecules.

$\pi$ -bonds will overlap with one another if given the opportunity. Since the electrons in  $\pi$ -bonds are delocalized across p-orbitals (Figure 6.1),  $\pi$ -bonds are able to easily interact with other molecules that contain p-orbitals oriented in the same direction, which results in stacking of aromatic rings and other  $\pi$ -bonds (Miller et al., 1997). Overlap can occur when the energy of the p-orbitals in one molecule is similar to the energy of the p-orbitals in another.  $\pi$ -bonds commonly occur across carbon atoms, which have the same energies since they are the same atom; however, other atoms that are bound to these carbons can change energy levels of the orbital of the electrons available to bind.

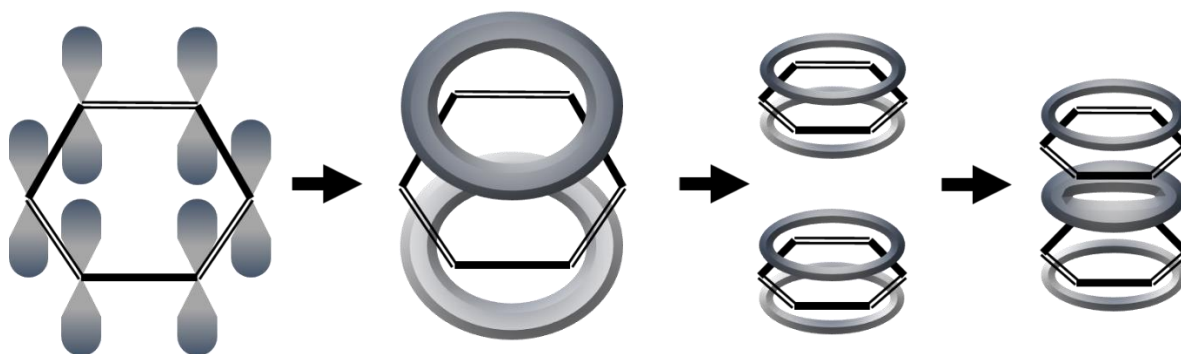


Figure 6.1: Overlap of p-orbitals and  $\pi$ -bonds.

It is also possible for other p-orbitals to stack with  $\pi$ -bonds, since  $\pi$ -bonds are delocalized p-orbitals. If the p-orbitals are oriented in the appropriate geometry, then  $\pi$ -bonds are able to stack on top of the p-orbitals, as they would stack on  $\pi$ -bonds. For example, three fluorine atoms on a carbon have p-orbitals capable of this. Each fluorine atom has a p-orbital in the z-direction, which is not used in bonding with the carbon. These p-orbitals (one on each of the fluorine atoms) are oriented in a trigonal planar geometry, essentially appearing as a ring. This planar geometry of

the p-orbitals is perfect for  $\pi$ -bonds stacking on p-orbitals (see also Figure 6.8 in Section 6.5.4, which discusses dominant sensing mechanisms for aromatics).

#### 6.1.4 Metal Coordination

Metal coordination only exists as a sensing mechanism when a metal or metal oxide is present in the sensing material. Coordination between an analyte and a metal is what allows basic catalysis to occur. Therefore, if chemical reactions involving a specific analyte are catalyzed by a specific metal oxide, such as platinum (Pt) used to oxidize methanol, then that metal oxide may improve the sensing properties (sensitivity and selectivity) of a polymeric sensing material (Xiong et al., 2013; Wang et al., 2013a).

Metals and metal oxides are commonly used as sensing materials and typically work on the basis of catalyzing (facilitating) an oxidation reaction. A typical mechanism for formaldehyde (HCHO) is shown below (see Equations 6.1 – 6.6). A similar mechanism occurs for the oxidation of any small organic molecule, where the oxygen gas ( $O_2$ ) comes from air and adsorbs to the surface of the metal or metal oxide (catalyst) (Wang et al., 2009a).



Oxidation utilizes the partial pressure of oxygen in the atmosphere. The oxygen is adsorbed onto the surface of the sensing material. As oxidation takes place, electrons ( $e^-$ ) are created that reduce the resistance of the sensor. This change in resistance is monitored as the sensor response. Very small amounts of other metals and metal oxides can be added to the sensing material to increase the amount of adsorbed oxygen onto the surface, thereby improving the sensitivity of the sensor (Lee et al., 2006).

When metals and metal oxides are incorporated into a polymer, the amount of adsorbed (or coordinated) oxygen onto the metal is significantly reduced due to reduced access of oxygen to the metal. This reduced access is caused by two things. First, there is a reduced amount of

coordination sites on the metal since the polymer is occupying some of the coordination sites (hence the metal, for instance, nickel (Ni), is bound to the polymer; see Figure 6.2). Second, the steric hindrance caused by the polymer repels some of the oxygen molecules so that the oxygen is not able to get close enough to coordinate to the metal.

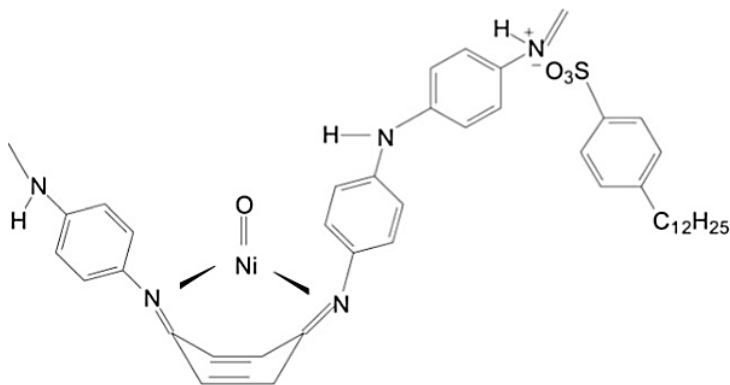


Figure 6.2: Ni coordination to the nitrogens in the quinoid ring (Han et al., 2006).

The geometry is important to consider when the metal or metal oxide is incorporated into a polymeric sensing material. The addition of a metal or metal oxide will cause the polymer to coordinate around the metal, creating a ‘kink’ (or change in conformation) in the polymeric chain (see Figure 6.2). This reduces the number of available spots for analyte coordination and also causes a steric interaction that creates a cavity within the polymer, which can improve the sorption of an analyte into the polymer.

Coordination of the polymer also, generally, creates strain on the bonds within the polymer, since the polymer bends (or changes conformation) to bind to the metal. The preferred conformation of an aromatic ring is a flat plane. This strain can be seen in Figure 6.2 by the “boat” conformation (the aromatic ring has been bent into the shape of a “boat”, with two carbons bent upwards) that is created when polyaniline (PANI) coordinates to the Ni. To bend into the “boat” conformation, the double bonds in the carbon ring have moved (the electron density has shifted) to allow the carbon to bend. If too much metal is added as a dopant, the polymer chains will become too strained and begin to break, thereby significantly reducing the benefit of the addition of the metal or metal oxide dopant.

It should also be noted that the metal oxide may not actually incorporate itself into the polymer because the strain is too great for the polymer to conform around the metal oxide. For example, poly (2,5-dimethyl aniline) (P25DMA) is unable to coordinate with zinc oxide (ZnO). In this case, the ZnO was added during the polymerization of P25DMA and resulted in minimal polymer formed around the ZnO nanoparticles because the strain was too great and the polymer chains could not withstand the strain caused by conforming around the ZnO (Stewart et al., 2015).

### ***6.1.5 Steric Hindrance***

The previous four primary effects are all attractive forces that draw an analyte towards the sensing material. Steric hindrance, on the other hand, is a repulsive force. Each atom is surrounded by an electron cloud that repels other atoms. Therefore, the larger (and bulkier) the molecule, the larger the electron cloud. However, the geometry of a molecule plays a role as well.

Steric hindrance is caused by the electronic repulsion of the electrons on molecules. All molecules are surrounded by a cloud of electrons that repel the molecule in question from other molecules. The bulkier a molecule (analyte), the larger the electronic cloud that surrounds it and therefore, the harder it is for that molecule to come near another molecule or fit into an interstitial space of a sensing material. Therefore, smaller, less bulky analytes (such as formaldehyde or methanol) are able to interact with a sensing material more easily than larger, bulkier analytes (such as triethylamine). This, as a result, can improve the selectivity of a sensing material.

Note that as more atoms are added onto the side group, the electron cloud gets larger. A t-butyl group (three methyl groups off one carbon atom) is much larger than hydrogen and therefore, exhibits more repulsion due to a larger electron density. A t-butyl group also requires more space due to the increased number of atoms and is therefore, a very bulky side group. Due to the bulkiness of t-butyl, it is much more difficult for an analyte to reach the central carbon. This can be thought of as the t-butyl group protecting the central carbon. This can be used to an advantage in sensing materials by excluding (and thus “protecting” the sensing material from) larger analytes, similar to a molecular sieve. The bulkiness can also be used to increase interstitial spaces or cavities in a sensing material to improve access of the analyte into the sensing material, thereby improving sensitivity.

### ***6.1.6 Dispersion and van der Waals Forces***

Electron density shifts around an atom and appears to have an average symmetric distribution around an atom; however, at any given time, the electron density may be greater on one side of an atom or compound. This results in a slight negative charge on that side and a slight positive charge on the opposite side. These charges last very briefly, but are enough to induce small electrostatic forces that bring molecules together in close proximity.

Dispersion and van der Waals forces are the result of induced dipoles created when two molecules come into close proximity. These induced dipoles are stabilized by electrostatic forces created with one molecule being slightly positive and the other slightly negative, where the two molecules are “touching”. The electron density does not shift between the two molecules, just around each molecule, such that one side of the molecule is positive and the other side is negative (Grate and Abraham, 1991).



## 6.2 Secondary Sensing Mechanisms

Secondary sensing mechanisms are effects that occur once the analyte is in close proximity to the sensing material. These effects are not what initially attracts the analyte to the sensing material; however, these secondary effects can also contribute considerably and often appear as part of the dominant mechanism.

### 6.2.1 Swelling

Absorption of an analyte (or multiple analytes) can reach a point where the analyte(s) pushes the polymer chains away from one another. When this happens, the polymer swells, increasing in overall volume. It should be noted that swelling of a conductive polymer, which is typically in a glassy state at room temperature, is expected to be low; however, swelling has been observed for multiple conductive polymers (Bai and Shi, 2007).

Polymer swelling can affect the response in different ways. For example, when water absorbs into polyaniline (PANI), swelling increases the resistance (reduces the conductivity); however, when water absorbs into polypyrrole (PPy), swelling reduces the resistance (increases the conductivity) (Joulazadeh et al., 2014).

PANI's conductivity is related to its conjugation and defects along the polymer chain and the conjugation between the polymer chains. When water molecules are absorbed into PANI, initially the water increases the conductivity by increasing the number of defects and altering the conjugation along the polymer chains. However, when too much water is absorbed, the water molecules push the polymer chains further apart, resulting in the polymer swelling, and reducing the amount of conjugation between polymer chains. This means that it is more difficult for a charge to be carried across multiple polymer chains, thus resulting in a decrease in PANI's conductivity (Joulazadeh et al., 2014).

Conversely, the absorption of water molecules into PPy initially causes a reduction in conductivity because the water molecules increase the space between polymer chains, causing minor swelling. This reduces the charge transfer between polymer chains and thus, reduces conductivity as well. However, as the concentration of water increases, a threshold is reached and the conductivity of PPy begins to increase with an increase in water concentration. This may be due to the water molecules forming a continuous layer between the PPy chains, effectively creating a charge transfer bridge between the conductive PPy chains (Joulazadeh et al., 2014).

### **6.2.2 Solvent Effects**

Swelling of a polymer may lead to solvent effects, where the analyte sorbs and diffuses into the polymer matrix to the point at which the analyte begins to behave as a “solvent”. When this occurs, the polymer chains become mobile. For conductive polymers, this may result in a decrease in conductivity because electrons may no longer be able to jump from one chain to another (Slater et al., 1993). However, the solvation of the polymer chains increases the conductivity if the solvent (analyte) has a higher electrical permittivity than the polymer (Vercelli et al., 2002).

### **6.3 Multiple Mechanisms**

Multiple mechanisms occur, sometimes simultaneously, when a gas analyte interacts with a sensing material. Some of these mechanisms may be the result of (triggered by) other mechanisms. For example, an analyte may be attracted to a polymer and sorb by hydrogen bonding or Lewis acid-base interactions. As more analyte sorbs, the sensing material begins to swell. This changes the properties of the sensing material and may result in more analyte sorbed than would be otherwise. In a sense, the partitioning characteristics of the target analyte change between the bulk phase and the polymer (interaction/sensing) sites. This, of course, affects the diffusivity characteristics of the analyte, whereby the movement of the polymer chains, as the sensing material swells, results in a change of pore size and distribution and thus, a corresponding change in the diffusion of the analyte into the sensing material. Swelling can also lead to solvent effects, whereby the analyte concentration has passed a threshold and begins to behave more like a “solvent” than an analyte.

In a crystalline polymer, as an analyte is sorbed, it enters the larger pores first. Many pores are interconnected and the analyte continues to move (diffuse) into the polymer with ease until all of these larger pores are saturated. Once these pores are saturated, the analyte can continue to migrate into smaller pores as the analyte begins to behave as a “solvent”, which results in some polymer chain mobility. As the chains move, some of the smaller pores are widened, which intensifies the solvent effects. This also results in further swelling of the polymer (and enhanced sorption). Eventually, the polymer is not able to swell any further, which results in no more analyte being able to sorb into the polymer since saturation has been reached (Bonavoglia et al., 2006). At that point, no more analyte can be sorbed onto the polymer and thus, the maximum limit (highest concentration) of how much analyte can be detected has been reached.

### **6.4 Solubility and Solubility Parameters**

Solubility, in general, is the ability of one substance to mix with another. Solubility between a solute and a solvent ranges from fully miscible, such as ethanol and water, to essentially insoluble, such as silver chloride in water. For gas sensors, the solubility of the target gas analyte, and the

interferents in the sensing material, particularly in the polymeric sensing material, is important. If the gas analytes are even somewhat soluble in the sensing material, then the gas analyte is able to diffuse into the sensing material, thereby increasing the amount of analyte that is able to bind and ultimately produce a measurable response.

Many factors affect the solubility of a substance in another substance; for example, the polarity of the two substances. The general rule is that polar molecules dissolve in other polar molecules and non-polar molecules dissolve in non-polar ones; however, solubility is much more complicated since other factors, not just polarity, influence a molecule's solubility.

Solubility parameters are useful indicators in assessing whether two molecules are miscible since they are based on both a molecule's chemical structure and physical state. Each substance (molecule) has a solubility parameter that in essence summarizes the forces with which the substance is likely to interact with another substance, given the substance's chemical nature and state. If the solubility parameters of two substances are similar, then they are likely soluble in one another.

It should be noted that these solubility parameters are either determined experimentally (where some error is always present) or calculated based on models (that always use certain approximations and assumptions). This often results in discrepancies between solubility parameters published in the literature.

There are two types of solubility parameters, the Hildebrand solubility parameter ( $\delta$ ) and the Hansen solubility parameters ( $\delta_D$ ,  $\delta_P$ ,  $\delta_H$ ). The Hildebrand solubility parameter summarizes the different contributions to the cohesive energy density (CED) function of the specific substance and therefore, some information about solubility is lost. On the other hand, the Hansen solubility parameters break down the CED of a substance into three types of contributions: dispersive energy ( $\delta_D$ ), polarity ( $\delta_P$ ), and ability to hydrogen bond ( $\delta_H$ ); see Tables 6.2 and 6.3. The Hildebrand and Hansen solubility parameters are related as per Equation 6.7 (Hansen, 2007).

$$\delta^2 = \delta_D^2 + \delta_P^2 + \delta_H^2 \quad (\text{Equation 6.7})$$

In general, if two compounds have similar Hildebrand parameters, then they are likely to dissolve within one another. For example, acetone ( $19.9 \text{ MPa}^{1/2}$ ) and aniline ( $21.1 \text{ MPa}^{1/2}$ ) should be fairly miscible due to their similar solubility parameters. However, due to the simplification of the calculation, this is not always the case. For instance, toluene ( $18.2 \text{ MPa}^{1/2}$ ), which is not capable of hydrogen bonding, has an identical Hildebrand parameter to ethyl acetate ( $18.2 \text{ MPa}^{1/2}$ ), which is capable of hydrogen bonding. However, their Hansen Solubility parameters are quite different (see Table 6.2); Grate and Abraham, 1991.

Therefore, the Hansen solubility parameters, which break down the solubility into dispersive energy ( $\delta_D$ ), polarity ( $\delta_P$ ), and ability to hydrogen bond ( $\delta_H$ ) contributions will give a better indication. If these three parameters are close in nature (i.e. when plotted against one another, the two substances are located close in the 3-D space), then the two substances are likely to be soluble. For example, benzene and chloroform have similar Hildebrand solubility parameters (18.6 MPa<sup>1/2</sup> and 19.0 MPa<sup>1/2</sup>, respectively), but different Hansen solubility parameters (see Table 6.2), whereas benzene and toluene have similar Hildebrand and Hansen solubility parameters.

Table 6.2: Hansen and Hildebrand Solubility Parameters for Various VOCs

Analyte	Hansen (MPa <sup>1/2</sup> ) <sup>1</sup>			Hildebrand (MPa <sup>1/2</sup> ) <sup>1</sup>
	$\delta_D$	$\delta_H$	$\delta_P$	$\delta$
Butane	14.1	0.0	0.0	14.1
Xylene	17.8	1.0	3.1	18.0
Ethyl Acetate	15.8	5.3	7.2	18.2
Toluene	18.0	1.4	2.0	18.2
Benzene	18.4	0.0	2.0	18.6
Chloroform	17.8	3.1	5.5	19.0
Tetrahydrofuran	16.8	5.7	8.0	19.4
Acetone	15.5	10.4	7.0	20.1
Dichloromethane	18.2	6.3	6.1	20.3
Acetaldehyde	14.7	8.0	11.3	21.1
Acetic Acid	14.5	8.0	13.5	21.3
Phenol	18.0	5.9	14.9	24.1
Acetonitrile	15.3	18.0	6.1	24.6
Formaldehyde	12.8	14.4	15.4	24.7
Ethanol	15.8	8.8	19.4	26.6
Methanol	15.1	12.3	22.3	29.7
Ethylene Glycol	17.0	11.0	26.0	32.9
Water	15.5	16.0	42.4	47.9

<sup>1</sup>Brandrup et al. (1999)

Note that the  $\delta_P$  of the Hansen solubility parameters for benzene is not zero (see Table 6.2), despite benzene being non-polar. This is because the electron density is constantly shifting across the atoms in a molecule, even in non-polar molecules, such as benzene. This can result in a small polarity for a brief moment, and thus have a non-zero polarity solubility parameter (Hansen, 2007). Therefore, an aromatic molecule such as benzene, which contains delocalized electrons, has a  $\delta_P$  of 2.0. Non-polar molecules, which cannot exchange electrons, such as butane, have both a  $\delta_P$  and  $\delta_H$  of zero, as seen in Table 6.2.

Table 6.3: Hansen and Hildebrand Solubility Parameters for Various Polymers

Polymer	Hansen (MPa <sup>1/2</sup> )			Hildebrand (MPa <sup>1/2</sup> )
	$\delta_D$	$\delta_H$	$\delta_P$	$\delta$
Polyethylene	-	-	-	16.2 <sup>1</sup>
Poly (butadiene- <i>co</i> -styrene)	17.55	3.36	2.7	18.07 <sup>1</sup>
Poly (2,6-dimethyl-1,4-phenylene oxide)	-	-	-	19.6 <sup>4</sup>
Poly (ethylene oxide)	17.3	3.0	9.4	19.9 <sup>1</sup>
Poly (2,5-dimethyl aniline)	-	-	-	21 <sup>2</sup>
Poly (vinyl chloride)	18.72	10.03	3.07	21.46 <sup>1</sup>
Polyaniline	17.4	8.1	10.7	22.2 <sup>3</sup>
Polystyrene (LG, BASF)	21.28	5.75	4.3	22.47 <sup>1</sup>
Poly (methyl methacrylate)	18.69	10.56	7.51	22.8 <sup>1</sup>
Poly (vinylidene fluoride)	17.2	12.5	9.2	23.2 <sup>1</sup>
Polypyrrole	-	-	-	25.2 <sup>5</sup>
Poly (vinyl pyrrolidone)	-	-	-	25.6 <sup>1</sup>
Poly (vinyl acetate)	-	-	-	19.2 <sup>1</sup>

<sup>1</sup>Brandrup et al. (1999) <sup>2</sup>Itoh et al. (2007a) <sup>3</sup>Shacklette and Han (1993) <sup>4</sup>Puskas et al. (2007) <sup>5</sup>Bradner et al. (1989)

Note that the solubility parameters for polymers are simply estimates. Typically, the solubility parameters of a polymer are experimentally obtained by dissolving the polymer in solvents and estimating the solubility of the polymer based on how well the polymer dissolves in different solvents (Duaij et al., 2013). Thus, typically, only the Hildebrand solubility parameter is available (if a parameter is available at all). Therefore, the Hildebrand solubility parameter is used in the discussion that follows as an indicator of solubility.

In addition, the solubility parameters of a monomer (i.e. aniline) will be different from those of its corresponding polymer (i.e. polyaniline (PANI)), although the values are close. For example, aniline has a Hildebrand solubility parameter of 21.1 MPa<sup>1/2</sup>, whereas PANI has a Hildebrand solubility parameter of 22.2 MPa<sup>1/2</sup> (Shacklette, 1994). Therefore, the solubility parameter for the monomer may be used as a very rough guide for that of the corresponding polymer, if the solubility parameter is not available.

Note that the composition of a polymer, including amorphous and crystalline fractions, copolymer composition, and crosslinking, all affect the solubility parameters of a polymer. Table 6.4 shows five different values observed for the Hildebrand solubility parameter for polystyrene, two values observed for poly (styrene-*co*-divinylbenzene), and the effect crosslinking has on the solubility parameters of poly (styrene-*co*-divinylbenzene).

Table 6.4: Hildebrand Solubility Parameters for Polystyrene

Polymer	Hildebrand (MPa <sup>1/2</sup> ) <sup>1</sup>
Polystyrene	17.5
	18.6
	18.6
	18.7
	20.2
	22.47
	22.47
Poly (styrene- <i>co</i> -divinylbenzene)	14.8
	17.4
5% Crosslinking	15.7
10% crosslinking	17.8
20% crosslinking	15.1

<sup>1</sup>Brandrup et al. (1999)

## 6.5 Dominant Mechanisms for Different Volatile Organic Compounds (VOCs)

The dominant mechanisms for how different analytes interact are discussed next. The analytes are classified by their functional groups such as alcohols and amines. In total, six different functional groups are discussed in the subsequent subsections (alcohols, aldehydes, alkanes, amines, aromatics, and ketones). At the end of each subsection, a table summarizes various sensing materials used for the detection of the analytes, as well as sensitivity (detection limit) and selectivity (if available). Note that in many of the tables in this section, there are no entries for selectivity. This is due to the fact that very few publications conduct or report any selectivity experiments (i.e. most often, only one analyte is used to evaluate the efficacy of a sensing material).

### 6.5.1 Alcohols

Alcohols are organic compounds that contain a hydroxyl (-OH) group, such as methanol and ethanol. These small alcohols are polar, due to the oxygen atom pulling electron density towards itself, away from the other atoms in the molecule, making the oxygen more electronegative and the other atoms more electropositive. Alcohols are also able to hydrogen bond because of the large dipole created between the oxygen and hydrogen. Therefore, alcohols are attracted to sensing materials that are polar, especially those able to hydrogen bond.

As an example, polyaniline (PANI) is a common sensing material for both methanol and ethanol (Athawale et al., 2006; Gao et al., 2008; Kim et al., 2005). PANI contains an amine group that makes it polar and able to hydrogen bond. PANI is also conductive when doped with an acid, which makes it an ideal sensing material in resistive type sensors (see Figure 6.3a). The doping

leads to positive charges on the nitrogen atoms, due to the additional hydrogen sharing electron density from the acid, and creates holes along the polymer chain that allow electrons to hop from one to another, thus making PANI conductive (Kukla et al., 1996). These positive charges also more strongly attract electronegative atoms and molecules, such as the oxygen in methanol and ethanol because of the larger dipole and therefore, stronger electrostatic forces. When an electronegative atom binds to the amine on PANI, by donating some electron density, the hole on the nitrogen is filled and the resistance on the polymer chain increases, which can be measured (Athawale et al., 2006).

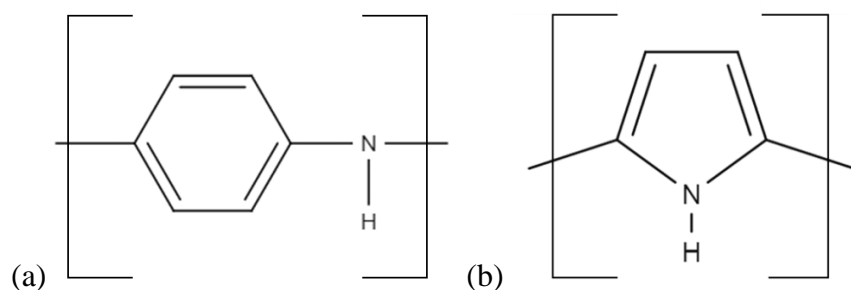


Figure 6.3: a) Polyaniline (PANI) and b) Polypyrrole (PPy)

By modifying PANI, the sensitivity and/or selectivity can be improved. Athawale and Kulkarni (2000) compared how different PANI derivatives responded to different aliphatic alcohols and found that selectivity was overall improved towards methanol when an ethyl group was added to the amine group. This ethyl group “protected” the nitrogen from the larger alcohols through steric hindrance, since an ethyl group is much larger than a single hydrogen atom. Due to methanol’s smaller size, methanol is able to more easily reach the nitrogen, despite the added steric hindrance from the ethyl group. In addition, methanol is more polar than ethanol and is, therefore, more strongly attracted to the nitrogen on the polymer.

Polypyrrole (PPy) is very similar to PANI (see Figure 6.3b), containing a conjugated chain and an amine group. The conjugated chain allows electrons to migrate down the PPy chain and is thus, conductive, making it a common sensing material in resistive type sensors (Babaei and Alizadeh, 2013; Mabrook et al., 2006). PPy attracts alcohols through electrostatic forces with its amine group (slightly positively charged hydrogen on a nitrogen). The amine is able to hydrogen bond with the  $-OH$  in the alcohol (Das et al., 2014). Because the amine is a secondary amine in nature (it is bonded to two carbon atoms, and one hydrogen atom), there is some steric hindrance surrounding the positively charged nitrogen. Due to the rigid nature of PPy, the chains are able to pack more closely together, creating smaller interstitial spaces for the analytes to diffuse into (Fonner et al., 2010). The combination of the polar amine ( $-NH$ ) on PPy, which is more attracted to other, more polar species that are able to hydrogen bond (such as small alcohols), with the steric hindrance that repulses larger molecules than methanol, explains the selectivity shown by Mabrook et al. (2006). Similarly, Babaei and Alizadeh (2013) demonstrated better selectivity by using

perchlorate as a dopant. The perchlorate is negatively charged and thus attracted to the positively charged hydrogen on the amine group. By binding to the amine, the perchlorate “protected” some of the amines, thus reducing the number of available sensing sites (amine groups, in this case) for the analytes to bond to. Since perchlorate was only used as a dopant, not every amine would be protected.

Table 6.5 summarizes various polymeric sensing materials used for either methanol or ethanol. Selectivity values towards the target analyte are also shown in Table 6.5. The higher the value for the selectivity, the lower the response from the interferent. Typical interferents were other alcohols (e.g. methanol, ethanol, and propanol) and aromatics (e.g. benzene and toluene), amongst others.

Poly (diallyldimethyl ammonium chloride) (PDDAC) (see Figure 6.4a) contains a positively charged nitrogen that acts as a Lewis acid. The oxygen on an alcohol, such as ethanol, has two lone pairs of electrons, capable of acting as a Lewis base. The electrostatic force draws the ethanol towards the PDDAC. Zhan et al. (2013) doped PDDAC with tin oxide ( $\text{SnO}_2$ ), a common inorganic sensing material for volatile organic compounds (VOCs). By incorporating  $\text{SnO}_2$  into the PDDAC, the  $\text{SnO}_2$  nanoparticles were stabilized in the PDDAC matrix, and therefore aggregation of the nanoparticles was reduced, allowing for more  $\text{SnO}_2$  to be available to interact, through metal coordination, with the analytes. This resulted in the doped PDDAC being more sensitive to ethanol than either PDDAC or  $\text{SnO}_2$  alone. It should be noted that Zhan et al. (2013) claimed high selectivity towards ethanol by using inorganic gases as a comparison, which often behave differently than organic gases.

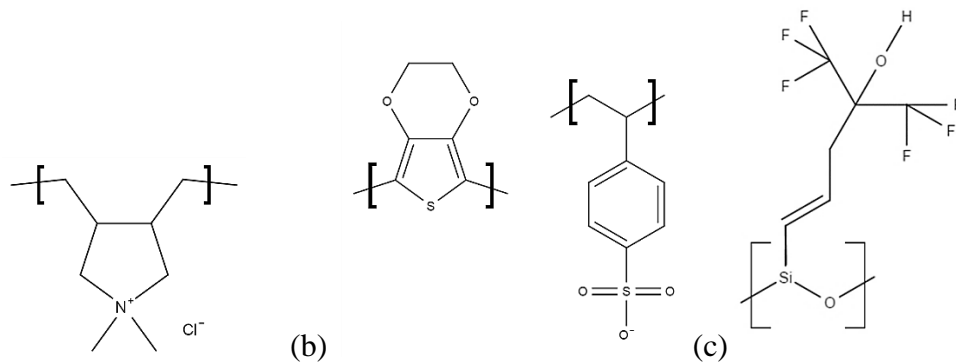


Figure 6.4: a) Poly (diallyldimethyl ammonium chloride) (PDDAC), b) Poly(3,4-ethylenedioxy thiophene): poly(styrene sulfonate) (PEDOT: PSS), c) OV 275



Table 6.5: Polymeric Sensing Materials for Alcohols

Analyte	Sensing Material	Dopant	Detection Limit	Selectivity	Reference
Methanol	Poly ( <i>N</i> -ethyl aniline) PNEA	HCl		Propanol (1.48) Ethanol (1.86) Butanol (2.88) Heptanol (18.40)	Athawale and Kulkarni (2000)
Methanol	Polyaniline (PANI)	Pd	1 ppm		Athawale et al. (2006)
Methanol	Polypyrrole (PPy)	Perchlorate (ClO <sub>4</sub> )	300 ppm	Nitromethane (4.5) Ethanol (4.9) Acetonitrile (7.5) Acetone (10.3) 1-propanol (11.5) Ethyl Acetate (12.5) Chloroform (13) 2-propanol (16.9) Toluene (20.5)	Babaei and Alizadeh (2013)
Methanol	Polyaniline (PANI)		100 ppm	Diimine Triethylamine Ethanol (1.3)	Gao et al. (2008)
Methanol	Polypyrrole (PPy)	None	5000 ppm	Propanol (1.6) Chloroform (2.2) Benzene (2.9)	Mabrook et al. (2006)
Ethanol	Polyaniline (PANI)	Poly (vinylidene fluoride) (PVF <sub>2</sub> )	100 ppm	Methanol (2.0) Benzene (5.0) Toluene (3.3)	Kim et al. (2005)
Ethanol	Poly (2,5-dimethyl aniline) (P25DMA)	None	3 ppm	Methanol (3.5) Benzene (4.8)	Stewart et al. (2015)
Ethanol	Poly(diallyldimethyl ammonium chloride) (PDDAC)	Tin Oxide (SnO <sub>2</sub> )	10 ppm	Nitrogen dioxide (19.6) Hydrogen gas (9.9) Sulfur dioxide (95.6) Hydrogen Sulfide (49.0)	Zhan et al. (2013)
Ethanol	Poly(3,4-ethylenedioxythiophene): poly(styrene sulfonate) (PEDOT: PSS)	None	5000 ppm	-	Jung et al. (2008)
Ethanol	OV 275	None	500 ppm	Benzene (7.1) Methanol (8.8)	Chen et al. (2015b)

Poly(3,4-ethylenedioxythiophene): poly(styrene sulfonate) (PEDOT: PSS) (see Figure 6.4b) also is likely to interact with ethanol through Lewis acid-base interactions, with the sulfur and oxygen

atoms on the PEDOT:PSS behaving as Lewis bases with their lone pairs of electrons. Ethanol, a Lewis acid, is able to hydrogen bond to the PEDOT:PSS. Similarly, the cyano groups on OV 275 (see Figure 6.4c) behave as Lewis acids and the ethanol is able to hydrogen bond to the nitrogen in the cyano group. In terms of selectivity, ethanol probably has a similar solubility to OV 275, compared to methanol, despite ethanol and methanol being chemically similar. The Hildebrand solubility parameters of ethanol and methanol are 26.6 and 29.7, respectively (see Table 6.2).

### 6.5.2 Aldehydes and Ketones

Aldehydes and ketones are very similar. Aldehydes have at least one double bonded oxygen (C=O) on a terminal carbon and ketones have at least one double bonded oxygen on a non-terminal carbon (see Figure 6.5). This oxygen draws electron density towards itself, resulting in a dipole with a slight negative charge on the oxygen, thus aldehydes and ketones are polar, but not as polar as alcohols. The two lone pairs on the oxygen act as a Lewis base, thus sensing materials that behave as Lewis acids are ideal. In addition, the high electronegativity of oxygen allows other molecules capable of hydrogen bonding to hydrogen bond to the oxygen in the aldehyde or ketone.

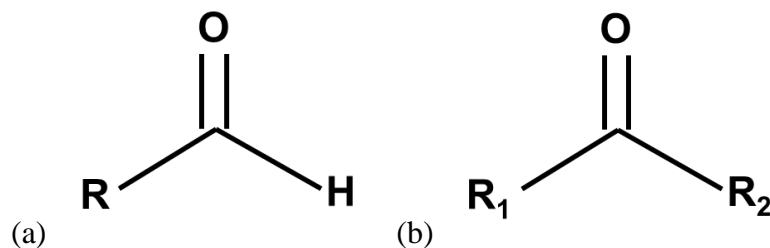


Figure 6.5: Schematic of an (a) aldehyde and a (b) ketone.

Due to the double bonded oxygen drawing electron density away from the carbon, both aldehydes and ketones are susceptible to nucleophilic attack from a nucleophile. In addition, the planar geometry of aldehydes and ketones limits steric hindrance; thus, the carbon is easily accessed by the nucleophile. However, ketones are more sterically hindered than aldehydes due to the fact that the ketone is surrounded by two carbon chains and an aldehyde has a hydrogen on one side. Nucleophilic attack is similar to Lewis acid-base interactions where the Lewis base (the nucleophile) donates electron density to the Lewis acid (electron deficient carbon) in the aldehyde or ketone. While Lewis acid-base interactions are likely to occur when hydrogen bonding is a possibility, it is more likely the dominant mechanism is hydrogen bonding due to the electrostatic forces (Zhang et al., 2016).

Formaldehyde is the simplest aldehyde, containing only one carbon. Many sensing materials have been investigated for formaldehyde due to its role in poor indoor air quality (WHO, 2010). It should be noted however, that many papers which describe sensing materials for formaldehyde use formalin (liquid formaldehyde) as their formaldehyde source (Antwi-Boampong and

BelBruno, 2013; Zhang et al., 2016; Alizadeh and Soltani, 2013; Wang et al., 2010b). The problem is that formalin is 37% formaldehyde and 10 - 15% of stabilizer, typically methanol, in water. Therefore, it is difficult to assess whether the response is from formaldehyde or methanol, unless methanol is used as an interferent. If methanol shows a much poorer response than what was observed from formalin, then it can be assumed the response from the formalin is indeed from the formaldehyde. Otherwise, it is likely that response from the formalin is at least partially from both formaldehyde and methanol; however, it is impossible to distinguish which gas produces what percentage of the response. Therefore, the best method to evaluate a formaldehyde sensor is to use formaldehyde in gaseous form from a compressed gas cylinder rather than the vapour from formalin.

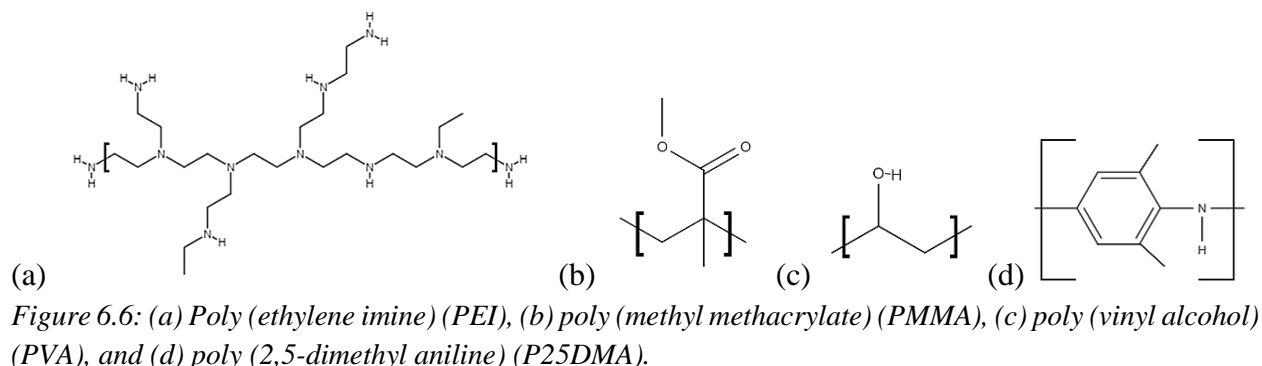
For example, for both polyaniline (PANI) doped with silver (Ag) nanoparticles (Zhang et al., 2016) and graphene-poly (methyl methacrylate) (graphene-PMMA) nanocomposite (Alizadeh and Soltani, 2013), the combination of methanol, formaldehyde and water is more likely to cause the response observed than formaldehyde alone. This is due to the ability of both methanol and water to hydrogen bond.

PANI is hydrophilic and both water and methanol are able to hydrogen bond to either the nitrogen or hydrogen in the amine; however, the hydrogen in PANI's amine is only able to hydrogen bond to formaldehyde. This effectively means that two molecules of methanol and/or water can bind to one amine (sensing site) on PANI (with one bound to the nitrogen and the other to the hydrogen) and only one formaldehyde molecule can bind to the amine. So for each sensing site (amine) on PANI, half as much formaldehyde is able to bond as its interferents, water and methanol. This results in a more sensitive sensor for the interferents than for formaldehyde. Additionally, this is why PANI is often used as a sensing material for methanol, as shown in Table 6.5.

Zhang et al. (2016) modified PANI by doping it with silver (Ag). The addition of Ag largely increased the porosity of the PANI matrix, which allowed more surface area, and therefore more sensing sites, for the analytes to bond to. The authors suggested nucleophilic attack as to why formaldehyde produced a larger response than the interferents tested; however, since formalin was used as the source for formaldehyde, this is not likely the case. Hydrogen bonding may be more likely between the amine group and the oxygen on formaldehyde, due to the electrostatic forces, since formaldehyde is polar (2.33 D). This may also explain why there was such a large response to formaldehyde and methanol (which is capable of hydrogen bonding). In addition, acetone was tested as an interferent and a smaller response was observed for acetone than formaldehyde. This is despite the fact that acetone (2.91 D) is more polar than formaldehyde (2.33 D), also behaves as a Lewis base (electrophile), and is susceptible to nucleophilic attack. However, Ag is often used to catalyze the oxidation of methanol into formaldehyde for industrial applications and thus, methanol and formaldehyde would be highly attracted to the Ag (more than acetone) and both are

able to easily coordinate with the Ag, thus increasing the response observed for formalin (Lefferts et al., 1986).

In some cases, the combination of methanol and formaldehyde can improve the sensitivity to formaldehyde. For example, Antwi-Boampong and BelBruno (2013) combined PANI and poly (ethylene imine) (PEI) (see Figure 6.6a) and doped it with formic acid to create a selective sensing material for formaldehyde. PANI, which is conductive, has increased resistance when an analyte sorbs onto it and thus was the responsive part of the sensing material. PEI was used to protect the PANI and improved its selectivity. The authors suggested a mechanism in which the PEI “trapped” the formaldehyde, which then was able to interact with PANI, resulting in a response. However, this does not explain the selectivity since PEI would “trap” many of the other interferents such as acetone, methanol, and ammonia, in a similar way to formaldehyde (acetone) or through hydrogen bonding (methanol and ammonia). A better explanation as to why formaldehyde produced such a large response, compared to the other interferents tested, is due to the way in which the materials were tested. The six interferents are all liquid at room temperature, whereas formaldehyde is not. Since formalin was used for formaldehyde, three vapours (formaldehyde, methanol, and water) were simultaneously exposed to the sensing material and thus, would result in all three gases interacting with the sensing material. Since methanol and water are able to hydrogen bond, they would more readily bind to the amine groups in PEI, reducing the number of available sorption sites on PEI. Formaldehyde would then not be able to bind to the PEI; however, it could bind to PANI, resulting in a large response since PANI’s conductivity decreases as more analyte sorbs onto it.



Similarly, Alizadeh and Soltani (2013) created a graphene-poly (methyl methacrylate) (graphene-PMMA) nanocomposite that used the less hydrophilic nature of PMMA (see Figure 6.6b) to “protect” the graphene from highly polar analytes such as water. The PMMA sorbs interferents capable of hydrogen bonding, such as methanol and ethanol, and sterically repels larger interferents such as tetrahydrofuran and acetonitrile. Small molecules that cannot hydrogen bond, such as formaldehyde, are able to diffuse through the PMMA and sorb onto the alkoxy functional groups on graphene, reducing graphene’s conductivity, and thus producing a response.

The morphology of the sensing material is also important. Wang et al. (2010a) compared flat and nanofibrous membranes of polyethyleneimine/poly (vinyl alcohol) (PEI/PVA) (see Figure 6.6c) as a sensing material for formaldehyde. It was found that the nanofibrous membrane was about three times more responsive than the flat membrane. The nanofibers created a more porous membrane that allowed for easier diffusion into the matrix. This also resulted in a much higher specific surface area of the nanofibers than the flat membrane. A higher surface area results in more sensing sites available to the analytes and therefore, a potential for a larger response.

Wang et al. (2010a) also compared different compositions of PEI/PVA and found that more than just morphology affected the sensing material's response. Two sensing materials were made with different PEI-PVA compositions that had similar specific surface area; however, the material with the higher PEI content produced a larger response. The authors suggest that PEI interacting with formaldehyde through Lewis acid-base interactions is the dominant sensing mechanism, with the formaldehyde acting as a Lewis base. However, both PEI and PVA are able to hydrogen bond to formaldehyde and thus, hydrogen bonding seems to be the dominant mechanism. In addition, the amines in PEI are stronger nucleophiles and Lewis bases and thus, if Lewis acid-base interactions did occur, it was more likely for formaldehyde to act as a Lewis acid. Further evidence for hydrogen bonding as the dominant mechanism exists when comparing ethanol and formaldehyde, which are of similar size. Ethanol is capable of hydrogen bonding, but formaldehyde is not; however, formaldehyde produced a much larger response. Steric interactions can explain why acetone, which is also susceptible to nucleophilic attack (acts as a Lewis acid), produces a much lower response than formaldehyde since formaldehyde is smaller than acetone. In addition, aldehydes are more reactive (stronger Lewis acids) than ketones.

Itoh et al. (2007a) created a sensor able to detect aldehydes, with acetaldehyde producing a larger response than formaldehyde. The sensor used intercalated layers of poly (2,5-dimethyl aniline) (P25DMA) (see Figure 6.6d) and molybdenum trioxide ( $\text{MoO}_3$ ). The  $\text{MoO}_3$  is used as a catalyst to oxidize alcohols into aldehydes and ketones (Velusamy et al., 2004 and Maiti et al., 2004). Therefore, alcohols, ketones, and aldehydes are all able to coordinate with Mo. The greater sensitivity to acetaldehyde and formaldehyde, than to ethanol, methanol, and acetone, suggests that the  $\text{MoO}_3$  was protected by the P25DMA and the analytes had to first diffuse through the P25DMA to reach the  $\text{MoO}_3$ . The aromatic interferents would have much larger steric hindrance due to their larger size and bulkier configuration and thus, they did not readily diffuse into the P25DMA. In addition, the aromatic compounds may have bonded to the P25DMA through  $\pi$ -stacking with the aromatic rings in P25DMA; however, the change in resistance came from binding with the Mo, not the P25DMA.

Comparing the solubility parameters of P25DMA to these analytes (see Table 6.6), shows that P25DMA has a similar Hildebrand solubility parameter to acetaldehyde. The Hildebrand solubility parameter essentially amalgamates many of the different factors that affect solubility,

thus giving a general rule for determining whether two compounds are miscible with one another. The Hansen solubility parameters are related to the Hildebrand solubility parameter (see Equation 6.1); they break down the solubility into three different contributions/parameters ( $\delta_D$ ,  $\delta_H$ , and  $\delta_P$ , which correspond to the dispersion forces, hydrogen bonding, and polar intermolecular forces, respectively). If two compounds have similar solubility parameters, they are likely to be miscible with one another. Therefore, P25DMA is more soluble in acetaldehyde than the other eight interferents, and vice versa. This can be extended to diffusion, where more soluble analytes are able to more readily diffuse into the polymer matrix. Thus, acetaldehyde is more likely to diffuse into the P25DMA and be able to coordinate with the  $\text{MoO}_3$  creating a response from the resistive sensor.

Table 6.6: Hansen and Hildebrand Solubility Parameters for P25DMA, PANI, and Gas Analytes

Polymer/ Analyte	Hansen			Hildebrand
	$\delta_D$	$\delta_H$	$\delta_P$	$\delta$
<b>P25DMA</b>	-	-	-	<b>21<sup>1</sup></b>
<b>PANI</b>	<b>17.4</b>	<b>8.1</b>	<b>10.7</b>	<b>22.2<sup>2</sup></b>
Xylene	17.8	1	3.1	18.0 <sup>3</sup>
Toluene	18	1.4	2	18.2 <sup>3</sup>
Benzene	18.4	0	2	18.6 <sup>3</sup>
Chloroform	17.8	3.1	5.5	19.0 <sup>3</sup>
Acetone	15.5	10.4	7	20.1 <sup>3</sup>
Acetaldehyde	14.7	8	11.3	21.1 <sup>3</sup>
Formaldehyde	12.8	14.4	15.4	24.7 <sup>3</sup>
Ethanol	15.8	8.8	19.4	26.6 <sup>3</sup>
Methanol	15.1	12.3	22.3	29.7 <sup>3</sup>

<sup>1</sup>*Itoh et al. (2007a)*

<sup>2</sup>*Shacklette and Han (1993)*

<sup>3</sup>*Brandrup et al. (1999)*

Acetone is the simplest ketone. Acetone will interact with PANI in a similar manner to formaldehyde, although acetone is bulkier. When comparing the detection limits of acetone and formaldehyde in Table 6.7, note that PANI has been doped with various metal oxides or used in a copolymer, which would affect the response.

A blend of polypyrrole (PPy) and poly methyl methacrylate (PMMA) was also used as a sensing material for acetone. The amine group on PPy would behave similarly to the amine in PANI, hydrogen bonding to the double bonded oxygen in acetone. Ruangchuay et al. (2003) noted that while acetone reversibly bound to PPy, acetic acid (which was evaluated as an interferent) permanently bound to PPy. This is because PPy, which contains conjugated bonds (alternating double and single bonds), will partially oxidize in the presence of an anionic dopant such as  $\alpha$ -naphthalene sulfonate ( $\alpha\text{-NS}^-$ ). This results in a positively charged nitrogen (=N-) on PPy that is able to stabilize the negatively charged dopant. When acetic acid is present, the  $\alpha\text{-NS}^-$  steals a hydrogen from acetic acid, resulting in the acetic acid becoming its conjugate base (acetate), which

then strongly binds to the positively charged PPy through electrostatic interactions (see Figure 6.7).

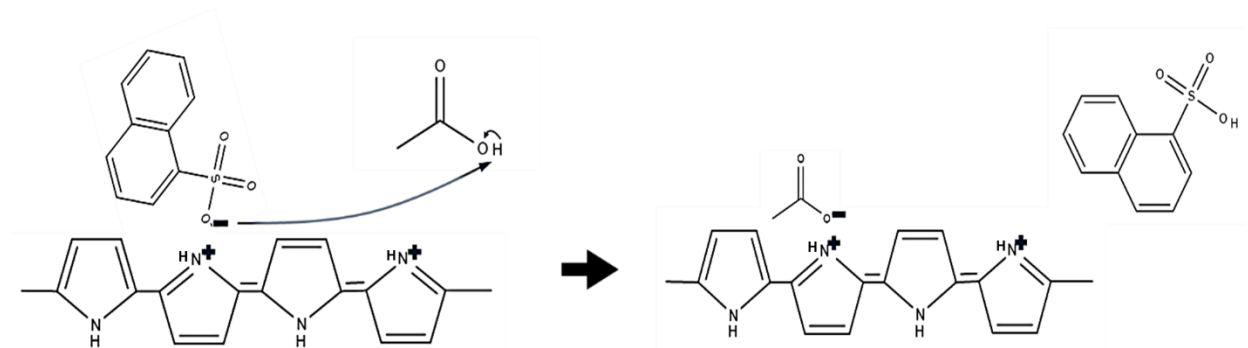


Figure 6.7: Substitution of  $\alpha$ -naphthalene sulfonate ( $\alpha$ -NS<sup>-</sup>) with acetic acid in polypyrrole (PPy).

The addition of PMMA to PPy resulted in a polymer that swelled when analyte was present, which pushed the conductive PPy chains apart and reduced the conductivity of the sensing material. The greater the swelling of a polymer, the greater the resistance, and the larger the response observed. When acetone interacted with PPy/ $\alpha$ -NS<sup>-</sup>/PMMA, a lot of swelling occurred when acetone absorbed into the sensing material to hydrogen bond to PPy. However, when acetic acid absorbed into the sensing material, it displaced the  $\alpha$ -NS<sup>-</sup> molecules by first neutralizing the  $\alpha$ -NS, and subsequently stabilizing the positively charged =N<sup>-</sup> in PPy. Therefore, the  $\alpha$ -NS would be free to migrate through the sensing material matrix to a spot where the  $\alpha$ -NS had more space (and was less sterically repulsed). This would result in less swelling of the PMMA, since acetic acid is smaller than  $\alpha$ -NS; however, the PMMA would not shrink since the  $\alpha$ -NS would still be in the polymer matrix. The difference in swelling results in a larger response to acetone than to acetic acid, thereby creating a sensor that is more selective towards acetone (Ruangchuy et al., 2003).

Table 6.7: Polymeric Sensing Materials for Aldehydes and Ketones

Analyte	Sensing Material	Dopant	Detection Limit	Selectivity	Reference
Form-aldehyde	Polyaniline/ Poly (ethylene imine) (PANI/PEI)	Formic Acid	38 ppm	Chloroform (4068) Acetone (2582) Dichloromethane (2469) Water (186) Methanol (121) Ammonia (91)	Antwi-Boampong and BelBruno (2013)
Form-aldehyde	Polyaniline (PANI)	NiO (5 wt. %) Al <sub>2</sub> O <sub>3</sub> (wt.15%)	5 ppm	Acetaldehyde (1.79) Benzene (2.11) Ethanol (1.86)	Stewart et al. (2012)
Form-aldehyde	Polyaniline (PANI)	Ag (25 mol %) Nitric acid	1.24 ppm	Acetone (112) Hexane (105) Chloroform (25) Benzene (3)	Zhang et al. (2016)
Form-aldehyde	Graphene-Poly (methyl methacrylate) (Graphene-PMMA)	None	0.01 ppm	Dichloromethane (27.4) Acetone (11.4) Water (11.4) Acetonitrile (10.5) Tetrahydrofuran (8.6) Ethanol (6.9) Methanol (6.2) Ethanol (7.4) Acetone (9.6) Benzene (125) Dicholoromethane (125) Toluene (125) Chloroform (125)	Alizadeh and Soltani (2013)
Form-aldehyde	Poly (ethylene imine) (PEI)	Poly (vinyl alcohol) (PVA) (~40 wt.%)	10 ppm	Acetone (9.6) Benzene (125) Dicholoromethane (125) Toluene (125) Chloroform (125)	Wang et al. (2010b)
Acet-aldehyde	Poly (2,5-dimethyl aniline)/ Molybdenum trioxide (P25DMA/ MoO <sub>3</sub> )	None	0.91 ppm	Formaldehyde (1.3) Chloroform (9.2) Methanol (235) Ethanol (235) Acetone (47.1) Benzene (235) Toluene (42.8) Xylene (118)	Itoh et al. (2007a)
Acetone	Polyaniline (PANI)	HCl	29 ppm	-	Do and Wang (2013)
Acetone	Polypyrrole/ Poly (methyl methacrylate) (PPy/ PMMA)	$\alpha$ -naphthalene sulfonate ( $\alpha$ -NS <sup>-</sup> ) (~8%)	30.3%	Acetic Acid (3.9)	Ruangchuay et al., 2003



### 6.5.3 Amines

Despite the emphasis on how volatile organic compounds (VOCs) interact with polymeric sensing materials, ammonia has been included even though it is not a VOC. Ammonia has been included because it is essentially the simplest form of an amine group, where all R-groups are hydrogens.

Ammonia is a small, polar molecule capable of behaving as a Lewis base and able to hydrogen bond. Ammonia is electrostatically attracted to sensing materials that are also polar and able to hydrogen bond. This includes polymers that have polar functional groups, including amines such as polyaniline (PANI) (Gong et al., 2010; Venditti et al., 2013) and polypyrrole (PPy) (Bhat et al., 2001); carboxylic acids such as poly (acrylic acid) (PAA) (Lee et al., 2010); and esters such as poly (methyl methacrylate) (PMMA) (Matsugushi et al., 2002).

The amine groups in PANI and PPy are able to hydrogen bond to ammonia. Acid-doped PANI and PPy are both conductive and have better conductivity when the polymer chains are more crystalline, which results in closer stacking of the polymer chains (Andreatta et al., 1988). The small size of ammonia means it is less sterically hindered and thus, still able to diffuse into the smaller interstitial spaces of PANI and PPy. In addition, the acid doping results in positively charged amine groups (acid) on both polymers that attract the slightly negative nitrogen in ammonia (base), resulting in a Lewis acid-base interaction (Bhat et al., 2001).

Similarly, ammonia is able to hydrogen bond to the OH in the carboxylic acid on PAA; however, ammonia is also able to hydrogen bond to the double bonded oxygen as well. It should be noted that ammonia and carboxylic acids commonly undergo acid-base reactions, creating an amide, and therefore, ammonia can chemically bind to the PAA, making it extremely difficult to remove and thus reduce the reusability of the sensing material. This was observed by Lee et al. (2010).

Multiple sensors listed in Table 6.8 used titanium dioxide (TiO<sub>2</sub>) nanoparticles to improve the sensitivity towards ammonia. TiO<sub>2</sub> is commonly used to oxidize ammonia into nitrogen monoxide (NO) and nitrogen dioxide (NO<sub>2</sub>) (Kebede et al., 2013). Therefore, ammonia will coordinate well with TiO<sub>2</sub>. In addition, TiO<sub>2</sub> was able to coordinate well with both PAA and PANI. Gold (Au) nanoparticles were also used as a dopant in PANI (Venditti et al., 2013); however, it was not likely that Au improved the sensitivity to ammonia. It is more likely that the mercaptans (which in this case contain an SO<sub>3</sub><sup>-</sup> group) that stabilized the Au nanoparticles are what improved the response to ammonia, compared to undoped PANI. The negatively charged mercaptan electrostatically attracted the slightly positively charged hydrogens on ammonia.

Triethylamine (TEA) contains three ethyl (C<sub>2</sub>H<sub>5</sub>) groups instead of three hydrogen atoms around a nitrogen atom. TEA is therefore much bulkier than ammonia, and it is also less polar than ammonia. In both cases, the nitrogen carries a slight negative charge; however, TEA is unable to

hydrogen bond unless it bonds to something capable of hydrogen bonding like an amine or alcohol. Ji et al. (2008) used a copolymer of PANI-PMMA doped with toluene sulfonic acid (TSA). The TSA protonated the amine on PANI and also provided some steric hindrance (since TSA is a bulky acid), increasing the interstitial spaces between the polymer chains, thus making the amines on PANI more accessible. The slightly negatively charged nitrogen in TEA was attracted to the positively charged amine on PANI.

Note that doping a sensing material may improve non-sensing properties, such as mechanical or electrical, and thus, doping may not always be beneficial in terms of sensitivity and selectivity. The addition of poly (vinyl alcohol) (PVA) to PPy was to improve the mechanical properties of PPy (Bhat et al., 2001). While the PVA likely increased the interstitial spaces in the polymeric material, thereby improving diffusion into the polymer, the alcohol groups on PVA were also able to hydrogen bond to ammonia. This would have reduced the sensor's sensitivity, since sorption onto PPy is what created a change in conductivity (in this case) and thus, a measurable response. Any ammonia bound to PVA would not have produced a measurable response.

Table 6.8: Polymeric Sensing Materials for Amines

Analyte	Sensing Material	Dopant	Detection Limit	Selectivity	Reference
Ammonia	Poly (methyl methacrylate)- Polyaniline (PMMA-PANI)	bis(2-ethyl hexyl) hydrogen phosphate (DiOHP)	10 ppm	-	Matsugushi et al. (2002)
Ammonia	Titanium dioxide/ poly(acrylic acid) (TiO <sub>2</sub> /PAA)	None	0.11 ppm	Butyl amine (1.9) Pyridine (3.8) Ethanol (13.8) Toluene (20.4) Chloroform (43.6)	Lee et al. (2010)
Ammonia	Titanium dioxide (TiO <sub>2</sub> )	Polyaniline (PANI) Hydrochloric Acid (HCl)	50 ppt*	-	Gong et al. (2010)
Ammonia	Polypyrrole (PPy)	Poly (vinyl alcohol) PVA (5 w/v %) Gold (Au)	1000 ppm	-	Bhat et al. (2001)
Ammonia	Polyaniline (PANI)	3-mercapto-1-propane sulfonic acid (3MPS)	10.8 ppm	Ethanol Toluene Acetonitrile	Venditti et al. (2013)
Triethyl-amine	PMMA/ PANI	Toluene sulfonic acid (TSA)	20 ppm	-	Ji et al. (2008)

\*parts per trillion (ppt)

#### 6.5.4 Aromatics

Aromatics are molecules that contain conjugated (alternating single and double bonds) planar rings. The alternating single and double bonds, combined with the planar geometry, result in delocalized electron density across the p-orbitals in the aromatic ring. Filled p-orbitals that are oriented such that the delocalization is in a planar geometry allow for  $\pi$ -stacking and therefore, aromatics are attracted to other aromatics. There are cases where an aromatic can  $\pi$ -stack with other functional groups such as a trifluoro-group (as in SXFA, see Figure 6.8), where the  $p_z$ -

orbitals of the three fluorine atoms are in a planar configuration and benzene, which is also planar, is able to  $\pi$ -stack (Chen et al., 2015b).

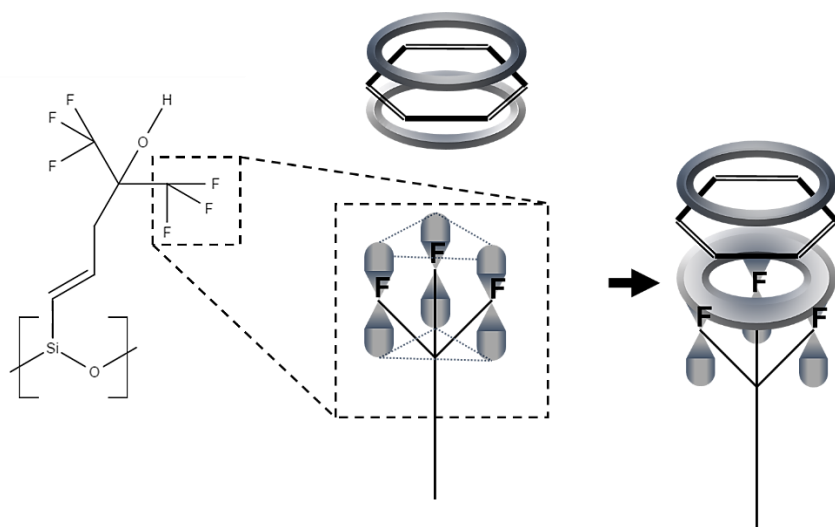


Figure 6.8: Benzene  $\pi$ -stacking onto SXFA.

All of the polymeric materials used for aromatic analyte detection are at least partly conjugated and thus, have an aromatic component to them. This is what the aromatic rings in benzene, toluene, and xylene are able to  $\pi$ -stack with. Because aromatic compounds are typically the only VOCs that are able to  $\pi$ -stack, many non-aromatic interferents will not bind very well and thus high selectivity will be observed towards the aromatic compounds (Li et al., 2007). Aromatic molecules are also bulkier than the other VOCs discussed and therefore, need larger interstitial spaces to easily diffuse into the polymer matrix.

For example, as shown in Figure 6.9 a, a copolymer (poly (methyl methacrylate-*co*-chloromethyl styrene) modified with *N,N*-dimethyl-1,3-propanediamine (MCD)) contains multiple aromatic rings and other long R-chains that create large interstitial spaces between the polymer chains. These larger interstitial spaces allow toluene to diffuse into MCD more easily and bind to the aromatic rings through  $\pi$ -stacking, which pulls charge density away from the conductive MCD. This effectively makes it harder for the charge to travel along the copolymer chains, which results in a reduction of MCD's conductivity (Matsuguchi et al., 2013). Note that this displacement of charge density while the polymer and aromatic analytes interact through  $\pi$ -stacking results in a change in conductivity. This is how most of the responses are measured for the sensors listed in Table 6.9. Resistive-type sensors are commonly used for aromatic analytes because a conjugated polymer is typically conductive (Barisci et al., 2002).

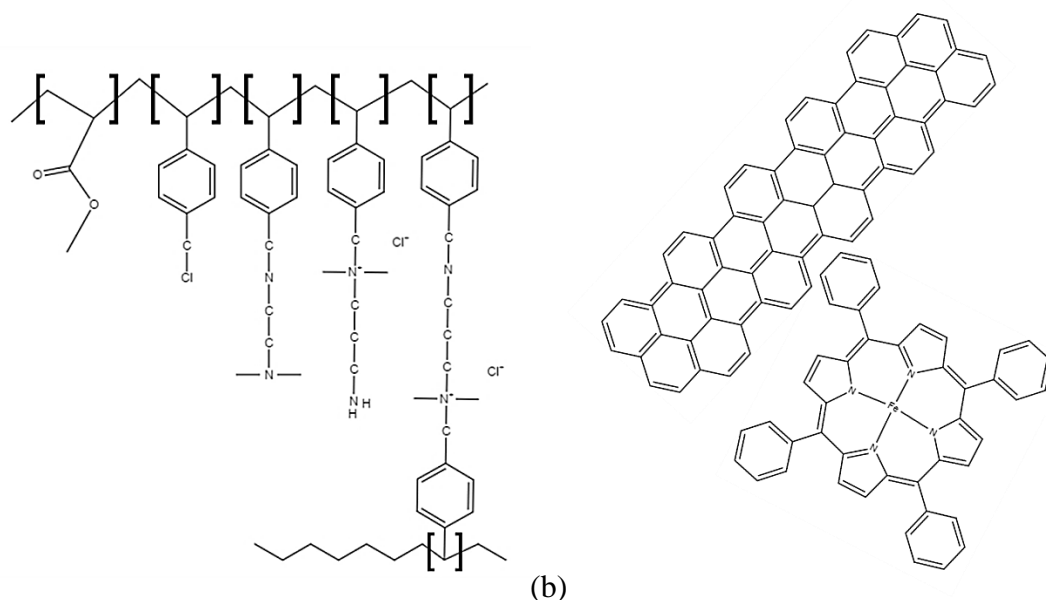


Figure 6.9: (a) MCD and (b) single wall carbon nanotubes doped with iron-tetraphenylporphyrin (SWCNT-Fe-TPP)

Toluene has one methyl functional group and thus, has a small dipole moment (0.36 D). However, it is below 0.4 D and therefore, toluene is still considered non-polar. Xylene, on the other hand, is considered polar with a dipole moment of 0.64 D. This is why polymers, such as polyaniline (PANI) and polypyrrole (PPy), are slightly more selective towards xylene than toluene and benzene. The electrostatic forces are why xylene is favoured over toluene and benzene when interacting with PANI (Li et al., 2009) and PPy (Lin et al., 2003). Note that while ethylbenzene is also polar (0.58 D), it is slightly less polar than xylene; ethylbenzene is also bulkier, which means ethyl benzene is also more sterically hindered than xylene.

Rushi et al. (2014) did, however, demonstrate that single wall carbon nanotubes doped with iron-tetraphenylporphyrin (SWCNT-Fe-TPP) (see Figure 6.9b) had slightly better selectivity towards toluene than xylene, despite all three aromatic compounds (benzene, toluene, and xylene) being able to  $\pi$ -stack with the aromatic rings on both the porphyrin and SWCNT. This is due to the incorporation of Fe. Toluene coordinates well with Fe and thus, is more preferentially bound than xylene and benzene (Albonetti et al., 2010).

Table 6.9: Polymeric Sensing Materials for Aromatics

Analyte	Sensing Material	Dopant	Detection Limit	Selectivity	Reference
Benzene	SXFA	None	500 ppm	Ethanol (11.3) Methanol (12.5)	Chen et al. (2015b)
Toluene	MMA-CMSt-DMPDA	Carbon Black (~10%)	50 ppm	-	Matsuguchi et al. (2013)
Toluene	Single wall carbon nanotubes (SWNT)	Iron-tetraphenyl porphyrin (Fe-TPP)	500 ppb	Xylene (1.8) Benzene (2.8)	Rushi et al. (2014)
Toluene	P3HT-benzyl		1 ppm	Methanol (6.1) Ethanol (>4000) Isopropanol (>4000) Acetone (>4000) Methylene Chloride (4.6) Acetonitrile (6.8) Benzene (2.1) Hexane (>4000) Cyclohexane (>4000)	Li et al. (2007)
Xylene	Polyaniline	HCl	200 ppm	Toluene (1.3) Benzene (1.9)	Li et al. (2009)
Xylene	Polypyrrole	Cl <sup>-</sup>	67 ppm	Ethylbenzene (2) Toluene (4) Benzene (10)	Lin et al. (2003)

### 6.5.5 Alkanes

Unlike most of the volatile organic compounds (VOCs) discussed, alkanes are non-polar. Therefore, alkanes are not attracted to sensing materials through large electrostatic forces from dipoles. Instead, alkanes are attracted by very small van der Waals forces, which only occur at very short distances.

Alkanes are simple hydrocarbons that only have singly bonded carbons and hydrogens. They can be either linear or branched; branched alkanes are bulkier and thus more sterically hindered. As an example, methane, the simplest hydrocarbon and alkane is discussed.

Methane is a small, non-polar molecule which is typically detected through the catalytic oxidation over metal and metal oxide catalysts (Simplicio et al., 2006). In some cases, a polymer matrix is used to support the catalytic metal oxide (see Table 6.10). For example, Xie et al. (2010) used a polyaniline (PANI) doped with camphor sulfonic acid as a matrix for palladium oxide (PdO). PdO

is used as a catalyst to oxidize methane and thus, readily coordinates with methane. It is important that these materials have a porous structure that allows methane (and O<sub>2</sub>) to diffuse through the polymer and reach the metal oxide, as is the case for the PANI-PdO nanocomposite. The PANI matrix was used to “filter” out interferences such as water (humidity), since PANI is hydrophilic and water is able to hydrogen bond to the amines in PANI. The removal of water as an interference is important, since water reduces PdO’s effectiveness as a catalyst for methane (Fujimoto et al., 1998).

Supramolecular cryptophane-A, which has a cage-like structure (see Figure 6.10), has also been used as a sensing material for methane (Benounis et al., 2005; Sun et al., 2009). Cryptophane-A has a shell-like structure and is able to form a stable complex with methane (Garel et al., 1993). Methane’s small size means it is not easily sterically hindered and thus can enter the cryptophane-A, since it is not being electrostatically repelled. This lack of repulsion is also due to methane’s non-polar nature. The complex formed between methane and cryptophane-A is a result of van der Waals forces (Sun et al., 2009).

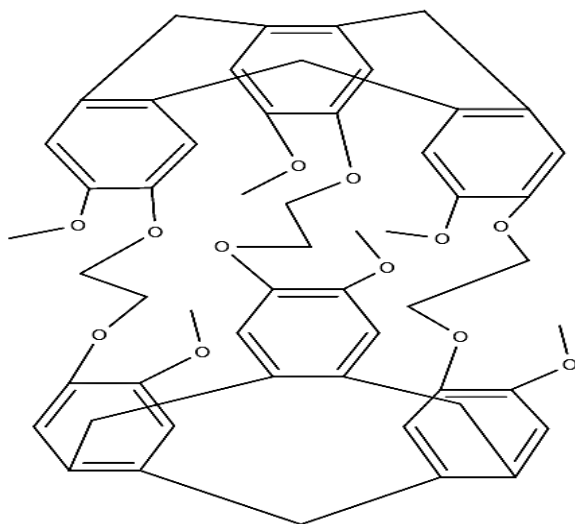


Figure 6.10: Cryptophane-A

Table 6.10: Polymeric Sensing Materials for Alkanes

Analyte	Sensing Material	Dopant	Detection Limit	Selectivity	Reference
Methane	Polyaniline (PANI)	PdO (17%) Camphor sulfonic acid (CSA)	3000 ppm	-	Xie et al. (2010)
Methane	Cryptophane-A	None	5000 ppm	-	Benounis et al. (2005)
Methane	Cryptophane-A	None	20 000 ppm	Ammonia (1.4) Nitrogen Dioxide (3.2) Carbon Monoxide (51.5) Hydrogen Gas (9.4)	Sun et al. (2009)

## 6.6 Final Remarks about Sensing Mechanisms

By examining the way an analyte interacts with a sensing material, it is possible to determine the dominant sensing mechanisms. This chapter examined a multitude of potential sensing mechanisms and what the likely dominant mechanisms are for various types of volatile organic compounds (VOCs). Identifying the dominant mechanisms of a target analyte can improve sensing material selection since the sensing materials and analytes interact via these mechanisms.

Chapter 7 further explores these sensing mechanisms through case studies (and counter-examples). In addition, practical prescriptions are suggested which can be used to improve the efficiency of designing and tailoring sensing materials for target analytes. These prescriptions are then followed to select potential sensing materials for ethanol.





## **7. Results and Discussion: Selecting a Sensing Material**

When designing or selecting sensing materials for gas analytes, there are a few factors to be considered. The first step is to choose a target analyte (volatile organic compound, VOC) for a specific application. Then, examining the chemical nature of the target analyte, determine which functional group(s) are present on the analyte. These functional groups will dictate the dominant sensing mechanisms with which the sensing material and analyte will interact.

Before continuing with sensing material selection, it is important to look at the type of sensor that will be used since the type of sensor may constrain the types of polymers used. For example, a resistive type sensor requires a conductive polymer and a capacitive sensor may require a polymer that is capable of swelling. If the type of sensor is unknown, then the issue becomes more complicated, but still a sensing material could be chosen that is able to work on a variety of different types of sensors.

In addition, the environment the sensor will be used in may also provide constraints. These include the types of interferences present which have an effect on selectivity, operational temperatures, size of sensor, response and recovery times. It is important to consider all these factors when selecting potential sensing materials.

### **7.1 Sensor Application Requirements**

A sensor's application will always carry some constraints such as operational temperature and sensitivity required. It is important to consider these constraints when designing a sensing material. The sensor application designates not only the target analyte, but also the environment in which the sensor will be used.

#### ***7.1.1 Sensitivity***

The sensor application determines how sensitive the sensor needs to be. For example, a formaldehyde sensor for indoor air quality must be able to detect formaldehyde below the concentration that has been determined as toxic. According to the World Health Organization (WHO), the concentration of formaldehyde should not exceed 0.08 ppm (80 ppb) over a 30 minute exposure (WHO, 2010). Therefore, a formaldehyde sensor for indoor air quality must be able to at least detect 0.08 ppm of formaldehyde (the target detection limit). Ideally, a sensor's sensitivity should be lower than the target detection limit.

To achieve such high sensitivity (low detection limit), the sensing material must have as many sensing sites as possible. This is because there is a correlation between the amount of analyte that sorbs and the sensitivity; the more the analyte sorbs, the more sensitive the sensing material. In

addition, when less analyte is present (i.e. lower concentration), less analyte sorbs onto the sensing material. Therefore, having more sensing sites available is likely to increase the number of analyte molecules that sorb (barring steric hindrance and other counterbalancing sensing mechanisms), thereby increasing the sensitivity of the sensing material.

Furthermore, the sensitivity of the sensor should not be limited by the sensor electronics. The noise should be at least three times lower than the response of the sensor to the target analyte at the detection limit. The sensitivity of the sensor must be evaluated with the sensing material on the sensor, since some sensing materials work better (have better sensitivity) than other materials on the same sensor. Also, two different sensing materials may produce different noise levels (one material may produce more noise than the other) on the same sensor (Stewart et al., 2015).

### ***7.1.2 Selectivity***

In any given environment, there will be the target analyte, as well as other interferents present. The application, and thus the environment the sensor will be used in, determines what these interferents are. For example, in an indoor air quality sensor, where the target analyte is formaldehyde, common interferents include acetone, ammonia, butanol, formic acid, toluene, and xylene (Wolkoff, 2013). Therefore, a selective sensor for formaldehyde must selectively identify formaldehyde when all of these other VOCs are present.

It is important to note that the concentrations of all VOCs present in an environment are not equal. Some interferents may be at concentrations an order of magnitude lower than the target analyte's concentration. If this is the case, the interferents present in the environment at very low concentrations (i.e. present at the ppb level when the concentration of the target analyte is at the ppm level) can be ignored (considered negligible), since they are not likely to create a response from the sensor at such low concentrations (Wolkoff, 2013).

### ***7.1.3 Operational Temperature***

The operational temperature is an important consideration, especially with regards to polymeric materials. It is important that the polymeric sensing materials are in their glassy states, since polymers above their glass transition temperature ( $T_g$ ) begin to soften and “flow”. If this occurs while a sensor is in operation, a response may not be detectable or the softened polymer chains may produce an erroneous or biased response. Because of this, the  $T_g$  of a potential sensing material should be above (ideally, well above) the operational temperature. Therefore, the operational temperature may eliminate some potential polymeric sensing materials. The operational temperature may also be optimized to improve the selectivity of the sensor (Lee et al., 2007).

In addition to the temperature at which the analyte is being sensed, the temperature at which the sensor recovery takes place may also be a consideration. This is the case for sensors with built-in heaters that are used to speed up the recovery times of a sensor by providing more energy (heat) to break the bond between the analyte and sensing material, regenerating the sensing material (Lee et al., 2006). Therefore, the  $T_g$  of potential polymeric sensing materials must be above the temperature at which the sensor is heated, not just the sensing temperature.

#### ***7.1.4 Response and Recovery Times***

Most applications require fast response and recovery times, ideally in the order of seconds or quicker. The response time is the time needed to reach 90% of the final signal (100% response); recovery time is the time the response takes to return to the baseline. Generally, the recovery time is longer than the response time.

It is possible to reduce the response time by doping a polymeric material with a metal or metal oxide dopant, especially in conductive sensors. For example, the incorporation of platinum (Pt) into polyaniline (PANI) increases the conversion rate between conductor and insulator, which decreases both the response and recovery times (Ulmann et al., 1992). The recovery time can also be reduced by heating the sensing layer, which gives energy to the analyte molecules and breaks the physical bonds formed between the analyte and sensing material (Nicolas-Debarnot and Poncin-Epaillard, 2003).

### **7.2 Target Analyte's Chemistry (Mechanisms)**

When choosing sensing materials for a target analyte, it is important to look at the functional groups of the target analyte. For example, ethanol has a hydroxyl (alcohol) group, formaldehyde has an aldehyde group, and benzene is aromatic. The functional groups dictate the chemistry with which the analyte will interact with the polymeric sensing materials. Therefore, the functional groups on the polymeric materials are also important. Chapter 6 described the dominant mechanisms for different volatile organic compounds (VOCs). Determining the mechanisms by which the target analyte is likely to interact with a sensing material will help narrow down potential sensing materials for a target analyte.

For example, ethanol contains an alcohol functional group and thus, ethanol is a polar molecule with a hydrogen attached to an oxygen. Therefore, ethanol is able to hydrogen bond. Consequently, a corresponding sensing material that would show affinity to ethanol should also be polar and ideally be able to hydrogen bond. Polymers that fall into this category are, for example, polymers containing alcohols, amines, and carboxylic acids.

## 7.3 Case Studies

This section provides examples and counter examples of the dominant mechanisms that occur. In some cases, it is more difficult to determine the dominant sensing mechanism because more than one mechanisms have a strong effect and the mechanisms may compete with one another.

### 7.3.1 Examples

#### 7.3.1.1 Effect of Hydrogen Bonding

Polyaniline (PANI) and poly (*N*-methyl aniline) (PNMA) were evaluated using ethanol and acetone to determine if ethanol interacted with PANI through hydrogen bonding. Both PANI and PNMA were synthesized as described in Section 3.3 using their respective monomers: aniline (A.C.S. reagent, Sigma-Aldrich, Oakville, Ontario, Canada) and *N*-methyl aniline (A.C.S. reagent, Sigma-Aldrich, Oakville, Ontario, Canada). It was hypothesized that ethanol's OH group hydrogen bonded to the NH group on PANI. PNMA was chosen as a counter example since PNMA is chemically similar to PANI, except the amine group on PNMA is "protected" through steric hindrance by a methyl group (see Figure 7.1). Acetone was chosen as a counter example (to ethanol) since PANI may still hydrogen bond to the double bonded oxygen (=O) on acetone, but acetone itself cannot hydrogen bond and thus would not sorb onto PNMA. It should be noted that acetone is a little larger than ethanol (77.5 cm<sup>3</sup>/mol and 62.6 cm<sup>3</sup>/mol, respectively; however, acetone is more polar than ethanol (2.91 D and 1.69 D, respectively). Despite these differences, on the whole, acetone and ethanol are similar molecules.

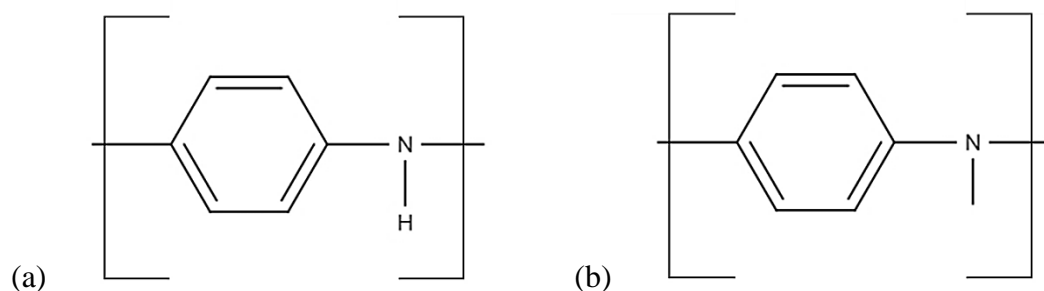


Figure 7.1: Schematic of (a) polyaniline (PANI) and (b) poly (*N*-methyl aniline) (PNMA)

Acetone is able to act as a Lewis-base; however, PANI would prefer to hydrogen bond since the hydrogen in the amine on PANI is electron deficient and wants to gain electron density through hydrogen bonding. The electronegative oxygen (on acetone) will seek out the positively charged hydrogen, resulting in a hydrogen bond. The tertiary amine on PNMA will act as a Lewis-base and does not have a hydrogen attached to its amine able to hydrogen bond to acetone. Therefore, acetone is unable to bond with PNMA. However, ethanol is still capable of hydrogen bonding to the tertiary amine on PNMA because of the alcohol (OH) group in ethanol.

Both PANI and PNMA were subjected to 5 ppm of ethanol (balance of nitrogen) and 5.5 ppm of acetone (balance of nitrogen), separately. The amount of gas (ethanol or acetone) that sorbed onto the sensing material (PANI or PNMA) was subsequently measured using the test system described in Chapter 3. It was found that significantly more ethanol and acetone sorbed onto PANI than onto PNMA. In addition, significantly more ethanol sorbed onto both PANI and PNMA than acetone (see Figure 7.2).

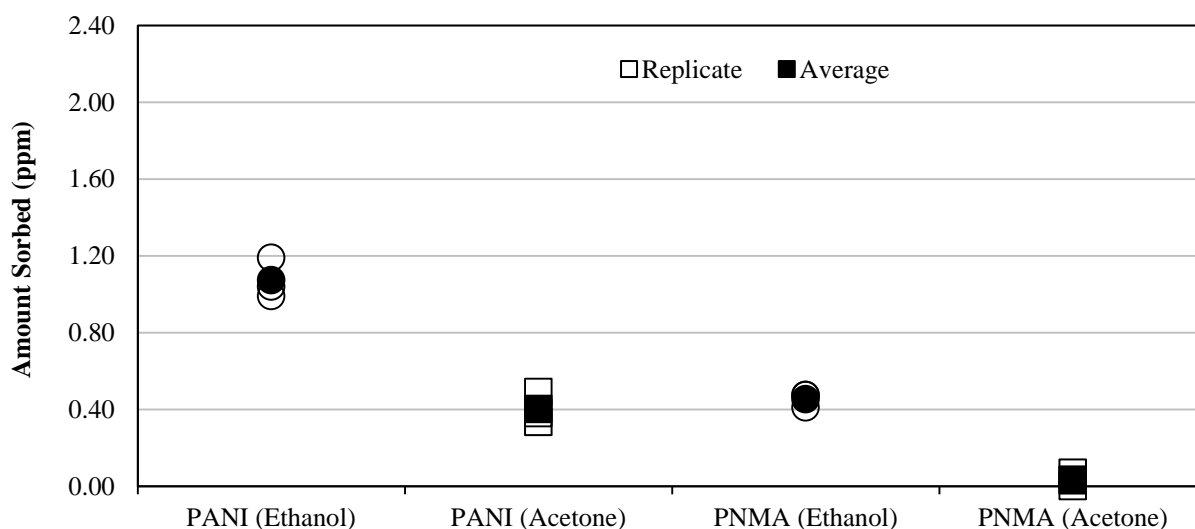


Figure 7.2: Amount of ethanol (circles) and acetone (squares) sorbed onto both PANI and PNMA.

Despite acetone being more polar than ethanol, acetone is only a hydrogen bond acceptor, which means that it doesn't have a hydrogen capable of hydrogen bonding. This results in acetone being attracted to both PANI and PNMA through electrostatic forces, but is limited in physically bonding with these polymeric sensing materials. Ethanol's ability to hydrogen bond allows it to sorb onto both PANI and PNMA. Since PANI is also able to hydrogen bond and PNMA is only a hydrogen bond acceptor, due to PNMA's a tertiary amine, PANI will more readily sorb both acetone and ethanol.

There is some steric hindrance that occurs as well, which enhances the difference in sorption between ethanol and acetone. Acetone is larger than ethanol and has a bulkier shape. Acetone is trigonal planar in shape, whereas ethanol is linear and has one less carbon atom. This means that acetone is more sterically hindered. It should be noted that the polar attractive forces and the steric repulsion do compete against one another and given that acetone is not that bulky, in general, the attractive forces are likely to win out, especially for PANI, where the amine is unprotected. However, the steric repulsion is more of an issue when it comes to PNMA, where the amine is somewhat "protected" by a methyl group, which would exert greater steric repulsion.

### 7.3.1.2 Incorporation of Metal Oxide Dopants into a Polymeric Sensing Material

The incorporation of a metal oxide nanoparticle into a polymer (doping) can improve both the sensitivity and selectivity of a sensing material. For example, doping poly (2,5-dimethyl aniline) (P25DMA) with just 5 wt. % alumina ( $\text{Al}_2\text{O}_3$ ) improved both the sensitivity to ethanol, as well as the selectivity (see Figure 7.3). The P25DMA was synthesized using 2,5-dimethyl aniline (A.C.S. reagent, Sigma-Aldrich, Oakville, Ontario, Canada) with 5 wt. %  $\text{Al}_2\text{O}_3$  nanoparticles (particle size <50 nm, 10 wt. % dispersion in  $\text{H}_2\text{O}$ , Sigma-Aldrich, Oakville, Ontario, Canada), as described in Section 3.3 in Chapter 3.

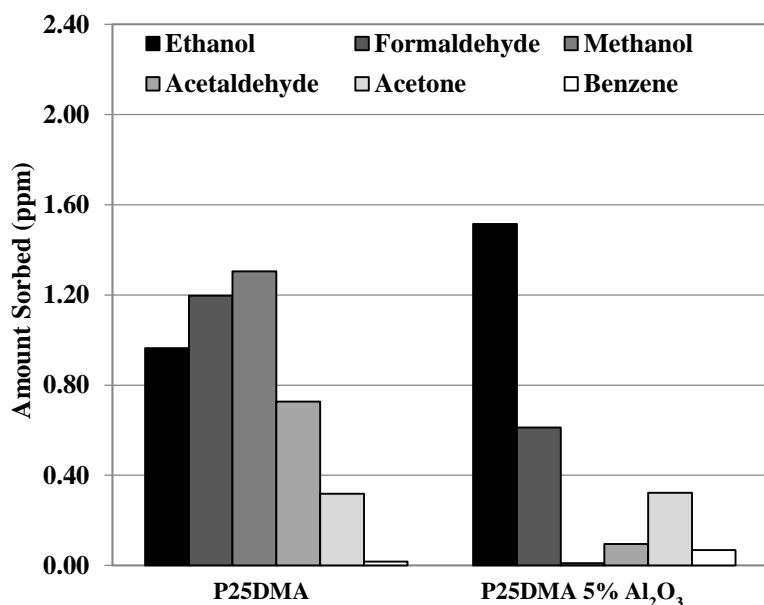


Figure 7.3: Sorption of different gases (left to right, ethanol, formaldehyde, methanol, acetaldehyde, acetone, and benzene) to P25DMA and P25DMA 5%  $\text{Al}_2\text{O}_3$ .

$\text{Al}_2\text{O}_3$  was added to increase the sensitivity (Yang et al., 2009a) and selectivity of P25DMA to ethanol (Papadopoulos et al., 1996). Ethanol more readily decomposes on  $\text{Al}_2\text{O}_3$  than other volatile organic compounds (VOCs) such as methanol and acetaldehyde (Cordi and Falconer, 1996). Therefore, ethanol may be able to coordinate better with the Al amongst other factors. Note that decomposition is influenced by more than just coordination with the catalyst. Thus, adding  $\text{Al}_2\text{O}_3$  should ideally improve the selectivity of P25DMA, which it did.

The addition of  $\text{Al}_2\text{O}_3$  to P25DMA also changed the morphology of the sensing material. The addition of  $\text{Al}_2\text{O}_3$  created “kinks” along the P25DMA chain, resulting in polymer chains that could not stack as neatly. This resulted in an increase in surface area available for the analytes to sorb to. In addition, the structure became more porous (see Figure 7.4), which also increased the number of sensing sites for the analytes to bond to. This increase in number of sensing sites improved the selectivity of the P25DMA.

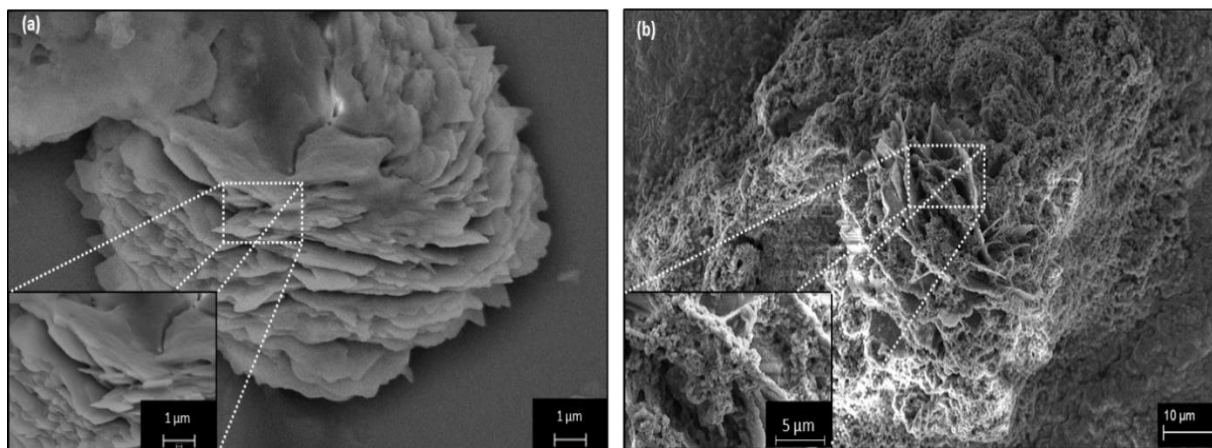


Figure 7.4: SEM images of (a) P25DMA and (b) P25DMA doped with  $Al_2O_3$ .

### 7.3.1.3 Competing Mechanisms

Poly (2,5-dimethyl aniline) (P25DMA) was doped with nickel oxide (NiO) nanoparticles and exposed to ethanol gas to evaluate P25DMA doped with NiO as a potential sensing material for ethanol (see Figure 7.5). The P25DMA was synthesized using 2,5-dimethyl aniline (A.C.S. reagent, Sigma-Aldrich, Oakville, Ontario, Canada), with 5 wt. %, 10 wt. %, and 20 wt. % NiO nanoparticles (particle size < 50 nm, concentration of 99.8%, Sigma-Aldrich, Oakville, Ontario, Canada) as described in Section 3.3.

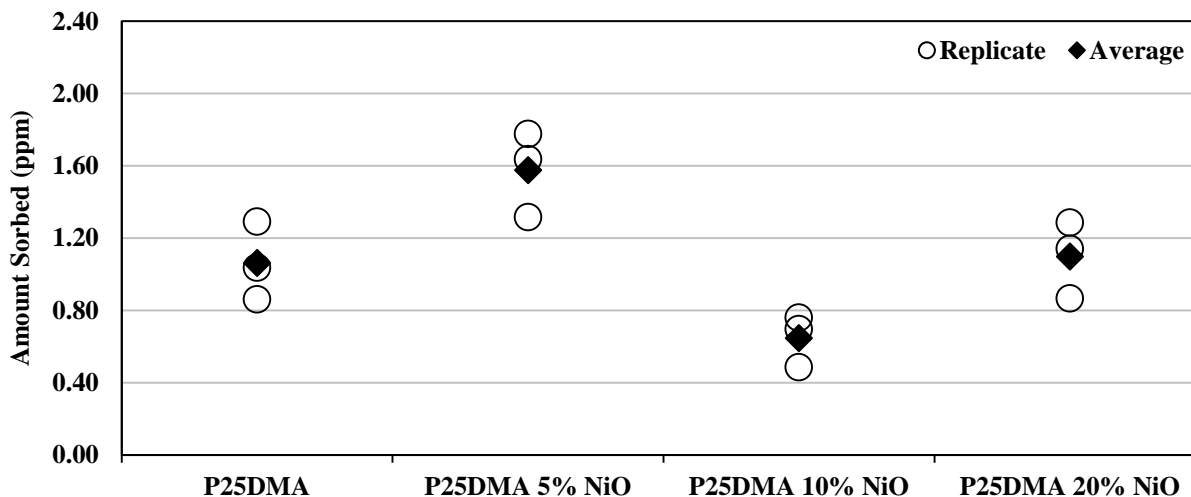


Figure 7.5: Ethanol sorption on P25DMA and P25DMA doped with different concentrations of NiO.

P25DMA primarily interacts with ethanol through hydrogen bonding. Adding 5% NiO created “kinks” in the polymer chain, where the P25DMA changed conformation to reduce strain caused by the bond between the Ni and the amine groups on P25DMA (Han et al., 2006). This created



larger interstitial spaces in the polymer and thus, improved diffusivity into the polymer. This resulted in the amount of ethanol sorbed which significantly increased for P25DMA 5% NiO compared to the undoped P25DMA. Even with the added NiO, the dominant mechanism for P25DMA 5% NiO was still hydrogen bonding, although metal coordination did play a minor role in the improved sorption observed.

Further increasing the amount of NiO to 10 wt. % resulted in a large and significant drop in ethanol sorption, likely due to competing mechanisms. At a concentration of 10 wt. %, metal coordination likely began to take over. The larger and more numerous interstitial spaces created by the kinks in the polymer chain would have increased the diffusion into the polymer matrix where most of the NiO resided. Note that the NiO bound to multiple amine groups in the polymers, thereby reducing the number of sites (amines) to which ethanol hydrogen bonded. This reduction in sensing sites coupled with reduced access to NiO (where metal coordination occurs) resulted in a reduced amount of ethanol sorbed.

By increasing the amount of NiO to 20 wt. %, the amount of ethanol sorbed increased again, although not back to the level of P25DMA 5% NiO. This increase in ethanol sorption from 10% to 20% NiO was likely due to the higher availability of NiO with which ethanol was able to coordinate. P25DMA 20% NiO had the most kinks in the polymer chains and thus, an increased number of larger interstitial spaces to improve diffusion (and therefore, less steric hindrance). In addition, the increased amount of NiO allowed more ethanol to coordinate to the Ni, despite the NiO reducing the number of amines on the P25DMA to which the ethanol could hydrogen bond.

In the case for P25DMA doped with NiO, two competing mechanisms dominated. At low concentrations of NiO (5 wt. %), hydrogen bonding dominated and resulted in a large amount of ethanol sorption. As more NiO was added, the NiO coordinated to more and more amine sites on the P25DMA, significantly reducing the number of amines available to which ethanol could hydrogen bond. However, as the concentration of NiO increased, the dominance of metal coordination increased. At 20 wt. %, the increased NiO content allowed metal coordination to dominate due to the availability of NiO and reduction in hydrogen bonding sites on the P25DMA.

### ***7.3.2 Counter Examples***

Sometimes the dominant mechanism for a target analyte and/or sensing material can have detrimental effects on sensitivity and selectivity. For example, a sensing material that is capable of hydrogen bonding, such as polyethyleneimine (PEI), may sorb interferents more preferentially or may bind too strongly to certain analytes to be useful. Another example is when a metal oxide is added to improve the sensing properties of a polymer, but instead it is either not incorporated into the polymer matrix or destroys the polymer matrix, resulting simply in polymer coated nanoparticles.

### 7.3.2.1 Competing Analytes (Poor Selectivity)

Polyethyleneimine (PEI) was chosen as a potential sensing material for ethanol due to its numerous amine groups (see Figure 7.6). PEI (50 wt. % in water, Sigma-Aldrich, Oakville, Ontario, Canada) was dried at room temperature (21 °C) for two months, then purged with nitrogen (5.0 grade) for 4 hours before being evaluated with 5 ppm of ethanol (balance of nitrogen). It was found that PEI sorbed only 0.05 ppm, which can be considered negligible, since the error was determined as 1% (based on three independent replicates).

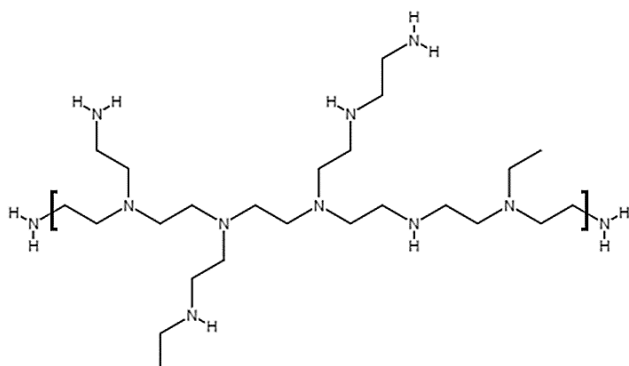


Figure 7.6: Schematic of polyethyleneimine (PEI).

Based on the chemical structure of PEI, it would appear that there is a high density of sensing sites due to all the amines present. In addition, the branching would reduce the polymers ability to pack, increasing the interstitial spaces between the polymer chains, thereby improving diffusion of an analyte into the polymeric material. However, because of these amine groups, PEI is extremely hydrophilic and thus, PEI was saturated with water molecules, even after PEI had been dried, which left no open sensing sites for ethanol. A few ethanol molecules may have sorbed onto the water molecules through hydrogen bonding, but it was a negligible amount.

While it may have been possible to remove more water from the PEI, its use as a sensing material is limited due to its affinity to water. In atmospheric conditions, where water vapour is present (relative humidity), water vapour will preferentially bind to PEI since it is much more polar than any other polar analyte. Note that PEI has been used in sensor applications; however, it has been combined with other materials such as poly (vinyl alcohol) for a formaldehyde sensor (Wang et al., 2010b) or combined with multi-walled carbon nanotubes for a humidity sensor (Yu et al., 2006).

### 7.3.2.2 Incompatible Metal Oxides and Polymers

There are cases where a metal oxide either does not bind to the polymer at all or only a small percentage will be incorporated. In the case where the metal oxide is not incorporated into the

polymer, the polymer is not considered doped with the metal oxide. In the case where only a small percentage of metal oxide is incorporated, despite adding more metal oxide (i.e. only 5% of a metal oxide is taken up, despite 20% being available), the polymer is considered doped. These two cases are the result of poor coordination between the metal oxide and the polymer.

Copper (II) oxide (CuO) (particle size <50 nm, Sigma-Aldrich, Oakville, Ontario, Canada) was polymerized with 2,5-dimethyl aniline (A.C.S. reagent, Sigma-Aldrich, Oakville, Ontario, Canada) at three concentrations of CuO (5 wt.%, 10 wt.%, and 20 wt.%, based on amount added during polymerization) to form a doped poly (2,5-dimethyl aniline) (P25DMA). Note that the three samples will be referred to as P25DMA 5% CuO, P25DMA 10% CuO, and P25DMA 20% CuO. However, none of the CuO was incorporated into the final polymer. The lack of CuO was confirmed by electron dispersive spectroscopy (Ametek EDAX, New Jersey, USA); see Table 7.1. In addition, there was no significant difference between the amount of ethanol sorbed between P25DMA 5% CuO, P25DMA 10% CuO, and P25DMA 20% CuO (see Figure 7.7) and the scanning electron microscopy (SEM) images showed that P25DMA 5% CuO, P25DMA 10% CuO, and P25DMA 20% CuO all had similar morphologies (see Figure 7.8). It was, however, interesting to note that the morphology of the P25DMA made in the presence of CuO had a different morphology and sorption response to ethanol than P25DMA made without any dopant added during polymerization (see Figures 7.7 and 7.8).

Table 7.1: EDAX Measurements for P25DMA Doped with CuO

Polymeric Nanocomposite	Weight Percent of Cu
P25DMA 5% CuO	0.16
P25DMA 10% CuO	0.07
P25DMA 20% CuO	0.11

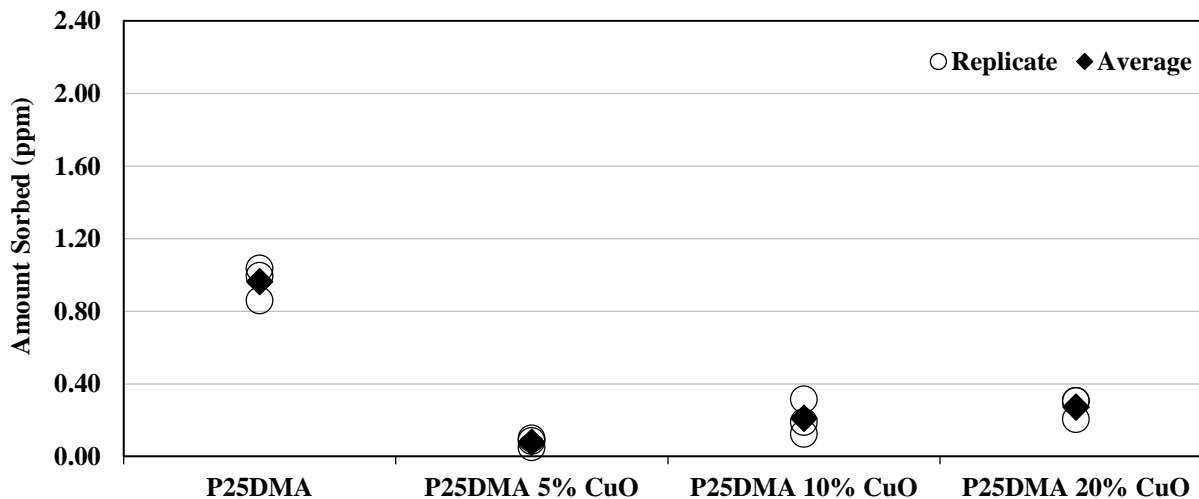


Figure 7.7: Amount of ethanol sorbed onto P25DMA doped with CuO.

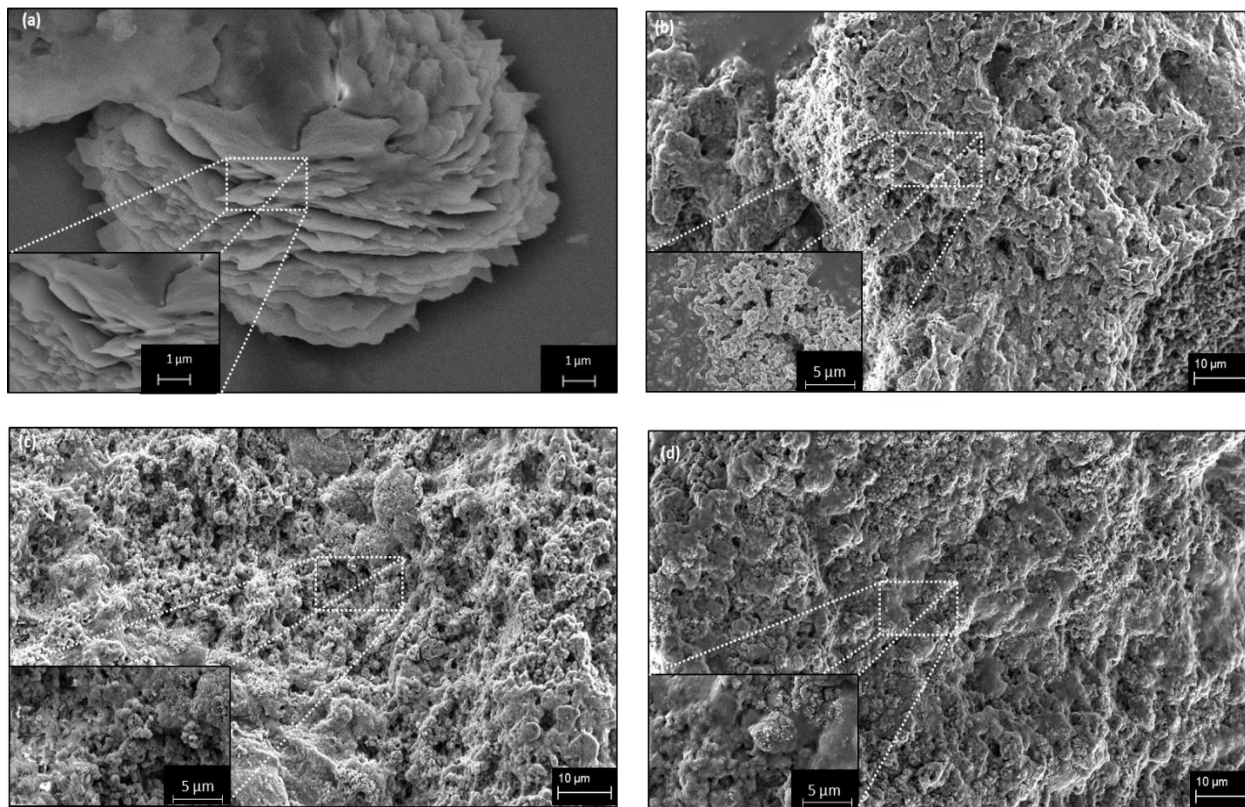


Figure 7.8: SEM images of (a) P25DMA, (b) P25DMA doped with 5% CuO, (c) P25DMA doped with 10% CuO, and (d) P25DMA doped with 20% CuO.

This suggests that despite the CuO not incorporating into the P25DMA matrix, it did have an effect on the synthesis. It is likely that the CuO created “kinks” along the P25DMA chain as the polymer attempted to conform around a CuO nanoparticle as the polymer chain grew; however the strain was too great and the weak bond between Cu and the P25DMA would break to relieve this strain. The “kinks” would, however, remain and result in a more porous morphology since the polymer chains would not be able to stack more closely together. Note that a more porous morphology does not necessarily mean the polymer has a larger number of accessible sensing sites. This is the case for the CuO doped P25DMA versus the undoped P25DMA.

The conformational strain of a polymer chain when the polymer is bound to the metal oxide nanoparticle results in a polymer coated nanoparticle, as is the case of P25DMA with 20 wt. % zinc oxide (ZnO) (Thompson et al., 2001). By coating the ZnO nanoparticle with P25DMA, the ZnO is no longer accessible by the analyte and thus, the ZnO cannot interact with the analyte. In addition, the P25DMA is essentially ‘destroyed’ and thus the ZnO decreases the number of sorption sites on P25DMA, resulting in significantly reduced sensing ability of the P25DMA to ethanol (Stewart et al., 2015).

Both of these examples, P25DMA with CuO and ZnO, show that choosing dopants that coordinate well with the polymer matrix is important. However, this may not always be evident, and as such, dopants are chosen based on their likelihood to improve sorption of the target analyte. Therefore, preliminary screening tests are important to determine if the dopant (metal oxide) is incorporated well into the polymer matrix and if the dopant has an effect on the sensing properties.

## 7.4 Practical Prescriptions

### 7.4.1 Practical Prescriptions

The prescriptions herein are for designing and selecting polymeric sensing materials for volatile organic compounds (VOC); see Figure 7.9 for an overview. They take into consideration the previously described dominant sensing mechanisms with which the analytes and sensing materials interact (see Chapter 6).

When designing a sensing material for a target analyte, it is best to begin by looking at the chemistry of the target analyte. Determining the type of functional group(s) on the target analyte will help narrow down the types of polymers that could work as sensing materials. In addition, the size of the target analyte is a consideration. If the target analyte is bulky such as benzene or trimethylamine, then a polymer whose chains do not pack as tightly (i.e. has larger interstitial spaces) would be better; however, a small molecule such as methanol or formaldehyde can more easily penetrate smaller interstitial spaces due to reduced steric hindrance.

The type of functional groups on the target analyte will determine the dominant mechanisms with which the target analyte and the polymeric sensing material interact. See Section 6.5 for further details about which mechanisms dominate for which functional groups. Based on the sensing mechanisms, potential polymer classes can be selected, which will be further refined by other constraints.

The next step is to look at the target application. The target application will have some constraints such as operational temperature and environmental stability. The polymer must be able to remain in its glassy state at the operating temperature (range). Therefore, the glass transition temperature ( $T_g$ ) must be above the operational temperature of the sensor. In addition, the polymer must have good mechanical and environmental stability to withstand repeated and long term use.

The main constraint is sensitivity (detection limit). For a particular application, the detection limit of a sensor must be lower than the target limit. In general, a sensing material with more “sensing sites” has a lower limit of detection and is thus more sensitive. The more accessible (available) sensing sites are on the surface of the sensing material; thus, a morphology with high surface area-to-volume ratios is best.

The target application will also determine the types of typical analytes (interferents) present with the analyte, as well as typical concentrations of all analytes. If the interferents are present at an order of magnitude (or more) lower than the target analyte, then those interferents may not appreciably interact with a sensing material. In addition, the list of potential polymers may be reduced by considering the chemistry and functional groups of the interferents. For example, the response from larger interferents can be reduced through steric hindrance since the larger interferents will be repelled by steric effects and thus not be able to sorb onto the sensing material and produce a response. Therefore, polymers with bulkier side groups/chains may be eliminated from the list of potential polymers. Another example is using hydrophobic and hydrophilic copolymers to reduce a response caused by water vapour (humidity).

The type of sensor used will significantly affect the types of polymers considered. If a resistive (conductive)-based sensor is used, then the sensing material must be conductive. Therefore, a conductive polymer is needed for resistive type sensors. Currently, resistive type sensors are most commonly used. Other types of sensors include capacitive-based sensors, where a conductive polymer may hinder the sensor performance, and mass-based sensors, where polymeric sensing materials are advantageous because they are of light weight compared to metal and metal oxide sensing materials.

The list of potential polymers has now been reduced through dominant mechanisms, application constraints, and types of sensor. The resulting polymers can also be modified by adding, removing, and/or changing some functional groups on a polymer backbone. This can be done to improve any number of properties. Two or more polymers can be combined, creating a copolymer to change the properties. In addition, dopants can also be added. In some cases, dopants can be used to make a polymer conductive, such as adding acid to polyaniline. In many cases, metal and metal oxide dopants are added to improve the sensitivity and/or selectivity of the polymeric material. It is important to note that not all metals are able to coordinate with all polymers.

Once a final list of potential polymers has been selected, they can be ranked in terms of what may be the most effective in terms of sensitivity and/or selectivity. These polymers can now be synthesized and evaluated as sensing materials for the target analyte.

Note that selection of potential sensing materials is a two pronged approach. The selection combines the chemical nature of the target analyte and how it is likely to interact with a polymeric sensing material with the practical constraints placed on the application of the final sensor. Therefore, when looking at the chart in Figure 7.9, begin at the top. There are three paths (factors) to consider: target analyte, target application constraints, and typical interferents. Combining these three factors will result in a set of potential polymeric materials. Next, dopants can also be added. These polymers (with or without dopants) can then be evaluated as sensing materials for the target analyte and application.

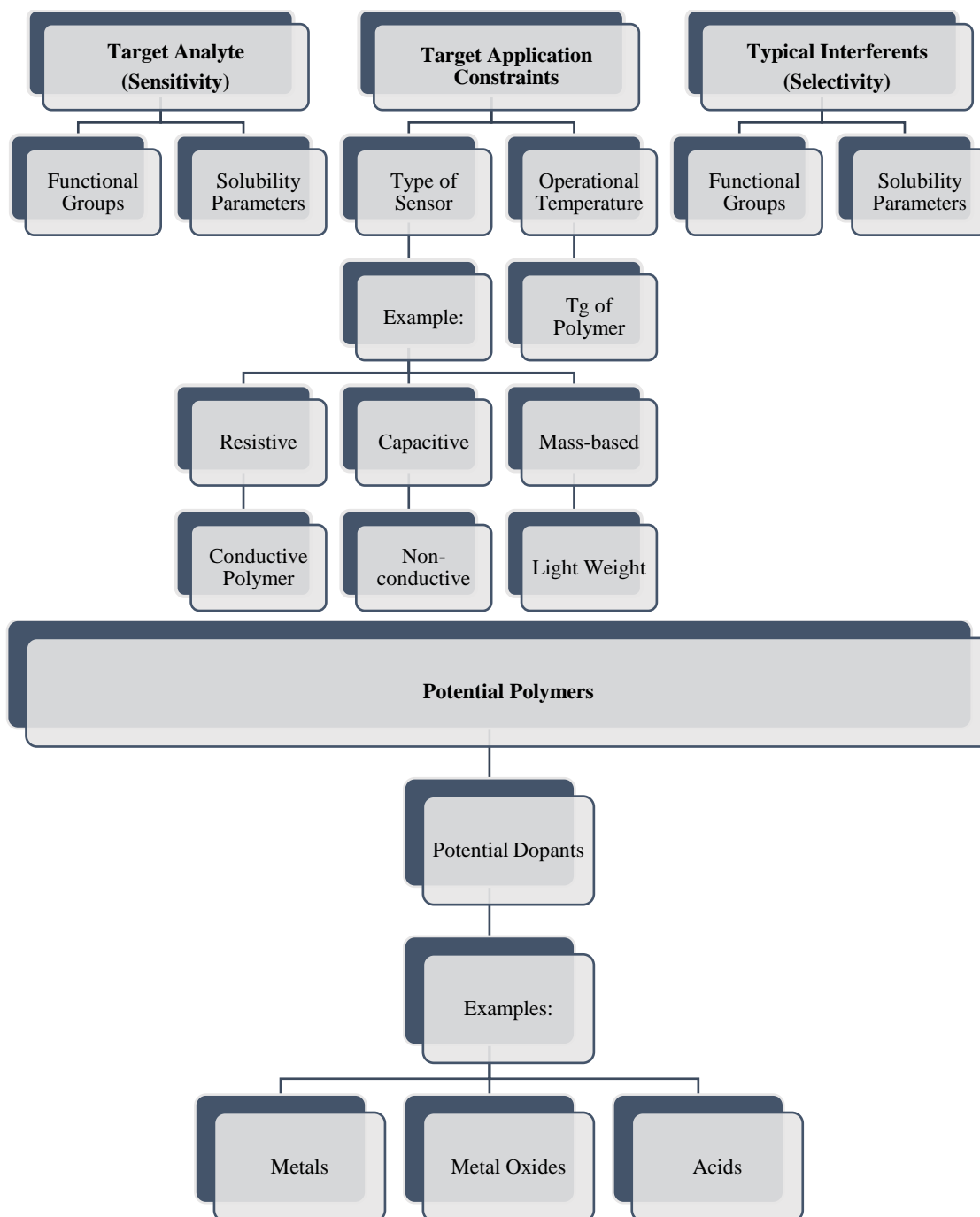


Figure 7.9: Prescription Flow Chart for Sensing Material Selection.

### 7.4.2 Polymeric Sensing Material Selection Example

As an example, an ethanol gas sensor will be used, with a target detection limit of 5 ppm. This sensor will typically operate at room temperature (around 21°C) and may be either a resistive or mass-based sensor. The sensor will be used where appreciable amounts of methanol and acetone may also be present as interferents.

Initially, looking at ethanol, it has an alcohol group and therefore, it is able to hydrogen bond. It can also act as a Lewis-base; however, hydrogen bonding is the dominant mechanism. Therefore, potential polymers should include amines, alcohols, carboxylic acids, ethers, esters, amides, etc. This is a long list that needs to be pared down. For this example, one may start with 30 – 50 possible candidate polymers (see Appendix I), reducing this list down to 12 potential polymers to be considered further (see Table 7.2).

For a sensor working at room temperature, the polymers need to be in a glassy state above room temperature. Given that sensors are often pushed outside their typical operational range, the sensing material must not soften considerably or begin to flow. Therefore, for this application which can result in storage near 50°C, a  $T_g$  above 60°C is preferable. This drops the list of 12 candidates in Table 7.2 down to 8.

Looking at the functional groups of the main interferents (acetone and methanol) reduced the list of potential materials further. Methanol, similar to ethanol, is also an alcohol and thus, is also able to hydrogen bond. Acetone, on the other hand, cannot hydrogen bond, but as a ketone, will behave as a Lewis base. Therefore, keeping polymers that are not able to hydrogen bond, but have oxygen or nitrogen that ethanol is able to hydrogen bond to may improve selectivity. Therefore, the OH, COOH, and NH functionalized polymer chains will be eliminated, leaving 4 candidate polymers at this stage, namely, PETE, PMMA, PVP, and PPO.

A check with the Hildebrand solubility parameters, where ethanol is 26.6 MPa<sup>1/2</sup>, shows that the Hildebrand solubility parameter of PPy is 25.15 MPa<sup>1/2</sup>, which is close to that of ethanol. Therefore PPy will be added back to the list, bringing the number up to 5 potential polymeric sensing materials. PETE (21.9 MPa<sup>1/2</sup>) and PPO (19.6 MPa<sup>1/2</sup>) were the most different in terms of Hildebrand solubility parameters. To reduce the list to 4 potential polymers, PETE was eliminated and PPO was kept because PPO is conductive and PETE is not. This leaves 2 polymers that are conductive (PPy and PPO) and 2 polymers that are non-conductive (PMMA and PVP). This allows for flexibility on the type of sensor that may be used.



Table 7.2: Potential Polymeric Sensing Materials for Ethanol

Polymer	Glass Transition Temperature, $T_g$ ( $^{\circ}\text{C}$ ) <sup>1</sup>	Hildebrand Solubility Parameter ( $\text{MPa}^{1/2}$ ) <sup>1</sup>	Structure	Functional Groups
Poly (ethylene oxide) (PEO)	-43	19.9		-O-
Poly (vinyl acetate) (PVAc)	30	19.2		COOR
Polyamide (PA)	50 <sup>2</sup>	23.02		CONR <sub>2</sub>
Poly (lactic acid) (PLA)	57	21		COOR
Poly (ethylene terephthalate) (PETE)	67	21.9		COOR x2
Poly (vinyl alcohol) (PVA)	85	21.7		OH
Polyaniline (PANI)	100	22.2		NH
Poly (methyl methacrylate) (PMMA)	105	22.8		COOR
Poly (acrylic acid) (PAA)	106	19.2		COOH
Poly (vinyl pyrrolidone) (PVP)	128	25.6		CONR <sub>2</sub>
Poly (2,6-dimethyl-1,4-phenylene oxide) (PPO)	215	19.6		-O-
Polypyrrole (PPy)	270	25.15		NH

<sup>1</sup>Brandrup et al. (1999)

<sup>2</sup>For the structure shown

These four polymers (PMMA, PVP, PPO, and PPy) were evaluated with respect to their sorption of ethanol, methanol, and acetone. PMMA (Average  $M_w$  = 15,000, Sigma-Aldrich, Oakville, Ontario, Canada), PVP (Average  $M_w$  = 40,000, Sigma-Aldrich, Oakville, Ontario, Canada), PPO (Average  $M_w$  = 30,000 Sigma-Aldrich, Oakville, Ontario, Canada), and PPy (Conductivity 10 – 50 S/cm, pressed pellet, Sigma-Aldrich, Oakville, Ontario, Canada) were all used as obtained, without further modification. The polymer samples were prepared in round bottom flasks and tested using the gas test system as described in Section 3.5 of Chapter 3.

All four polymers showed good sorption of ethanol. In addition, all four polymers showed poorer sorption of methanol and acetone (see Figure 7.10). Therefore, all four polymers had good selectivity towards ethanol with respect to methanol and especially to acetone. From here, only a couple of polymers need to be deposited onto a sensor for further evaluation. If a resistive type sensor is chosen, then PPy and PPO can be used; if a mass-based sensor is selected, then any of the four polymers could be employed; however PVP had the best selectivity and thus would be the best choice, despite PVP sorbing the least ethanol of the four polymers. This demonstrates that the practical prescriptions can significantly improve the efficiency of choosing (and further testing) potential sensing materials. When coupled with preliminary evaluation of a sensing material's sorption characteristics to specific gas analytes, the cost of deposition and sensor testing is also significantly reduced.

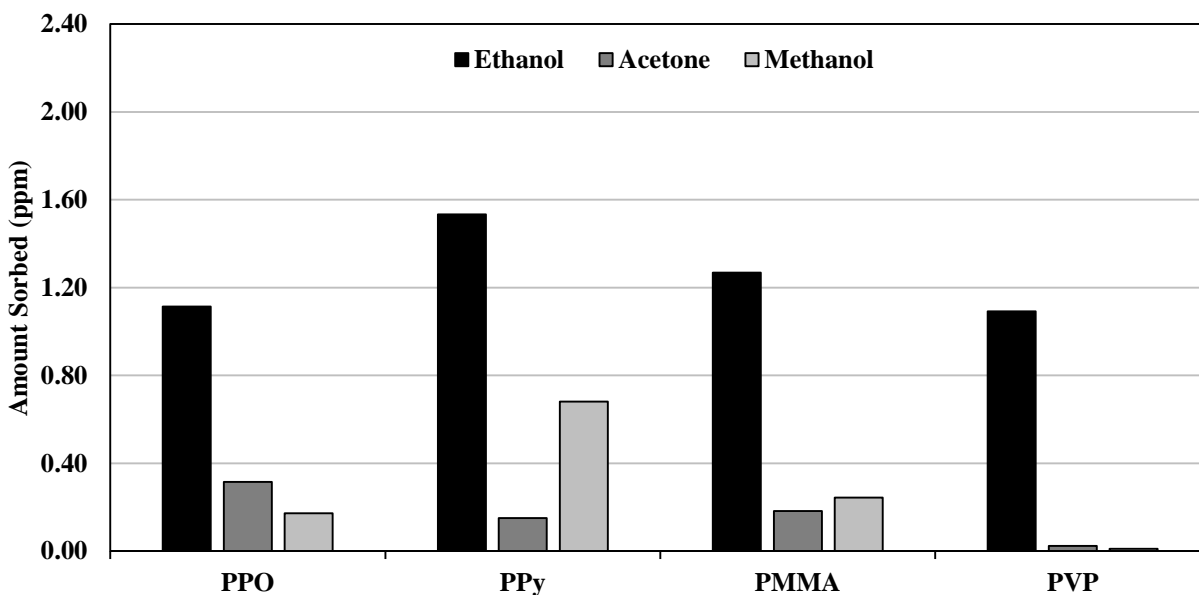


Figure 7.10: Sorption of the four polymers to ethanol, methanol, and acetone.



## 8. Concluding Remarks and Recommendations

### 8.1 Concluding Remarks

There were three main objectives for this thesis: to design sensitive and selective polymeric sensing materials for ethanol; to identify the main sensing mechanisms with which sensing materials and analytes interact; and to create general prescriptions that could be used to design new polymeric sensing materials. All three of these main objectives were met.

In total, 22 different polymers and polymeric nanocomposites were synthesized and evaluated as sensing materials for ethanol. In addition, 8 other commercially available sensing materials were also evaluated as sensing materials for ethanol. From these 30 polymeric sensing materials, it was found that poly (2,5-dimethyl aniline) (P25DMA) doped TiO<sub>2</sub>, NiO, and Al<sub>2</sub>O<sub>3</sub>, and polypyrrole (PPy) had the highest sensitivity to ethanol based on sorption tests. However, when comparing the selectivity, P25DMA 5% Al<sub>2</sub>O<sub>3</sub> and P25DMA 10% TiO<sub>2</sub> had the best selectivity out of the polymeric nanocomposites and poly (vinyl pyrrolidone) (PVP) had the best selectivity of the commercially available polymers.

High selectivity was also achieved using five partially selective polymeric sensing materials. P25DMA and P25DMA doped with 5% Al<sub>2</sub>O<sub>3</sub>, NiO, TiO<sub>2</sub>, and ZnO were used to create a sensor array capable of detecting six different gas analytes (acetaldehyde, acetone, benzene, ethanol, formaldehyde, and methanol). This was done using principal component analysis (PCA) as a filtering algorithm.

Two different sensors, a radio frequency identification (RFID) capacitive sensor and a microelectromechanical system (MEMS) microcantilever sensor, were used to evaluate various sensing materials. It was found that on the various types of RFID sensors P25DMA doped with 20% NiO had the best sensitivity and selectivity towards ethanol and had a limit of detection of 3 ppm on the rigid type RFID sensor. On the MEMS microcantilever, P25DMA had a limit of detection of 5 ppm for ethanol.

The information obtained from these experiments (sensitivity and selectivity to ethanol) also improved the understanding of how sensing materials and gas analytes interact. Based on carefully chosen polymeric sensing materials, it was determined that both the polymer backbone and the side chains (functional groups) have an effect on the sensing properties. This led to the exploration of various sensing mechanisms with which volatile organic compounds (VOCs) and polymeric sensing materials interact.

Combining the information obtained from the experiments with that in the literature has led to an evaluation of sensing mechanisms for various classes of VOCs. Some of these mechanisms were

evaluated with carefully chosen polymeric sensing materials and gas analytes, which confirmed the dominant mechanisms. Based on these sensing mechanisms, as well as sensor application constraints, general prescriptions were developed that can be used to select potential polymeric sensing materials for VOC sensor applications. These prescriptions were evaluated by selecting potential sensing materials for ethanol. Four potential sensing materials were evaluated for sensitivity and selectivity. It was found that all four of the polymeric sensing materials evaluated had good sensitivity and overall, good selectivity, especially PVP.

Therefore, all three main objectives for this thesis were met. In addition, many smaller side-concepts that contributed to the main objectives were explored.

The experimental test set-up (Chapter 3; used throughout the thesis) was discussed in detail in “Novel Test System for Gas Sensing Materials and Sensors” published in *Macromolecular Symposia* (Stewart et al., 2013).

The polymeric nanocomposites made with poly (2,5-dimethyl aniline) (P25DMA) doped with Al<sub>2</sub>O<sub>3</sub>, CuO, NiO, TiO<sub>2</sub> (Chapter 4) has been accepted in the *Journal of Macromolecular Science A: Pure and Applied Chemistry* under the title “Evaluation of Polymeric Nanocomposites for the Detection of Toxic Gas Analytes” (Stewart and Penlidis, 2016a). In addition, a paper discussing the sensor array (also from Chapter 4) has been accepted in *Macromolecular Symposia* under the title “Detection of Six Volatile Organic Compounds using a Sensor Array”.

The sensors onto which the polymeric sensing materials were deposited and evaluated (Chapter 5) were done in collaboration with two other groups. The RFID sensors were done in collaboration with Wei Ting (Scott) Chen who designed the various RFID sensors, onto which my sensing materials were placed and analyzed using my test system. The results from these experiments are published in multiple papers including “Doped Poly (2,5-dimethyl aniline) for the Detection of Ethanol” (Stewart et al., 2015), “Novel Undercoupled Radio-frequency (RF) Resonant Sensor for Gaseous Ethanol and Interferents Detection” (Chen et al., 2015b), and “Wearable RF Sensor Array Implementing Coupling-Matrix Readout Extraction Technique” (Chen et al., 2015a). The MEMS-based microcantilever was done in collaboration with Mahmoud Khater and the results are published under “Binary MEMS Gas Sensors” (Khater et al., 2014).

An overview of sensing mechanisms and how they can be used to select potential sensing materials for a target gas analyte and application (Chapters 6 and 7) has been published in *Polymers for Advanced Technologies* under the title “Designing Polymeric Sensing Materials: What are we Doing Wrong?” (Stewart and Penlidis, 2016b). In addition, a shorter paper entitled “Designing Polymeric Sensing Materials for Analyte Detection and Related Mechanisms” that presents a systematic approach to selecting sensing materials using sensing mechanisms has been published in *Macromolecular Symposia* (Stewart and Penlidis, 2016c).

In total, the work presented in this thesis has produced results that have been published in 9 refereed papers (6 of which are “first author”, 2 are “second author”, and one other).

## **8.3 Future Work**

### ***8.3.1 Short Term Goals***

#### *8.3.1.1 Improve the Sensor Array for Six VOCs*

The sensor array described in Section 4.6 could be improved to be able to identify the components of gas mixtures as well. By evaluating known concentrations of gas analytes in various mixtures (two gases, three gases, and so forth), it may be possible to identify multiple gas analytes in a mixture of gases. To accomplish this, a more sophisticated “neural net” or filtering algorithm may be needed to achieve this separation of VOCs.

#### *8.3.1.2 Improve Understanding of Sensing Mechanisms and Dopant Incorporation*

A greater understanding of how analytes (and interferents) interact with polymeric sensing materials will result in more efficient and better selection of sensing materials for future sensor development. In addition, a better understanding of how dopants, especially metal oxides, incorporate themselves into a polymeric matrix will improve sensing material synthesis and dopant selection. This will also improve polymer nanocomposite selection in a variety of applications such as membrane separation and catalysis. Note that multiple sensing mechanisms occur simultaneously when an analyte interacts with a sensing material; therefore, it may be difficult to identify the dominant mechanisms in operation (only based on theory).

#### *8.3.1.3 Improve Understanding of Sensing Mechanisms for Inorganic Analytes*

Inorganic compounds such as nitrogen oxides ( $\text{NO}_x$ ) (EPA, 1999), sulfur oxides ( $\text{SO}_x$ ) (Shahbazi et al., 2016), and carbon monoxide (CO) (Smith, 1987) all contribute to environmental and air pollution. The majority of sensing materials for inorganic analytes are based on metals and metal oxides (Shinde et al., 2012; Korotcenkov, 2013); however, the selectivity towards a specific analyte may not be sufficient (Comini et al., 2002). As a potential solution to increase selectivity of sensing materials for inorganic analytes, polymeric materials could be used instead since they can be tailored to interact with a target analyte. Analyzing trends in literature could lead to identifying sensing mechanisms for inorganic analytes and understanding how inorganic analytes and polymeric sensing materials interact. This improved understanding of how inorganic analytes (and interferents) interact with polymeric sensing materials will result in more efficient and better selection of sensing materials for future sensor development.

### **8.3.2 Long Term Goals**

#### *8.3.2.1 Build and Evaluate a Prototype of the Ethanol Sensing Device for a Vehicle*

One of the ultimate objectives of this research was to build a prototype for an ethanol sensor that could be placed inside a vehicle. The goal was to have an ignition interlock system that would be triggered by the sensor, if ethanol was detected from a person's skin above a set threshold. Therefore, further evaluation of the most promising sensing materials for ethanol should be conducted on various sensors, creating complete sensors. These complete sensors must be evaluated for their sensing ability and their durability in a vehicle.

#### *8.3.2.2 Design, Synthesize, and Evaluate Sensing Materials for Acetone*

Acetone is an indicator for disease, including diabetes (Fleischer et al., 2002). A sensor able to detect low concentrations of acetone in the breath, similar to breathalyzers for ethanol, could be used as a non-invasive method for screening for diabetes. A sensor for acetone needs a limit of detection below 1 ppm and a high selectivity to avoid false positives (Deng et al., 2004).

Note that a highly sensitive and selective sensing material may be difficult to create; however, designing multiple sensing materials that are sensitive to acetone and/or other common interferents to be used in a sensor array or electronic nose could be a viable solution.

#### *8.3.2.3 Design, Synthesize, and Evaluate Sensing Materials for Benzene*

Benzene is toxic, even at very low concentrations (no safe level of benzene can be recommended by WHO) (WHO, 2010) and therefore, contributes to poor indoor air quality. Benzene is also a by-product of industrial processes and vehicle exhaust (Lee et al., 2002). Because of its high toxicity, it is important to monitor benzene levels in air.

Similar to acetone, a sensor array could be used to improve the selectivity towards benzene. This would require designing multiple sensing materials for benzene and/or other common interferents present in the target application. Note that the sensing materials required for an indoor air application and those for monitoring benzene in industrial by-products or vehicle exhaust are likely to be very different. This is because the environment with which the sensor needs to function is very different, especially in terms of temperature.

#### *8.3.2.4 Sensing Materials for Inorganic Pollutants*

Inorganic compounds such as nitrogen oxides (NO<sub>x</sub>) (EPA, 1999), sulfur oxides (SO<sub>x</sub>) (Shahbazi et al., 2016), and carbon monoxide (CO) (Smith, 1987) all contribute to air pollution. NO<sub>x</sub> and SO<sub>x</sub> are pollutants released from a variety of industrial processes, including pulp and paper and combustion engines (Bajpai, 2015). All three cause environmental air pollution and thus, it is important to monitor and reduce the amount released into the air.

To detect all three, amongst other inorganic analytes (such as CO<sub>2</sub>, O<sub>3</sub>, and H<sub>2</sub>S), a sensor array that is able to identify many different gas analytes would be the best solution. A sensor array could be designed to detect threshold concentrations of each analyte, where the threshold concentration is the maximum “safe level” determined by government standards.

#### *8.3.2.5 Sensing Materials for Toxic Aqueous Analytes*

There are many toxic analytes that affect the quality of drinking water. These toxic analytes include heavy metals (such as mercury (Nolan et al., 2006) and arsenic (Akpoy and Muchie, 2010)), sulfide ions (Hassan et al., 2002), and chlorophenols (Kuleyin, 2007). It is important to both monitor and remove these toxic analytes. Therefore, designing sensing materials and absorbents capable of detecting and sorbing low concentrations (ppb levels) of these toxic analytes would improve the quality of drinking water.

#### *8.3.2.6 Modelling of the Interactions between Sensing Materials and Analytes*

Molecular orbital theory can be used to evaluate potential sensing materials and gas analytes. When an analyte molecule sorbs onto a sensing material, there is an interaction between the molecular orbitals of both molecules. The energies of these orbitals can be predicted using molecular orbital theory and can be modelled using various computational chemistry software and wave function approximations such as Hartree-Fock. Note that two compounds will only bind, even temporarily, if their highest occupied molecular orbital (HOMO) and their lowest unoccupied molecular orbital (LUMO) are similar in energy. This could also be extended to determine how well certain metal oxides will bind to a polymer to create polymeric nanocomposites.





## References

- Acevedo, C. A., E. Y. Sánchez, J. G. Reyes, and M. E. Young. "Volatile Organic Compounds Produced by Human Skin Cells" *Biological Research* **40** (2007) 347-355.
- Abdul Rahim, H. and S. D. Syed Hassan. "Breathalyzer Enabled Ignition Switch System" The 2010 6<sup>th</sup> International Colloquium on Signal Processing and Its Applications, May 21-23, 2010, Melaka, Malaysia.
- Agbor, N. E., M. C. Petty, and A. P. Monkman. "Polyaniline Thin Films for Gas Sensing" *Sensors and Actuators B* **28** (1995) 173-179.
- Agilent Technologies. "Pulsed Discharge Helium Ionization Detector (PDHID): User Information" Agilent Technologies, USA 2006, p. 8.
- Ai, L., J.-C. Mau, W.-F. Liu, M.-Y. Fu, and T.-C. Chen. "Ammonia Gas Fiber Sensor Based on Polyaniline Sensing Film Coated on Superstructure Fiber Bragg Gratings" *Microwave and Optical Technology Letters* **49** (2007) 3036-3066.
- Akpor, O. B. and M. Muchie. "Remediation of heavy metals in Drinking Water and Wastewater Treatment Systems: Processes and Applications" *International Journal of Physical Sciences* **5**, 12 (2010) 1807-1817.
- Albonetti, S., R. Bonelli, R. Delaigle, C. Femoni, E. M. Gaigneaux, V. Morandi, L. Ortolani, C. Tiozzo, S. Zacchini, and F. Trifirò. "Catalytic Combustion of Toluene over Cluster-derived Gold/Iron Catalysts" *Applied Catalysis A: General* **372** (2010) 138-146.
- Alizadeh, T. and L. H. Soltani. "Graphene/Poly(methyl methacrylate) Chemiresistor Sensor for Formaldehyde Odor Sensing" *Journal of Hazardous Materials* **248-249** (2013) 401-406.
- Andreatta, A., Y. Cao, J. C. Chang, A. J. Heeger, and P. Smith. "Electrically-conductive Fibers of Polyaniline Spun Solutions in Concentrated Sulfuric Acid" *Synthetic Metals* **26** (1988) 383-389.
- Antwi-Boampong, S. and J. J. BelBruno. "Detection of Formaldehyde Vapor using Conductive Polymer Films" *Sensors and Actuators B* **182** (2013) 300-306.
- Arshak, K. I., L. M. Cavanagh, I. Gaidan, E. G. Moore, S. A. Clifford, R. Phelan, C. Cunniffe, J. A. Harris, and G. M. Lyons. "NiO-TiO<sub>2</sub> Thick-films for Detection of Alcohol Vapours at Room Temperature" *IEEE* (2004).

Arsuaga, J. M., A. Sotto, G. del Rosario, A. Martinez, S. Molina, S. B. Teli, and J. de Abajo. "Influence of the Type, Size, and Distribution of Metal Oxide Particles on the Properties of Nanocomposite Ultrafiltration Membranes" *Journal of Membrane Science* **428** (2013) 131-141.

Ashley, D. L., M. A. Bonin, F. L. Cardinali, J. M. McCraw, J. S. Holler, L. L. Needham, and D. G. Patterson, Jr. "Determining Volatile Organic Compounds in Human Blood from a Large Sample Population by Using Purge and Trap Gas Chromatography/Mass Spectrometry" *Analytical Chemistry* **64** (1992) 1021-1029.

Athawale, A. A., and M. V. Kulkarni. "Polyaniline and its Substituted Derivatives as a Sensor for Aliphatic Alcohols" *Sensors and Actuators B* **67** (2000) 173-177.

Athawale, A. A., S. V. Bhagwat, and P. P. Katre. "Nanocomposite of Pd-Polyaniline as a Selective Methanol Sensor" *Sensors and Actuators B* **114** (2006) 263-267.

Aussawasathien, D., S. Sahasithiwat, L. Sahasithiwat, and C. Teerawattananon. "Poly(o-anisidine)-polystyrene nanocomposite Fibers via Electrospinning Process: Surface Morphology and Chemical Vapor Sensing" *Sensors and Actuators B* **151** (2011) 341-350.

Babaei, M. and N. Alizadeh. "Methanol Selective Gas Sensor Based on Nano-structured Conducting Polypyrrole Prepared by Electrochemically on Interdigital Electrodes for Biodiesel Analysis" *Sensors and Actuators B* **183** (2013) 617-626.

Bai, H. and G. Shi. "Gas Sensors Based on Conducting Polymers" *Sensors* **7**, 3 (2007) 267-307.

Bai, X., H. Ji, P. Gao, Y. Zhang, and X. Sun. "Morphology, Phase Structure and Acetone Sensitive Properties of Copper-doped Tungsten Oxide Sensors" *Sensors and Actuators B* **193** (2014) 100-106.

Bajpai, P. *Green Chemistry and Sustainability in Pulp and Paper Industry*. Springer, Switzerland 2015.

Barisci, J. N., G. G. Wallace, M. K. Andrews, A. C. Partridge, and P. D. Harris. "Conducting Polymer Sensors for Monitoring Aromatic Hydrocarbons using an Electronic Nose" *Sensors and Actuators B* **84** (2002) 252-257.

Barreca, D., E. Comini, A. Gasparotto, C. Maccato, C. Sada, G. Sberveglieri, and E. Tondello. "Chemical Vapor Deposition of Copper Oxide Films and Entangled Quasi-1D Nanoarchitectures as Innovative Gas Sensors" *Sensors and Actuators B* **141**, 1 (2009) 270-275.

Bavastrello, V., E. Stura, S. Carrara, V. Erokhin, and C. Nicolini. "Poly(2,5-dimethylaniline)-MWNTs Nanocomposite: A New Material for Conductometric Acid Vapours Sensor" *Sensors and Actuators B* **98** (2004) 247-253.

Beckers, N. A., M. T. Taschuk, and M. J. Brett. "Selective Room Temperature Nanostructured Thin Film Alcohol Sensor as a Virtual Sensor Array" *Sensors and Actuators B* **176** (2013) 1096-1102.

Beltrán, N. H., M. A. Duarte-Mermoud, V. A. Soto, S. A. Salah, and M. A. Bustos. "Chilean Wines Classification based only on Aroma Information" *International Journal of Electrical and Computer Engineering* **1**, 5 (2006) 378-383.

Benounis, M., N. Jaffrezic-Renault, J.-P. Dustasta, K. Cherif, and A. Abdelghani. "Study of a New Evanescent Wave Optical Fiber Sensor for Methane Detection Based on Cryptophane Molecules" *Sensors and Actuators B* **107** (2005) 32-39.

Bhat, N. V., A. P. Gadre, and V. A. Bambole. "Structural, Mechanical, and Electrical Properties of Electropolymerized Polypyrrole nanocomposite Films" *Journal of Applied Polymer Science* **80** (2001) 2511-2517.

Bonavoglia, B., G. Storti, M. Morbidelli, A. Rajendran, and M. Mazzotti. "Sorption and Swelling of Semicrystalline Polymers in Supercritical CO<sub>2</sub>" *Journal of Polymer Science Part B* **44**, 11 (2006) 1531-1546.

Bradner, F. P., J. S. Shapiro, H. J. Bowley, D. L. Gerrard, and W. Maddams. "Some Insights into the Microstructure of Polypyrrole" *Polymer* **30**, 5 (1989) 914-917.

Bandrup, J., E. H. Immergut, E. A. Grulke. "Polymer Handbook Fourth Edition" John and Wiley Sons, Inc., USA 1999, p. 683-711.

Bocchini, S., A. Chiolerio, S. Porro, D. Accardo, N. Garino, K. Bejtka, D. Perrone, and C. F. Pirri. "Synthesis of Polyaniline-based Inks, Doping Thereof and Test Device Printing towards Electronic Applications" *Journal of Materials Chemistry C* **1** (2013) 5101-5109.

Calestani, D., R. Mosca, M. Zanichelli, M. Villani, and A. Zappettini. "Aldehyde Detection by ZnO Tetrapod-based Gas Sensors" *Journal of Materials Chemistry* **21** (2011) 15532-15536.

Callister, W. D. Jr. *Fundamentals of Materials Science and Engineering: An Integrated Approach* Second Edition. John Wiley & Sons, Inc., United States of America 2005.

Campanella, L. and M. Battilotti. "Suitable Solid State Chemical Sensor for HCHO Determination" *International Journal of Environment and Pollution* **27**, 4 (2006) 313-323.

Cao, X., Z. Zhang, and X. Zhang. "A Novel Gaseous Acetaldehyde Sensor Utilizing Cataluminescence on Nanosized BaCO<sub>3</sub>" *Sensors and Actuators B* **99** (2004) 30-35.

Chen, Z.-K., S.-C. Ng, S. F. Y. Li, L. Zhong, L. Xu and H. S. O. Chan. "The Fabrication and Evaluation of a Vapour Sensor Based on Quartz Crystal Microbalance Coated with Poly(o-anisidine) Langmuir-Blodgett Layers" *Synthetic Metals* **87** (1997) 201-204.

Chen, X., J. Sun, and J. Shen. "Patterning of Layer-by-Layer Assembled Organic-Inorganic Hybrid Films: Imprinting Versus Lift-off" *Langmuir* **25** (2009) 3316-3350.

Chen, W. T., K. M. E. Stewart, J. Carroll, R. Mansour, E. Abdel-Rahman, and A. Penlidis. "Novel Gaseous Phase Ethanol Sensor Implemented with Underloaded RF Resonator for Sensor-embedded Passive Chipless RFIDs" *Proceedings at The 17<sup>th</sup> International Conference on Solid-state Sensors, Actuators and Microsystems (TRANSDUCERS & EUROSENSORS XXVII) IEEE*, June 2013, pp. 2059-2062.

Chen, W. T., K. M. E. Stewart, C. K. Yang, R. R. Mansour, J. Carroll, and A. Penlidis. "Wearable RF Sensor Array Implementing Coupling-Matrix Readout Extraction Technique" *IEEE Transactions and Microwave Theory and Techniques* **63**, 12 (2015a) 4157-4168.

Chen, W. T., K. M. E. Stewart, R. R. Mansour, and A. Penlidis. "Novel Undercoupled Radio-frequency (RF) Resonant Sensor for Gaseous Ethanol and Interferents Detection" *Sensors and Actuators A* **230** (2015b) 63-73.

Chen, W. T. (2015c) *Wearable RF Resonant Gaseous Chemical Sensor Array*. PhD Thesis, University of Waterloo.

Cheng, J. P., B. B. Wang, M. G. Zhao, F. Liu, and X. B. Zhang. "Nickel -doped Tin Oxide Hollow Nanofibers Prepared by Electrospinning for Acetone Sensing" *Sensors and Actuators B* **190** (2014) 78-85.

Chiang, C.-J., K.-T. Tsai, Y.-H. Lee, H.-W. Lin, Y.-L. Yang, C.-C. Shih, C.-Y. Lin, H.-A. Jeng, Y.-H. Weng, Y.-Y. Cheng, K.-C. Ho, and C.-A. Dai. "In Situ Fabrication of Conducting Polymer nanocomposite Film as a Chemical Resistive CO<sub>2</sub> Gas Sensor" *Microelectronic Engineering* **111** (2013) 409-415.

Choi, S.-J. , I. Lee, B.-H. Jang, D.-Y. Youn, W.-H. Ryu, C. O. Park, and I.-D. Kim. “Selective Diagnosis of Diabetes using Pt-Functionalized WO<sub>3</sub> Hemitube Networks as a Sensing Layer of Acetone in Exhaled Breath” *Analytical Chemistry* **85**, 3 (2013) 1792-1796.

Choopun, S., N. Hongsith, P. Mangkorntong, and N. Mangkorntong. “Zinc Oxide Nanobelts by RF Sputtering for Ethanol Sensor” *Physica E* **39** (2007) 53–56.

Choudhury, A. “Polyaniline/Silver Nanocomposite: Dielectric Properties and Ethanol Vapour Sensitivity” *Sensors and Actuators B* **138** (2009) 318-325.

Cindemir, U., P. C. Lansåker, L. Österlund, G. A. Niklasson, and C.-G. Granqvist. “Sputter-deposited Indium-Tin Oxide Thin Films for Acetaldehyde Gas Sensing” *Coatings* **6**, 2 (2016) doi: 10.3390/coatings6020019.

Comini, E., G. Faglia, G. Sberveglieri, Z. Pan, and Z. L. Wang. “Stable and Highly Sensitive Gas Sensors based on Semiconducting Oxide Nanobelts” *Applied Physics Letters* **81**, 10 (2002) 1869-1871.

Cordi, E. M. and J. L. Falconer. “Oxidation of Volatile Organic Compounds on Al<sub>2</sub>O<sub>3</sub>, Pd/Al<sub>2</sub>O<sub>3</sub>, and PdO/Al<sub>2</sub>O<sub>3</sub> Catalysts” *Journal of Catalysis* **162** (1996) 104-117.

Coulson, C. A. “The dipole Moment of the C-H Bond” *Transactions of the Faraday Society* **38** (1942) 433-444.

Curran, A. M., S. I. Rabin, P. A. Prada, and K. G. Furton. “Comparison of the Volatile Organic Compounds Present in Human Odor using SPME-GC/MS” *Journal of Chemical Ecology* **31**, 7 (2005) 1607-1619.

Dahnke, H., G. Von Basum, K. Kleinermanns, P. Hering, and M. Mürtz. “Rapid Formaldehyde Monitoring in Ambient Air by Means of Mid-infrared Cavity Leak-out Spectroscopy” *Applied Physics B: Lasers and Optics* **75** (2002) 311-316.

Das, D., P. Choudhury, L. J. Borthakur, I. R. Kamrupi, U. Gogoi, and S. K. Dolui. “Methanol Vapour Sensor Based on Poly (styrene-co-butylacrylate)/Polypyrrole-EG Core-shell Nanocomposites” *Sensors and Actuators B* **199** (2014) 320-329.

De Wit, M., E. Vanneste, H. J. Geise, and L. J. Nagels. “Chemiresistive Sensors of Electrically Conducting Poly(2,5-thienylene vinylene) and Copolymers: Their Response to Nine Organic Vapours” *Sensors and Actuators B* **50** (1998) 164-172.

Deng, C., J. Zhang, X. Yu, W. Zhang, and X. Zhang. "Determination of Acetone in Human Breath by Gas Chromatography-Mass Spectrometry and Solid-phase Microextraction with on-fiber Derivatization" *Journal of Chromatography B* **810**, 2 (2004) 269-275.

Deore, M. K. and G. H. Jain. "Studies on Ethanol Gas Sensing Properties of Al<sub>2</sub>O<sub>3</sub>-doped ZnO Thick Films" *Journal of Petroleum Science Research* **3**, 2 (2014) 60-67

Dirksen, J. A., K. Duval, T. A. Ring. "NiO Thin-film Formaldehyde Gas Sensors" *Sensors and Actuators B* **80** (2001) 106-115.

Do, J.-S. and S.-H. Wang. "On the Sensitivity of Conductimetric Acetone Gas Sensor Based on Polypyrrole and Polyaniline Conducting Polymers" *Sensors and Actuators B* **185** (2013) 39-46.

Duajj, O. K., A. Alghamdi, and Z. Y. Al-Sigh. "Solubility and Surface Thermodynamics of Conducting Polymers by Inverse Gas Chromatography. III. Polypyrrole Chloride" *Journal of Chromatography A* **1291** (2013) 137-145.

Endo, T., Y. Yenagida, and T. Hatsuzawa. "Colourimetric Detection of Volatile Organic Compounds using Colloidal Crystal-based Chemical Sensor for Environmental Applications" *Sensors and Actuators B* **125** (2007) 589-595.

EPA (United States Environmental Protection Agency) Office of Air Quality. Nitrogen Oxides (NO<sub>x</sub>), Why and How they are Controlled, North Carolina, 1999.

Fan, H., Z. Peng, H. Yang, and K. Zhou. "A New Cataluminescence-based Gas Sensor for Simultaneously Discriminating Benzene and Ammonia" *Analytical Methods* **8** (2016) 1257-1264.

Fink, J. K. "Polymeric Sensors and Actuators" Scrivener Publishing, Beverly, Massachusetts, USA 2012.

Fleischer, M., E. Simon, E. Rumpel, H. Ulmer, M Harbeck, M. Wendel, C. Fietzek, U. Weimar, and H. Meixner. "Detection of Volatile Compounds Correlated to Human Disease through Breath Analysis with Chemical Sensors" *Sensors and Actuators B* **83** (2002) 245-249.

Fonner, J. M., C. E. Schmidt, and P. Ren. "A Combined Molecular Dynamics and Experimental Study of Doped Polypyrrole" *Polymer* **51**, 21 (2010) 4985-4993.

Fujimoto, K.-I., F. H. Ribeiro, M. Avalos-Borja, and E. Iglasia. "Structure and Reactivity of PdO<sub>x</sub>/ZrO<sub>2</sub> Catalysts for Methane Oxidation at Low Temperatures" *Journal of Catalysis* **179** (1998) 431-442.

Gallagher, M., C. J. Wysocki, J. J. Leyden, A. I. Spielman, X. Sun, and G. Preti. "Analysis of Volatile Organic Compounds from Human Skin" *British Journal of Dermatology* **159** (2008) 780-791.

Gao, J. and A. Penlidis. "Mathematical Modeling and Computer Simulation/Database for Emulsion Polymerization" *Progress in Polymer Science* **27**, 3 (2002) 403-535.

Gao, Y., X. Li, J. Gong, B. Fan, Z. Su, and L. Qu. "Polyaniline Nanotubes Prepared using Fiber Mats Membrane as the Template and their Gas-response Behaviour" *Journal of Physical Chemistry C* **112** (2008) 8215-8222.

Garel, L. J.-P. Dustasta, and A. Collet. "Complexation of Methane and Chlorofluorocarbons by Cryptophane-A in Organic Solution" *Angewandte Chemie International Edition* **32**, 8 (1993) 1169-1171.

Garzella, C., E. Comini, E. Tempesti, C. Frigeri, and G. Sberveglieri. "TiO<sub>2</sub> Thin Films by a Novel Sol-gel Processing for Gas Sensor Applications" *Sensors and Actuators B* **68** (2000) 189-196.

Giberti, A., M. C. Carotta, B. Fabbri, S. Gherardi, V. Guidi, and C. Malagù. "High-sensitivity Detection of Acetaldehyde" *Sensors and Actuators B* **174** (2012) 402-405.

Gomes de Souza, F. Jr., T. K. Anzai, M. V. A. Rodrigues, P. A. Melo Jr., M. Nele, and J. C. Pinto. "*In Situ* Determination of Aniline Polymerization Kinetics through Near-infrared Spectroscopy" *Journal of Applied Polymer Science* **112**, 1 (2009) 157-162.

Gong, J., Y. Li, Z. Hu, Z. Zhou, and Y. Deng. "Ultrasensitive NH<sub>3</sub> Gas Sensor from Polyaniline Nanograin Enchased TiO<sub>2</sub> Fibers" *Journal of Physical Chemistry C* **114** (2010) 9970-9974.

González-Chavarri, J., I. Castro-Hurtado, I. Ayerdi, E. Castaño, and G. G. Mandayo. "ZnO Conductometric Sensor for Indoor Air Quality Measurement inside Buildings" *IEEE 10<sup>th</sup> Spanish Conference on Electron Devices (CDE)*, Madrid, Spain, February 11-13, 2015.

Gou, X., G. Wang, J. Yang, J. Park, and D. Wexler. "Chemical Synthesis, Characterization and Gas Sensing Performance of Copper Oxide Nanoribbons" *Journal of Materials Chemistry* **18** (2008) 965-969.

Gràcia, I., P. Ivanov, F. Blanco, N. Sabaté, X. Vilanova, X. Correig, L. Fonseca, E. Figueras, J. Santander, and C. Cané. "Sub-ppm Gas Sensor Detection via Spiral  $\mu$ -preconcentrator" *Sensors and Actuators B* **132** (2008) 149-154.



Grate, J. W. and M. H. Abraham. "Solubility Interactions and the Design of Chemically Selective Sorbent Coatings for Chemical Sensors and Arrays" *Sensors and Actuators B* **3** (1991) 85-111.

Grob, R. L. and E. F. Barry, "Modern Practice of Gas Chromatography", 4<sup>th</sup> ed. J. Wiley & Sons, USA 2004, p. 25.

Gupta, M. C. and S. S. Umare. "Studies on Poly (*o*-methoxyaniline)" *Macromolecules* **25** (1992) 138-142.

Gurbuz, Y. W. P. Kang, J. L. Davidson, and D. V. Kerns. "Diamond Microelectronic Gas Sensor for Detection of Benzene and Toluene" *Sensors and Actuators B* **99** (2004) 207-215.

Hamedani, N. F., A. R. Mahjoub, A. A. Khodadadi, and Y. Mortazavi. "Microwave Assisted Fast Synthesis of Various ZnO Morphologies for Selective Detection of CO, CH<sub>4</sub>, and Ethanol" *Sensors and Actuators B* **156** (2011) 737-742.

Han, J., G. Song, R. Guo. "Synthesis of Rectangular Tubes of Polyaniline/NiO nanocomposites" *Journal of Polymer Science Part A: Polymer Chemistry* **44** (2006) 4229-4234.

Han, S.-D. and Y.-S. Sohn. "Thin Film Gas Sensor for Detection of Toxic Gases from Microbial" *IEEE Transducers 2011*, Beijing, China, June 5-9, 2011, pg 178-181.

Hansen, C. M. "Hansen Solubility Parameters: A User's Handbook, Second Edition" CRC Press, United States of America, 2007.

Hassan, S. S. M., S. A. M. Marzouk, and H. E. M. Sayour. "Methylene Blue Potentiometric Sensor for Selective Determination of Sulfide Ions" *Analytica Chimica Acta* **466** (2002) 47-55.

Haynes, W. M. "CRC Handbook of Chemistry and Physics, 93<sup>rd</sup> Edition" CRC Press, United States of America, 2012.

He, J.-Q., J. Yin, D. Liu, L.-X. Zhang, F.-S. Cai, and L.-J. Bie. "Enhanced Acetone Gas-sensing Performance of La<sub>2</sub>O<sub>3</sub>-doped Flowerlike ZnO Structure Composed of Nanorods" *Sensors and Actuators B* **182** (2013) 170-175.

HersHKovitz, Y., I. Eshkenazi, C. E. Campbell, J. Rishpon. "An Electrochemical Biosensor for Formaldehyde" *Journal of Electroanalytical Chemistry* **491** (2000) 182-187.

Hirayama, K. Y. Sakai, K. Kameoka, K. Noda, and R. Naganawa. "Preparation of a Sensor Device with Specific Recognition Sites for Acetaldehyde by Molecular Imprinting Technique" *Sensors and Actuators B* **86** (2002) 20-25.

Horstjann, M., Y. A. Bakhirkin, A. A. Kosterev, R. F. Curl, F. K. Tittel, C. M. Wong, C. J. Hill, and R. Q. Yang. "Formaldehyde Sensor Using Interband Cascade Laser Based Quartz-enhanced Photoacoustic Spectroscopy" *Applied Physics B: Lasers and Optics* **79** (2004) 799-803.

Hosono, K., I. Matsubara, N. Murayama, S. Woosuck, and N. Izu. "Synthesis of Polypyrrole/MoO<sub>3</sub> Hybrid Thin Films and Their Volatile Organic Compound Gas-sensing Properties" *Chemical Materials* **17** (2005) 349-354.

Hosseini, S. H., S. H. A. Oskooei, and A. A. Entezani. "Toxic Gas and Vapour Detection by Polyaniline Gas Sensor" *Iranian Polymer Journal* **14**, 4 (2005) 333-344.

Howarth, R. W., R. Santoro, and A. Ingraffea. "Methane and the Greenhouse-gas Footprint of Natural Gas Shale Formations" *Climatic Change* **106** (2011) 679-690.

Hsu, C.-L., Y.-D. Gao, Y.-S. Chen, and T.-J. Hsueh. "Vertical Ti Doped ZnO Nanorods based on Ethanol Gas Sensor Prepared on Glass by Furnace System with Hotwire Assistance" *Sensors and Actuators B* **192** (2014) 550-557.

Hu, P., G. Du, W. Zhou, J. Cui, J. Lin, H. Liu, D. Liu, J. Wang, and S. Chen. "Enhancement of Ethanol Vapour Sensing of TiO<sub>2</sub> Nanobelts by Surface Engineering" *Applied Materials and Interfaces* **2**, 11 (2010) 3263-3269.

Huang, J., X. Xu, C. Gu, W. Wang, B. Geng, Y. Sun, and J. Liu. "Effective VOCs Gas Sensor Based on Porous SnO<sub>2</sub> Microcubes Prepared via Spontaneous Phase Segregation" *Sensors and Actuators B* **173** (2012) 599-606.

Ibupoto, Z. H., M. A. Abbasi, X. Liu, M. S. Alsalhi, and M. Willander. "The Synthesis of NiO/TiO<sub>2</sub> Heterostructures and Their Valence Band Offset Determination" *Journal of Nanomaterials* **2014** (2014) doi/10.1155/2014/928658.

Itoh, T., I. Matsubara, W. Shin, and N. Izu. "Layered Hybrid Thin Film of Molybdenum Trioxide with Poly (2,5-dimethylaniline) for Gas Sensor Sensitive to VOC Gases in ppm Level" *Chemistry Letters* **36**, 1 (2007a) 100-101.

Itoh, T., I. Matsubara, W. Shin, N. Izu, and M. Nishibori. "Highly Aldehyde Gas-Sensing Responsiveness and Selectivity of Layered Organic-Guest/MoO<sub>3</sub>-Host Hybrid Sensor" *Journal of the Ceramic Society of Japan* **115**, 11 (2007b) 742-744.

Itoh, T., I. Matsubara, W. Shin, and N. Izu. "Synthesis and Characterization of Layered Organic/Inorganic Hybrid Thin Films Based on Molybdenum Trioxide with Poly(*N*-methylaniline) for VOC Sensor" *Materials Letters* **61** (2007c) 4031-4034.

Itoh, T., I. Matsubara, W. Shin, N. Izu, and M. Nishibori. "Characterizations of Interlayer Organic-Inorganic Nanohybrid of Molybdenum Trioxide with Polyaniline and Poly (*o*-anisidine)" *Materials Chemistry and Physics* **110**, 1 (2008) 115-119.

Ji, S., Y. Li, and M. Yang. "Gas Sensing Properties of a nanocomposite Composed of Electrospun Poly(methyl methacrylate) Nanofibers and in situ Polymerized Polyaniline" *Sensors and Actuators B* **133** (2008) 644-649.

Jia, Q., H. Ji, Y. Zhang, Y. Chen, X. Sun, and Z. Jin. "Rapid and Selective Detection of Acetone Using Hierarchical ZnO Gas Sensor for Hazardous Odor Markers Application" *Journal of Hazardous Materials* **276** (2014) 262-270.

Jiang, Z., J. Wang, L. Meng, Y. Huang, and L. Liu. "A Highly Efficient Chemical Sensor Material for Ethanol: Al<sub>2</sub>O<sub>3</sub>/Graphene Nanocomposites Fabricated from Graphene Oxide" *Chemical Communications* **47** (2011) 6350-6352.

Jones, A. W., V. Lagesson, and C. Tagesson. "Correspondence" *Journal of Clinical Pathology* **48** (1995) 979-980.

Joulazadeh, M., A. H. Navarchian, and M. Niroomand. "A comparative Study on Humidity Sensing Performances of Polyaniline and Polypyrrole Nanostructures" *Advances in Polymer Technology* **33**, S1 (2014) DOI: 10.1002/adv.21461.

Jun, J.-M., Y.-H. Park, and C.-S. Lee "Characteristics of a Metal-loaded SnO<sub>2</sub>/WO<sub>3</sub> Thick Film Gas Sensor for Detecting Acetaldehyde Gas" *Bulletin of the Korean Chemical Society* **32**, 6 (2011) 1865-1872.

Jung, Y. S., W. C. Jung, H. L. Tuller, and C. A. Ross. "Nanowire Conductive Polymer Gas Sensor Patterned Using Self-assembled Block Copolymer Lithography" *Nano Letters* **8**, 11 (2008) 3776-3780.

Kanable, R. "Nation without Drunk Driving: Technology will Help Achieve the Goal" *Law Enforcement Technology* **33**, 10 (2006) 46-53.

Kao, K.-W., M.-C. Hsu, Y.-H. Chang, S. Gwo, and J. A. Yeh. "A Sub-ppm Acetone Gas Sensor for Diabetes Detection Using 10 nm Thick Ultrathin InN FETs" *Sensors* **12** (2012) 7157-7168.

Kaur, N., E. Comini, D. Zappa, N. Poli, and G. Sberveglieri. "Nickel Oxide Nanowires: Vapour Liquid Solid Synthesis and Intergration into a Gas Sensing Device" *Nanotechnology* **27** (2016) 205701-205709.

Kawamura, K., K. Kerman, M. Fujihara, N. Nagatani, T. Hashiba, and E. Tamiya. "Development of a Novel Hand-held Formaldehyde Gas Sensor for the Rapid Detection of Sick Building Syndrome" *Sensors and Actuators B* **105** (2005) 495-501.

Kawamura, K., M. Vestergaard, M. Ishiyama, N. Nagatani, T. Hashiba, and E. Tamiya. "Development of a Novel Hand-held Toluene Gas Sensor: Possible Use in the Prevention and Control of Sick Building Syndrome" *Measurement* **39**, 6 (2006) 490-496.

Ke, M.-T., M.-T. Lee, C.-Y. Lee, and L.-M. Fu. "A MEMS-based Benzene Gas Sensor with a Self-heating WO<sub>3</sub> Sensing Layer" *Sensors* **9**, 4 (2009) 2895-2906.

Kebede, M. A., M. E. Varner, N. K. Scharko, R. B. Gerber, and J. D. Raff. "Photooxidation of Ammonia on TiO<sub>2</sub> as a Source of NO and NO<sub>2</sub> under Atmospheric Conditions" *Journal of the American Chemical Society* **135**, 23 (2013) 8606-8615.

Khater, M. E., E. M. Abdel-Rahman, and A. H. Nayfeh. "A Mass Sensing Technique for Electrostatically Activated MEMS" *Proceeding of the ASME International Design Engineering Technical Conferences & Computers and Information in Engineering Conference*, August 30 - September 2, 2009. San Diego, California, USA.

Khater, M. E., M. Al-Ghamdi, S. Park, K. M. E. Stewart, E. M. Abdel-Rahman, A. Penlidis, A. H. Nayfeh, A K. S. Abdel-Aziz, M. Basha. "Binary MEMS Gas Sensors" *Journal of Micromechanics and Microengineering* **24**, 6 (2014) 065007-065015.

Kim, J.-S., S.-O. Sohn, and J.-S. Huh. "Fabrication and Sensing Behavior of PVF<sub>2</sub> Coated-polyaniline Sensor for Volatile Organic Compounds" *Sensors and Actuators B* **108** (2005) 409-413.

Kim, K.-W., P.-S. Cho, S.-J. Kim, J.-H. Lee, C.-Y. Kang, J.-S. Kim, and S.-J. Yoon. "The Selective Detection of C<sub>2</sub>H<sub>5</sub>OH using SnO<sub>2</sub>-ZnO Thin Film Gas Sensor Prepared by Combinatorial Solution Deposition" *Sensors and Actuators B* **123** (2007) 318-324.

Kim, K.-S., W.-H. Baek, J.-M. Kim, T.-S. Yoon, H. H. Lee, C. J. Kang, and Y.-S. Kim. "A Nanopore Structured High Performance Toluene Gas Sensor Made by Nanoimprinting Method" *Sensors* **10**, 1 (2010) 765-774.

Kim, N.-H., S.-J. Choi, D.-J. Yang, J. Bae, J. Park, and I.-D. Kim. "Highly Sensitive and Selective Hydrogen Sulfide and Toluene Sensors using Pd Functionalized WO<sub>3</sub> Nanofibers for Potential Diagnosis of Halitosis and Lung Cancer" *Sensors and Actuators B* **193** (2014) 574-581.

Knake, R., P. Jacquinot, and P. C. Hauser. "Amperometric Detection of Gaseous Formaldehyde in the ppb Range" *Electroanalysis* **13**, 8 (2001) 631-634.

Kolla, H. S., S. P. Surwade, X. Zhang, A. G. MacDiarmid, and S. K. Manohar. "Absolute Molecular Weight of Polyaniline" *Journal of the American Chemical Society* **127** (2005) 16770-16771.

Konwer, S., A. K. Guha, and S. K. Dolui. "Graphene Oxide-filled Conducting Polyaniline nanocomposites as Methanol-sensing Materials" *Journal of Material Science* **48** (2013) 1729-1739.

Korotcenkov, G. *Handbook of Gas Sensor Materials. Properties, Advantages and Shortcomings for Applications Volume 1: Conventional Approaches*. Springer, New York, USA, 2013.

Kukla, A. L., Y. M. Shirshov, and S. A. Piletsky. "Ammonia Sensors based on Sensitive Polyaniline Films" *Sensors and Actuators B* **37** (1996) 135-140.

Kuleyin, A. "Removal of Phenol and 4-chlorophenol by Surfactant-modified Natural Zeolite" *Journal of Hazardous Materials* **144** (2007) 307-315.

Lee, S. C., M. Y. Chiu, K. F. Ho, S. C. Zou, and X. Wang. "Volatile Organic Compounds (VOCs) in Urban Atmosphere of Hong Kong" *Chemosphere* **48**, 3 (2002) 375-382.

Lee, C.-Y., P.-R. Hsieh, C.-H. Lin, P.-C. Chou, L.-M. Fu, and C.-M. Chiang. "MEMS-based Formaldehyde Gas Sensor Integrated with a Micro-hotplate" *Microsystems Technology* **12** (2006) 893-898.

Lee, C.-Y., C.-M. Chiang, Y.-H. Wang, and R.-H. Ma. "A Self-heating Gas Sensor with Integrated NiO Thin-film for Formaldehyde Detection" *Sensors and Actuators B* **122** (2007) 503-510.

Lee, Y.-I., K.-J. Lee, D.-H. Lee, Y.-K. Jeong, H. S. Lee, and Y.-H. Choa. "Preparation and Gas Sensitivity of SnO<sub>2</sub> Nanopowder Homogeneously Doped with Pt Nanoparticles" *Current Applied Physics* **9** (2009) 579-581.

Lee, S.-W., N. Takahara, S. Korposh, D.-H. Yang, K. Toko, and T. Kunitake. "Nanoassembled Thin Film Gas Sensors. III. Sensitive Detection of Amine Odors Using TiO<sub>2</sub>/Poly (acrylic acid) Ultrathin Film Quartz Crystal Microbalance Sensors" *Analytical Chemistry* **82**, 6 (2010) 2228-2236.

Lee, I., S.-J. Choi, K.-M. Park, S. S. Lee, S. Cho, I.-D. Kim, and C. O. Park. "The Stability, Sensitivity and Response Transients of ZnO, SnO<sub>2</sub> and WO<sub>3</sub> Sensors under Acetone, Toluene and H<sub>2</sub>S Environments" *Sensors and Actuators B* **197** (2014) 300-307.

Lefferts, L., J. G. van Ommen, and J. R. H. Ross. "The Oxidative Dehydrogenation of Methanol to Formaldehyde over Silver Catalysts in Relation to the Oxygen-silver Interaction" *Applied Catalysis* **23** (1986) 385-402.

Li, G., C. Martinez, and S. Semancik. "Controlled Electrophoretic Patterning of Polyaniline from a Colloidal Solution" *Journal of the American Chemical Society* **127** (2005) 4903-4909.

Li, B., S. Santhanam, L. Schultz, M. Jefferies-EL, M. C. Iovu, G. Sauvé, J. Cooper, R. Zhang, J. C. Revelli, A. G. Kusne, J. L. Snyder, T. Kowalewski, L. E. Weiss, R. D. McCullough, G. K. Fedder, and D. N. Lambeth. "Inkjet Printed Chemical Sensor Array Based on Polythiophene Conductive Polymers" *Sensors and Actuators B* **123** (2007) 651-660.

Li, W., N. D. Hoa, Y. Cho, D. Kim, and J.-S. Kim. "Nanofibers of Conducting Polyaniline for Aromatic Organic Compound Sensors" *Sensors and Actuators B* **143** (2009) 132-138.

Li, B., J. Liu, G. Shi, and J. Liu. "A Research on Detection and Identification of Volatile Organic Compounds Utilizing Cataluminescence-based Sensor Array" *Sensors and Actuators B* **177** (2013a) 1167-1172.

Li, X. B., S. Y. Ma, F. M. Li, Y. Chen, Q. Q. Zhang, X. H. Yang, C. Y. Wang, and J. Zhu. "Porous Spheres-like ZnO Nanostructure as Sensitive Gas Sensors for Acetone Detection" *Materials Letters* **100** (2013b) 119-123.

Li, Z. "Template-free Fabrication of NiO Nanobelts: Promising Candidate for Ethanol Gas Sensor at Room Temperature" *Microelectronics International* **33**, 2 (2016).

Liewhiran, C., A. Camenzind, A. Teleki, S. E. Pratsinis, and S. Phanichphant. "High Performance Ethanol Sensor for Control Drunken Driving Based on Flame-made ZnO Nanoparticles" *Proceedings of the 2<sup>nd</sup> IEEE International Conference on Nano/Micro Engineered and Molecular Systems*, January 16-19, 2007, Bangkok, Thailand.

Lin, C. W., Y. L. Liu, and R. Thangamuthu. "Investigation of the Relationship between Surface Thermodynamics of the Chemically Synthesized Polypyrrole Films and their Gas-sensing Responses to BTEX Compounds" *Sensors and Actuators B* **94** (2003) 36-45.

Lin, Y., Y. Wang, W. Wei, L. Zhu, S. Wen, and S. Ruan. "Synergistically Improved Formaldehyde Gas Sensing Properties of SnO<sub>2</sub> Microspheres by Indium and Palladium Co-doping" *Ceramics International* **41**, 6 (2015) 7329-7336.

Liu, Y., J. Dong, P. J. Hesketh, and M. Liu. "Synthesis and Gas Sensing Properties of ZnO Single Crystal Flakes" *Journal of Materials Chemistry* **15** (2005a) 2316-2320.

Liu, J., X. Wang, Q. Peng, and Y. Li. "Vanadium Pentoxide Nanobelts: Highly Selective and Stable Ethanol Sensor Materials" *Advanced Materials* **17**, 6 (2005b) 764-767.

Liu, M. (2010) *Synthesis of ZnO Nanowires and Applications as Gas Sensors*. PhD Thesis, University of Saskatchewan.

Liu, L., S. Li, L. Wang, C. Guo, Q. Dong, and W. Li. "Enhancement Ethanol Sensing Properties of NiO-SnO<sub>2</sub> Nanofibers" *Journal of the American Ceramic Society* **94**, 3 (2011a) 771-775.

Liu, L., S. Li, J. Zhang, L. Wang, J. Zhang, H. Li, Z. Liu, Y. Han, X. Jiang, and P. Zheng. "Improved Selective Acetone Sensing Properties of Co-doped ZnO Nanofibers by Electrospinning" *Sensors and Actuators B* **155** (2011b) 782-788.

Lou, Z., L. Wang, T. Fei, and T. Zhang. "Enhanced Ethanol Sensing Properties of NiO-doped SnO<sub>2</sub> Polyhedra" *New Journal of Chemistry* **36** (2012) 1003-1007.

Lv, P., Z. Tang, G. Wei, J. Yu, and Z. Huang. "Recognizing Indoor Formaldehyde Binary Gas Mixtures with a Micro Gas Sensor Array and a Neutral Network" *Measurement Science and Technology* **18** (2007) 2997-3004.

Mabrook, M. And P. Hawkins. "A Rapidly-responding Sensor for Benzene, Methanol, and Ethanol Vapours Based on Films of Titanium Dioxide Dispersed in a Polymer Operating at Room Temperature" *Sensors and Actuators B* **75** (2001) 197-202.

Mabrook, M. F., C. Pearson, and M. C. Petty. "Inkjet-printed Polypyrrole Thin Films for Vapour Sensing" *Sensors and Actuators B* **115** (2006) 547-551.

Maiti, S. K., K. M. Abdul Malik, R. Bhattacharyya. "Oxoperoxo-molybdenum and -Tungsten (VI) Complexes: Their Synthesis, Structure and Catalytic Uses in the Peroxidic Oxidation of Alcohols to Aldehydes and Ketones" *Inorganic Chemistry Communications* **7** (2004) 823-828.

Mani, G. K., and J. B. B. Rayappan. "ZnO Nanoarchitectures: Ultrahigh Sensitive Room Temperature Acetaldehyde Sensor" *Sensors and Actuators B* **223** (2016) 343-351.

Matsugushi, M., J. Io, G. Sugiyama, and Y. Sakai. "Effect of NH<sub>3</sub> Gas on the Electrical Conductivity of Polyaniline Blend Films" *Synthetic Metals* **128** (2002) 15-19.

Matsuguchi, M., K. Asahara, and T. Mizukami. "Highly Sensitive Toluene Vapor Sensors Using Carbon Black/Amino-Functional Copolymer nanocomposites" *Journal of Applied Polymer Science* **127**, 4 (2013) 2529-2535.

Meng, Q., T. Han, G. Wang, N. Zheng, C. Cao, and S. Xie. "Preparation of a Natural Dye Dosed Ormosil Coating for the Detection of Formaldehyde in the Optical Gas Sensor" *Sensors and Actuators B* **196** (2014) 238-244.

Miekisch, W., J. K. Schubert, and G. F. E. Noeldge-Schomburg. "Diagnosis Potential of Breath Analysis- Focus on Volatile Organic Compounds" *Clinica Chimica Acta* **347** (2004) 25-39.

Miller, L. L., R. G. Dunn, D. C. Tully, and D. A. Tomalia. "Electrically Conducting Dendrimers" *Journal of the American Chemical Society* **119** (1997) 1005-1010.

Mitsubayashi, K., K. Yokoyama, T. Takeuchi, and I. Karube. "Gas-Phase Biosensor for Ethanol" *Analytical Chemistry* **66** (1994) 3297-3302.

Mitsubayashi, K. and Y. Hashimoto. "Bioelectronic Sniffer Device for Trimethylamine Vapour using Flavin Containing Monooxygenase" *IEEE Sensors Journal* **2**, 3 (2002) 133-139.

Mitsubayashi, K., H. Amagai, H. Watanabe, and Y. Nakayama. "Bioelectronic Sniffer with a Diaphragm Flow-cell for Acetaldehyde Vapour" *Sensors and Actuators B* **95** (2003) 303-308.



Mlsna, T. E., S. Cemalovic, M. Warburton, S. T. Hobson, D. A. Mlsna, and S. V. Patel. "Chemicapacitive Microsensors for Chemical Warfare Agent and Toxic Industrial Chemical Detection" *Sensors and Actuators B* **116** (2006) 192-201.

Mochalski, P., J. King, K. Unterkofler, H. Hinterhuber, and A. Amann. "Emission Rates of Selected Volatile Organic Compounds from Skin of Healthy Volunteers" *Journal of Chromatography B* **959** (2014) 62-70.

Mondin, A., D. Badocco, and P. Pastore. "Use of Silver/Octadecanethiol Coating and a Reference-gas Correction Algorithm to Minimize the Water Effect in Determining Oxygen with a Light Emission Based Optical Sensor" *Sensors and Actuators B* **190** (2014) 775-781.

Mu, S., C. Chen, and J. Wang. "The Kinetic Behaviour for the Electrochemical Polymerization of Aniline in Aqueous Solution" *Synthetic Metals* **88** (1997) 249-254.

Mu, H., Z. Zhang, X. Zhao, F. Liu, K. Wang, and H. Xie. "High Sensitive Formaldehyde Graphene Gas Sensor Modified by Atomic Layer Deposition Zinc Oxide Films" *Applied Physics Letters* **105** (2014) 033107 doi: 10.1063/1.4890583.

Muthukrishnan, K., M. Vanaraja, S. Boomadevi, R. K. Karn, J. B. B. Rayappan, V. Singh, and K. Pandiyan. "Highly Selective Acetaldehyde Sensor using Sol-gel Dip Coated Nano Crystalline TiO<sub>2</sub> Thin Film" *Journal of Materials Science: Materials in Electronics* **26**, 7 (2015) 5135-5139.

Mwakikunga, B. Wa., M. Mokwena, J. Dewar, S. S. Ray, I. Geibelhaus, T. Singh, T. Fischer, and S. Mathur. "Tin dioxide Nano-wire Device for Sensing Kinetics of Acetone and Ethanol towards Diabetes Monitoring" *Proceedings at 2013 IEEE Sensors*, November 2013, p. 1-4.

Na, C. W., H.-S. Woo, J.-H. Lee. "Design of Highly Sensitive Volatile Organic Compound Sensors by Controlling NiO Loading on ZnO Nanowire Networks" *RSC Advances* **2** (2012) 414-417.

Nagomi, M., T. Maeda, and T. Uma. "A Methanol Gas Sensor based on Inorganic Glass Thin Films" *Sensors and Actuators B* **137** (2009) 603-607.

Nair, P. R. and M. A. Alam. "Design Considerations of Silicon Nanowire Biosensors" *IEEE Transactions on Electron Devices* **54**, 12 (2007) 3400-3408.

Natile M. M. and A. Glisenti. "Surface Reactivity of NiO: Interaction with Methanol" *Chemical Materials* **14** (2002) 4895-4903.

- Nehete, K., R. A. Sharma, L. Chaudhari, S. Bhattacharya, V. Singal, and D. D'Melo. "Study of Erosion Resistance and Mechanical Properties of Unsaturated Polyester based Nano-composites" *IEEE Transactions on Dielectrics and Electrical Insulation* **19**, 2 (2012) 373-382.
- Nguyen, V. Q., A. M. Vu, V. L. Nguyen, N. H. Vu, and V. H. Nguyen. "Gas Sensing Properties at Room Temperature of Quartz Crystal Microbalance Coated with ZnO Nanorods" *Sensors and Actuators B* **153** (2011) 188-193.
- Nguyen, D. K., D. T. Do, V. D. Nguyen, D. H. Nguyen, and V. H. Nguyen. "Design of SnO<sub>2</sub>/ZnO Hierarchical Nanostructures for Enhanced Ethanol Gas-sensing Performance" *Sensors and Actuators B* **174** (2012) 594-601.
- Nicolas-Debarnot, D. and F. Poncin-Epaillard. "Polyaniline as a New Sensitive Layer for Gas Sensors" *Analytica Chimica Acta* **475** (2003) 1-15.
- Nolan, E. M., M. E. Racine, and S. J. Lippard. "Selective Hg(II) Detection in Aqueous Solution with Thiol Derivatized Fluoresceins" *Inorganic Chemistry* **45** (2006) 2742-2749.
- Okabayashi, T., T. Fujimoto, I. Yamamoto, K. Utsunomiya, T. Wada, Y. Yamashita, N. Yamashita, and M. Nakagawa. "High Sensitive Hydrocarbon Gas Sensor Utilizing Cataluminescence of  $\gamma$ -Al<sub>2</sub>O<sub>3</sub> Activated with Dy<sup>3+</sup>" *Sensors and Actuators B* **64** (2000) 54-58.
- Palaniappan, S. and C. Saravanan. "Polyaniline-maleicacid-dodecylhydrogensulfate salt as Sensor Material for Toxic Gases" *Journal of Applied Polymer Science* **118** (2010) 518-524.
- Panchal, J. N., S. G. Patel, and V. S. Vaishnav. "Room Temperature Detection of Benzene Vapours by Tin Oxide Nano Clusters" *Sensors and transducers* **190**, 7 (2015) 35-39.
- Pandey, G. and E. T. Thostenson. "Carbon Nanotubes-based Multifunctional Polymer Nanocomposites" *Sensors and Actuators B* **52**, 3 (2012) 355-416.
- Papadopoulos, C. A., D. S. Vlachos, and J. N. Avaritsiotis. "Comparative Study of Various Metal-oxide-based Gas-sensor Architectures" *Sensors and Actuators B* **32** (1996) 61-69.
- Park, H. J., N.-J. Choi, H. Kang, M. Y. Jung, J. W. Park, K. H. Park, and D.-S Lee. "A ppb-level Formaldehyde Gas Sensor based on CuO Nanotubes Prepared using a Polyol Process" *Sensors and Actuators B* **203** (2014) 282-288.
- Parmar, M., C. Balamurugan, and D.-W. Lee. "PANI and Graphene/PANI Nanocomposite Films-Comparative Toluene Gas sensing Behaviour" *Sensors* **13**, 12 (2013) 16611-16624.

Patel, N. G., P. D. Patel, V. S. Vaishnav. "Indium Tin Oxide (ITO) Thin Film Gas Sensor for Detection of Methanol at Room Temperature" *Sensors and Actuators B* **96** (2003) 180-189.

Patil, D. R., L. A. Patil, and D. P. Amalnerkar. "Ethanol Gas Sensing Properties of Al<sub>2</sub>O<sub>3</sub>-doped ZnO Thick Film Resistors" *Bulletin of Material Science* **30**, 6 (2007) 553-559.

Phillips, M. "Method for the Collection and Assay of Volatile Organic Compounds in Breath" *Analytical Biochemistry* **247** (1997) 272-278.

Pich, A., Y. Li, V. Boyko, S. Richter, K.-F. Arndt, and H.-J. P. Adler. "Thermo-sensitive Poly(*N*-vinylcaprolactam-co-acetoacetoxyethylmethacrylate) Microgels. 3. Incorporation of Polypyrrole by Selective Microgel Swelling in Ethanol-water Mixtures" *Polymer* **45** (2004) 1079-1087.

Pourfayaz, F., A. Khodadadi, Y. Mortazavi, and S. S. Mohajerzadeh. "CeO<sub>2</sub> doped SnO<sub>2</sub> Sensor Selective to Ethanol in Presence of CO, LPG, and CH<sub>4</sub>" *Sensors and Actuators B* **108** (2005) 172-176.

Puskas, J. E., Y. Kwon, V. Altstädt, and M. Kontopoulou. "Blends of Poly (2,6-dimethyl-1,4-phenylene oxide) (PPO) with Polystyrene-based Thermoplastic Rubbers: A Comparative Study" *Polymer* **48** (2007) 590-597.

Putzbach, W. and N. J. Ronkainen. "Immobilization Techniques in the Fabrication of Nanomaterial-based Electrochemical Biosensors: A Review" *Sensors* **13**, 4 (2013) 4811-4840.

Qi, Q., T. Zhang, L. Liu, X. Zheng, Q. Yu, Y. Zeng, and H. Yang. "Selective Acetone Sensor Based on Dumbbell-like ZnO with Rapid Response and Recovery" *Sensors and Actuators B* **134** (2008) 166-170.

Rahman, M. M., A. Khan, and A. M. Asiri. "Chemical Sensor Development Based on Poly (*o*-anisidine) Silverized-MWCNT Nanocomposites Deposited on Glassy Carbon Electrodes for Environmental Remediation" *RCS Advances* **5** (2015) 71370-71378.

Raksa, P., A. Gardchareon, T. Chairuang Sri, P. Mangkorntong, N. Mangkorntong, and S. Choopun. "Ethanol Sensing Properties of CuO Nanowires Prepared by an Oxidation Reaction" *Ceramics International* **35**, 2 (2009) 649-652.

Ramamurthy, P. C., A. N. Mallaya, A. Joseph, W. R. Harrell, and R. V. Gregory. "Synthesis and Characterization of High Molecular Weight Polyaniline for Organic Electronic Applications" *Polymer Engineering and Science* (2012) doi:10.1002/pen.23096.

Rao, B. B. "Zinc Oxide Semi-conductor Gas Sensor for Ethanol Vapour" *Materials Chemistry and Physics* **64** (2000) 62-65.

Rawat, N. K., A. K. Sinha, and S. Ahmad. "Conducting Poly (*o*-anisidine-*co*-*o*-phenyldiammine) Nanorod Dispersed Epoxy nanocomposite Coatings: Synthesis, Characterization and Corrosion Protective Performance" *RCS Advances* **5** (2015) 94933-94948.

Rezlescu, N., N. Iftimie, E. Rezlescu, C. Doroftei, and P. D. Popa. "Semiconducting Gas Sensor for Acetone Based on the Fine Grained Nickel Ferrite" *Sensors and Actuators B* **114** (2006) 427-432.

Righettoni, M., A. Tricoli, and S. E. Pratsinis. "Si:WO<sub>3</sub> Sensors for Highly Selective Detection of Acetone for Easy Diagnosis of Diabetes by Breath Analysis" *Analytical Chemistry* **82**, 9 (2010) 3581-3587.

Righettoni, M., A. Amann, and S. E. Pratsinis. "Breath Analysis by Nanostructured Metal Oxides as Chemo-resistive Gas Sensors" *Materials Today* **18**, 3 (2015) 163-171.

Rochat, S. and T. M. Swager. "Conjugated Amplifying Polymers for Optical Sensing Applications" *ACS Applied Materials and Interfaces* **5** (2013) 4488-4502.

Ruangchuay, L., A. Sirivat, and J. Schwank. "Polypyrrole/poly(methylmethacrylate) blend as selective sensor for acetone in lacquer" *Talanta* **60** (2003) 25-30.

Ruchika, V. K. and, S. C. Sood, G. S. Viridi. "Fabrication and Characterization of Zinc Oxide Based Thick and Thin Film Ethanol Sensors Doped with Aluminum Oxide" *International Journal of Applied Sciences and Engineering Research* **5**, 1 (2016) 81-89.

Rushi, A. D., K. P. Datta, P. S. Ghosh, A. Mulchandani, and M. D. Shirsat. "Selective Discrimination among Benzene, Toluene, and Xylene: Probing Metalloporphyrin-functionalized Single-walled Carbon Nanotube-based Field Effect Transistors" *Journal of Physical Chemistry C* **118** (2014) 24034-24041.

Ruzsanyi, V., P. Mochalski, A. Schmid, H. Wiesenhofer, M. Klieber, H. Hinterhuber, and A. Amann. "Ion Mobility Spectrometry for Detection of Skin Volatiles" *Journal of Chromatography B* **911** (2012) 84-92.

Safavi, A., N. Maleki, F. Farjami, and E. Farjami. "Electrochemical Oxidation of Formaldehyde on Palladium Nanoparticles Electrodeposited on Carbon Ionic Liquid nanocomposite Electrode" *Journal of Electroanalytical Chemistry* **626** (2009) 75-79.

Sahay, P. P. "Zinc Oxide Thin Film Gas Sensor for Detection of Acetone" *Journal of Materials Science* **40** (2005) 4383-4385.

Sahay, P. P., S. Tewari, S. Jha, and M. Shamsuddin. "Sprayed ZnO Thin Films for Ethanol Sensors" *Journal of Materials Science* **49** (2005) 4791-4793.

Sapurina, I. Y. and M. A. Shishov. "Oxidative Polymerization of Aniline: Molecular Synthesis of Polyaniline and the Formation of Supramolecular Structures" (2012) doi:10.5772/48758.

Sapurina, I. and J. Steskal. "The Mechanism of the Oxidative Polymerization of Aniline and the Formation of Supramolecular Polyaniline Structures" *Polymer International* **57** (2008) 1295-1325.

Sarkar, T., S. Srinives, S. Sarkar, R. C. Haddon, and A. Mulchandani. "Single-walled Carbon Nanotube-Poly (porphyrin) Hybrid for Volatile Organic Compound Detection" *Journal of Physical Chemistry C* **118** (2014) 1602-1610.

Sawyer, B. D. and P. A. Hancock. "An Evaluation of Drivers using an Ignition Interlock Device: Breath Tests while Driving" *Proceedings of the Human Factors and Ergonomics Society 58<sup>th</sup> Annual Meeting* (2014) 2098-2101.

Scott, A. J. and A. Penlidis. "Nitrile Rubber Reactor Operation Troubleshooting with Principal Component Analysis" *Journal of Macromolecular Science, Part A: Pure and Applied Chemistry* **50**, 8 (2013) 803-811.

Shacklette, L. W. and C. C. Han. "Solubility and Dispersion Characteristics of Polyaniline" *MRS Proceedings* **328** (1993) 157.

Shacklette, L. W. "Dipole and Hydrogen-bonding Interactions in Polyaniline: A Mechanism for Conductivity Enhancement" *Synthetic Metals* **65** (1994) 123-130.

Shahbazi, H., M. Reyhanian, V. Hosseini, and H. Afshin. "The Relative Contributions of Mobile Sources to Air Pollutant Emissions in Tehran, Iran: An Emission Inventory Approach" *Emission Control Science and Technology* **2** (2016) 44-56.

Shan, H., C. Liu, L. Liu, S. Li, L. Wang, X. Zhang, X. Bo, and X. Chi. "Highly Sensitive Acetone Sensors based on La-doped  $\alpha$ -Fe<sub>2</sub>O<sub>3</sub> Nanotubes" *Sensors and Actuators B* **184** (2013) 243-247.

Shen, R. S., X. P. Li, X. C. Xia, H. W. Liang, G. G. Wu, Y. Liu, C. H. Cheng, and G. T. Du. "Comparative Investigation of Three Types of Ethanol Sensor Based on NiO-SnO<sub>2</sub> nanocomposite Nanofibers" *Chinese Science Bulletin* **57**, 17 (2012) 2087-2093.

Shim, Y.-B. and S.-M. Park. "Electrochemistry of Conductive Polymers VII. Autocatalytic Rate Constant for Polyaniline Growth" *Synthetic Metals* **29** (1989) E169-E174.

Shinde, S. D., G. E. Patil, D. D. Kajale, V. B. Gaikwad, and G. H. Jain. "Synthesis of ZnO Nanorods by Spray Pyrolysis for H<sub>2</sub>S Gas Sensor" *Journal of Alloys and Compounds* **528**, 5 (2012) 109-114.

Shirasu, M. and K. Touhara. "The Scent of Disease: Volatile Organic Compounds of the Human Body Related to Disease and Disorder" *Journal of Biochemistry* **150**, 3 (2011) 257-266.

Simplicio, L. M. T., S. T. Brandão, E. A. Sales, L. Lietti, F. Bozon-Verduraz. "Methane Combustion over PdO-alumina Catalysts: The Effect of Palladium Precursors" *Applied Catalysis B* **63**, 1 (2006) 9-14.

Singh, R. C., O. Singh, M. P. Singh, and P. S. Chandi. "Synthesis of Zinc Oxide Nanorods and Nanoparticles by Chemical Route and their Comparative Study as Ethanol Sensors" *Sensors and Actuators B* **135** (2008) 352-357.

Singh, S., H. Haur, V. N. Singh, K. Jain, and T. D. Senguttuvan. "Highly Sensitive and Pulse-like Response towards Ethanol of Nbdoped TiO<sub>2</sub> Nanorods based Gas Sensors" *sensors and Actuators B* **171** (2012) 899-906.

Slater, J. M., J. Paynter, and E. J. Watt. "Multi-layer Conducting Polymer Gas Sensor Arrays for Olfactory Sensing" *Analyst* **118** (1993) 379-384.

Smith, K. *Biofuels, Air Pollution, and Health: A Global Review*. Plenum Press, New York, USA, 1987.

Soini, H. A., K. E. Bruce, I. Klouckova, R. G. Brereton, D. J. Penn, and M. V. Novotny. "In Situ Surface Sampling of Biological Objects and Preconcentration of their Volatiles for Chromatographic Analysis" *Analytical Chemistry* **78**, 20 (2006) 7161-7168.

Solomon, R., J. Cardy, I. Noble, and R. Wulkan. *The 2012 Provincial and Territorial Legislative Review, MADD*, March 31, 2012.

Stambolova, I., K. Konstantinov, S. Vassilev, P. Peshev, and T. Tsacheva. "Lanthanum doped SnO<sub>2</sub> and ZnO Thin Films Sensitive to Ethanol and Humidity" *Materials Chemistry and Physics* **63** (2000) 104-108.

Steiskal, J. and R. G. Gilbert. "Polyaniline. Preparation of a Conducting Polymer" (IUPAC Technical Report) *Pure and Applied Chemistry* **74**, 5 (2002) 857-867.

Stewart, K. M. E., N. T. McManus, E. Abdel-Rahman, and A. Penlidis. "Doped Polyaniline for the Detection of Formaldehyde" *Journal of Macromolecular Science, Part A* **49**, 1 (2012) 1-6.

Stewart, K. M. E. and A. Penlidis. "Novel Test System for Gas Sensing Materials and Sensors" *Macromolecular Symposia* **324** (2013) 11-18.

Stewart, K. M. E., W. T. Chen, R. R. Mansour, and A. Penlidis. "Doped Poly (2,5-dimethyl aniline) for the Detection of Ethanol" *Journal of Applied Polymer Science* **132** (2015) 42259-42264.

Stewart, K. M. E. and A. Penlidis. "Designing Polymeric Sensing Materials for the Detection of Ethanol" *Macromolecular Symposia* **360** (2016a) 123-132.

Stewart, K. M. E. and A. Penlidis. "Evaluation of Polymeric Nanocomposites for the Detection of Toxic Gas Analytes" *Journal of Macromolecular Science, Part A Pure and Applied Chemistry* **53**, 10 (2016b) 610-618.

Stewart, K. M. E. and A. Penlidis. "Designing Polymeric Sensing Materials: What are we doing Wrong?" *Polymers for Advanced Technologies* **133**, 42 (2016c) doi:10.1002/pat.3893.

Suematsu, K., Y. Shin, Z. Hua, K. Yoshida, M. Yuasa, T. Kida, and K. Shimanoe. "Nanoparticle Cluster Gas Sensor: Controlled Clustering of SnO<sub>2</sub> Nanoparticles for Highly Sensitive Toluene Detection" *Applied Materials and Interfaces* **6** (2014) 5319-5326.

Sullivan, A. "Ending Drunk Driving with a Flash of Light" *Richmond Journal of Law and Technology* **21**, 4 (2015).

Sun, P., Y. Jiang, G. Xie, X. Du, and J. Hu. "A Room Temperature Supramolecular-based Quartz Crystal Microbalance (QCM) Methane Gas Sensor" *Sensors and Actuators B* **141** (2009) 104-108.

Sun, Y.-F., S.-B. Liu, F.-L. Meng, J.-Y. Liu, Z. Jin, L.-T. Kong, and J.-H. Liu. "Metal Oxide Nanostructures and Their Gas Sensing Properties: A Review" *Sensors* **12**, 3 (2012) 2610-2631.

Surwade, S. P., S. R. Agnihotra, V. Dua, H. S. Kolla, X. Zhang, and S. K. Manohar. "Chromism and Molecular Weight of Polyaniline Derivatives" *Synthetic Metals* **159** (2009) 2153-2156.

Svetlicic, V., A. J. Schmidt, and L. L. Miller. "Conductometric Sensors Based on the Hypersensitive Response of Plasticized Polyaniline Films to Organic Vapours" *Chemistry of Materials* **10** (1998) 3305-3307.

Talwar, V., O. Singh, and R. C. Singh. "ZnO Assisted Polyaniline Nanofibers and its Application as Ammonia Gas Sensor" *Sensors and Actuators B* **191** (2014) 276-282.

Tan, C. K. and D. J. Blackwood. "Interactions between Polyaniline and Methanol Vapour" *Sensors and Actuators B* **71** (2000) 184-191.

Tang, H., K. Prasad, R. Sanjinés, and F. Lévy. "TiO<sub>2</sub> Anatase Thin Film as Gas Sensors" *Sensors and Actuators B* **26** (1995) 71-75.

Tang, L., Y. Li, K. Xu, X. Hou, and Y. Li. "Sensitive and Selective Acetone Sensor Based on its Cataluminescence from Nano-LaO<sub>2</sub> Surface" *Sensors and Actuators B* **132** (2008) 243-249.

Tavoli, F. and N. Alizadeh. "Optical Ammonia Gas Sensor Based on Nanostructure Dye-doped Polypyrrole" *Sensors and Actuators B* **176** (2013) 761-767.

Thompson, R. B., V. V. Ginzburg, M. W. Matsen, and A. C. Balazs. "Predicting the Mesophases of Copolymer-Nanoparticle Composites" *Science* **292**, 5526 (2001) 2469-2472.

Ulmann, M., R. Kostecki, J. Augustynski, D. J. Strike, and M. Koudelka-Hep. "Modification des Polymères Conducteurs avec de Petites Particules Métalliques; Propriétés des Films de Polypyrrole et de Polyaniline Platinés" *Chimia* **46** (1992) 138-140.

Vaddiraju, S. and K. K. Gleason. "Selective Sensing of Volatile Organic Compounds using Novel Conducting Poly-metal Nanoparticle Hybrids" *Nanotechnology* **21** (2010) 125503-125511.

Valentini, L., V. Bavastrello, E. Stura, I. Armentano, C. Nicolini, and J. M. Kenny. "Sensors for Inorganic Vapour Detection Based on Carbon Nanotubes and Poly (*o*-anisidine) Nanocomposite Material" *Chemical Physical Letters* **383** (2004) 617-622.

Velusamy, S., M. Ahamed, and T. Punniyamurthy. "Novel Polyaniline-supported Molybdenum-catalyzed Aerobic Oxidation of Alcohols to Aldehydes and Ketones" *Organic Letters* **6**, 26 (2004) 4821-4824.

Venditti, I. I. Fratoddi, M. V. Russo, and A. Bearzotti. "A Nanostructured nanocomposite based on Polyaniline and Gold Nanoparticles: Synthesis and Gas Sensing Properties" *Nanotechnology* **24** (2013) 155503-155509.



Vercelli, B., S. Zecchin, N. Comisso, G. Zotti, A. Berlin, E. Dalcanale, and L. Groenendaal. "Solvoconductivity of Polyconjugated Polymers: The Role of Polymer Oxidation Degree and Solvent Electrical Permittivity" *Chemistry of Materials* **14** (2002) 4768-4774.

Virji, S., J. Huang, R. B. Kaner, and B. H. Weiller. "Polyaniline Nanofiber Gas Sensors: Examination of Response Mechanisms" *Nano Letters* **4**, 3 (2004) 491-496.

Wan, Q., Q. H. Li, Y. J. Chen, T. H. Wang, and X. L. He. "Fabrication and Ethanol Sensing Characteristics of ZnO Nanowire Gas Sensors" *Applied Physics Letters* **84** (2004) 3654-3656.

Wang, J., M. Ichiro, N. Murayama, S. Woosuck, and N. Izu. "The Preparation of Polyaniline Intercalated MoO<sub>3</sub> Thin Films and its Sensitivity to Volatile Organic Compounds" *Thin Film Solids* **514** (2006) 329-333.

Wang, Y.-H., C.-Y. Lee, C.-H. Lin, and L.-M. Fu. "Enhanced Sensing Characteristics on MEMS-based Formaldehyde Gas Sensors" *Microsystems Technology* **14** (2008) 995-1000.

Wang, J., B. Zou, S. Ruan, J. Zhao, F. Wu. "Synthesis, Characterization, and Gas-sensing Property for HCHO of Ag-doped In<sub>2</sub>O<sub>3</sub> Nanocrystalline Powders" *Materials Chemistry and Physics* **117** (2009a) 489-493.

Wang, J., P. Zeng, J.-Q. Qi, and P.-J. Yao. "Silicon-based Micro-gas Sensors for Detecting Formaldehyde" *Sensors and Actuators B* **136** (2009b) 399-404.

Wang, C., L. Yin, L. Zhang, Y. Qi, N. Lun, and N. Liu. "Large Scale Synthesis and Gas-sensing Properties of Anatase TiO<sub>2</sub> Three Dimensional Hierarchical Nanostructures" *Langmuir* **26**, 15 (2010a) 12841-12848.

Wang, X., B. Ding, M. Sun, J. Yu, and G. Sun. "Nanofibrous Polyethyleneimine Membranes as Sensitive Coatings for Quartz Crystal Microbalance-based Formaldehyde Sensors" *Sensors and Actuators B* **144** (2010b) 11-17.

Wang, L., Y. Kang, X. Liu, S. Zhang, W. Huang, and S. Wang. "ZnO Nanorod Gas sensor for Ethanol Detection" *Sensors and Actuators B* **162**, 1 (2012) 237-243.

Wang, H., Y. Wang, Z. Zhu, A. Sapi, K. An, G. Kennedy, W. D. Michalak, and G. A. Somorjai. "Influence of Size-Induced Oxidation State of Platinum Nanoparticles on Selectivity and Activity in Catalytic Methanol Oxidation in the Gas Phase" *Nano Letters* **13**, 6 (2013a) 2976-2979.

Wang, L., S. Wang, M. Xu, X. Hu, H. Zhang, Y. Wang, and W. Huang. "A Au-functionalized ZnO Nanowire Gas Sensor for Detection of Benzene and Toluene" *Physical Chemistry Chemical Physics* **15** (2013b) 17179-17186.

Webster, G. D. and H. C. Gabler. "Feasibility of Transdermal Ethanol Sensing for the Detection of Intoxicated Drivers" *Annual Proceedings of the Association of Advanced Automotive Medicine* **51** (2007) 449-464.

Wei, Y., X. Tang, and Y. Sun. "A Study of the Mechanism of Aniline Polymerization" *Journal of Polymer Science Part A: Pure and Applied Chemistry* **27** (1989) 2385-2396.

WHO Regional Office for Europe WHO "Guidelines for Indoor Air Quality: Selected Pollutants" Copenhagen, Denmark, 2010.

Winther-Jensen, O., R. Kerr, and B. Winther-Jensen. "Alcohol Vapour Detection at the Three Phase Interface using Enzyme-Conducting Polymer nanocomposites" *Biosensors and Bioelectronics* **52** (2014) 143-146.

Wolkoff, P. "Indoor Air Pollutants in Office Environments: Assessment of Comfort, Health, and Performance" *International Journal of Hygiene and Environmental Health* **216**, 4 (2013) 371-394.

Xie, G., P. Sun, X. Yan, X. Du, and Y. Jiang. "Fabrication of Methane Gas Sensor by Layer-by-layer Self-assembly of Polyaniline/PdO Ultra Thin Films on Quartz Crystal Microbalance" *Sensors and Actuators B* **145** (2010) 373-377.

Xie, H., C. Sheng, X. Chen, X. Wang, Z. Li, and J. Zhou. "Multi-wall Carbon Nanotube Gas Sensor Modified with Amino-group to Detect Low Concentration of Formaldehyde" *Sensors and Actuators B* **168** (2012) 34-38.

Xing, R.-Q., L. Xu, Y.-S. Zhu, J. Song, W.-F. Qin, Q.-L. Dai, D.-L. Liu, and H.-W. Song. "Three-dimensional Ordered SnO<sub>2</sub> Inverse Opals for Superior Formaldehyde Gas-Sensing Performance" *Sensors and Actuators B* **188** (2013) 235-241.

Xiong, B., Y. Zhou, Y. Zhao, J. Wang, X. Chen, R. O'Hayre, and Z. Shao. "The Use of Nitrogen-doped Graphene Supporting Pt Nanoparticles as a Catalyst for Methanol Electrocatalytic Oxidation" *Carbon* **52** (2013) 181-192.

Xu, J., Q. Pan, Y. Shun, and Z. Tian. "Grain Size Control and Gas Sensing Properties of ZnO Gas Sensor" *Sensors and Actuators B* **66** (2000) 277-279.

Xu, J., Y. Chen, Y. Li, and J. Shen. "Gas Sensing Properties of ZnO Nanorods Prepared by Hydrothermal Method" *Journal of Material Science* **40** (2005) 2919-2921.

Yang, M., X. G. Zhang, and H. L. Li. "Differential-pulse Voltammetric Determination of Trace Formaldehyde using Magnetic Microspheres and Magnetic Electrode" *The Analyst* **126** (2001) 676-678.

Yang, D. and B. R. Mattes. "Polyaniline Emeraldine Base in *N*-methyl-2-pyrrolidinone Containing Secondary Amine Additives: A Rheological Investigation of Solutions" *Journal of Polymer Science B: Polymer Physics* **40**, 23 (2002) 2702-2713.

Yang, K., H. Sun, and P. Kurup. "Development and Calibration of a Portable Air Sampler" *Journal of Macromolecular Science, Part A: Pure and Applied Chemistry* **46** (2009a) 1233-1237.

Yang, Z., Y. Huang, G. Chen, Z. Guo, S. Cheng, and S. Huang. "Ethanol Gas Sensor Based on Al-doped ZnO Nanomaterial with Many Gas Diffusing Channels" *Sensors and Actuators B* **140**, 2 (2009b) 549-556.

Yebo, N. A., P. Lommens, Z. Hens, and R. Baets. "An integrated Optic Ethanol Vapour Sensor Based on a Silicon-on-insulator Microring Resonator Coated with a Porous ZnO Film" *Optics Express* **18**, 11 (2010) 11859-11866.

Yu, H., T. Cao, L. Zhou, E. Gu, D. Yu, and D. Jiang. "Layer-by-Layer Assembly and Humidity Sensitive Behaviour of Poly(ethyleneimine)/Multiwall Carbon Nanotube nanocomposite Films" *Sensors and Actuators B* **119**, 2 (2006) 512-515.

Yu, X. L., Y. Wang, H. L. W. Chan, and C. B. Cao. "Novel Gas Sensing Materials Based on CuS Hollow Spheres" *Microporous and Mesoporous Materials* **118** (2009) 423-426.

Zhan, Z., J. Lu, W. Song, D. Jiang, and J. Xu. "Highly Selective Ethanol In<sub>2</sub>O<sub>3</sub>-based Gas Sensor" *Materials Research Bulletin* **42** (2007) 228-235.

Zhan, S., D. Li, S. Liang, X. Chen, and X. Li. "A Novel Flexible Room Temperature Ethanol Gas Sensor Based on SnO<sub>2</sub> Doped Poly-diallyldimethylammonium Chloride" *Sensors* **13** (2013) 4378-4389.

Zhang, Z.-M., J.-J. Cai, G.-H. Ruan, and G.-K. Li. "The Study of Fingerprint Characteristics of the Emanations from Human Arm Skin using the Original Sampling System by SPME-GC/MS" *Journal of Chromatography B* **822** (2005) 244-252.

Zhang, J., J. Liu, Q. Peng, X. Wang, and Y. Li. "Nearly Monodisperse Cu<sub>2</sub>O and CuO Nanospheres: Preparation and Applications for Sensitive Gas Sensors" *Chemistry of Materials* **18** (2006) 867-871.

Zhang, Y., W. He, H. Zhao, and P. Li. "Template-free to Fabricate Highly Sensitive and Selective Acetone Gas Sensor based on WO<sub>3</sub> Microspheres" *Vacuum* **95** (2013) 30-34.

Zhang, Y., Q. Liu, J. Zhang, Q. Zhu, and Z. Zhu. "A Highly Sensitive and Selective Formaldehyde Gas Sensor Using a Molecular Imprinting Technique based on Ag-LaFeO<sub>3</sub>" *Journal of Materials Chemistry C* **2** (2014) 10067-10072.

Zhang, D., A. Liu, H. Chang, and B. Xia. "Room-temperature High Performance Acetone Gas sensor based on Hydrothermal Synthesized SnO<sub>2</sub>-reduced Graphene Oxide Hybrid Composite" *RSC Advances* **5** (2015) 3016-3022.

Zhang, J., P. Guan, W. Li, Z. Shi, and H. Zhai. "Synthesis and Characterization of a Polyaniline/Silver Nanocomposite for the Determination of Formaldehyde" *Instrumentation Science & Technology* **44**, 3 (2016) 249-258.

Zheng, J., G. Li, X. Ma, Y. Wang, G. Wu, and Y. Cheng. "Polyaniline–TiO<sub>2</sub> Nano-composite-based Trimethylamine QCM Sensor and its Thermal Behavior Studies" *Sensors and Actuators B* **133** (2008) 374–380.

Zheng, L., L. Wang, T. Fei, and T. Zhang. "Enhanced Ethanol Sensing Properties of NiO-doped SnO<sub>2</sub> Polyhedra" *New Journal of Chemistry* **36** (2012) 1003–1007.

Zhou, K., R. Wang, B. Xu, and Y. Li. "Synthesis, Characterization, and Catalytic Properties of CuO Nanocrystals with Various Shapes" *Nanotechnology* **17** (2006) 3939-3943.

Zhou, Z.-L., T.-F. Kang, Y. Zhang, and S.-Y. Cheng. "Electrochemical Sensor for Formaldehyde Based on Pt-Pd Nanoparticles and a Nafion-modified Glassy Carbon Electrode" *Microchimica Acta* **164** (2009) 133-138.

Zhou, K., C. Gu, D. Ma, and H. Cao. "Real-time Monitoring of Acetaldehyde in Air by Cataluminescence-based Gas Sensor" *Applied Mechanics and Materials* **268-270** (2013) 1594-1597.

Zhou, X., J. Liu, C. Weng, P. Sun, X. Hu, X. Li, K. Shimano, N. Yamazoe, and G. Lu. "Highly Sensitive Acetone Gas Sensor based on Porous ZnFe<sub>2</sub>O<sub>4</sub> Nanospheres" *Sensors and Actuators B* **206** (2015) 577-583.

Zhu, Y., J. Shi, Z. Zhang, C. Zhang, and X. Zhang. "Development of a Gas Sensor Utilizing Chemiluminescence on Nanosized Titanium Dioxide" *Analytical Chemistry* **74** (2002) 120-124.

Zhu, B. L., C. S. Xie, W. Y. Wang, K. J. Huang, and J. H. Hu. "Improvement in Gas Sensitivity of ZnO Thick Film to Volatile Organic Compounds (VOCs) by Adding TiO<sub>2</sub>" *Material Letters* **58**, 5 (2004) 624-629.

Zhu, Q., Y. M. Zhang, J. Zhang, Z. Q. Zhu, and Q. J. Liu. "A New and High Response Gas Sensor for Methanol using Molecularly Imprinted Technique" *Sensors and Actuators B* **207** (2015) 398-403.

Zou, R., G. He, K. Xu, Q. Liu, Z. Zhang, and J. Hu. "ZnO Nanorods on Reduced Graphene Sheets with Excellent Field Emission, Gas Sensor and Photocatalytic Properties" *Journal of Materials Chemistry A* **1** (2013) 8445-8452.

## Appendix A: Volatile Organic Compounds (VOCs) Emitted from the Human Body

Appendix A summarizes the VOCs that have been measured from a person in either the blood, breath, or off the skin (transdermally). This is a much more comprehensive list than that shown in Section 3.2. The concentration of each of these VOCs is also included, where possible (i.e. as reported in the literature).

Table A.1: Selected VOCs Emitted from the Human Body

Volatile Organic Compound (VOC)	In Blood (ppb)	In Breath	From Skin (ppb)
1,2-dichloroethane	0.028 a		
1,2-pentadiene		X j	
1,3-dichlorobenzene	0.079 a		
1-butanol			X h
1-hexadecanol			X c
1-methoxyhexane			X h
1-methyl hexyl acetate			X h
2-(2-propyl)-5-methyl-1-cyclohexanol (menthol)			X h
2-butanone	2.1 a		
2-pentanone		X j	
2-propanol		X g	
3-hexanol			X h
Acetaldehyde		X g	
Acetic acid			X h
Acetone (2-propanone)	520 a	X g,j	X h
Ammonia		Xg	X d
Benzaldehyde	X f		1.5 d X e,f,h,i
Benzene	0.094 a		

<b>Volatile Organic Compound (VOC)</b>	<b>In Blood (ppb)</b>	<b>In Breath</b>	<b>From Skin (ppb)</b>
Benzoic acid			X h
Benzyl Alcohol			X f
Carbon disulfide	11 a	X g	
Carbon tetrachloride	0.094 a		
Chlorobenzene	0.034 a	X j	
Chloroform	0.054 a		
Cyclohexanol			X e
Cyclopentadecane			X i
Decanal			4.7 d X c,f,h,i
Dimethylamine		X g	
Dimethylsulfide		X g,j	
Diphenyl ether			X i
Dodecanal			X h
Dodecane		X j	X f,i
Dodecanoic acid			X f,h
Ethane		X g	
Ethanol		X g	X d
Ethyl carbamate (urethane)			X h
Ethylbenzene	0.17 a		
Heptanal	X f	X f	X f
Hexadecane			X f,i
Hexanoic acid			X h
Isoprene		X b,g,j	
Lactic acid			X h

Volatile Organic Compound (VOC)	In Blood (ppb)	In Breath	From Skin (ppb)
<i>m/p</i> -xylene	0.23 a	X j	
Methanol		X g	
Methyl mercaptanes		X g	
Methyl salicylate			X i
Methylene chloride	0.069 a		
<i>n</i> -Butyl acetate			X d
Naphthalene			X f
Octanal			4.3 d X f,h,i
Octanoic acid			X h
Pentadecane			X i
Pentane		X b,g	
Phenol			X f,h
Propane-1,2,3-triol (glycerin)			X h
Propanoic acid			X h
Styrene	0.057 a		X e
Toluene	0.55 a X f		X f
Trichloroethene	0.057 a		
Triethylamine		X g	
Undecanal			X f
Undecane		X f	X f,i

*X denotes the compound is present, but has not been quantified.*



- a. Ashley et al. (1992)
- b. Jones et al. (1995)
- c. Soini et al. (2006)
- d. Ruzsanyi et al. (2012)
- e. Acevedo et al. (2007)
- f. Curran et al. (2005)
- g. Miekisch et al. (2004)
- h. Gallagher et al. (2008)
- i. Zhang et al. (2005)
- j. Phillips (1997)

## Appendix B: Sensing Materials for Volatile Organic Compounds

Appendix B contains multiple overview tables of different sensing materials used for various gas analytes (VOCs), briefly discussed in Section 2.4.5. These tables summarize what has been presented in the literature for both polymeric and inorganic (metal and metal oxide) sensing materials. The tables are divided by gas analyte and include the sensing material, any dopants, limit of detection (LoD), operational temperature, and response and recovery times. Note that not all of this data was present in some of the papers and the missing data is marked by a dash (-). In addition, estimated response and recovery times are preceded by a tilde (~).

Table B.1: Sensing Materials for Acetone

Sensing Material	Dopant	Detection Limit	Operational Temperature	Response Time	Recovery Time	Reference
Polyaniline	HCl	29 ppm	25 °C	1 minute	3 minutes	Do and Wang (2013)
Polypyrrole/ Poly (methyl methacrylate) (PPy/ PMMA)	$\alpha$ -naphthalene sulfonate ( $\alpha$ -NS <sup>-</sup> ) (~8%)	30.3%	25 °C	-	-	Ruangchuay et al., 2003
Single wall carbon nanotubes-poly (tetraphenyl-porphorin)	None	9 ppm	Room Temperature	~ 10 minutes	~15 minutes	Sarkar et al. (2014)
$\alpha$ -Fe <sub>2</sub> O <sub>3</sub>	La (7 wt. %)	50 ppm	240 °C	3 seconds	10 seconds	Shan et al. (2013)
InN	None	400 ppb	200 °C	1260 seconds	3740 seconds	Kao et al. (2012)

Sensing Material	Dopant	Detection Limit	Operational Temperature	Response Time	Recovery Time	Reference
La <sub>2</sub> O <sub>3</sub>	None	0.08 µg/mL (~65 ppm)	360 °C	5 seconds	25 seconds	Tang et al. (2008)
NiFe <sub>2</sub> O <sub>4</sub>	Co <sub>0.01</sub> , Mn <sub>0.02</sub>	-	215 °C	3 minutes	5.5 minutes	Rezlescu et al. (2006)
SnO <sub>2</sub>	None	200 ppm	-	Minutes	Minutes	Mwakikunga et al. (2013)
SnO <sub>2</sub>	Ni (5 at. %)	2 ppm	340 °C	7 seconds	30 seconds	Cheng et al. (2014)
SnO <sub>2</sub> -reduced graphene oxide	None	10 ppm	Room Temperature	107 seconds	146 seconds	Zhang et al. (2015)
WO <sub>3</sub>	None	100 ppm	200 °C	32 seconds	45 seconds	Zhang et al. (2013)
WO <sub>3</sub>	Cu (3 mol %)	20 ppm	300 °C	5 seconds	20 seconds	Bai et al. (2014)
WO <sub>3</sub>	Pt	120 ppb	300 °C	~ 2 minutes	~3 minutes	Lee et al. (2014)
WO <sub>3</sub>	Pt	120 ppb	350 °C	~ 4 minutes	~ 2 minutes	Choi et al. (2013)
WO <sub>3</sub>	Si (10 mol %)	100 ppb	400 °C	~ 1.5 minutes	~1.5 minutes	Righettoni et al. (2010)

<b>Sensing Material</b>	<b>Dopant</b>	<b>Detection Limit</b>	<b>Operational Temperature</b>	<b>Response Time</b>	<b>Recovery Time</b>	<b>Reference</b>
ZnO	Co (0.5 wt. %)	5 ppm	360 °C	6 seconds	4 seconds	Liu et al. (2011b)
ZnO	La <sub>2</sub> O <sub>3</sub> (1.0 wt. %)	10 ppm	350 °C	9 seconds	13 seconds	He et al. (2013)
ZnO	None	250 ppb	230 °C	3 seconds	-	Jia et al. (2014)
ZnO	None	2 ppm	310 °C	3-5 seconds	4-5 seconds	Li et al. (2013b)
ZnO	None	4 ppm	300 °C	1.5 seconds	3 seconds	Qi et al. (2008)
ZnO	None	8.1 ppm	260 °C	1.5 seconds	3 seconds	Qi et al. (2008)
ZnO	TiO <sub>2</sub> (10 wt.%)	100 ppm	370 °C	10 seconds	5 seconds	Zhu et al. (2004)
ZnO <sub>2</sub>	None	1000 ppm	325 °C	~ 2 minutes	5 minutes	Sahay (2005)
ZnFe <sub>2</sub> O <sub>4</sub>	None	30 ppm	200 °C	9 seconds	272 seconds	Zhou et al. (2015)

Table B.2: Sensing Materials for Acetaldehyde

Sensing Material	Dopant	Detection Limit	Operational Temperature	Response Time	Recovery Time	Reference
Polyaniline (PANI)	None	560 ppm	-	-	-	Ai et al. (2007)
Polyaniline (PANI)	HClO <sub>4</sub>	5 ppm	20 °C	90 seconds	4 minutes	Kukla et al. (1996)
Polyaniline (PANI)	Dodecyl-hydrogen sulfate salt and maleic acid	10 ppm	Room Temperature	5 minutes	2 minutes	Palaniappan and Saravanan (2010)
Poly (2,5-dimethyl aniline) (P25DMA)	MoO <sub>3</sub>	0.96 ppm	40 °C	20 minutes	-	Itoh et al. (2007a)
Poly (5,6,7,8-tetrahydro-1-naphthyl-amine) (PTHNA)	MoO <sub>3</sub>	25 ppb	-	-	-	Itoh et al. (2007b)
Ethylene dimethacrylate	Methyl methacrylate (0.5 mol %)	9886 ppm	-	30 seconds	-	Hirayama et al. (2002)
Al <sub>2</sub> Ti <sub>2</sub> O <sub>7</sub>	None	~400 ppb (0.5 mg/m <sup>3</sup> )	295 °C	-	-	Zhou et al. (2013)
BaCO <sub>3</sub>	None	0.5 ppm	225 °C	-	-	Cao et al. (2004)
In <sub>2</sub> O <sub>3</sub>	Au	10 ppm	250 °C	~10 seconds	~10 seconds	Han and Sohn (2011)
SnO <sub>2</sub>	In (10 %)	200 ppb	200 °C	~ 15 minutes	~15 minutes	Cindemir et al. (2016)

Sensing Material	Dopant	Detection Limit	Operational Temperature	Response Time	Recovery Time	Reference
Ti	SnO <sub>2</sub> (10 mol %)	10 ppb	500 °C	-	-	Giberti et al. (2012)
TiO <sub>2</sub>	None	5 ppm	Room Temperature	~30 seconds	~30 seconds	Muthukrishnan et al. (2015)
WO <sub>3</sub>	Ru (1 wt. %) SnO <sub>2</sub> (5 wt. %)	20 ppm	300 °C	10 seconds	20 seconds	Jun et al. (2011)
ZnO	Co (5 wt. %)	10 ppm	Room Temperature	~200 seconds	~200 seconds	Mani and Rayappan (2016)
ZnO	None	10 ppb	450 °C	-	-	Giberti et al. (2012)
ZnO	None	50 ppb	250 °C	35 seconds	5 minutes	Calestani et al. (2011)

Table B.3: Sensing Materials for Benzene

<b>Sensing Material</b>	<b>Dopant</b>	<b>Detection Limit</b>	<b>Operational Temperature</b>	<b>Response Time</b>	<b>Recovery Time</b>	<b>Reference</b>
Poly (dimethyl siloxane)	Polystyrene (2.0 (w/v) %)	10 ng/mL	-	-	-	Endo et al. (2007)
Bi <sub>4</sub> SnV <sub>2</sub> O <sub>13</sub>	None	~100 ppb (0.12 mg/m <sup>3</sup> )	150 °C	-	-	Fan et al. (2016)
Pd/i-diamond/ p-diamond	None	~1300 ppm (1 torr)	200 °C	~100 seconds	~100 seconds	Gurbuz et al. (2004)
SnO <sub>2</sub>	Au (1%)	150 ppb	30 °C	2 seconds	1 second	Gràcia et al. (2008)
SnO <sub>2</sub>	None	220 ppb	240 °C	3 seconds	12 seconds	Huang et al. (2012)
SnO <sub>2</sub>	None	300 ppm	Room Temperature	-	-	Panchal et al. (2015)
WO <sub>3</sub>	None	200 ppb	300 °C	35 seconds	-	Ke et al. (2009)
ZnO	Au (6.5 wt. %)	1 ppm	340 °C	80 seconds	11 seconds	Wang et al. (2013b)
ZnO	TiO <sub>2</sub> (10 wt. %)	10 ppm	375 °C	10 seconds	5 seconds	Zhu et al. (2004)

Table B.4: Sensing Materials for Ethanol

Sensing Material	Dopant	Detection Limit	Operational Temperature	Response Time	Recovery Time	Reference
Poly (2,5-dimethyl aniline)	NiO (20 wt.%)	24 ppm	21 °C	60 seconds	60 Seconds	Stewart et al. (2015)
Poly (2,5-dimethyl aniline)	None	3 ppm	21 °C	35 seconds	100 Seconds	Stewart et al. (2015)
Polyaniline (PANI)	NiO (10 wt. %)	0.31 ppm	21 °C	-	-	Stewart et al. (2012)
Polyaniline (PANI)	TiO <sub>2</sub>	150 ppm	Room Temperature	280 seconds	-	Zheng et al. (2008)
Alcohol oxidase	None	0.348 ppm	Room temp.	120 seconds	120 seconds	Mitsubayashi et al. (1994)
Alcohol oxidase	None	268.6 ppm	-	-	-	Mitsubayashi et al. (2003)
Bis [(E)-1,1,1-trifluoro-2-(thrifluoromethyl) pent-4-en-2-ol] siloxane (ADIOL)	None	-	20 °C	90 seconds	2 seconds	Yang et al. (2009a)
Cu <sub>2</sub> O	-	10 ppm	200 °C	170 seconds	180 seconds	Barreca et al. (2009)
Cu <sub>2</sub> O	-	10 ppm	210 °C	15 seconds	-	Zhang et al. (2006)
CuO	-	100 ppm	240 °C	110 seconds	120 seconds	Raksa et al. (2009)



Sensing Material	Dopant	Detection Limit	Operational Temperature	Response Time	Recovery Time	Reference
CuO	Au	5 ppm	200 °C	4 seconds	7 seconds	Gou et al. (2008)
CuO	Pt	5 ppm	200 °C	4 seconds	7 seconds	Gou et al. (2008)
CuS Hollow Spheres	None	3 ppm	250 °C	15 seconds	15 seconds	Yu et al. (2009)
Graphene	Al <sub>2</sub> O <sub>3</sub>	1225 ppm	200 °C	10 seconds	100 seconds	Jiang et al. (2011)
NiO	None	10 ppm	Room Temperature	-	-	Li (2016)
NiO	None	5 ppm	300 °C	-	-	Kaur et al. (2016)
NiO	TiO <sub>2</sub> (25 wt. %)	2000 ppm	Room Temperature	9 seconds	16 seconds	Arshak et al. (2004)
SnO <sub>2</sub>	Lao (3 at. %)	-	300	10 seconds	10 seconds	Stambolova et al. (2000)
SnO <sub>2</sub>	NiO (5 mol %)	5 ppm	300 °C	2 seconds	3 seconds	Liu et al. (2011a)
SnO <sub>2</sub>	NiO	6.7 ppm	280°C	0.6 seconds	10 seconds	Lou et al. (2012)
SnO <sub>2</sub>	Pt (0.3 wt. %)	2 ppm	400	~30 seconds	-	Lee et al. (2009)
TiO <sub>2</sub>	Ag	5 ppm	250 °C	1 second	2 seconds	Hu et al. (2010)
TiO <sub>2</sub>	None	20 ppm	350 °C	12 seconds	9 seconds	Wang et al. (2010a)

Sensing Material	Dopant	Detection Limit	Operational Temperature	Response Time	Recovery Time	Reference
TiO <sub>2</sub>	None	40 µg/mL (~26 000 ppm)	440 °C	50 seconds	160 seconds	Zhu et al. (2002)
TiO <sub>2</sub>	None	40 ppm	400 °C	1 second	10 seconds	Tang et al. (1995)
ZnO	Al <sub>2</sub> O <sub>3</sub> (1 wt. %)	100 ppm	300 °C	18 seconds	40 seconds	Patil et al. (2007)
ZnO	Al <sub>2</sub> O <sub>3</sub> (2 at. %)	1000 ppm	290 °C	8 seconds	10 seconds	Yang et al. (2009b)
ZnO	Al <sub>2</sub> O <sub>3</sub> (1 wt. %)	400 ppm	300 °C	6 seconds	20 seconds	Ruchika et al. (2016)
ZnO	Al <sub>2</sub> O <sub>3</sub> (1 wt. %)	500 ppm	400 °C	10 seconds	40 seconds	Deore and Jain (2014)
ZnO	Lao (3 at. %)	-	300	60 seconds	-	Stambolova et al. (2000)
ZnO	NiO	0.3 ppm	450 °C	~60 seconds	~60 seconds	Na et al. (2012)
ZnO	None	1 ppm	300	-	-	Wan et al. (2004)
ZnO	None	1 ppm	320 °C	35 seconds	24 seconds	Wang et al. (2012)
ZnO	None	10 ppm	400 °C	25 seconds	~20 seconds	Singh et al. (2008)
ZnO	None	10 ppm	400 °C	5 seconds	5 / 10 seconds	Singh et al. (2008)
ZnO	None	1000 ppm	350	120 seconds	90 seconds	Sahay et al. (2005)

Sensing Material	Dopant	Detection Limit	Operational Temperature	Response Time	Recovery Time	Reference
ZnO	None	25 ppm	400	60 seconds	Minutes	Liewhiran et al. (2007)
ZnO	None	50 ppm	220 °C	25 seconds	50 seconds	Choopun et al. (2007)
ZnO	Ti (1.86 at %)	50 ppm	250 °C	~200 seconds	~60 seconds	Hsu et al. (2014)
ZnO	TiO <sub>2</sub> (10 wt. %)	100 ppm	370 °C	10 seconds	5 seconds	Zhu et al. (2004)
ZnO	TiO <sub>2</sub> (10 wt. %)	100 ppm	320 °C	-	-	Zhu et al. (2004)
ZnO Flakes	None	300 ppm	400	62 seconds	62 Seconds	Liu et al. (2005a)
ZnO nanorods	None	10 ppm	330	10 seconds	30 seconds	Xu et al. (2005)
ZnO-Graphene	None	5 ppm	-	10 seconds	10 seconds	Zou et al. (2013)
$\gamma$ -Al <sub>2</sub> O <sub>3</sub>	Dy <sup>3+</sup> (1 mol %)	500 ppm	450 °C	-	-	Okabayashi et al. (2000)

Table B.5: Sensing Materials for Formaldehyde

<b>Sensing Material</b>	<b>Dopant</b>	<b>Detection Limit</b>	<b>Operational Temperature</b>	<b>Response Time</b>	<b>Recovery Time</b>	<b>Reference</b>
Polyaniline (PANI)	MoO <sub>3</sub>	-	-	-	-	Wang et al. (2006)
Polyaniline (PANI)	NiO (15 wt. %)	0.3 ppm	21 °C	-	-	Stewart et al. (2012)
Polyaniline (PANI)	NiO (5 wt. %) Al <sub>2</sub> O <sub>3</sub> (15 wt. %)	1 ppm	21 °C	-	-	Stewart et al. (2012)
Polyaniline (PANI)	None	500 ppm	20 °C	60 minutes	-	Hosseini et al. (2005)
Cascade laser based quartz-enhanced photoacoustic spectroscopy	None	25 ppbv	-	10 seconds	-	Horstjann et al. (2004)
Cavity Leak-out Spectroscopy (CALOS)	None	2 ppb	25 °C	5 seconds	-	Dahnke et al. (2002)
Cu <sub>2</sub> O	None	6 ppb	250 °C	~150 seconds	~75 seconds	Park et al. (2014)

<b>Sensing Material</b>	<b>Dopant</b>	<b>Detection Limit</b>	<b>Operational Temperature</b>	<b>Response Time</b>	<b>Recovery Time</b>	<b>Reference</b>
Fe <sub>3</sub> O <sub>4</sub> magnetic microspheres with acylhydrazine groups on the surface	pH 5.5	10 µg/L (0.3µg/L estimated)	-	-	-	Yang et al. (2001)
Gold coated Nafion	None	13 ppb	25 °C	2 minutes	-	Knake et al. (2001)
Graphene	ZnO	180 ppb	Room Temperature	36 seconds	~1500 seconds	Mu et al. (2014)
Graphene-Poly (methyl methacrylate)	None	10 ppb	Room Temperature	~ 600 seconds	-	Alizadeh and Soltani (2013)
In <sub>2</sub> O <sub>3</sub>	Ag (8 wt. %)	2 ppm	100 °C	10 seconds	60 seconds	Wang et al. (2009a)
LaFeO <sub>3</sub>	Ag (1 mol %)	500 ppb	40 °C	67 seconds	104 seconds	Zhang et al. (2014)
Multiwall carbon nanotubes (MWCNT)	Amino groups (18.19%)	20 ppb	Room Temperature	7 – 10 seconds	100s seconds	Xie et al. (2012)
NAD <sup>+</sup> /NADH	pH 8 0.1M potassium phosphate	0.2 ppbv	Room Temperature	~ 60 seconds	~120 seconds	Hershkovitz (2000)

<b>Sensing Material</b>	<b>Dopant</b>	<b>Detection Limit</b>	<b>Operational Temperature</b>	<b>Response Time</b>	<b>Recovery Time</b>	<b>Reference</b>
Nafion	Pd-Pt	3 $\mu$ M	-	-	-	Zhou et al. (2009)
NiO	None	1.2 ppm	280 °C	13 seconds	-	Lee et al. (2006)
NiO	PANI (20 wt. %)	10 <sup>-7</sup> mol/L	-	90 minutes	-	Campanella and Battilotti (2006)
NiO/Al <sub>2</sub> O <sub>3</sub>	None	40 ppb	280 °C	7 seconds	-	Wang et al. (2008)
Pd Nanoparticles	0.1M NaOH	0.01M	25 °C	-	-	Safavi et al. (2009)
SnO <sub>2</sub>	Au, Cu, Pt, Pd	0.06 ppm	200 °C	15 minutes	-	Lv et al. (2007)
SnO <sub>2</sub>	In (4.43 at. %) Pd (0.66 at. %)	5 ppm	160 °C	3 seconds	6 seconds	Lin et al. (2015)
SnO <sub>2</sub>	None	10 ppb	215 °C	14 seconds	140 seconds	Xing et al. (2013)

Table B.6: Sensing Materials for Methanol

<b>Sensing Material</b>	<b>Dopant</b>	<b>Detection Limit</b>	<b>Operational Temperature</b>	<b>Response Time</b>	<b>Recovery Time</b>	<b>Reference</b>
Graphene oxide-PANI	None	100 ppm	110 °C	~5 seconds	~15 seconds	Konwer et al. (2013)
Poly ( <i>o</i> -anisidine) (PoANI)	HCl	-	Room Temperature	10 minutes	10 minutes	Athawale and Kulkarni (2000)
Poly (2,3-dimethyl aniline) (P2,3DMA)	HCl	-	Room Temperature	10 minutes	10 minutes	Athawale and Kulkarni (2000)
Poly (methyl acrylic acid)	None	1 ppm	130 °C	40 seconds	50 seconds	Zhu et al. (2015)
Polyaniline	HCl	-	Room Temperature	10 minutes	10 minutes	Athawale and Kulkarni (2000)
Polyaniline colloid	None	25 ppm	-	3 seconds	90 seconds	Li et al. (2005)
Polypyrrole	ClO <sub>4</sub>	300 ppm	30 °C	< 1 second	3500 seconds	Babaei and Alizadeh (2013)
In <sub>2</sub> O <sub>3</sub>	SnO <sub>2</sub> (17 %)	200 ppm	Room Temperature	-	-	Patel et al. (2003)
SiO <sub>2</sub>	P <sub>2</sub> O <sub>5</sub> (5 mol %)	10,000 ppm (1%)	25 °C	~10 seconds	~90 seconds	Nagomi et al. (2009)
TiO <sub>2</sub>	None	100 ppm	500 °C	½ minute	< 1 minute	Garzella et al. (2000)

Table B.7: Sensing Materials for Toluene

<b>Sensing Material</b>	<b>Dopant</b>	<b>Detection Limit</b>	<b>Operational Temperature</b>	<b>Response Time</b>	<b>Recovery Time</b>	<b>Reference</b>
Poly (dimethyl siloxane)	Polystyrene (2.0 (w/v)%)	10 ng/mL	-	-	-	Endo et al. (2007)
Polyethyleneimine (PEI)	None	200 ppm	20 °C	90 seconds	2 seconds	Yang et al. (2009b)
Polyaniline (PANI)	None	100 ppm	30	11 minutes	22 minutes	Parmar et al. (2013)
Pd/i-diamond/ p-diamond	None	~1300 ppm (1 torr)	150 °C	~100 seconds	~100 seconds	Gurbuz et al. (2004)
ZnO	Au (6.5 wt. %)	1 ppm	340 °C	60 seconds	10 seconds	Wang et al. (2013b)
SnO <sub>2</sub>	None	90 ppb	240 °C	3 seconds	13 seconds	Huang et al. (2012)
TiO <sub>2</sub>	Pd	50 ppm	Room Temperature	~ 90 seconds	~200 seconds	Kim et al. (2010)
IO <sub>5</sub>	None	50 ppb	Room Temperature	-	-	Kawamura et al. (2006)
SnO <sub>2</sub>	Pd (0.2 mol %)	100 ppb	300	-	-	Suematsu et al. (2014)
WO <sub>3</sub>	Pd (1 wt. %)	20 ppb	350	11 seconds	16 seconds	Kim et al. (2014)
ZnO	TiO <sub>2</sub> (10 wt. %)	10 ppm	375 °C	10 seconds	5 seconds	Zhu et al. (2004)





## Appendix C: Selectivity towards Ethanol

Appendix C contains an overview table of selective gas sensing materials for ethanol. This table includes the sensing material and any dopants. The selectivity (ratio between the responses of ethanol to that of an interferent) towards different gas interferents is listed.

Table C.1: Selectivity of Sensors towards Ethanol with Respect to Other VOCs

Sensing Material	Dopant	Selectivity with Respect to							Reference
		Acetone	Acetal- dehyde	Ammonia	Benzene	Form- aldehyde	Methane	Methanol	
Cu <sub>2</sub> O	None	1.1							Barreca et al. (2009)
CuS Hollow Spheres	None	~4.6		~5.75		~11.5			Yu et al. (2009)
In <sub>2</sub> O <sub>3</sub>	Pt 4.5 wt.% La <sub>2</sub> O <sub>3</sub> 1.35 wt.%						~325	~2.6	Zhan et al. (2007)
NiO	None	1.5							Kaur et al. (2016)
NiO	TiO <sub>2</sub> (25 wt. %)							2.8	Arshak et al. (2004)
Poly (2,5-dimethyl aniline)	NiO 20 wt. %	4.2			6.6			72.3	Stewart et al. (2015)
Poly (2,5-dimethyl aniline)	None	1.6			5.3			11.4	Stewart et al. (2015)
Polyaniline	NiO (10 wt. %)		1.2		6.2	1.1			Stewart et al. (2012)

Sensing Material	Dopant	Selectivity with Respect to								Reference
		Acetone	Acetaldehyde	Ammonia	Benzene	Formaldehyde	Methane	Methanol	Octane/LPG	
Polyaniline	Poly (vinylidene fluoride)				5			2		Kim et al. (2005)
Polyaniline	TiO <sub>2</sub>		1.8			1.3				Zheng et al. (2008)
SnO <sub>2</sub>	CeO <sub>2</sub> 2 wt. %							~3.5	~35	Pourfayaz et al. (2005)
SnO <sub>2</sub>	NiO (5 mol %)	3.2			18.7		10.2			Liu et al. (2011a)
SnO <sub>2</sub>	NiO					3.4	8.1			Lou et al. (2012)
SnO <sub>2</sub>	None							~6666		Beckers et al. (2013)
SnO <sub>2</sub>	Pt 0.3 wt. %					~2.5				Lee et al. (2009)
SnO <sub>2</sub>	ZnO	~2								Kim et al. (2007)
SnO <sub>2</sub>	ZnO			~3.1					~4.8	Nguyen et al. (2012)
TiO <sub>2</sub>	Nb 3 wt. %								~14	Singh et al. (2012)
TiO <sub>2</sub>	None	~2								Zhu et al. (2002)

Sensing Material	Dopant	Selectivity with Respect to								Reference
		Acetone	Acetal- dehyde	Ammonia	Benzene	Form- aldehyde	Methane	Methanol	Octane/ LPG	
VO <sub>5</sub>	None			Good <sup>1</sup>						Liu et al. (2005b)
ZnO	Al <sub>2</sub> O <sub>3</sub> (1 wt. %)			12						Deore and Jain (2014)
ZnO	Al <sub>2</sub> O <sub>3</sub> (1 wt. %)								6.1	Patil et al. (2007)
ZnO	La <sub>2</sub> O <sub>3</sub> -Pd								~5	Rao (2000)
ZnO	NiO		~3.3		~4	~2.9				Na et al. (2012)
ZnO	NiO	7.3			9.7					Na et al. (2012)
ZnO	None		~1.7							Calestani et al. (2011)
ZnO	None						~5			Hamedani et al. (2011)
ZnO	None			~8.5		~4.25			~1.7	Xu et al. (2005)
ZnO	TiO <sub>2</sub> (10 wt. %)	1.9								Zhu et al. (2004)
ZnO-Graphene	None	1.5		6.8		3.3				Zou et al. (2013)

LPG- liquid petroleum gas

<sup>1</sup>Authors did not show number in a table or graph. They just stated that they had good selectivity.



## Appendix D: Miscellaneous Chromatograms

Appendix D has two sections. Section D.1 provides a sample of the gas chromatograms obtained while evaluating the various sensing materials. Section D.2 contains typical gel permeation chromatography (GPC) responses (traces) obtained.

### D.1: Gas Chromatograms

These additional chromatograms, to those presented in Section 3.1, show additional details. Figure D.1 shows the good separation achieved between the different gas interferents used. The proximity of methanol and acetaldehyde (as seen in the inset in Figure D.1) did not pose a problem since these two analytes were never run at the same time (i.e. mixed); however, at a different column temperature, these two gases could be separated a little more.

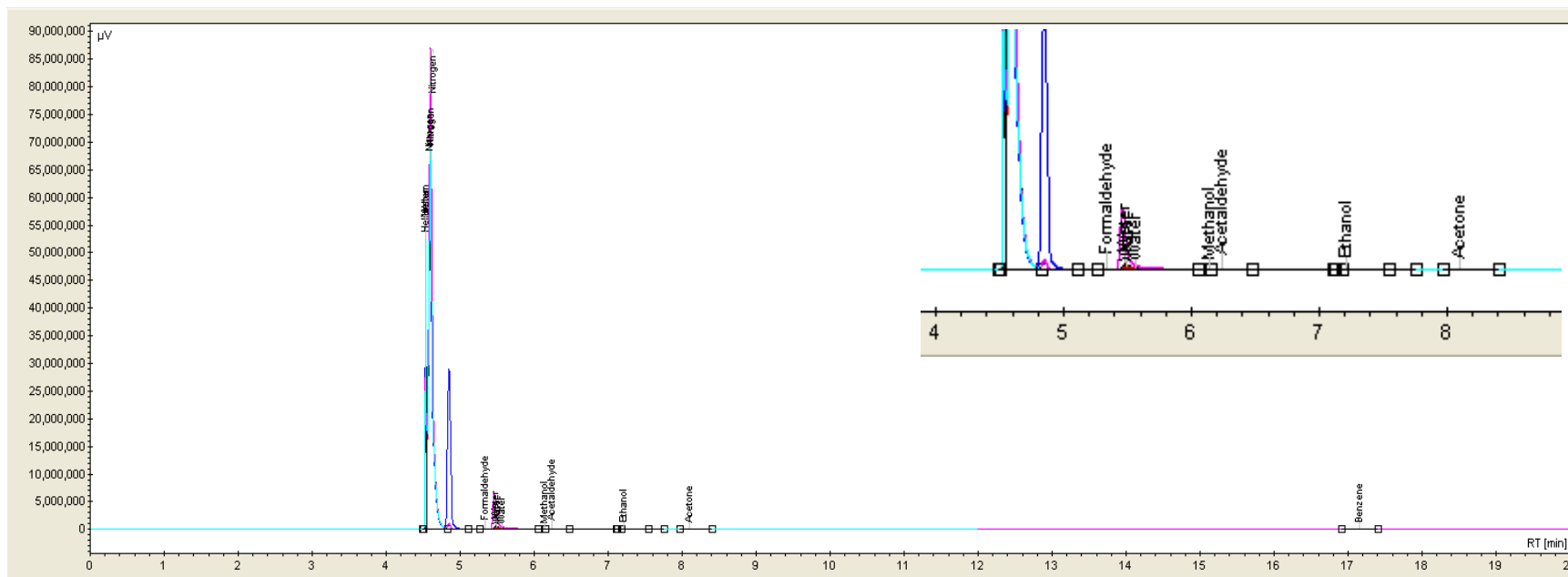


Figure D.1: Gas chromatogram of all six gas analytes evaluated. Note the separation between all the gases, except methanol and acetaldehyde. Benzene eluted after 17 minutes (lone peak on the right). There was also a water peak to the right of formaldehyde around 5.5 minutes.

Figure D.2 shows two consecutive measurements taken at 48 and 60 minutes for one ethanol sample. The fact that both chromatograms are on top of one another shows that equilibrium has been reached. For all of the samples, except benzene, the GC run took 12 minutes; hence the 48 and 60 minute sampling times. The runs containing benzene took 20 minutes and had 40 and 60 minute sampling times for the equilibrium runs (instead of 48 and 60).

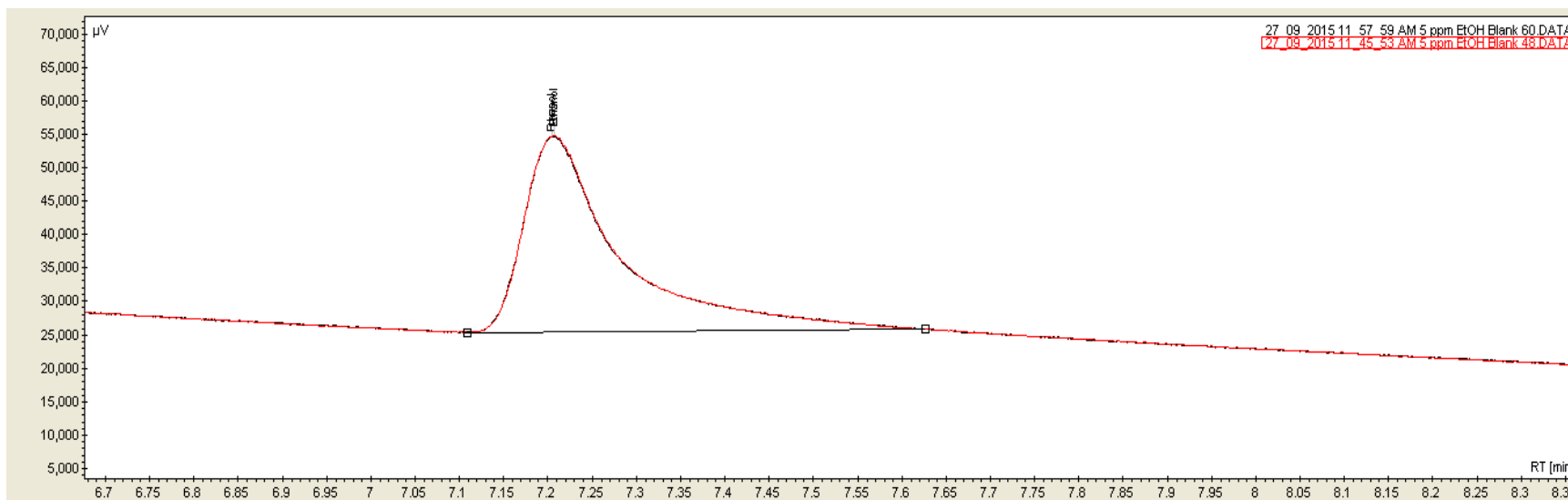


Figure D.2: Two ethanol chromatograms measured at 48 minutes (red) and 60 minutes (black). Note that the two chromatograms are on top of one another. This shows that equilibrium has been reached.

Figures D.3 – D.8 show the peaks observed for each gas analyte tested. Acetaldehyde, acetone, benzene, ethanol, formaldehyde, and methanol eluted out at 6.4, 8.1, 17.2, 7.2, 5.7, and 6.1, respectively when the column temperature was 110 °C. The acetaldehyde and methanol peaks were too close to separate had the two been in the same; however, this was not an issue.

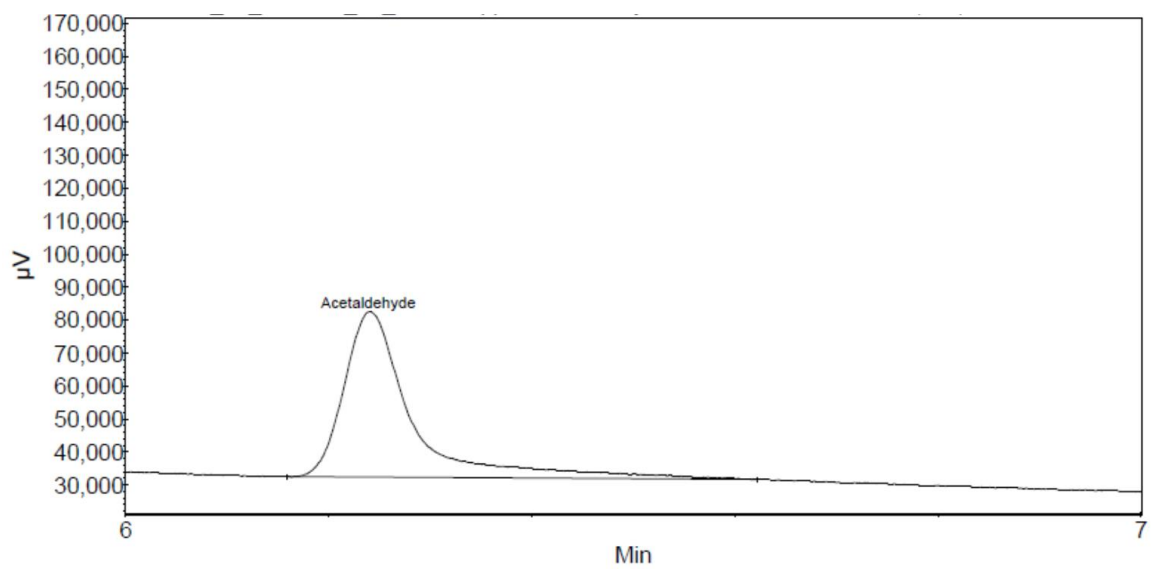


Figure D.3: Gas chromatogram of acetaldehyde.

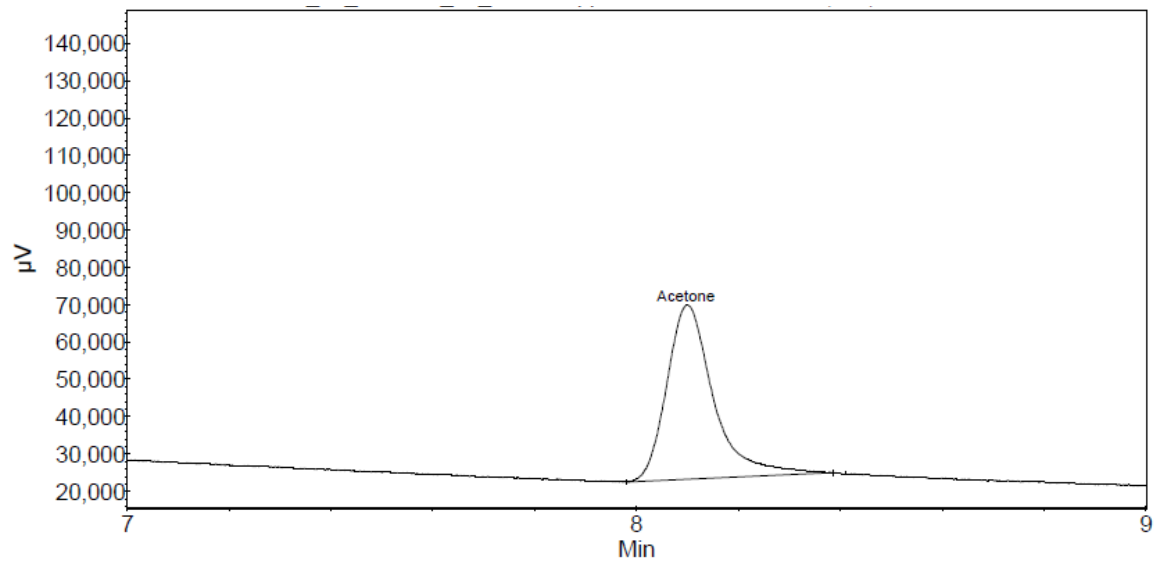


Figure D.4: Gas chromatogram of acetone.



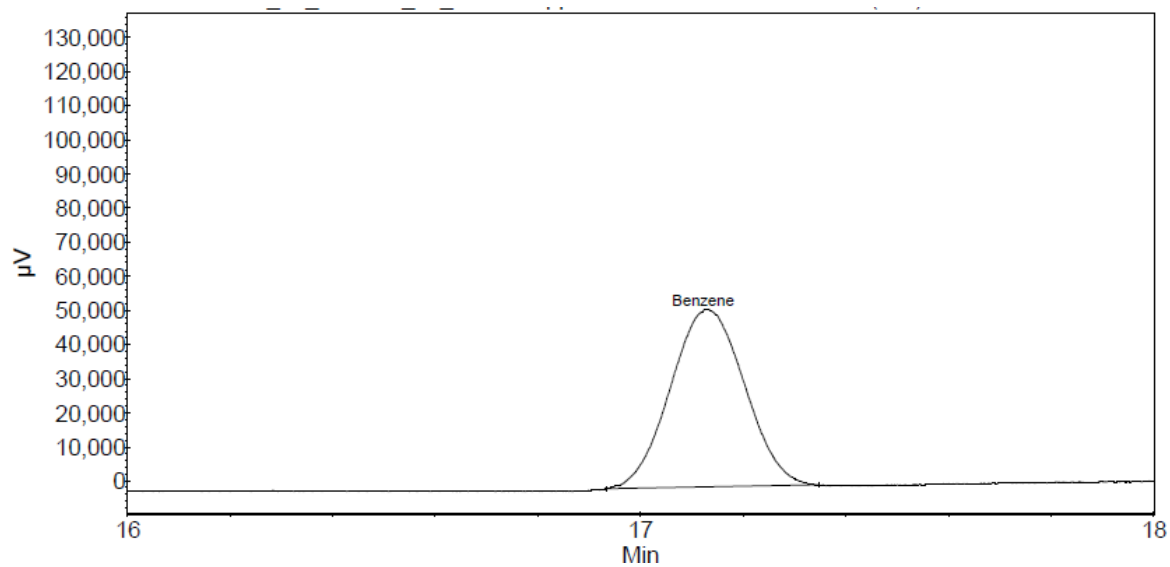


Figure D.5: Gas chromatogram of benzene.

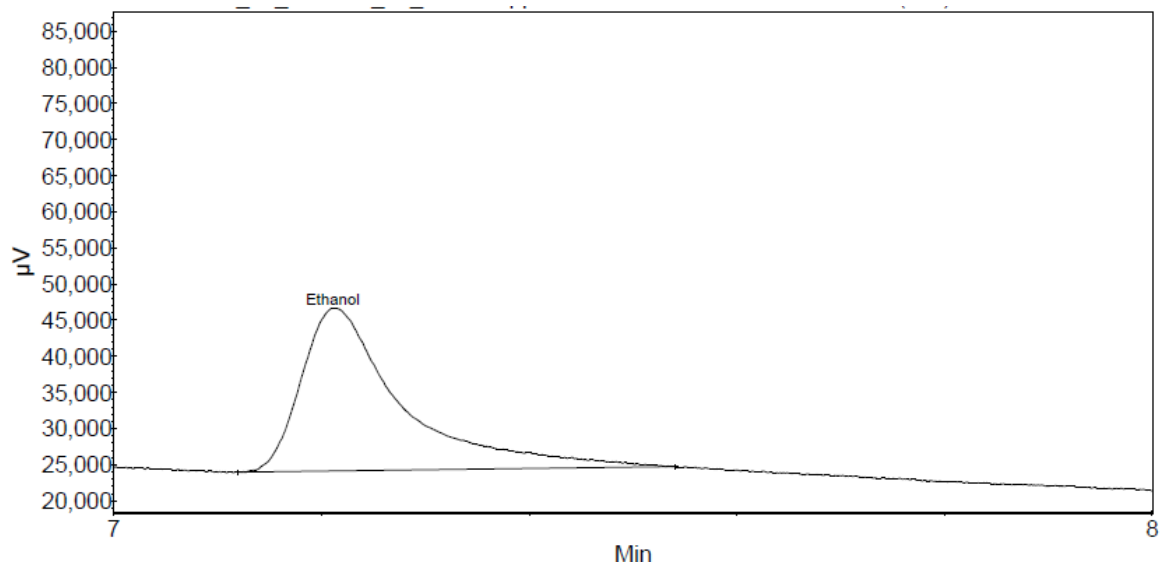


Figure D.6: Gas chromatogram of ethanol.

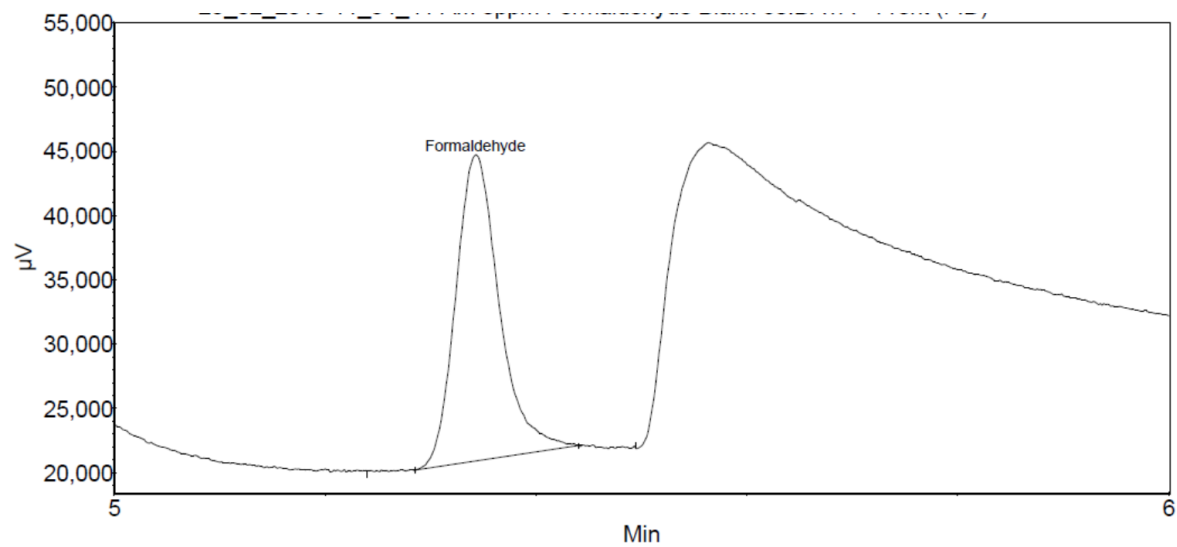


Figure D.7: Gas chromatogram of formaldehyde.

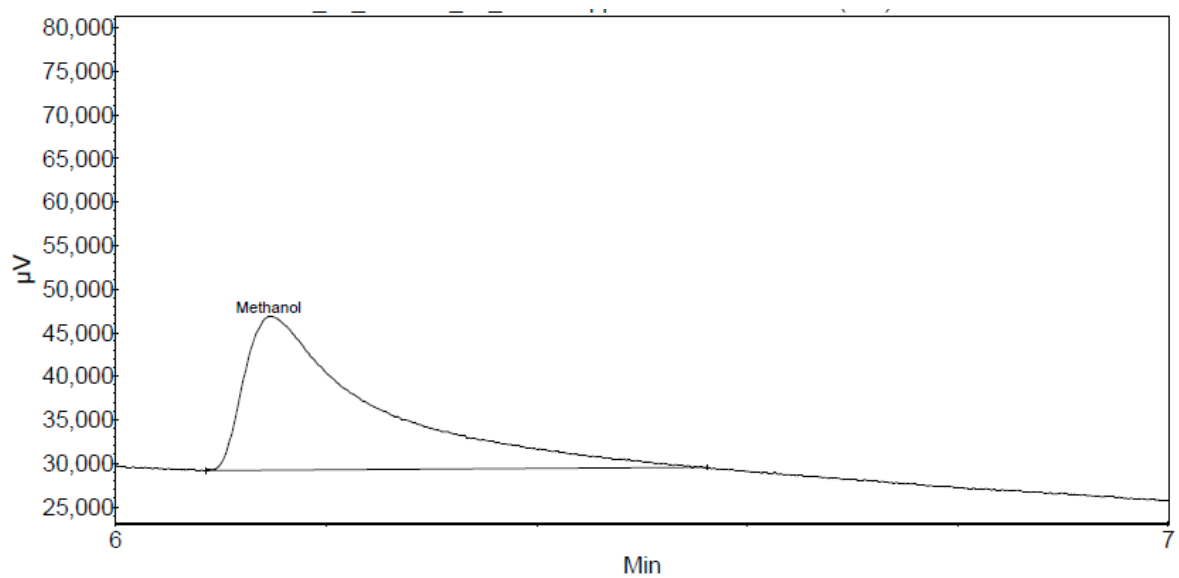


Figure D.8: Gas chromatogram of methanol.

## D.2 Gel Permeation Chromatography (GPC) Responses

The molecular weights measured (see also section 3.7) were obtained using a Viscotek TDA 305 GPC, with refractive index (RI), right angle light scattering (RALS), and low angle light scattering (LALS) detectors. Since no value for the  $dn/dc$  for PANI in DMSO could be found in the literature, and the value calculated by the GPC software was 0.0012 (which seemed excessively low and resulted in molecular weights that were not detectable on the GPC set-up used), two values of  $dn/dc$  were used to estimate the average molecular weight of PANI. Therefore,  $dn/dc$  values were estimated based on PANI in other solvents (see Table D.1).

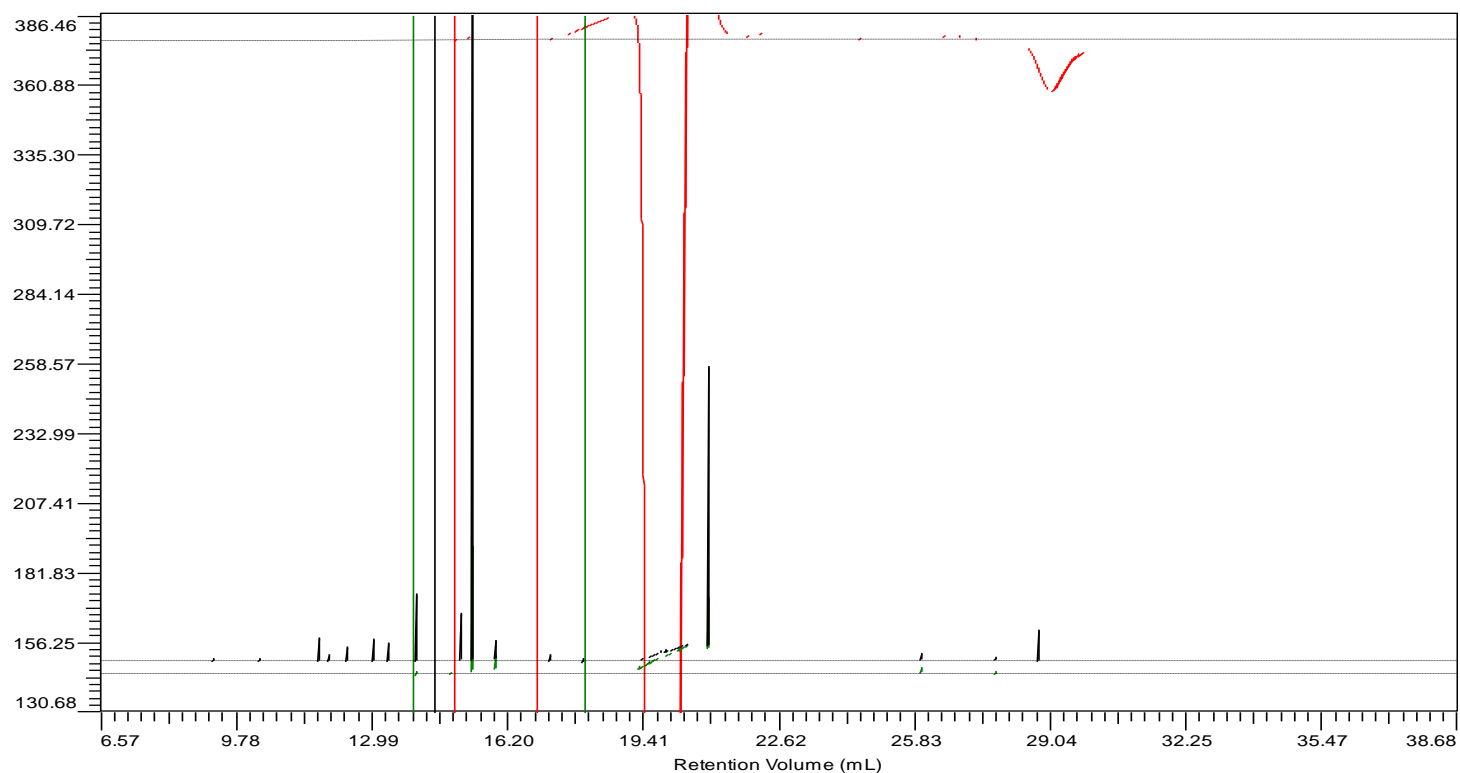


Figure D.9: Gel permeation chromatogram of polyaniline (PANI), where the RI is red, the RALS is green, and the LALS is black.

Table D.1: dn/dc Values

Polymer	Solvent	dn/dc (mL/g)	$\lambda_0$ (nm)	Reference
PANI	NMP/LiBF <sub>4</sub>	0.41	785	Kolla et al. (2005)
PANI	NMP/LiBF <sub>4</sub>	0.43	632	Surwade et al. (2009)
PANI	Chloroform	0.48	632	Surwade et al. (2009)
Poly (acrylamide)	Water	0.182	546	Brandrup et al. (1999)
Poly (acrylamide)	Acetic Acid	0.194	546	Brandrup et al. (1999)
Poly (acrylamide)	DMSO	0.089	546	Brandrup et al. (1999)
Poly (acrylonitrile)	DMF	0.080	546	Brandrup et al. (1999)
Poly (acrylonitrile)	DMSO	0.042	546	Brandrup et al. (1999)

*N*-methyl-2-pyrrolidone (NMP); dimethyl sulfoxide (DMSO); dimethyl formide (DMF)

Given that the measured dn/dc values for PANI were around 0.4 in different solvents, 0.4 was used as an estimate of dn/dc to calculate the average molecular weight of PANI. However, since the dn/dc for poly (acrylamide) and poly (acrylonitrile) in DMSO was about half that of the dn/dc in other solvents, a dn/dc of 0.2 was also used to calculate molecular weights of PANI (see Table D.2).

Table D.2: Molecular Weight Averages of PANI

Sample	dn/dc (estimate)	M <sub>w</sub> (Da)	M <sub>n</sub> (Da)	PDI
PANI 1	0.4	386,866	176,975	2.186
PANI 2	0.4	407,761	204,761	1.995
PANI 1	0.2	773,733	353,950	2.186
PANI 2	0.2	815,521	408,807	1.995

Note that PANI was dissolved in DMSO and run through a Viscotek GPC with an RI, RALS, and LALS detector.

A known standard was also run to obtain a measure of reproducibility for the system (see Table D.3).

Table D.3: Pullulan Standard ( $M_w = 108,000$  Da)

	<b>Standard 1</b>	<b>Standard 2</b>	<b>Average</b>	<b>Standard Deviation</b>	<b>Percent Error (%)</b>
<b><math>M_n</math> (Da)</b>	97,591	99,461	98,526	1322	1.3
<b><math>M_w</math> (Da)</b>	104,392	108,129	106,261	262	2.5
<b>PDI</b>	1.070	1.087			

*dn/dc in DMSO is 0.066.*

## Appendix E: Data

Appendix E contains all of the data that were collected experimentally for this thesis. This appendix has been separated into subsections that correspond to subsections in the text. This was done for ease of relating the data to the analysis described in the corresponding chapters.

### E.1 Chapter 4 Data

#### *E.1.1 Polyaniline (PANI) Nanocomposites (Section 4.3.2)*

Table E.1 Amount of Ethanol Sorbed onto Each PANI Nanocomposite

Polymer Sample	Average Amount of Ethanol Sorbed (ppm)		
PANI	0.600	0.630	0.617
PANI 10% NiO	0.683	0.540	0.680
PANI 20% NiO	0.557	0.530	0.540
PANI 10% ZnO	0.723	0.880	0.727
PANI 20% ZnO	0.630	0.540	0.493

#### *E.1.2 Poly (o-anisidine) (PoANI) Nanocomposites (Section 4.3.2)*

Table E.2 Amount of Ethanol Sorbed onto Each PoANI Nanocomposite

Polymer Sample	Average Amount of Ethanol Sorbed (ppm)		
PoANI	0.253	0.387	0.400
PoANI 10% NiO	0.220	0.227	0.203
PoANI 20% NiO	0.697	0.633	0.693
PoANI 10% ZnO	0.920	1.060	0.980
PoANI 20% ZnO	0.807	1.050	1.007

**E.1.3 Poly (2,5-dimethyl aniline) (P25DMA) Nanocomposites (Section 4.3.3)**

Table E.3: Amount of Ethanol Sorbed onto the P25DMA Nanocomposites

Time (min)	Amount Sorbed (ppm)					
	60	72	60	72	60	72
P25DMA	1.04	0.95	0.94	0.78	0.71	0.83
P25DMA 5% Al <sub>2</sub> O <sub>3</sub>	1.42	1.44	1.36	1.41	1.76	1.70
P25DMA 10% Al <sub>2</sub> O <sub>3</sub>	1.19	1.15	1.5	1.48	1.62	1.46
P25DMA 20% Al <sub>2</sub> O <sub>3</sub>	1.04	1.03	1.39	1.53	1.62	1.45
P25DMA 5% CuO	0.10	0.10	0.11	0.06	0.10	0.00
P25DMA 10% CuO	0.08	0.17	0.34	0.29	0.24	0.14
P25DMA 20% CuO	0.19	0.22	0.4	0.21	0.28	0.33
P25DMA 5% NiO	1.26	1.37	1.63	1.64	1.82	1.73
P25DMA 10% NiO	0.88	0.64	0.66	0.31	0.80	0.59
P25DMA 20% NiO	0.81	0.92	1.34	1.23	1.28	1.00
P25DMA 5% TiO <sub>2</sub>	1.16	1.13	0.92	0.98	1.46	1.47
P25DMA 10% TiO <sub>2</sub>	1.49	1.54	1.41	1.45	1.58	1.39
P25DMA 20% TiO <sub>2</sub>	1.66	1.56	1.51	1.58	1.94	1.92
P25DMA 5% ZnO	0.84	0.87	1.48	1.37	1.58	1.49
P25DMA 10% ZnO	0.33	-0.19	0.53	0.18	0.48	0.19
P25DMA 20% ZnO	-0.07	-0.26	-0.49	-0.36	-0.24	-0.47

Table E.4: Amount of Acetaldehyde Sorbed onto the P25DMA Nanocomposites

Time (min)	Amount Sorbed (ppm)					
	36	48	36	48	36	48
P25DMA	0.73	0.68	0.80	0.69	0.76	0.70
P25DMA 5% Al <sub>2</sub> O <sub>3</sub>	-0.17	-0.19	-0.11	-0.09	0.27	0.30
P25DMA 5% NiO	0.50	0.50	0.50	0.54	0.62	0.70
P25DMA 10% NiO	0.70	0.47	0.87	0.56	0.53	0.47
P25DMA 20% NiO	0.43	0.63	0.40	0.45	0.60	0.49
P25DMA 5% ZnO	0.32	0.29	0.38	0.32	0.40	0.35
P25DMA 5% TiO <sub>2</sub>	0.24	0.23	0.18	0.17	0.21	0.20
P25DMA 10% TiO <sub>2</sub>	0.24	0.33	0.13	0.16	0.24	0.21
P25DMA 20% TiO <sub>2</sub>	0.76	0.69	0.66	0.66	0.70	0.66

Table E.5: Amount of Acetone Sorbed onto the P25DMA Nanocomposites

Time (min)	Amount Sorbed (ppm)					
	60	72	60	72	60	72
<b>P25DMA</b>	0.29	0.25	0.24	0.17	0.34	0.32
<b>P25DMA 5% Al<sub>2</sub>O<sub>3</sub></b>	0.23	0.17	0.33	0.33	0.22	0.17
<b>P25DMA 5% NiO</b>	0.41	0.40	0.29	0.27	0.47	0.44
<b>P25DMA 10% NiO</b>	0.50	0.53	0.49	0.51	0.57	0.56
<b>P25DMA 20% NiO</b>	0.59	0.57	0.70	0.70	0.59	0.59
<b>P25DMA 5% ZnO</b>	0.22	0.14	0.03	0.02	0.14	0.07
<b>P25DMA 5% TiO<sub>2</sub></b>	0.21	0.20	0.30	0.28	0.28	0.24
<b>P25DMA 10% TiO<sub>2</sub></b>	0.29	0.32	0.08	0.13	0.13	0.13
<b>P25DMA 20% TiO<sub>2</sub></b>	0.47	0.45	0.33	0.28	0.90	0.77

Table E.6: Benzene onto the P25DMA Nanocomposites

Time (min)	Amount Sorbed (ppm)					
	40	60	40	60	40	60
<b>P25DMA</b>	0.08	0.07	-0.05	-0.12	0.05	-0.01
<b>P25DMA 5% Al<sub>2</sub>O<sub>3</sub></b>	0.10	0.06	0.27	0.06	-0.03	-0.04
<b>P25DMA 5% NiO</b>	0.13	0.08	-0.05	-0.07	0.02	0.00
<b>P25DMA 10% NiO</b>	0.21	0.18	0.24	0.23	0.24	0.23
<b>P25DMA 20% NiO</b>	1.23	1.20	0.36	0.30	0.31	0.29
<b>P25DMA 5% ZnO</b>	-0.02	-0.04	0.34	0.05	-0.04	-0.07
<b>P25DMA 5% TiO<sub>2</sub></b>	0.03	0.02	0.04	0.03	-0.10	-0.14
<b>P25DMA 10% TiO<sub>2</sub></b>	0.03	0.01	0.09	0.10	0.11	0.11
<b>P25DMA 20% TiO<sub>2</sub></b>	0.38	0.25	0.41	0.29	0.27	0.14

Table E.7: Formaldehyde onto the P25DMA Nanocomposites

Time (min)	Amount Sorbed (ppm)					
	48	60	48	60	48	60
<b>P25DMA</b>	1.44	1.42	1.09	0.97	1.16	1.1
<b>P25DMA 5% Al<sub>2</sub>O<sub>3</sub></b>	0.41	0.48	0.68	0.78	0.73	0.59
<b>P25DMA 5% NiO</b>	1.29	1.18	1.42	1.42	1.44	1.43
<b>P25DMA 10% NiO</b>	0.97	0.97	0.8	0.82	0.83	0.85
<b>P25DMA 20% NiO</b>	1.05	1.08	1.02	1.02	0.98	0.94
<b>P25DMA 5% ZnO</b>	0.76	0.82	0.9	0.74	0.97	0.86
<b>P25DMA 5% TiO<sub>2</sub></b>	1.17	1.09	1.08	1.02	1.15	1.27
<b>P25DMA 10% TiO<sub>2</sub></b>	0.75	0.72	0.86	0.87	0.74	0.76
<b>P25DMA 20% TiO<sub>2</sub></b>	1.03	0.95	1.4	1.33	1.47	1.49



Table E.8: Methanol onto the P25DMA Nanocomposites

Time (min)	Amount Sorbed (ppm)					
	72	84	72	84	72	84
<b>P25DMA</b>	1.27	1.18	1.61	1.52	1.31	0.94
<b>P25DMA 5% Al<sub>2</sub>O<sub>3</sub></b>	-0.03	-0.10	-0.70	-0.62	-0.30	-0.30
<b>P25DMA 5% NiO</b>	0.47	0.43	0.96	0.94	0.32	0.28
<b>P25DMA 10% NiO</b>	0.49	0.50	0.91	0.63	0.72	0.50
<b>P25DMA 20% NiO</b>	0.67	0.65	0.83	0.79	0.83	0.70
<b>P25DMA 5% ZnO</b>	0.75	0.58	0.21	0.02	0.31	0.12
<b>P25DMA 5% TiO<sub>2</sub></b>	0.15	0.21	-0.18	-0.39	-0.06	-0.20
<b>P25DMA 10% TiO<sub>2</sub></b>	0.26	0.27	0.44	0.35	0.46	0.29
<b>P25DMA 20% TiO<sub>2</sub></b>	1.06	0.96	1.01	0.77	0.98	0.98

## E.2 Chapter 5 Data

### E.2.1 RFID Sensor (Section 5.1.1)

Table E.9: Flexible vs. Rigid RFID Sensor

Gas Mixture	Ethanol Concentration	Rigid			Flexible		
		OV 275	OV 225	SXFA	OV 275	OV 225	SXFA
Ethanol	1250	1.35	0.73	1.01	1.08	0.41	1.47
Methanol	1250	1.03	0.64	1.86	1.47	1.25	1.46
Benzene	1250	0.43	0.12	0.65	0.41	0.16	0.71
Acetone	1250	1.75	1.35	1.74	1.42	0.82	1.35
E-M	1250	2.28	1.18	3.08	2.71	1.25	2.85
	625	1.54	0.86	2.07	1.97	0.91	2.4
E-A	1250	2.44	1.17	2.81	2.39	1.14	2.76
	625	1.54	0.69	2.11	1.85	0.63	2.17
E-B	1250	1.82	0.87	1.53	1.61	0.73	1.44
	625	1.33	0.36	2.19	1.12	0.42	1.95
E-M-A	1250	3.56	2.81	4.17	3.53	2.67	4.21
	625	3.42	2.74	4.13	3.47	2.59	3.97
E-M-B	1250	2.65	1.27	3.21	2.81	1.44	3.13
	625	2.13	0.71	2.74	2.27	1.79	2.87
E-A-B	1250	3.57	2.31	3.45	3.31	1.98	3.47
	625	2.99	1.78	2.65	2.76	1.44	2.79
E-M-B-A	1250	3.66	2.91	5.44	3.69	2.78	4.89
	625	3.68	2.48	4.98	3.66	2.66	4.68

Note that E, M, A, and B are ethanol, methanol, acetone, and benzene, respectively.

Table E.10: Rigid vs Flexible Sensor

Gas Mixture	Ethanol Concentration	Rigid			Flexible		
		P25DMA	20% NiO	20% ZnO	P25DMA	20% NiO	20% ZnO
Ethanol	1250	1.51	3.92	0.01	1.22	4.75	0.02
Methanol	1250	0.91	1.21	0.03	0.70	1.35	0.05
Benzene	1250	0.39	0.18	0.71	0.29	0.13	0.59
Acetone	1250	0.71	0.64	0.00	0.69	0.43	0.02
E-M	1250	2.53	5.33	0.06	2.21	5.71	0.07
	625	1.51	3.34	0.04	1.45	3.11	0.04
E-A	1250	2.18	4.74	0.01	1.97	5.01	0.01
	625	1.63	2.89	0.02	1.48	2.65	0.01
E-B	1250	1.85	4.33	0.75	1.71	4.28	0.51
	625	1.00	2.35	0.72	1.03	2.07	0.52
E-M-A	1250	2.97	6.35	0.06	2.88	6.39	0.07
	625	2.41	3.44	0.06	2.19	3.47	0.06
E-M-B	1250	2.73	6.00	0.73	2.36	6.18	0.51
	625	2.11	3.49	0.73	1.97	3.1	0.5
E-A-B	1250	2.69	4.99	0.73	2.37	5.07	0.52
	625	1.94	2.88	0.72	1.73	2.61	0.52
E-M-B-A	1250	3.27	6.3	0.76	3.41	6.47	0.71
	625	2.53	4.05	0.78	2.56	4.01	0.68

Note that E, M, A, and B are ethanol, methanol, acetone, and benzene, respectively.

Table E.11. RFID Sensor Array Data

Gas Mixture	Ethanol Concentration	Rigid			Flexible		
		P25DMA	20% NiO	20% ZnO	P25DMA	20% NiO	20% ZnO
Ethanol	1250	1.35	0.73	1.01	1.51	3.92	0.01
Methanol	1250	1.03	0.64	1.86	0.91	1.21	0.03
Benzene	1250	0.43	0.12	0.65	0.39	0.18	0.71
Acetone	1250	1.75	1.35	1.74	0.71	0.64	0.00
E-M	1250	2.28	1.18	3.08	2.53	5.33	0.06
	625	1.54	0.86	2.07	1.51	3.34	0.04
E-A	1250	2.44	1.17	2.81	2.18	4.74	0.01
	625	1.54	0.69	2.11	1.63	2.89	0.02
E-B	1250	1.82	0.87	1.53	1.85	4.33	0.75
	625	1.33	0.36	2.19	1.00	2.35	0.72
E-M-A	1250	3.56	2.81	4.17	2.97	6.35	0.06
	625	3.42	2.74	4.13	2.41	3.44	0.06
E-M-B	1250	2.65	1.27	3.21	2.73	6.00	0.73
	625	2.13	0.71	2.74	2.11	3.49	0.73
E-A-B	1250	3.57	2.31	3.45	2.69	4.99	0.73
	625	2.99	1.78	2.65	1.94	2.88	0.72
E-M-B-A	1250	3.66	2.91	5.44	3.27	6.3	0.76
	625	3.68	2.48	4.98	2.53	4.05	0.78

Note that E, M, A, and B are ethanol, methanol, acetone, and benzene, respectively.

### E.2.2 MEMS Sensor (Section 5.1.2)

Table E.12: MEMS Sensor

Sensing Material	Set-off Voltage	Ethanol Concentration (ppm)
PANI 10% NiO	20	1000
	15	100
	1	50
P25DMA	5	50
	1	5

### E.2.3 Backbone Studies (Section 5.2)

Table E.13: PANI vs PPy to Ethanol

Time (min)	Amount Not Sorbed (ppm)					
	60	72	60	72	60	72
PANI	3.78	3.80	3.96	4.02	3.99	3.89
PPy	3.40	3.49	3.43	3.48	3.39	3.49

Table E.14: P25DMA vs PDPMO to Ethanol

Time (min)	Amount Not Sorbed (ppm)					
	60	72	60	72	60	72
P25DMA	3.39	3.48	3.05	3.14	3.35	3.72
PDMPO	4.71	4.66	4.33	4.30	4.46	4.52

### E.2.4 Functional Group Studies (Section 5.3)

Table E.15: PMMA vs PVP to Ethanol

Time (min)	Amount Not Sorbed (ppm)					
	60	72	60	72	60	72
PMMA	3.64	3.64	3.65	3.70	3.97	3.67
PVP	4.14	4.10	3.47	3.77	3.91	3.94

Table E.16: PANI and Derivatives to Ethanol

Time (min)	Amount Not Sorbed (ppm)					
	60	72	60	72	60	72
PANI	4.33	4.44	4.32	4.46	4.32	4.42
PoANI	4.71	4.88	4.57	4.69	4.86	5.00
P25DMA	3.66	4.05	4.06	4.22	3.76	4.17

Table E.17: Percent Response to Ethanol, Methanol, and Acetone

	Percent Response Change (%)		
	Ethanol	Acetone	Methanol
<b>OV275</b>	3.72	5.76	3.99
	3.85	4.88	3.75
<b>OV225</b>	1.54	3.57	2.46
	1.36	3.49	2.21
<b>SXFA</b>	4.76	5.58	7.13
	4.78	5.03	6.84

***E.2.5 Batch to Batch Comparison (Section 5.5.1)***

Table E.18: Amount of Ethanol Sorbed onto Two Batches of PANI 5% NiO

	Amount Sorbed (ppm)	
	Sample 1	Sample 2
<b>Batch 1</b>	3.12	3.22
<b>Batch 2</b>	3.28	3.15

*Note 10 ppm of ethanol was used instead of 5 ppm.*

***E.2.6 Operator Comparison (Section 5.5.2)***

Table E.19: Amount of Ethanol Sorbed onto PANI 5% NiO Prepared by Two Operators

	Amount Sorbed (ppm)		
	Sample 1	Sample 2	Sample 3
Operator 1	3.48	3.37	3.49
Operator 2	3.53	3.35	3.36

*Note 10 ppm of ethanol was used instead of 5 ppm.*

***E.2.7 Day to Day Comparison (Section 5.5.3)***

Table E.20: Amount of Ethanol Sorbed onto PANI 5% NiO Measured on Different Days

	Amount Sorbed (ppm)	
	Sample 1	Sample 2
Day 1	3.48	3.53
Day 2	3.37	3.35
Day 3	3.49	3.36

*Note 10 ppm of ethanol was used instead of 5 ppm.*

### E.2.8 Powder vs. Film (Section 5.5.4)

Table E.21: Amount of Ethanol Sorbed onto PVP and PMMA Powders and Films

Time (min)	Amount of Ethanol Sorbed (ppm)					
	60	72	60	72	60	72
<b>PVP Film</b>	0.86	0.90	1.14	1.18	1.09	1.06
<b>PVP Powder</b>	0.77	0.76	1.07	0.98	1.3	1.09
<b>PMMA Film</b>	1.36	1.36	1.35	1.30	1.07	1.02
<b>PMMA Powder</b>	1.03	0.74	0.86	0.73	1.41	1.13

## E.3 Chapter 7 Data

### E.3.1 PANI vs. PNMA (Section 7.3.1.1)

Table E.22: Amount of Analyte Sorbed onto PANI and PNMA

Time (min)	Amount Sorbed (ppm)					
	60	72	60	72	60	72
<b>Ethanol-PANI</b>	1.20	1.18	1.02	0.96	0.99	1.09
<b>Acetone-PANI</b>	0.38	0.38	0.32	0.35	0.48	0.50
<b>Ethanol-PNMA</b>	0.51	0.44	0.42	0.40	0.47	0.48
<b>Acetone-PNMA</b>	0.00	0.00	0.09	0.05	0.03	0.03

### E.3.2 Commercial Polymers (Section 7.4.2)

Table E.23: Amount of Ethanol Sorbed

Time (min)	Amount of Ethanol Sorbed (ppm)					
	60	72	60	72	60	72
<b>PPO</b>	0.91	1.20	1.50	1.48	0.78	0.81
<b>PPy</b>	1.58	1.49	1.55	1.50	1.59	1.49
<b>PMMA</b>	1.34	1.34	1.33	1.28	1.01	1.31
<b>PVP</b>	0.84	0.88	1.51	1.21	1.07	1.04
<b>PEI</b>	0.01	0.04	0.13	0.05	-0.01	0.01

Table E.24: Amount of Acetone Sorbed

Time (min)	Amount of Acetone Sorbed (ppm)					
	60	72	60	72	60	72
<b>PPO</b>	0.31	0.27	0.29	0.28	0.38	0.36
<b>PPy</b>	0.09	0.13	0.14	0.13	0.23	0.18
<b>PMMA</b>	0.17	0.18	0.09	0.09	0.27	0.29
<b>PVP</b>	0.00	0.00	0.00	0.09	0.05	0.00

Table E.25: Amount of Methanol Sorbed

<b>Time (min)</b>	<b>Amount of Methanol Sorbed (ppm)</b>					
	<b>60</b>	<b>72</b>	<b>60</b>	<b>72</b>	<b>60</b>	<b>72</b>
<b>PPO</b>	0.00	0.00	0.33	0.36	0.20	0.14
<b>PPy</b>	0.61	0.52	0.79	0.65	0.79	0.72
<b>PMMA</b>	0.00	0.02	0.39	0.32	0.35	0.38
<b>PVP</b>	0.00	0.00	0.00	0.00	0.00	0.00



## Appendix F: Statistical Analysis Tables

Appendix F contains all the statistical analysis that was done with the data shown in Appendix E. The data were analyzed using analysis of variance (ANOVA), Bonferroni's t-test and Fisher's least significant difference (LSD). Again, this appendix has been divided into subsections similar to Appendix E, for ease of relating the data to the analysis.

The Analysis of Variance (ANOVA) tables list the sum of squares (SS) (see Equations F.2 – F.4), the degrees of freedom (DF) (see Equations F.5 – F.7), and mean square (MS) (see Equations F.8 – F.9), as well as the  $F_{\text{observed}}$  (see Equation F.10) and the  $F_{\text{critical}}$  (from the F-table). Note that B stands for 'between treatments', and W stands for 'within treatment' (a.k.a. error). In addition, all these equations assume N is the total number of samples, where n is the sample size for k treatments.

$$\text{Correction for mean} = \frac{1}{\sum_{t=1}^k n_t} \left( \sum_{t=1}^k \sum_{i=1}^{n_t} y_{ti} \right)^2 \quad (\text{Equation F.1})$$

$$SS_B = \sum_{t=1}^k n_t (\bar{y}_t - \bar{y})^2 = \sum_{t=1}^k \frac{(\text{treatment totals})^2}{n_t} - \text{Correction for mean} \quad (\text{Equation F.2})$$

$$SS_W = \sum_{t=1}^k \sum_{i=1}^{n_t} (y_{ti} - \bar{y}_t)^2 = SS_{\text{Total}} - SS_B \quad (\text{Equation F.3})$$

$$SS_{\text{Total}} = \sum_{t=1}^k \sum_{i=1}^{n_t} (y_{ti} - \bar{y})^2 = \sum_{t=1}^k \sum_{i=1}^{n_t} \text{Obs}^2 - \text{Correction for mean} \quad (\text{Equation F.4})$$

$$df_B = k - 1 \quad (\text{Equation F.5})$$

$$df_W = \sum_{t=1}^k (n_t - 1) = df_{\text{Total}} - df_B \quad (\text{Equation F.6})$$

$$df_{\text{Total}} = \sum_{t=1}^k n_t - 1 \quad (\text{Equation F.7})$$

$$MS_B = \frac{SS_B}{df_B} \quad (\text{Equation F.8})$$

$$MS_W = \frac{SS_W}{df_W} \quad (\text{Equation F.9})$$

$$F_{\text{observed}} = \frac{MS_B}{MS_W} \quad (\text{Equation F.10})$$



If blocking was used to separate the effects of the blocks from the treatments (as was the case for the sensing materials (blocks) on different sensors (treatments)), then the following equations (see Equations F.11 – F.17) were used instead of Equations F.1 – F. 10 for the ANOVA table.

$$\text{Correction for the mean} = \frac{1}{kn} \left( \sum_{t=1}^k \sum_{i=1}^n y_{it} \right)^2 \quad (\text{Equation F.11})$$

$$S_{\text{Treatment}} = \frac{1}{n} \sum_{t=1}^k (\text{Treatment Totals})^2 - \text{Correction for the mean} \quad (\text{Equation F.12})$$

$$df_{\text{Treatment}} = k - 1 \quad (\text{Equation F.13})$$

$$S_{\text{Block}} = \frac{1}{k} \sum_{i=1}^n (B; \text{lock Totals})^2 - \text{Correction for the mean} \quad (\text{Equation F.14})$$

$$df_{\text{Block}} = k - 1 \quad (\text{Equation F.15})$$

$$S_{\text{Total}} = \sum_t \sum_i y_{ti}^2 - \text{Correction for the mean} \quad (\text{Equation F.16})$$

$$df_{\text{Total}} = n \cdot k - 1 \quad (\text{Equation F.17})$$

When the null hypothesis was rejected, a paired comparison test was needed to identify which pairs of means ( $\mu$ ) were significantly different from one another. Therefore the Bonferroni t-test (see Equations F.18 – F.20) and the Fisher's Least Significant Difference (LSD) (see Equations F.20 - F.22) were used.

$$s = \sqrt{MS_W} \quad (\text{Equation F.18})$$

$$T_{\text{observed}} = \frac{\bar{y}_i - \bar{y}_j}{s \sqrt{\frac{1}{n_i} + \frac{1}{n_j}}} \quad (\text{Equation F.19})$$

$$t_{N-k, \frac{\alpha}{2}}, \text{ where } N = \sum_{t=1}^k n_t \quad (\text{Equation F.20})$$

$$s.e. = \sqrt{\frac{2s^2}{n}} \quad (\text{Equation F.21})$$

$$LSD = s.e. \cdot t_{N-k, \frac{\alpha}{2}} \quad (\text{Equation F.22})$$

Below are the ANOVA tables that summarize the data evaluated in Chapters 4 and 6. In addition, the paired comparisons are also summarized in tables, with the significantly different means ( $\mu$ ) highlighted. Also, the percent error (see Equations F.23 – F.26) corresponding to the data analyzed by ANOVA is summarized in a table below the appropriate ANOVA table (i.e. for each comparison made in the thesis, the ANOVA table and percent error are listed together).

$$\bar{X} = \frac{1}{n} \sum_{i=1}^n X_i \quad (\text{Equation F.23})$$

$$S^2 = \frac{\sum_{i=1}^n (X_i - \bar{X})^2}{n-1} = \frac{1}{n-1} \left\{ \sum_{i=1}^n X_i^2 - \frac{1}{n} (\sum_{i=1}^n X_i)^2 \right\} \quad (\text{Equation F.24})$$

$$s = \sqrt{S^2} \quad (\text{Equation F.25})$$

$$\% \text{ error} = \frac{s}{\bar{X}} \times 100 \quad (\text{Equation F.26})$$

## F.1 Analysis from Chapter 4

### F.1.1 Analysis for PANI and Its Derivatives (Section 4.3.1)

Table F.1: ANOVA Comparing Ethanol Sorption on PANI, PoANI, and P25DMA

Source	SS	df	MS	F <sub>observed</sub>	F <sub>2,6,0.05</sub>
<b>Between Polymers</b>	0.40	2	0.20	<b>39.69</b>	<b>5.14</b>
<b>Within Polymers</b>	0.03	6	0.01		
<b>Total</b>	0.43	8			

There is a significant difference between at least one pair of means, therefore the Bonferroni t-test and Fisher's LSD were used to determine which means were different. The means highlighted in red in Table F.2 were significantly different. The polymers are labelled A-C in Table F.3, which also lists the percent error based on three independent replicates for each polymer.

Table F.2: Bonferroni t-test and Fisher's LSD Comparing Ethanol Sorption PANI and Its Derivatives

Mean Comparison	T <sub>obs</sub>	LSD
<b>A-B</b>	4.67	0.269
<b>A-C</b>	4.24	0.244
<b>B-C</b>	8.91	0.513

See Table F.3 for polymer designations A-C. Highlighted rows are those that have means that are significantly different. Note that  $t_{6,0.0005} = 5.959$  and  $LSD = 0.343$ .

Table F.3 Percent Error for Ethanol Sorption onto PANI, PoANI, and P25DMA

	Polymer	Average (ppm)	Standard Deviation	Percent Error (%)
<b>A</b>	PANI	0.62	0.02	<b>0.34</b>
<b>B</b>	PoANI	0.35	0.08	<b>1.75</b>
<b>C</b>	P25DMA	0.88	0.12	<b>2.98</b>

*F.1.2 Analysis for Doped PANI and PoANI (Section 4.3.2)*

Table F.4: ANOVA Comparing Ethanol Sorption on Doped and Undoped PANI and PoANI

Source	SS	df	MS	F <sub>observed</sub>	F <sub>9,20,0.05</sub>
<b>Between Polymers</b>	1.56	9	0.17	<b>34.89</b>	<b>2.39</b>
<b>Within Polymers</b>	0.10	20	0.01		
<b>Total</b>	1.66	29			

There is a significant difference between at least one pair of means, therefore the Bonferroni t-test and Fisher’s LSD were employed to determine which means were different. The means highlighted in red in Table F.5 were significantly different. The polymers are labelled A-J in Table F.6, which also lists the percent error based on three independent replicates for each polymer.

Table F.5: Bonferroni t-test and Fisher’s LSD Comparing Ethanol Sorption on Doped and Undoped PANI and PoANI

Mean Comparison	T <sub>obs</sub>	LSD	Mean Comparison	T <sub>obs</sub>	LSD	Mean Comparison	T <sub>obs</sub>	LSD
<b>A-B</b>	0.32	0.019	<b>B-I</b>	6.12	0.352	<b>E-F</b>	3.61	0.208
<b>A-C</b>	1.27	0.073	<b>B-J</b>	5.56	0.320	<b>E-G</b>	5.86	0.338
<b>A-D</b>	2.80	0.161	<b>C-D</b>	4.07	0.234	<b>E-H</b>	2.08	0.120
<b>A-E</b>	1.06	0.061	<b>C-E</b>	0.21	0.012	<b>E-I</b>	7.51	0.432
<b>A-F</b>	4.67	0.269	<b>C-F</b>	3.40	0.196	<b>E-J</b>	6.95	0.400
<b>A-G</b>	6.93	0.399	<b>C-G</b>	5.65	0.326	<b>F-G</b>	2.26	0.130
<b>A-H</b>	1.02	0.059	<b>C-H</b>	2.29	0.132	<b>F-H</b>	5.69	0.328
<b>A-I</b>	6.44	0.371	<b>C-I</b>	7.71	0.444	<b>F-I</b>	11.11	0.640
<b>A-J</b>	5.89	0.339	<b>C-J</b>	7.16	0.412	<b>F-J</b>	10.56	0.608
<b>B-C</b>	1.60	0.092	<b>D-E</b>	3.86	0.222	<b>G-H</b>	7.95	0.458
<b>B-D</b>	2.47	0.142	<b>D-F</b>	7.47	0.430	<b>G-I</b>	13.37	0.770
<b>B-E</b>	1.39	0.080	<b>D-G</b>	9.72	0.560	<b>G-J</b>	12.81	0.738
<b>B-F</b>	4.99	0.288	<b>D-H</b>	1.78	0.102	<b>H-I</b>	5.42	0.312
<b>B-G</b>	7.25	0.418	<b>D-I</b>	3.65	0.210	<b>H-J</b>	4.87	0.280
<b>B-H</b>	1.02	0.040	<b>D-J</b>	3.09	0.178	<b>I-J</b>	0.56	0.032

See Table F.6 for polymer designations A-J. Highlighted rows are those that have means that are significantly different. Note that  $t_{20, 0.0005} = 3.850$  and  $LSD = 0.222$ .

Table F.6: Percent Error Comparing Ethanol Sorption on Doped and Undoped PANI and PoANI

	<b>Polymer</b>	<b>Average (ppm)</b>	<b>Standard Deviation</b>	<b>Percent Error (%)</b>
<b>A</b>	PANI	0.62	0.02	<b>0.34</b>
<b>B</b>	PANI 10% NiO	0.63	0.08	<b>1.87</b>
<b>C</b>	PANI 20% NiO	0.54	0.01	<b>0.31</b>
<b>D</b>	PANI 10% ZnO	0.78	0.09	<b>2.12</b>
<b>E</b>	PANI 20% ZnO	0.55	0.07	<b>1.57</b>
<b>F</b>	PoANI	0.35	0.08	<b>1.75</b>
<b>G</b>	PoANI 10% NiO	0.22	0.01	<b>0.26</b>
<b>H</b>	PoANI 20% NiO	0.67	0.04	<b>0.83</b>
<b>I</b>	PoANI 10% ZnO	0.99	0.07	<b>1.75</b>
<b>J</b>	PoANI 20% ZnO	0.95	0.13	<b>3.21</b>

*F.1.3 Analysis for Doped P25DMA (Section 4.3.3)*

Table F.7: ANOVA Comparing Ethanol Sorption on P25DMA and P25DMA Doped with Al<sub>2</sub>O<sub>3</sub>

<b>Source</b>	<b>SS</b>	<b>df</b>	<b>MS</b>	<b>F<sub>observed</sub></b>	<b>F<sub>3,8,0.05</sub></b>
<b>Between Polymers</b>	0.71	3	0.24	<b>5.90</b>	<b>4.07</b>
<b>Within Polymers</b>	0.32	8	0.04		
<b>Total</b>	1.03	11			

There is a significant difference between at least one pair of means, therefore the Bonferroni t-test and Fisher’s LSD were used to determine which means were different. The means highlighted in red in Table F.8 were significantly different. The polymers are labelled A-D in Table F.9, which also lists the percent error based on three independent replicates for each polymer.

Table F.8: Bonferroni t-test and Fisher’s LSD Comparing Ethanol Sorption on P25DMA and P25DMA Doped with Al<sub>2</sub>O<sub>3</sub>

<b>Mean Comparison</b>	<b>T<sub>obs</sub></b>	<b>LSD</b>
<b>A-B</b>	<b>0.640</b>	<b>3.91</b>
<b>A-C</b>	0.525	3.20
<b>A-D</b>	0.468	2.86
<b>B-C</b>	0.115	0.70
<b>B-D</b>	0.172	1.05
<b>C-D</b>	0.057	0.35

See Table F.9 for polymer designations A-D. Highlighted rows are those that have means that are significantly different. Note that  $t_{8, 0.0005} = 3.355$  and  $LSD = 0.550$ .

Table F.9: Percent Error Comparing Ethanol Sorption on P25DMA and P25DMA Doped with CuO

	<b>Polymer</b>	<b>Average (ppm)</b>	<b>Standard Deviation</b>	<b>Percent Error (%)</b>
<b>A</b>	P25DMA	0.88	0.12	<b>2.98</b>
<b>B</b>	P25DMA 5% Al <sub>2</sub> O <sub>3</sub>	1.52	0.17	<b>4.87</b>
<b>C</b>	P25DMA 10% Al <sub>2</sub> O <sub>3</sub>	1.40	0.19	<b>5.20</b>
<b>D</b>	P25DMA 20% Al <sub>2</sub> O <sub>3</sub>	1.34	0.25	<b>6.87</b>

Table F.10: ANOVA Comparing Ethanol Sorption on P25DMA and P25DMA Doped with CuO

<b>Source</b>	<b>SS</b>	<b>df</b>	<b>MS</b>	<b>F<sub>observed</sub></b>	<b>F<sub>3,8,0.05</sub></b>
<b>Between Polymers</b>	1.12	3	0.37	<b>57.36</b>	<b>4.07</b>
<b>Within Polymers</b>	0.05	8	0.01		
<b>Total</b>	1.18	11			

There is a significant difference between at least one pair of means, therefore the Bonferroni t-test and Fisher's LSD were employed to determine which means were different. The means highlighted in red in Table F.11 were significantly different. The polymers are labelled A-D in Table F.12, which also lists the percent error based on three independent replicates for each polymer.

Table F.11: Bonferroni t-test and Fisher's LSD Comparing Ethanol Sorption on P25DMA and P25DMA Doped with CuO

<b>Mean Comparison</b>	<b>T<sub>obs</sub></b>	<b>LSD</b>
<b>A-B</b>	11.26	0.743
<b>A-C</b>	9.17	0.605
<b>A-D</b>	8.23	0.543
<b>B-C</b>	2.10	0.138
<b>B-D</b>	3.03	0.200
<b>C-D</b>	0.93	0.062

See Table F.12 for polymer designations A-D. Highlighted rows are those that have means that are significantly different. Note that  $t_{8, 0.0005} = 3.355$  and  $LSD = 0.221$ .

Table F.12: Percent Error Comparing Ethanol Sorption on P25DMA and P25DMA Doped with CuO

	<b>Polymer</b>	<b>Average (ppm)</b>	<b>Standard Deviation</b>	<b>Percent Error (%)</b>
<b>A</b>	P25DMA	0.88	0.12	<b>2.98</b>
<b>B</b>	P25DMA 5% CuO	0.08	0.06	<b>1.18</b>
<b>C</b>	P25DMA 10% CuO	0.21	0.10	<b>2.06</b>
<b>D</b>	P25DMA 20% CuO	0.27	0.08	<b>1.74</b>

Table F.13: ANOVA Comparing Ethanol Sorption on P25DMA and P25DMA Doped with NiO

<b>Source</b>	<b>SS</b>	<b>df</b>	<b>MS</b>	<b>F<sub>observed</sub></b>	<b>F<sub>3,8,0.05</sub></b>
<b>Between Polymers</b>	1.41	3	0.47	<b>14.00</b>	<b>4.07</b>
<b>Within Polymers</b>	0.27	8	0.03		
<b>Total</b>	1.68	11			

There is a significant difference between at least one pair of means, therefore the Bonferroni t-test and Fisher's LSD were used to determine which means were different. The means highlighted in red in Table F.14 were significantly different. The polymers are labelled A-D in Table F.15, which also lists the percent error based on three independent replicates for each polymer.

Table F.14: Bonferroni t-test and Fisher's LSD Comparing Ethanol Sorption on P25DMA and P25DMA Doped with NiO

<b>Mean Comparison</b>	<b>T<sub>obs</sub></b>	<b>LSD</b>
<b>A-B</b>	4.15	0.700
<b>A-C</b>	4.67	0.228
<b>A-D</b>	1.52	0.240
<b>B-C</b>	1.60	0.928
<b>B-D</b>	6.20	0.460
<b>C-D</b>	3.07	0.468

See Table F.15 for polymer designations A-D. Highlighted rows are those that have means that are significantly different. Note that  $t_{8, 0.0005} = 3.355$  and  $LSD = 0.502$ .

Table F.15: Percent Error Comparing Ethanol Sorption on P25DMA and P25DMA Doped with NiO

	<b>Polymer</b>	<b>Average (ppm)</b>	<b>Standard Deviation</b>	<b>Percent Error (%)</b>
<b>A</b>	P25DMA	0.88	0.12	<b>2.98</b>
<b>B</b>	P25DMA 5% NiO	1.58	0.22	<b>6.30</b>
<b>C</b>	P25DMA 10% NiO	0.65	0.20	<b>4.53</b>
<b>D</b>	P25DMA 20% NiO	1.10	0.22	<b>5.53</b>

Table F.16: ANOVA Comparing Ethanol Sorption on P25DMA and P25DMA Doped with TiO<sub>2</sub>

Source	SS	df	MS	F <sub>observed</sub>	F <sub>3,8,0.05</sub>
<b>Between Polymers</b>	1.14	3	0.38	<b>12.20</b>	<b>4.07</b>
<b>Within Polymers</b>	0.25	8	0.03		
<b>Total</b>	1.39	11			

There is a significant difference between at least one pair of means, therefore the Bonferroni t-test and Fisher's LSD were used to determine which means were different. The means highlighted in red in Table F.17 were significantly different. The polymers are labelled A-D in Table F.18, which also lists the percent error based on three independent replicates for each polymer.

Table F.17: Bonferroni t-test and Fisher's LSD Comparing Ethanol Sorption on P25DMA and P25DMA Doped with TiO<sub>2</sub>

Mean Comparison	T <sub>obs</sub>	LSD
<b>A-B</b>	2.16	0.312
<b>A-C</b>	4.17	0.602
<b>A-D</b>	5.61	0.808
<b>B-C</b>	2.01	0.290
<b>B-D</b>	3.44	0.497
<b>C-D</b>	1.43	0.207

See Table F.18 for polymer designations A-D. Highlighted rows are those that have means that are significantly different. Note that  $t_{8, 0.0005} = 3.355$  and  $LSD = 0.484$ .

Table F.18: Percent Error Comparing Ethanol Sorption on P25DMA and P25DMA Doped with TiO<sub>2</sub>

Polymer	Average (ppm)	Standard Deviation	Percent Error (%)
<b>A</b> P25DMA	0.88	0.12	<b>2.98</b>
<b>B</b> P25DMA 5% TiO <sub>2</sub>	1.19	0.23	<b>6.12</b>
<b>C</b> P25DMA 10% TiO <sub>2</sub>	1.48	0.07	<b>2.11</b>
<b>D</b> P25DMA 20% TiO <sub>2</sub>	1.70	0.19	<b>5.70</b>

Table F.19: ANOVA Comparing Ethanol Sorption on P25DMA and P25DMA Doped with ZnO

Source	SS	df	MS	F <sub>observed</sub>	F <sub>3,8,0.05</sub>
<b>Between Polymers</b>	3.45	3	1.15	<b>60.17</b>	<b>4.07</b>
<b>Within Polymers</b>	0.15	8	0.02		
<b>Total</b>	3.60	11			

There is a significant difference between at least one pair of means, therefore the Bonferroni t-test and Fisher's LSD were employed to determine which means were different. The means

highlighted in red in Table F.20 were significantly different. The polymers are labelled A-D in Table F.21, which also lists the percent error based on three independent replicates for each polymer.

Table F.20: Bonferroni t-test and Fisher's LSD Comparing Ethanol Sorption on P25DMA and P25DMA Doped with ZnO

Mean Comparison	T <sub>obs</sub>	LSD
A-B	4.40	0.497
A-C	5.51	0.622
A-D	10.74	1.212
B-C	9.91	1.118
B-D	15.14	1.708
C-D	5.23	0.590

See Table F.21 for polymer designations A-D. Highlighted rows are those that have means that are significantly different. Note that  $t_{8, 0.0005} = 3.355$  and  $LSD = 0.397$ .

Table F.21: Percent Error Comparing Ethanol Sorption on P25DMA and P25DMA Doped with ZnO

	Polymer	Average (ppm)	Standard Deviation	Percent Error (%)
A	P25DMA	0.88	0.12	<b>2.98</b>
B	P25DMA 5% ZnO	1.37	0.18	4.98
C	P25DMA 10% ZnO	0.25	0.26	5.49
D	P25DMA 20% ZnO	0.00	0.16	2.98

#### F.1.4 Analysis for Other Polymers (Section 4.3.4)

Table F.22: ANOVA Comparing Ethanol Sorption on the Other Polymers

Source	SS	df	MS	F <sub>observed</sub>	F <sub>4,10,0.05</sub>
Between Polymers	4.07	4	1.02	<b>35.38</b>	<b>3.478</b>
Within Polymers	0.29	10	0.03		
Total	4.36	14			

There is a significant difference between at least one pair of means, therefore the Bonferroni t-test and Fisher's LSD were used to determine which means were different. The means highlighted in red in Table F.23 were significantly different. The polymers are labelled A-E in Table F.24, which also lists the percent error based on three independent replicates for each polymer.



Table F.23: Bonferroni t-test and Fisher's LSD Comparing Ethanol Sorption on the Other Polymers

Mean Comparison	T <sub>obs</sub>	LSD
<b>A-B</b>	3.03	0.420
A-C	1.12	0.155
A-D	0.16	0.022
<b>A-E</b>	7.77	1.075
B-C	1.91	0.265
<b>B-D</b>	3.19	0.442
<b>B-E</b>	10.80	1.495
C-D	1.28	0.177
<b>C-E</b>	8.88	1.230
<b>D-E</b>	7.61	1.053

See Table F.24 for polymer designations A-E. Highlighted rows are those that have means that are significantly different. Note that  $t_{10, 0.0005} = 3.169$  and  $LSD = 0.439$ .

Table F.24: Percent Error Comparing Ethanol Sorption on the Other Polymers

	Polymer	Average (ppm)	Standard Deviation	Percent Error (%)
<b>A</b>	PPO	1.11	0.33	<b>8.47</b>
<b>B</b>	PPy	1.53	0.05	<b>1.33</b>
<b>C</b>	PMMA	1.27	0.13	<b>3.46</b>
<b>D</b>	PVP	1.27	0.25	<b>6.30</b>
<b>E</b>	PEI	0.04	0.05	<b>1.01</b>

#### *F.1.5 Analysis for Selectivity Studies (Section 4.4)*

Table F.25: ANOVA Comparing Different Analyte Sorption on P25DMA

Source	SS	df	MS	F <sub>observed</sub>	F <sub>9,20,0.05</sub>
<b>Between Polymers</b>	3.98	5	0.80	<b>59.30</b>	<b>3.151</b>
<b>Within Polymers</b>	0.16	12	0.01		
<b>Total</b>	4.14	17			

There is a significant difference between at least one pair of means, therefore the Bonferroni t-test and Fisher's LSD were used to determine which means were different. The means highlighted in red in Table F.26 were significantly different. The analytes are labelled A-F in Table F.27, which also lists the percent error based on three independent replicates for each analyte.

Table F.26: Bonferroni t-test and Fisher's LSD Comparing Different Analyte Sorption on P25DMA

Mean Comparison	T <sub>obs</sub>	LSD	Mean Comparison	T <sub>obs</sub>	LSD	Mean Comparison	T <sub>obs</sub>	LSD
A-B	4.97	0.46	B-C	2.73	0.25	C-E	12.33	1.13
A-C	7.70	0.71	B-D	6.54	0.60	C-F	14.77	1.35
A-D	1.57	0.14	B-E	9.60	0.88	D-E	3.06	0.28
A-E	4.63	0.42	B-F	12.04	1.10	D-F	5.50	0.50
A-F	7.07	0.65	C-D	9.27	0.85	E-F	2.44	0.22

See Table F.6 for analyte designations A-F. Highlighted rows are those that have means that are significantly different. Note that  $t_{12, 0.005} = 3.055$  and  $LSD = 0.199$ .

Table F.27: Percent Error Comparing Different Analyte Sorption on P25DMA

	Analyte	Average (ppm)	Standard Deviation	Percent Error (%)
A	Acetaldehyde	4.37	0.040	<b>0.91</b>
B	Acetone	5.24	0.064	<b>1.22</b>
C	Benzene	5.09	0.010	<b>0.20</b>
D	Ethanol	4.14	0.088	<b>2.11</b>
E	Formaldehyde	3.91	0.113	<b>2.88</b>
F	Methanol	3.30	0.222	<b>6.73</b>

## F.2 Analysis for Chapter 5

### F.2.1 Analysis for RFID Ethanol Sensitivity (Section 5.1.1)

Table F.28: ANOVA Comparing Rigid vs Flexible Sensors

Source	SS	df	MS	F <sub>observed</sub>	F <sub>9,20,0.05</sub>
<b>Sensors (target comparison)</b>	0.029	1	0.029	0.391	<b>4.45</b>
<b>Sensing Materials (blocks)</b>	45.05	5	9.011	119.88	<b>2.81</b>
<b>Error</b>	1.28	17	0.075		
<b>Total</b>	46.36	23			

There is a not a statistically significant difference between the types of RFID sensors, therefore the Bonferroni t-test and Fisher's LSD were not needed between the two types of sensors (rigid and flexible). However, the siloxane-based sensing materials and the P25DMA-based sensing materials did show a significant difference. Therefore, the Bonferroni t-test and the Fisher's LSD were used to determine which sensing materials were significantly different from one another on the rigid sensor (see Table F.29 and F.30).

Table F.29: Bonferroni t-test and Fisher's LSD Comparing the Rigid and Flexible Sensors

Mean Comparison	T <sub>obs</sub>	LSD	Mean Comparison	T <sub>obs</sub>	LSD	Mean Comparison	T <sub>obs</sub>	LSD
A-B	6.01	0.62	B-C	2.72	0.28	C-E	28.22	2.91
A-C	3.30	0.34	B-D	7.56	0.78	C-F	9.70	1.00
A-D	1.55	0.16	B-E	30.94	3.19	D-E	23.37	2.41
A-E	24.92	2.57	B-F	6.98	0.72	D-F	14.55	1.50
A-F	12.99	1.34	C-D	4.85	0.50	E-F	37.92	3.91

See Table F.30 for analyte designations A-F. Highlighted rows are those that have means that are significantly different. Note that  $t_{6, 0.0025} = 4.317$  and  $LSD = 0.509$ . Note that the C-D comparison was significantly different when using the t-test but not when using the LSD. At a higher confidence level, the t-test would show that the T<sub>obs</sub> is less than the t<sub>critical</sub> and therefore, SXFA and P25DMA did not have responses to ethanol that were statistically significantly different.

Table F.30: Percent Error Comparing the Siloxane-based and P25DMA-based Sensing Materials

Sensing Material		Average (% Change)	Standard Deviation	Percent Error (%)
A	OV 275	3.79	0.10	<b>2.42</b>
B	OV 225	1.45	0.13	<b>8.78</b>
C	SXFA	4.77	0.01	<b>0.30</b>
D	P25DMA	5.52	0.44	<b>7.94</b>
E	P25DMA 20% NiO	14.13	0.06	<b>0.45</b>
F	P25DMA 20% ZnO	0.10	0.01	<b>14.14</b>

### F.2.2 Analysis for Backbone Studies (Section 5.2)

Table F.31: PANI vs PPy

Source	SS	df	MS	F <sub>observed</sub>	F <sub>1,4, 0.05</sub>
Between Polymers	0.32	1	0.32	<b>58.28</b>	<b>7.71</b>
Within Polymers	0.02	4	0.01		
Total	0.34	5			

Therefore, there is a statistically significant difference between PANI and PPy.

Table F.32: Percent Error Comparing PANI and PPy

Polymer	Average (ppm)	Standard Deviation	Percent Error (%)
PANI	3.91	0.10	<b>2.57</b>
PPy	3.45	0.05	<b>1.33</b>

Table F.33: P25DMA vs PPO for Ethanol

Source	SS	df	MS	F <sub>observed</sub>	F <sub>1,4, 0.05</sub>
Between Polymers	0.01	1	0.01	<b>0.09</b>	<b>7.71</b>
Within Polymers	0.34	4	0.09		
<b>Total</b>	0.35	5			

Therefore, there is no significant difference between P25DMA and PPO when sorbing ethanol.

Table F.34: Percent Error Comparing P25DMA and PPO for Ethanol

Polymer	Average (ppm)	Standard Deviation	Percent Error (%)
P25DMA	1.06	0.22	<b>5.49</b>
PPO	1.11	0.33	<b>8.47</b>

Table F.35: P25DMA vs PPO for Methanol

Source	SS	df	MS	F <sub>observed</sub>	F <sub>1,4, 0.05</sub>
Between Polymers	1.98	1	1.98	<b>42.38</b>	<b>7.71</b>
Within Polymers	0.19	4	0.05		
<b>Total</b>	2.17	5			

Therefore, there is a statistically significant difference between P25DMA and PPO when sorbing methanol.

Table F.36: Percent Error Comparing P25DMA and PPO for Methanol

Polymer	Average (ppm)	Standard Deviation	Percent Error (%)
P25DMA	3.94	0.25	<b>7.54</b>
PPO	3.87	0.17	<b>3.73</b>

### *F.2.3 Analysis for Functional Group Studies (Section 5.3)*

Table F.37: PMMA vs PVP

Source	SS	df	MS	F <sub>observed</sub>	F <sub>1,4, 0.05</sub>
Between Polymers	0.05	1	0.05	<b>1.29</b>	<b>7.71</b>
Within Polymers	0.15	4	0.04		
<b>Total</b>	0.19	5			

Therefore, there is no significant difference between P25DMA and PPO when sorbing ethanol.

Table F.38: Percent Error Comparing PMMA vs PVP

Polymer	Average (ppm)	Standard Deviation	Percent Error (%)
PMMA	3.71	0.13	<b>3.46</b>
PVP	3.89	0.25	<b>6.30</b>

Table F.39: PANI, PoANI, P25DMA

Source	SS	df	MS	F <sub>observed</sub>	F <sub>2,6, 0.05</sub>
Between Polymers	0.67	2	0.34	<b>36.81</b>	<b>5.14</b>
Within Polymers	0.06	6	0.01		
Total	0.73	8			

There is a significant difference between at least one pair of means, therefore the Bonferroni t-test and Fisher's LSD were used to determine which means were different. The means highlighted in red in Table F.40 were significantly different. The analytes are labelled A-C in Table F.41, which also lists the percent error based on three independent replicates for each analyte.

Table F.40: Bonferroni t-test and Fisher's LSD Comparing

Mean Comparison	T <sub>obs</sub>	LSD
A-B	3.44	0.269
A-C	5.09	0.398
<b>B-C</b>	<b>8.53</b>	<b>0.667</b>

See Table F.41 for analyte designations A-C. Highlighted rows are those that have means that are significantly different. Note that  $t_{6, 0.005} = 5.959$  and  $LSD = 0.466$ .

Table F.41: Percent Error Comparing PANI, PoANI, P25DMA

	Polymer	Average (ppm)	Standard Deviation	Percent Error (%)
<b>A</b>	PANI	3.91	0.10	<b>2.57</b>
<b>B</b>	PoANI	4.29	0.15	<b>3.41</b>
<b>C</b>	P25DMA	3.99	0.23	<b>5.67</b>

Table F.42: OV 275, OV 225, SXFA

Source	SS	df	MS	F <sub>observed</sub>	F <sub>2,3, 0.05</sub>
Between Polymers	17.791	5	3.558	255.979	<b>4.39</b>
Within Polymers	0.083	6	0.014		
Total	17.874	11	1.625		

Table F.43: Bonferroni t-test and Fisher's LSD Comparing OV 275, OV 225, SXFA

Mean Comparison	T <sub>obs</sub>	LSD
<b>A-B</b>	6.01	0.62
A-C	3.30	0.34
B-C	2.72	0.28

See Table F.6 for analyte designations A-F. Highlighted rows are those that have means that are significantly different. Note that  $t_{6, 0.005} = 4.317$  and  $LSD = 0.509$ .

Table F.44: Percent Error Comparing OV 275, OV 225, SXFA

	Polymer	Average (% Change)	Standard Deviation	Percent Error (%)
<b>A</b>	OV 275	3.79	0.10	<b>2.42</b>
<b>B</b>	OV 225	1.45	0.13	<b>8.78</b>
<b>C</b>	SXFA	4.77	0.01	<b>0.30</b>

#### F.2.4 Analysis for Sample Stability (Section 5.4)

Table F.45 shows summary of the ANOVA. Since  $F_{\text{observed}}$  is larger than  $F_{\text{critical}}$ , the null hypothesis cannot be rejected, therefore there was no significant difference in the amount of ethanol sorbed onto each polymer. All of the polymers performed similarly. Thus, no further analysis was needed. The percent error for the amount of ethanol sorbed onto each polymer was obtained using three independent replicates are shown in Table F.46.

Table F.45: ANOVA Table Comparing Sample Stability of PANI

Source	SS	df	MS	F <sub>observed</sub>	F <sub>2,6, 0.05</sub>
<b>Between Polymers</b>	0.14	2.00	0.07	<b>3.42</b>	<b>5.14</b>
<b>Within Polymers</b>	0.12	6.00	0.02		
<b>Total</b>	0.26	8.00			

Table F.46: Percent Error Comparing Sample Stability of PANI

Polymer	Average (ppm)	Standard Deviation	Percent Error (%)
PANI (5 years)	8.00	0.22	<b>2.71</b>
PANI (2 years)	8.31	0.06	<b>0.67</b>
PANI (0 years)	8.16	0.10	<b>1.22</b>

#### F.2.5 Analysis for Batch to Batch Comparison (Section 5.5.1)

Table F.47 shows summary of the ANOVA. Since  $F_{\text{observed}}$  is larger than  $F_{\text{critical}}$ , the null hypothesis cannot be rejected, therefore there was no significant difference in the amount of ethanol sorbed onto each polymer batch. All of the batches performed similarly. Thus, no further analysis was

needed. The percent error for the amount of ethanol sorbed onto each polymer batch was obtained using two independent replicates is shown in Table F.48.

Table F.47: ANOVA Table Comparing Batches

Source	SS	df	MS	F <sub>observed</sub>	F <sub>1,2, 0.05</sub>
<b>Between Polymers</b>	0.0001	1	0.0001	<b>0.012</b>	<b>18.51</b>
<b>Within Polymers</b>	0.016	2	0.008		
<b>Total</b>	0.016	3			

Table F.48: Percent Error Comparing Batches

Polymer	Average (ppm)	Standard Deviation	Percent Error (%)
Batch 1	3.18	0.08	<b>2.45</b>
Batch 2	3.22	0.09	<b>2.86</b>

### *F.2.6 Analysis for Operator Comparison (Section 5.5.2)*

Table F.49 shows summary of the ANOVA. Since F<sub>observed</sub> is larger than F<sub>critical</sub>, the null hypothesis cannot be rejected, therefore there was no significant difference in the amount of ethanol sorbed onto each polymer made by different operators. Thus, no further analysis was needed. The percent error for the amount of ethanol sorbed onto each polymer made by different operators was obtained using two independent replicates is shown in Table F.50.

Table F.49: ANOVA Table Comparing Operators

Source	SS	df	MS	F <sub>observed</sub>	F <sub>2,3, 0.05</sub>
<b>Between Polymers</b>	0.021	2	0.011	<b>3.20</b>	<b>9.55</b>
<b>Within Polymers</b>	0.010	3	0.003		
<b>Total</b>	0.031	5			

Table F.50: Percent Error Comparing Operators

Polymer	Average (ppm)	Standard Deviation	Percent Error (%)
Operator 1	3.45	0.07	<b>1.93</b>
Operator 2	3.41	0.10	<b>2.96</b>

### *F.2.7 Analysis for Day to Day Comparison (Section 5.5.3)*

Table F.51 shows summary of the ANOVA. Since F<sub>observed</sub> is larger than F<sub>critical</sub>, the null hypothesis cannot be rejected, therefore there was no significant difference in the amount of ethanol sorbed onto each polymer when tested on different days. Thus, no further analysis was needed. The percent error for the amount of ethanol sorbed onto each polymer on different days was obtained using two independent replicates is shown in Table F.52.

Table F.51: ANOVA Table Comparing Days

Source	SS	df	MS	F <sub>observed</sub>	F <sub>1,4, 0.05</sub>
<b>Between Polymers</b>	0.002	1	0.002	<b>0.22</b>	<b>7.71</b>
<b>Within Polymers</b>	0.029	4	0.007		
<b>Total</b>	0.031	5			

Table F.52: Percent Error Comparing Days

Polymer	Average (ppm)	Standard Deviation	Percent Error (%)
Day 1	3.51	0.04	<b>1.01</b>
Day 2	3.36	0.01	<b>0.42</b>
Day 3	3.43	0.09	<b>2.68</b>

### *F.2.8 Analysis for Powder versus Film (Section 5.5.4)*

Table F.53 shows summary of the ANOVA. Since  $F_{\text{observed}}$  is larger than  $F_{\text{critical}}$ , the null hypothesis cannot be rejected, therefore there was no significant difference in the amount of ethanol sorbed onto the polymers deposited as a powder or a film. Thus, no further analysis was needed. The percent error for the amount of ethanol sorbed onto each polymer (powder and film) was obtained using three independent replicates is shown in Table F.54.

Table F.53: ANOVA Table Comparing Powder vs Film Deposition

Source	SS	df	MS	F <sub>observed</sub>	F <sub>3,8,0.05</sub>
<b>Between Polymers</b>	0.12	3	0.04	<b>0.95</b>	<b>4.07</b>
<b>Within Polymers</b>	0.32	8	0.04		
<b>Total</b>	0.44	11			

Table F.54: Percent Error Comparing Powder vs Film Deposition

Polymer	Average (ppm)	Standard Deviation	Percent Error (%)
PVP Film	3.96	0.13	<b>3.28</b>
PVP Powder	3.99	0.21	<b>5.19</b>
PMMA Film	3.76	0.16	<b>4.15</b>
PMMA Powder	4.00	0.26	<b>6.57</b>



## F.3 Analysis for Chapter 7

### F.3.1 Effect of Hydrogen Bonding (Section 7.3.1.1)

Table F.55: ANOVA Comparing PANI vs PNMA

Source	SS	df	MS	F <sub>observed</sub>	F <sub>3,8,0.05</sub>
Between Polymers	1.67	3	0.56	<b>112.53</b>	<b>4.07</b>
Within Polymers	0.04	8	0.005		
Total	1.71	11			

There is a significant difference between at least one pair of means, therefore the Bonferroni t-test and Fisher's LSD were used to determine which means were different. The means highlighted in red in Table F.56 were significantly different. The analytes are labelled A-D in Table F.57, which also lists the percent error based on three independent replicates for each analyte.

Table F.56: Bonferroni t-test and Fisher's LSD Comparing PANI and PNMA

Mean Comparison	T <sub>obs</sub>	LSD
<b>A-B</b>	11.68	0.672
<b>A-C</b>	10.78	0.620
<b>A-D</b>	18.09	1.040
<b>B-C</b>	0.90	0.052
<b>B-D</b>	6.41	0.368
<b>C-D</b>	7.31	0.420

See Table F.6 for analyte designations A-F. Highlighted rows are those that have means that are significantly different. Note that  $t_{8, 0.005} = 3.355$  and  $LSD = 0.193$ .

Table F.57: Percent Error Comparing PANI to PNMA

Sensing Material	Average (ppm)	Standard Deviation	Percent Error (%)
<b>A</b> PANI (Ethanol)	3.91	0.10	<b>2.57</b>
<b>B</b> PANI (Acetone)	5.10	0.07	<b>1.42</b>
<b>C</b> PNMA (Ethanol)	4.53	0.04	<b>0.90</b>
<b>D</b> PNMA (Acetone)	5.59	0.06	<b>1.11</b>

### F.3.2 Polymeric Sensing Material Selection Example (Section 7.4.2)

Table F.58: ANOVA Comparing Potential Sensing Materials for Ethanol

Source	SS	df	MS	F <sub>observed</sub>	F <sub>3,8,0.05</sub>
<b>Between Polymers</b>	0.27	3	0.09	<b>2.58</b>	<b>4.07</b>
<b>Within Polymers</b>	0.28	8	0.04		
<b>Total</b>	0.56	11			

Since  $F_{\text{observed}}$  is less than  $F_{\text{critical}}$ , there is no statistically significant difference between the sorption of ethanol onto these polymeric samples.

Table F.59: Percent Error Comparing Potential Sensing Materials for Ethanol

Sensing Material	Average (ppm)	Standard Deviation	Percent Error (%)
<b>A</b>	PPO	3.87	<b>8.47</b>
<b>B</b>	PPy	3.45	<b>1.33</b>
<b>C</b>	PMMA	3.71	<b>3.46</b>
<b>D</b>	PVP	3.89	<b>6.30</b>

Table F.60: ANOVA Comparing Potential Sensing Materials for Methanol

Source	SS	df	MS	F <sub>observed</sub>	F <sub>3,8,0.05</sub>
<b>Between Polymers</b>	0.75	3.00	0.25	<b>12.14</b>	<b>4.07</b>
<b>Within Polymers</b>	0.17	8.00	0.02		
<b>Total</b>	0.92	11.00			

Since  $F_{\text{observed}}$  is greater than  $F_{\text{critical}}$ , there is a statistically significant difference between the sorption of ethanol onto these polymeric samples. Therefore the Bonferroni t-test and Fisher's LSD were used to determine which means were different. The means highlighted in red in Table F.61 were significantly different. The analytes are labelled A-D in Table F.62, which also lists the percent error based on three independent replicates for each analyte.

Table F.61: Bonferroni t-test and Fisher's LSD Comparing Potential Sensing Materials for Methanol

Mean Comparison	T <sub>obs</sub>	LSD	Mean Comparison	T <sub>obs</sub>	LSD
<b>A-B</b>	4.440	0.517	<b>B-C</b>	3.789	0.445
<b>A-C</b>	0.610	0.072	<b>B-D</b>	7.834	0.920
<b>A-D</b>	3.435	0.403	<b>C-D</b>	4.045	0.475

See Table F.62 for analyte designations A-D. Highlighted rows are those that have means that are significantly different. Note that  $t_{8,0.005} = 5.041$  and  $LSD = 0.592$ .

Table F.62: Percent Error Comparing Potential Sensing Materials for Methanol

Sensing Material		Average (ppm)	Standard Deviation	Percent Error (%)
<b>A</b>	PPO	4.50	0.17	<b>3.73</b>
<b>B</b>	PPy	3.98	0.11	<b>2.69</b>
<b>C</b>	PMMA	4.43	0.20	<b>4.44</b>
<b>D</b>	PVP	4.90	0.15	<b>3.16</b>

Table F.63: ANOVA Comparing Potential Sensing Materials for Acetone

Source	SS	df	MS	F <sub>observed</sub>	F <sub>3,8,0.05</sub>
<b>Between Polymers</b>	0.13	3	0.04	<b>12.07</b>	<b>4.07</b>
<b>Within Polymers</b>	0.03	8	0.00		
<b>Total</b>	0.16	11			

Since  $F_{\text{observed}}$  is greater than  $F_{\text{critical}}$ , there is a statistically significant difference between the sorption of ethanol onto these polymeric samples. Therefore the Bonferroni t-test and Fisher's LSD were employed to determine which means were different. The means highlighted in red in Table F.64 were significantly different. The analytes are labelled A-D in Table F.65, which also lists the percent error based on three independent replicates for each analyte.

Table F.64: Bonferroni t-test and Fisher's LSD Comparing Potential Sensing Materials for Acetone

Mean Comparison	T <sub>obs</sub>	LSD	Mean Comparison	T <sub>obs</sub>	LSD
<b>A-B</b>	3.384	0.165	<b>B-C</b>	0.649	0.032
<b>A-C</b>	2.734	0.133	<b>B-D</b>	3.452	0.168
<b>A-D</b>	6.836	0.333	<b>C-D</b>	4.102	0.200

See Table F.65 for analyte designations A-D. Highlighted rows (in Table F.64) are those that have means that are significantly different. Note that  $t_{8,0.005} = 5.041$  and  $LSD = 0.246$ .

Table F.65: Percent Error Comparing Potential Sensing Materials for Ethanol

Sensing Material		Average (ppm)	Standard Deviation	Percent Error (%)
<b>A</b>	PPO	5.19	0.05	<b>0.87</b>
<b>B</b>	PPy	5.35	0.05	<b>0.91</b>
<b>C</b>	PMMA	5.32	0.09	<b>1.61</b>
<b>D</b>	PVP	5.52	0.09	<b>1.55</b>

## Appendix G: Characterization Details

Appendix G includes additional characterization data that were not included in the main text (complementary material to the information of Chapter 4).

### G.1 Additional Energy Dispersive X-ray (EDX) Data

Table G.1: EDX Data

Sample	Weight Percent (%)				
	C	N	O	Metal	S
P25DMA	75.99	10.74	6.25	-	4.51
P25DMA 5% Al <sub>2</sub> O <sub>3</sub>	44.42	15.58	33.18	0.61	6.21
P25DMA 10% Al <sub>2</sub> O <sub>3</sub>	32.69	9.57	16.70	0.57	40.46
P25DMA 20% Al <sub>2</sub> O <sub>3</sub>	71.02	7.49	17.46	0.49	3.54
P25DMA 5% CuO	69.31	9.25	19.78	0.08	0.06
P25DMA 10% CuO	71.94	6.66	19.41	0.07	0.19
P25DMA 20% CuO	68.22	9.64	18.77	0.07	0.24
P25DMA 5% NiO	59.56	6.15	14.94	5.58	5.71
P25DMA 10% NiO	40.09	7.38	32.04	8.11	7.89
P25DMA 20% NiO	47.90	5.05	21.06	19.14	2.27
P25DMA 5% TiO <sub>2</sub>	57.89	7.77	24.94	3.68	0.07
P25DMA 10% TiO <sub>2</sub>	44.75	7.32	31.65	12.37	1.88
P25DMA 20% TiO <sub>2</sub>	41.04	9.69	24.20	17.09	1.53
P25DMA 5% ZnO	66.44	6.10	17.89	0.20	3.75
P25DMA 10% ZnO	60.52	5.37	26.24	0.86	1.05
P25DMA 20% ZnO	19.17	1.52	22.63	46.89	4.58

Table G.2: Representative Percent Error for Three EDX Samples

Sample		C	N	O	Metal	S
P25DMA 5% ZnO	<b>Avg.</b>	66.30	6.55	23.68	0.34	2.89
	<b>Stdev</b>	0.12	0.08	0.36	0.01	0.04
	<b>% Error</b>	0.18	1.19	1.52	2.11	1.47
P25DMA 10% TiO <sub>2</sub>	<b>Avg.</b>	45.49	7.67	29.32	13.25	1.11
	<b>Stdev</b>	1.05	0.49	3.30	1.24	1.09
	<b>% Error</b>	2.30	6.37	11.24	9.34	98.10
P25DMA 20% Al <sub>2</sub> O <sub>3</sub>	<b>Avg.</b>	69.42	7.56	19.70	0.48	2.83
	<b>Stdev</b>	2.26	0.10	3.17	0.01	1.00
	<b>% Error</b>	3.26	1.31	16.08	2.95	35.48

*Note that two replicates each were used in these calculations.*

## G.2 Additional X-ray Diffraction (XRD) Data

Two independent replicates of P25DMA 5% NiO were measured using XRD (see Figure G.1). Note that the peaks appear at approximately the same angles for both replicates.

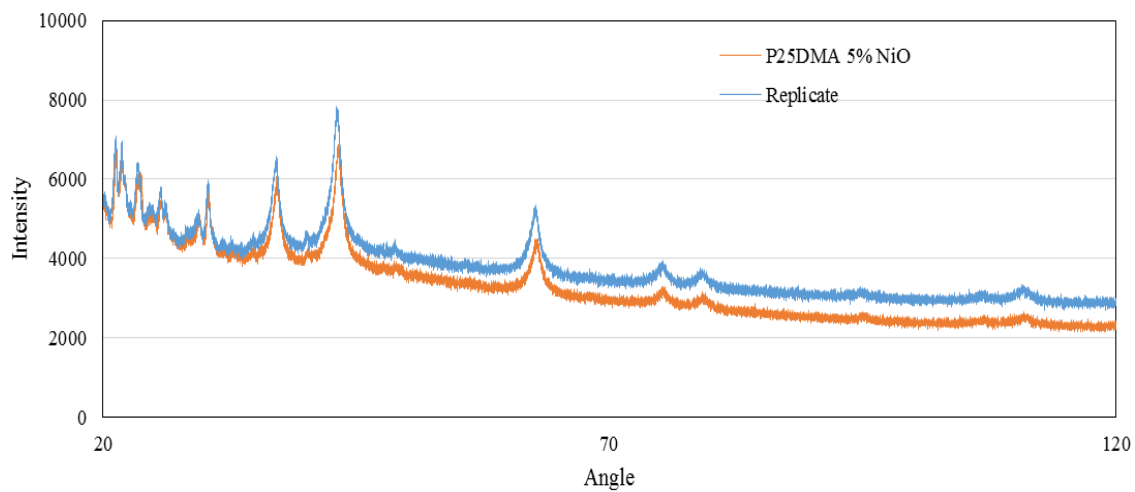


*Figure G.1: XRD for P25DMA 5% NiO and a P25DMA 5% NiO Replicate.*

## Appendix H: Sensor Array Analysis

Appendix H contains additional details about the principal component analysis (PCA) described in Sections 4.6 and 5.1.1.3. These include the data used in the PCA analysis, the factor coordinates of different cases (used to plot the Factors), the factor coordinates of variables, and the eigenvalues (used to create the scree plot).

### H.1 P25DMA Five Sensor Array (Section 4.6)

Table H.1: Data Used for the P25DMA Five Sensor Array

Case	P25DMA	P25DMA 5% Al <sub>2</sub> O <sub>3</sub>	P25DMA 5% NiO	P25DMA 5% ZnO	P25DMA 5% TiO <sub>2</sub>	Group <sup>1</sup>
1	0.76	0.00	0.57	0.4	0.23	1
2	0.70	0.00	0.51	0.35	0.19	1
3	0.80	0.00	0.5	0.38	0.21	1
4	0.69	0.00	0.54	0.32	0.2	1
5	1.09	0.68	1.42	0.9	1.17	2
6	1.42	0.78	1.42	0.76	1.09	2
7	1.16	0.73	1.44	0.82	1.02	2
8	1.10	0.59	1.43	0.74	1.08	2
9	1.27	0.00	0.47	0.21	0.00	3
10	1.18	0.00	0.43	0.02	0.00	3
11	1.61	0.00	0.32	0.31	0.00	3
12	1.52	0.00	0.28	0.12	0.00	3
13	1.04	1.42	1.63	1.48	1.16	4
14	0.95	1.44	1.64	1.37	1.13	4
15	0.94	1.36	1.82	1.58	0.92	4
16	0.78	1.41	1.73	1.49	0.98	4
17	0.29	0.33	0.40	0.22	0.30	5
18	0.25	0.33	0.41	0.14	0.28	5
19	0.24	0.23	0.47	0.14	0.28	5
20	0.17	0.17	0.44	0.07	0.24	5
21	0.05	0.10	0.02	0.00	0.03	6
22	0.00	0.06	0.00	0.00	0.02	6
23	0.00	0.00	0.00	0.00	0.04	6
24	0.00	0.00	0.00	0.00	0.03	6

<sup>1</sup>Where group 1, 2, 3, 4, 5, and 6 are acetaldehyde, formaldehyde, methanol, ethanol, acetone, and benzene.

Table H.2: Factor Coordinates of Cases for the P25DMA Five Sensor Array

<b>Case</b>	<b>Factor 1</b>	<b>Factor 2</b>	<b>Factor 3</b>	<b>Factor 4</b>	<b>Factor 5</b>
1	0.79888	0.314934	-0.001185	-0.403787	-0.041763
2	0.96393	0.223868	-0.027990	-0.349530	-0.027546
3	0.87385	0.396690	-0.039274	-0.332632	-0.098220
4	0.96255	0.207956	0.026551	-0.336770	0.027494
5	-2.08145	0.196998	0.724823	-0.120780	-0.167440
6	-2.12409	0.795445	0.615993	0.266129	0.004229
7	-1.94966	0.356046	0.520808	0.008456	0.066235
8	-1.77291	0.318547	0.802669	-0.102302	0.041810
9	1.03631	1.350877	-0.277734	-0.014917	0.137478
10	1.28927	1.216393	-0.097635	0.172620	0.264240
11	0.89405	1.957201	-0.456912	0.094438	-0.181728
12	1.14700	1.822717	-0.276813	0.281976	-0.054966
13	-3.41829	-0.394568	-0.333787	0.149887	-0.209940
14	-3.26677	-0.543799	-0.278477	0.245158	-0.057807
15	-3.31341	-0.488061	-0.701174	-0.244038	0.158634
16	-3.18485	-0.814038	-0.564251	-0.074330	0.104674
17	0.96671	-0.725089	0.040149	0.177561	-0.013943
18	1.07330	-0.779268	0.092021	0.235248	0.091237
19	1.12044	-0.741462	0.185929	0.059381	0.142252
20	1.33910	-0.813962	0.233259	0.030938	0.197440
21	2.07684	-0.928361	-0.091937	0.152226	-0.067726
22	2.16395	-0.995516	-0.077788	0.087530	-0.085913
23	2.19752	-0.968252	-0.000614	0.010022	-0.118962
24	2.20775	-0.965293	-0.016630	0.007514	-0.109769

Table H.3: Factor Coordinates of Variables for the P25DMA Five Sensor Array

<b>Variable</b>	<b>Factor 1</b>	<b>Factor 2</b>	<b>Factor 3</b>	<b>Factor 4</b>	<b>Factor 5</b>
P25DMA	-0.860587	-0.093836	0.075355	0.493083	-0.004609
P25DMA 5% Al <sub>2</sub> O <sub>3</sub>	-0.421810	-0.260193	-0.689165	-0.527827	0.019266
P25DMA 5% NiO	-0.247501	0.963506	0.023637	-0.097486	0.006925
P25DMA 5% ZnO	-0.268272	-0.252787	0.792929	-0.484276	0.025879
P25DMA 5% TiO <sub>2</sub>	-0.974124	-0.111747	0.046294	-0.167896	-0.088667

Table H.4: Eigenvalues for the P25DMA Five Sensor Array

<b>Factor</b>	<b>Eigenvalue</b>	<b>% Total</b>	<b>Cumulative</b>	<b>Cumulative</b>
1	3.742809	53.46869	3.742809	53.4687
2	1.146553	16.37933	4.889362	69.8480
3	1.120678	16.00968	6.010039	85.8577
4	0.842708	12.03868	6.852747	97.8964
5	0.094470	1.34958	6.947218	99.2460
6	0.033436	0.47766	6.980654	99.7236
7	0.019346	0.27638	7.000000	100.0000



## H.2 RFID Three Sensor Arrays (Section 5.1.1.3)

### H.2.1 RFID Siloxane-based Three Sensor Array

Table H.5: Data Used for the Siloxane-based RFID Three Sensor Array

Case	Ethanol	Methanol	Benzene	Acetone	P25DMA	P25DMA 20% NiO	P25DMA 20% ZnO
1	1250	0	0	0	1.35	0.73	1.01
2	0	1250	0	0	1.03	0.64	1.86
3	0	0	1250	0	0.43	0.12	0.65
4	0	0	0	1250	1.75	1.35	1.74
5	1250	1250	0	0	2.28	1.18	3.08
6	625	1250	0	0	1.54	0.86	2.07
7	1250	0	0	1250	2.44	1.17	2.81
8	625	0	0	1250	1.54	0.69	2.11
9	1250	0	1250	0	1.82	0.87	1.53
10	625	0	1250	0	1.33	0.36	2.19
11	1250	1250	0	1250	3.56	2.81	4.17
12	625	1250	0	1250	3.42	2.74	4.13
13	1250	1250	1250	0	2.65	1.27	3.21
14	625	1250	1250	0	2.13	0.71	2.74
15	1250	0	1250	1250	3.57	2.31	3.45
16	625	0	1250	1250	2.99	1.78	2.65
17	1250	1250	1250	1250	3.66	2.91	5.44
18	625	1250	1250	1250	3.68	2.48	4.98

Table H.6: Factor Coordinates of Cases for the Siloxane-based RFID Three Sensor Array

Case	Factor 1	Factor 2	Factor 3	Factor 4	Factor 5	Factor 6	Factor 7
1	1.89308	0.16523	0.01400	-1.79232	0.360346	-0.122906	0.014319
2	1.98425	-1.07138	-1.60590	0.87769	0.056694	-0.050704	0.013841
3	3.38903	0.31117	0.62781	1.28821	0.143305	-0.165325	-0.189848
4	1.04586	1.70905	-1.38742	0.79639	0.222799	0.001999	0.044145
5	-0.07206	-1.44616	-0.54844	-1.19327	-0.107575	-0.012335	0.185261
6	1.19305	-1.22100	-1.08397	-0.20192	0.086861	0.066973	-0.068668
7	-0.27377	1.25063	-0.31641	-1.33433	-0.552730	0.112197	0.034468
8	1.04261	1.41425	-0.85217	-0.31977	-0.652602	0.058486	-0.173120
9	1.27507	0.00600	1.67875	-0.80534	0.320869	-0.022304	-0.093471
10	1.88735	0.02069	1.18703	0.34489	-0.311349	-0.292982	0.319244
11	-2.72545	-0.13967	-0.97409	-0.72805	0.252070	-0.021799	-0.148254
12	-2.26700	0.02189	-1.47389	0.37546	0.342835	-0.040987	0.138909
13	-0.46441	-1.56816	1.11099	-0.24955	-0.035913	0.192822	-0.080323
14	0.61920	-1.42396	0.62029	0.77883	-0.216859	0.343502	-0.015292
15	-1.82256	1.21300	1.31790	-0.27217	0.270214	0.069029	0.093372
16	-0.60046	1.39751	0.81822	0.72441	0.244505	0.285974	0.022918
17	-3.42073	-0.40994	0.65870	0.33943	-0.227439	-0.415163	-0.203175
18	-2.68306	-0.22914	0.20860	1.37140	-0.196031	0.013524	0.105675

Table H.7: Factor Coordinates of Variables for the Siloxane-based RFID Three Sensor Array

Variable	Factor 1	Factor 2	Factor 3	Factor 4	Factor 5	Factor 6	Factor 7
Ethanol	-0.860587	-0.093836	0.075355	0.493083	-0.004609	0.041767	-0.003295
Methanol	-0.421810	-0.260193	-0.689165	-0.527827	0.019266	0.021192	-0.002220
Benzene	-0.247501	0.963506	0.023637	-0.097486	0.006925	-0.006885	-0.015524
Acetone	-0.268272	-0.252787	0.792929	-0.484276	0.025879	0.014101	-0.001189
P25DMA	-0.974124	-0.111747	0.046294	-0.167896	-0.088667	-0.019981	0.001207
P25DMA 20% NiO	-0.972977	-0.145724	-0.040321	0.154732	0.073962	-0.032172	0.002553
P25DMA 20% ZnO	-0.284534	0.950657	0.004965	-0.121781	0.005596	0.013370	0.015018

Table H.8: Eigenvalues for the Siloxane-based RFID Three Sensor Array

Factor	Eigenvalue	% Total	Cumulative	Cumulative
1	3.742809	53.46869	3.742809	53.4687
2	1.146553	16.37933	4.889362	69.8480
3	1.120678	16.00968	6.010039	85.8577
4	0.842708	12.03868	6.852747	97.8964
5	0.094470	1.34958	6.947218	99.2460
6	0.033436	0.47766	6.980654	99.7236
7	0.019346	0.27638	7.000000	100.0000

### H.2.2 RFID P25DMA-based Three Sensor Array

Table H.9: Data Used for the P25DMA-based RFID Three Sensor Array

Case	Ethanol	Methanol	Benzene	Acetone	P25DMA	P25DMA 20% NiO	P25DMA 20% ZnO
1	1250	0	0	0	1.51	3.92	0.01
2	0	1250	0	0	0.91	1.21	0.03
3	0	0	1250	0	0.39	0.18	0.71
4	0	0	0	1250	0.71	0.64	0.00
5	1250	1250	0	0	2.53	5.33	0.06
6	625	1250	0	0	1.51	3.34	0.04
7	1250	0	0	1250	2.18	4.74	0.01
8	625	0	0	1250	1.63	2.89	0.02
9	1250	0	1250	0	1.85	4.33	0.75
10	625	0	1250	0	1.00	2.35	0.72
11	1250	1250	0	1250	2.97	6.35	0.06
12	625	1250	0	1250	2.41	3.44	0.06
13	1250	1250	1250	0	2.73	6.00	0.73
14	625	1250	1250	0	2.11	3.49	0.73
15	1250	0	1250	1250	2.69	4.99	0.73
16	625	0	1250	1250	1.94	2.88	0.72
17	1250	1250	1250	1250	3.27	6.30	0.76
18	625	1250	1250	1250	2.53	4.05	0.78

Table H.10: Factor Coordinates of Cases for the P25DMA-based RFID Three Sensor Array

Case	Factor 1	Factor 2	Factor 3	Factor 4	Factor 5	Factor 6	Factor 7
1	0.43938	-1.03656	-0.08133	1.95585	-0.042649	0.080369	-0.025268
2	2.51760	-0.96941	-1.51563	-0.73024	-0.000612	-0.023785	0.001324
3	3.07850	2.07503	-0.20032	-0.04236	0.008377	-0.002190	0.003748
4	3.01458	-0.96319	1.21486	-0.63449	0.090342	-0.022638	-0.013548
5	-1.18578	-1.47931	-1.32478	0.71487	-0.168893	-0.026694	0.030433
6	0.79051	-1.21728	-1.43301	0.04795	0.127622	0.033097	-0.003008
7	-0.57092	-1.49444	1.39781	0.84988	0.048023	0.026044	-0.032994
8	1.02696	-1.23025	1.31226	0.07915	-0.028223	-0.116167	0.029671
9	-0.52901	1.59737	-0.01856	1.43788	-0.004202	0.053808	0.042749
10	1.33228	1.82394	-0.11800	0.73729	0.141095	0.039751	0.002611
11	-2.09994	-1.92629	0.13781	-0.32071	0.196713	-0.048182	0.020033
12	-0.16529	-1.61973	0.07384	-1.18419	-0.229610	0.101790	-0.003632
13	-2.10658	1.02406	-1.27589	0.27835	0.074610	-0.112116	-0.024993
14	-0.25364	1.31382	-1.35148	-0.53439	-0.162579	-0.050092	-0.027366
15	-1.59763	1.09514	1.47280	0.28608	-0.123414	-0.032977	-0.001072
16	0.22607	1.35637	1.38171	-0.45647	-0.109621	-0.037800	-0.005466
17	-2.88170	0.66355	0.20757	-0.85780	0.110831	0.045124	-0.018298
18	-1.03539	0.98717	0.12034	-1.62666	0.072190	0.092658	0.025075

Table H.11: Factor Coordinates of Variables for the P25DMA-based RFID Three Sensor Array

Variable	Factor 1	Factor 2	Factor 3	Factor 4	Factor 5	Factor 6	Factor 7
Ethanol	-0.860587	-0.093836	0.075355	0.493083	-0.004609	0.041767	-0.003295
Methanol	-0.421810	-0.260193	-0.689165	-0.527827	0.019266	0.021192	-0.002220
Benzene	-0.247501	0.963506	0.023637	-0.097486	0.006925	-0.006885	-0.015524
Acetone	-0.268272	-0.252787	0.792929	-0.484276	0.025879	0.014101	-0.001189
P25DMA	-0.974124	-0.111747	0.046294	-0.167896	-0.088667	-0.019981	0.001207
P25DMA 20% NiO	-0.972977	-0.145724	-0.040321	0.154732	0.073962	-0.032172	0.002553
P25DMA 20% ZnO	-0.284534	0.950657	0.004965	-0.121781	0.005596	0.013370	0.015018

Table H.12: Eigenvalues for the P25DMA-based RFID Three Sensor Array

<b>Factor</b>	<b>Eigenvalue</b>	<b>% Total</b>	<b>Cumulative</b>	<b>Cumulative</b>
1	3.028322	43.26174	3.028322	43.2617
2	2.006224	28.66034	5.034546	71.9221
3	1.113715	15.91021	6.148261	87.8323
4	0.832721	11.89601	6.980982	99.7283
5	0.014474	0.20676	6.995455	99.9351
6	0.004053	0.05790	6.999508	99.9930
7	0.000492	0.00702	7.000000	100.0000

## Appendix I: Potential Polymeric Sensing Materials for Ethanol

Appendix I contains a list of 50 potential polymeric sensing materials for ethanol, which were identified and ranked based on their likelihood to bind to ethanol. These 50 polymers were ordered based on their potential as sensing materials. The “best” materials are listed at the top and decrease in potential as the list continues. In general, the copolymers are more complicated since copolymer composition can significantly affect the properties. Therefore, the copolymers ranked lower on the list (see Table I.2).

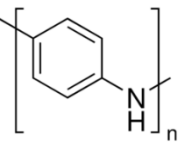
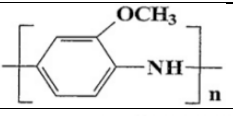
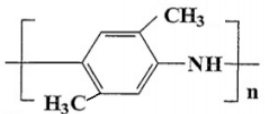
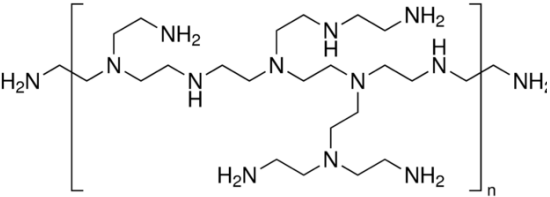
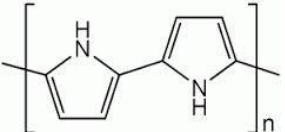
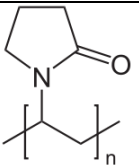
These polymers were chosen based on their chemical nature, using the sensing mechanisms discussed in Chapter 6. Based on the chemical nature of ethanol, three dominant sensing mechanisms, as discussed in Section 6.5.1, were determined for ethanol: hydrogen bonding, polarity, and Lewis acid-base interactions. Based on these sensing mechanisms, polymers were chosen as potential sensing materials for ethanol.

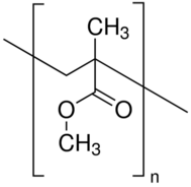
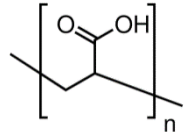
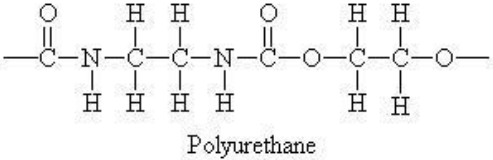
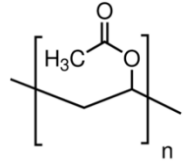
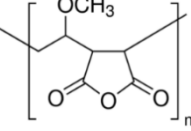
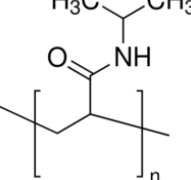
The dominant sensing mechanisms for each polymer are dictated by its functional groups. Table I.1 contains a list of nine functional groups with which ethanol may interact, based on the three dominant mechanisms identified for ethanol. The 50 potential polymeric sensing materials for ethanol all contain at least one of these functional groups and are listed in Table I.2 with their functional groups identified (marked by an x).

Table I.1: Sensing Mechanisms for Polymer Functional Groups

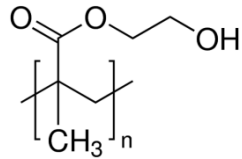
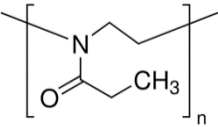
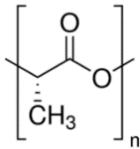
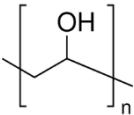
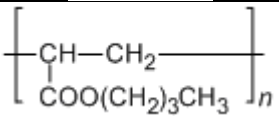
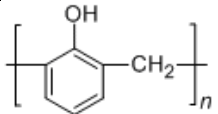
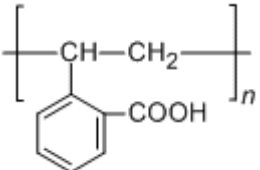
Functional Group		Sensing Mechanism		
		Hydrogen Bonding	Polarity	Lewis Acid-Base
Alcohol	OH	x	x	x
Amine	NH	x	x	x
Carboxylic Acid	COOH	x	x	x
Amide	CON		x	x
Cyano	CN		x	x
Double Bonded Oxygen	=O		x	x
Ester	COOR		x	x
Ether	COR		x	x
Trifluoro	CF <sub>3</sub>		x	x

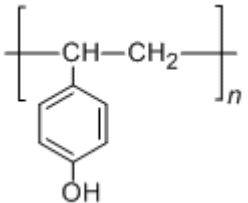
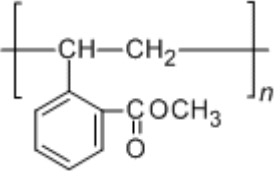
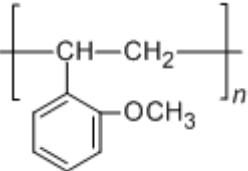
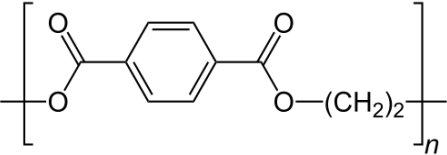
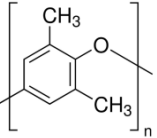
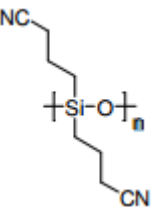
Table I.2: Potential Polymeric Sensing Materials and their Functional Groups

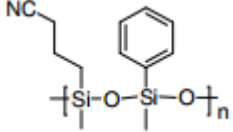
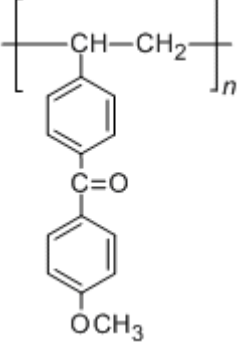
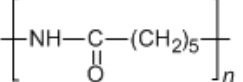
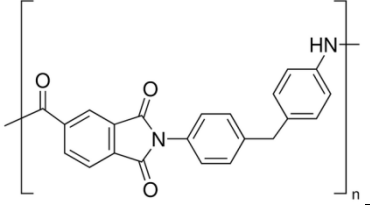
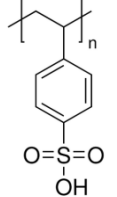
Polymer	Functional Groups Structure	OH	NH	COOH	CON	CN	=O	COOR	COR	CF <sub>3</sub>
Polyaniline			X							
Poly ( <i>o</i> -anisidine)			X						X	
Poly (2,5-dimethyl aniline)			X							
Poly (ethylene imine)			X							
Polypyrrole			X							
Polyvinyl-pyrrolidone					X					

Polymer	Functional Groups Structure	OH	NH	COOH	CON	CN	=O	COOR	COR	CF <sub>3</sub>
Poly (methyl methacrylate)								x		
Poly (acrylic acid)				x						
Polyurethane	 Polyurethane				x			x		
Poly (vinyl acetate)								x		
Poly (maleic anhydride)								x	x	
Poly ( <i>N</i> -isopropyl acrylamide)					x					



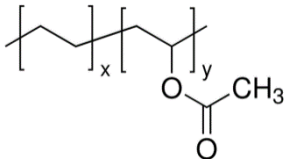
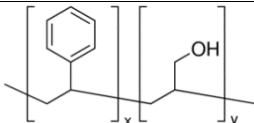
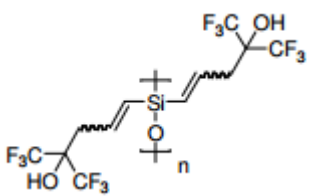
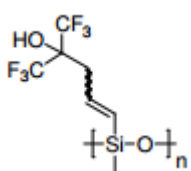
Polymer	Functional Groups Structure	OH	NH	COOH	CON	CN	=O	COOR	COR	CF <sub>3</sub>
		Poly (hydroxyethyl methacrylate)		x						x
Poly (2-oxazoline)					x					
Poly (L-lactide)								x		
Poly (vinyl alcohol)		x								
poly(butyl acrylate)								x		
poly(2-hydroxy-1,3-phenylenemethylene)		x								
poly(2-carboxystyrene)				x						

Polymer	Functional Groups Structure	OH	NH	COOH	CON	CN	=O	COOR	COR	CF <sub>3</sub>
		poly( <i>p</i> -vinylphenol)		x						
poly[2-(methoxycarbonyl)styrene]								x		
poly( <i>o</i> -methoxystyrene)									x	
Polyethylene terephthalate								x		
Poly (2,6-dimethyl-1,4-phenylene oxide)									x	
OV 275 (Seacoast)						x				

Polymer	Functional Groups Structure	OH	NH	COOH	CON	CN	=O	COOR	COR	CF <sub>3</sub>
		OV 225 (Seacoast)						x		
poly[4-(4-methoxybenzoyl)styrene]							x		x	
poly(ethyl 6-aminohexanoate)					x					
Poly(trimellitic anhydride chloride-co-4,4'-methylenedianiline)			x		x					
Poly (4-styrenesulfonic acid)		x					x			

Polymer	Functional Groups Structure	OH	NH	COOH	CON	CN	=O	COOR	COR	CF <sub>3</sub>
Poly (methacrylic acid) (sodium salt)										
poly(3,3'-carbonyldiphenylene 3,3',4,4'-benzophenonetetra carboxydiimide)										
Poly (3,4-ethylenedioxy thiophene)										
Poly (ethylene glycol)										
poly(methylene oxide)										
Poly (vinyl butyral-co-vinyl alcohol-co-vinyl acetate)										
poly[pyrrole-co-aniline]										

Polymer	Functional Groups Structure										
		OH	NH	COOH	CON	CN	=O	COOR	COR	CF <sub>3</sub>	
poly[aniline-co-(p-phenylenediamine)]			x								
Poly (1-vinylpyrrolidone-co-vinyl acetate)					x				x		
Poly ( <i>N</i> -isopropyl acrylamide-co-butylacrylate)					x				x		
Poly (methyl methacrylate-co-methacrylic acid)					x				x		
poly[acrylonitrile-co-(methyl methacrylate)]								x		x	
poly(trimethylene terephthalate)										x	
Poly (vinyl chloride-co-vinyl acetate-co-vinyl alcohol)		x								x	

Polymer	Functional Groups Structure	Functional									
		OH	NH	COOH	CON	CN	=O	COOR	COR	CF <sub>3</sub>	
Poly (ethylene- <i>co</i> -vinyl acetate)									x		
Poly (styrene- <i>co</i> -allyl alcohol)		x									
Adiol (Seacoast)		x									x
SXFA (Seacoast)		x									x



## Appendix J: Safety Considerations

Appendix J contains brief safety considerations (excerpt from the author's safety report).

Table J.1: Safety Precautions for Various Chemicals

Chemical Name	Carcinogen, Toxic, Etc.	Properties	Safety Precautions
Acetone	Toxic	Colourless liquid B.P. 56 C F.P. -16.99 C Highly flammable liquid and vapour	Safety glasses and gloves Incompatible and reactive with: Bases, oxidizing agents, reducing agents, phosphorous oxychloride Exposure through: inhalation, ingestion, eye or skin contact Symptoms: irritated eyes, nose, respiratory tract and skin, dizziness and drowsiness
Ammonium persulfate		White crystals	Safety glasses and gloves Incompatible and reactive with: acids alkalis, halides (fluorides, chlorides, bromides), combustible materials, heavy materials, moisture, reducing agents, heat Decomposes to form: fumes of sulfuric acid mist, oxygen Exposure through: inhalation Symptoms: irritated eyes, nose, respiratory tract and skin



<b>Chemical Name</b>	<b>Carcinogen, Toxic, Etc.</b>	<b>Properties</b>	<b>Safety Precautions</b>
Aniline	Toxic	Colourless, oily liquid B.P. 184 C F.P. 70C Combustible liquid and vapour Air and light sensitive	Safety glasses and gloves Work under fumehood Incompatible and reactive with: strong acids, strong oxidizers, albumin, solutions of iron, zinc aluminum, toluene diisocyanate, alkalis, red fuming nitric acid, and sodium, heat, ignition sources Burns to form: nitrogen oxides, carbon monoxide, carbon dioxide Exposure through: inhalation, ingestion, eye or skin contact Symptoms: bluish discolouration of lips and tongue, severe headache, dizziness, nausea, confusion, shock, irritated skin and eyes, blurred vision
Benzene	Highly carcinogenic	Colourless liquid MW 78.11 g/mol B.P. 80 C F.P. -11 C Combustible liquid and vapour	Safety glasses and gloves Work under a fumehood Incompatible and reactive with: oxidizing materials and halogens Exposure through: inhalation, ingestion, or skin contact Symptoms: irritated skin, and respiratory tract.
Ethanol	Mutagen	Colourless liquid Mild, pleasant odor B.P. 78 °C F.P. -16 °C Flammable	Safety glasses and gloves Work under a fumehood Has caused adverse reproductive and fetal effects in humans

<b>Chemical Name</b>	<b>Carcinogen, Toxic, Etc.</b>	<b>Properties</b>	<b>Safety Precautions</b>
Formaldehyde	Toxic Possible carcinogen	Clear, colourless liquid MW 30.17 g/mol B.P. 96 °C at 760mmHg F.P. 60 °C Combustible liquid and vapour	Safety glasses and gloves Work under a fumehood Incompatible and reactive with: oxidizing materials, alkalis, nitrogen dioxide (~180C), perchloric acid, perchloric acid-aniline mixtures, nitromethane, hydrochloric acid, heat, flames, and ignition sources Decompose to form: carbon monoxide Hazardous polymerization: trioxymethylene precipitate formed on long standing at very low temperature Exposure through: inhalation, ingestion, eye or skin contact Symptoms: irritated eyes, skin, and respiratory tract, severe abdominal pain, violent vomiting, dizziness, headache, blurred vision, shortness of breath
Methanol	Mutagen Toxic	Colourless liquid B.P. = 64.7 °C F.P. = 11 °C Flammable Very volatile	Safety glasses and gloves Work under a fumehood Incompatible and reactive with: strong oxidizing materials Exposure through: inhalation, ingestion, eyes, or skin contact Symptoms: irritated skin, eyes, and respiratory tract, coughing, dizziness, headache, nausea.

<b>Chemical Name</b>	<b>Carcinogen, Toxic, Etc.</b>	<b>Properties</b>	<b>Safety Precautions</b>
Nickel Oxide	Chronic toxicity Carcinogen Skin sensitizer	Dark grey solid powder M.W. 74.96 g/mol	Safety glasses and gloves Respirator Exposure through: inhalation, ingestion, eyes, or skin contact Symptoms: irritated skin, eyes, and respiratory tract
Nitrogen (gas)		Colourless Odorless Acts as an asphyxiant by displacing air	Safety glasses Can cause rapid suffocation
Titanium Oxide	Toxic Carcinogen	White solid powder M.W. 79.87 g/mol	Safety glasses and gloves Respirator Exposure through: inhalation, ingestion, eyes, or skin contact Symptoms: irritated skin, eyes, and respiratory tract
Zinc Oxide	Toxic	White liquid (particle suspension)	Safety glasses and gloves Respirator Exposure through: inhalation, ingestion, eyes, or skin contact Symptoms: irritated skin, eyes, and respiratory tract